PB90- 259557

UMTA-DC-06-0362-90-1

U.S. Department
of Transportation

**Urban Mass
Transportation
Administration**

RESEARCH, DEVELOPMENT AND DESIGN OF A STEERABLE TRANSIT TRUCK

PREPARED FOR

Washington Metropolitan Area Transit Authority
Washington, D.C.

UTDC Inc.
Kingston, Ontario, Canada

FINAL REPORT

March 1990

UMTA Technical Assistance Program

NOTICE

This document is disseminated under the sponsorship of the Department of Transportation in the interest of information exchange. The United States Government assumes no liability for its contents or use thereof.

The United States Government does not endorse products or manufacturers. Trade of manufacturers names appear herein solely because they are considered essential to the object of this report.

Technical Report Documentation Page

1. Report No.	2. Government Accession No. (NTIS)	3. Recipient's Catalog No.
UMTA-DC-06-0362-90-1		

4. Title and Subtitle	5. Report Date
Research and Development and Design of a Steerable Transit Truck	March 1990
	6. Performing Organization Code K9-10200
7. Author's	8. Performing Organization Report No.
J.W. Horwat, UTDC Inc.	TR 443 700 001
9. Performing Organization Name and Address	10. Grant or Project No.
Washington Metro Area Transit Authority 600 Fifth Street, N.W. Washington, D.C. 20001	11. Contract No. DC-06-0362
	13. Type of Report and Period Covered
12. Sponsoring Agency Name and Address **U.S. Department of Transportation** **Urban Mass Transportation Administration (UMTA)** **400 Seventh Street, S.W.** **Washington, D.C. 20590**	Final Project Report
	14. Sponsoring Agency Code UTS-21

15 Supplementary Notes WMATA - Program Manager - Edgar C. Green, Jr.

UTDC Inc.,
Post Office Box 70, Station "A", Kingston, Ontario, Canada K7M 6P9

16 Abstract

This program was initiated as the result of the findings of the WMATA wheel wear/track wear study. Because of the close wheel/track tolerance and flange profile, WMATA noted a wear rate in both wheel and track which was several times higher than anticipated. Because earlier studies of a steerable truck concept had never been completed, WMATA requested UMTA assistance to complete the evaluation.

The program objective was to design, analyze and recommend a steerable truck retrofit to the Washington Metro Rockwell trucks. The design features two-point, body-to-axle steering and replacement of the axle bearing rubber sleeve and end cap with an axle bearing box, top mount and laminated rubber/steel sandwiches. Steering input is by lever and push/pull rods. The brake housing-to-sideframe mountings are modified to ensure maximum pad/disc contact area. The incorporated design was computer analyzed mathematically for performance with respect to dynamic stability and curving ability. The results of the analyses define a stable vehicle within the dynamic envelope of the WMATA system and flange-free curving ability on curves of radii above 500 feet. Because of the large design change at the sideframe/axle interface, a finite element stres analysis was performed resulting in the requirement for a preliminary design sideframe reinforcing cap to be welded to the sideframe.

17. Key Words		18. Distribution Statement
Rapid Transit Noise Reduction Truck Dynamics Steerable Truck	Rail Wear Rail Cars	**Document available to the Public through National Technical Information Service (NTIS), Springfield, Virginia 22161.** **- telephone 703/487-4650**

19. Security Classif. (of this report)	20. Security Classif. (of this page)	21. No. of Pages	22. Price (NTIS)
Unclassified	**Unclassified**	213	

Form DOT F 1700.7 (8-72) Reproduction of completed page authorized

METRIC CONVERSION FACTORS

Approximate Conversions to Metric Measures

Symbol	When You Know	Multiply by	To Find	Symbol
		LENGTH		
in	inches	*2.5	centimeters	cm
ft	feet	30	centimeters	cm
yd	yards	0.9	meters	m
mi	miles	1.6	kilometers	km
		AREA		
in^2	square inches	6.5	square centimeters	cm^2
ft^2	square feet	0.09	square meters	m^2
yd^2	square yards	0.8	square meters	m^2
mi^2	square miles	2.6	square kilometers	km^2
	acres	0.4	hectares	ha
		MASS (weight)		
oz	ounces	28	grams	g
lb	pounds	0.45	kilograms	kg
	short tons (2000 lb)	0.9	tonnes	t
		VOLUME		
tsp	teaspoons	5	milliliters	ml
Tbsp	tablespoons	15	milliliters	ml
fl oz	fluid ounces	30	milliliters	ml
c	cups	0.24	liters	l
pt	pints	0.47	liters	l
qt	quarts	0.95	liters	l
gal	gallons	3.8	liters	l
ft^3	cubic feet	0.03	cubic meters	m^3
yd^3	cubic yards	0.76	cubic meters	m^3
		TEMPERATURE (exact)		
°F	Fahrenheit temperature	5/9 (after subtracting 32)	Celsius temperature	°C

*1 in = 2.54 (exactly). For other exact conversions and more detailed tables, see NBS Misc. Publ. 286, Units of Weights and Measures, Price $2.25, SD Catalog No. C13.10:286.

Approximate Conversions from Metric Measures

Symbol	When You Know	Multiply by	To Find	Symbol
		LENGTH		
mm	millimeters	0.04	inches	in
cm	centimeters	0.4	inches	in
m	meters	3.3	feet	ft
m	meters	1.1	yards	yd
km	kilometers	0.6	miles	mi
		AREA		
cm^2	square centimeters	0.16	square inches	in^2
m^2	square meters	1.2	square yards	yd^2
km^2	square kilometers	0.4	square miles	mi^2
ha	hectares (10,000 m^2)	2.5	acres	
		MASS (weight)		
g	grams	0.035	ounces	oz
kg	kilograms	2.2	pounds	lb
t	tonnes (1000 kg)	1.1	short tons	
		VOLUME		
ml	milliliters	0.03	fluid ounces	fl oz
l	liters	2.1	pints	pt
l	liters	1.06	quarts	qt
l	liters	0.26	gallons	gal
m^3	cubic meters	35	cubic feet	ft^3
m^3	cubic meters	1.3	cubic yards	yd^3
		TEMPERATURE (exact)		
°C	Celsius temperature	9/5 (then add 32)	Fahrenheit temperature	°F

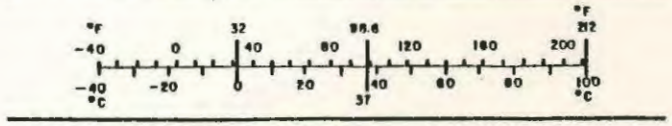

RESEARCH, DEVELOPMENT AND DESIGN

OF A

STEERABLE TRANSIT TRUCK

Prepared For The

WASHINGTON METROPOLITAN AREA TRANSIT AUTHORITY

Prepared By

J.W. HORWAT

UTDC INC.

March 1990

TABLE OF CONTENTS

TABLE OF CONTENTS (cont'd)

EXECUTIVE SUMMARY

This program is the result of a progressive steerable truck development program undertaken by the Transportation Systems Centre (USDOT) for use by US rail transit authorities. The objective was to design, analyze and recommend a steerable truck retrofit to the Washington Metro Rockwell trucks. The Urban Transportation Development Corporation was tasked to carry out the Program as Phase I (later 1a).

The design features two point body-to-axle steering, replacing the axle bearing rubber sleeve and end cap with an axle bearing box, top mount and laminated rubber/steel sandwiches. Steering input is by lever and push/pull rods. The brake housing-to-sideframe mountings are modified to ensure maximum pad/disc contact area.

The incorporated design was analyzed mathematically via high speed computer for performance with respect to dynamic stability and curving ability. The results showed a stable vehicle within the operating envelope of the WMATA system and flange-free curving ability on curves of radii above 500 ft.

Because of the large design change at the sideframe/axle interface a finite element stress analysis was performed resulting in the requirement for a preliminary design sideframe reinforcing cap to be welded to the sideframe.

1.0 INTRODUCTION

1.1 BACKGROUND

1.1.1 The Transportation Systems Center (TSC) of the U.S. Department of Transportation competitively awarded two parallel design feasibility studies aimed at developing rail rapid transit car steerable trucks for use by U.S. rail transit authorities. The Urban Transportation Development Corporation (UTDC) was awarded one contract to apply its design to the Chicago Transit Authority (CTA). This initial work was completed but the CTA withdrew from participation. The Washington Metropolitan Area Transit Authority (WMATA) expressed interest in replacing the CTA by applying the UTDC design to its trucks.

1.1.2 A research grant was based on the WMATA wheel and rail wear problems and the desire to maintain the original competition. Funding was approved, and the UTDC was awarded a contract for the design and analysis of a WMATA Rockwell truck, to be known as Phase 2A of the WMATA Program.

1.2 PROGRAM OBJECTIVE

1.2.1 The objective of this program was to design, analyze and recommend a steerable truck retrofit to the WMATA Rockwell trucks to WMATA specifications and system operating envelope.

1.1.3 The WMATA Program as envisioned by the UTDC was to begin with the gathering of data and end with a tested, acceptable, near-production, steering retrofit for the Rockwell truck. The Program was divided into three phases, Phase 1 being the gathering of data and the design, modelling and analysis of the retrofit and test on instrumented track, and Phase 3 encompassing the testing of the retrofitted truck on the WMATA track. This report contains the results obtained during Phase 1 (later renamed Phase 1A).

1.1.4 The retrofit to the existing WMATA trucks would yield economic and rider acceptance benefits to the WMATA operations and could form the basis for future truck orders. These benefits would be experienced in reduced wheel flange forces, contributing to a reduction in track maintenance and noise; a reduction in flange and tread wear which would bring about a reduction in wheel maintenance, and a diminution of rolling resistance for reduced energy costs.

2.0 DESIGN

2.0.1 Section 2.1 summarizes the design criteria contained in the WMATA Specification, Section S14, and other data provided by WMATA.

Section 2.2 is a description of the WMATA truck as designed by the manufacturer, Section 2.3 is the description as modified for steering by UTDC R&D, and Section 2.4 is a description of the steering operation of the steered truck.

2.1 SPECIFICATION

2.1.1 The following vehicle specifications were considered in the design of the steering retrofit:

a) vehicle weight - loaded - 105,000 lb.
- empty - 72,000 lb.

b) maximum speed - 80 mi/hr

c) track gauge - tangent - 4 ft. 8½ in.

d) wheel diameter - mean - 28 in.

e) truck height - 32½ in.

f) truck wheelbase - 87 in.

g) truck centre-to-centre - 52 ft.

h) journal bearing life - 1,000,000 mi.

i) running rail - 115 RE canted 1:40

j) minimum curve radius - 225 ft.

k) trucks fully interchangeable between either end of car

l) truck parts to withstand maximum loads imposed by forces acting on the frame, without exceeding stresses greater than 60% of the endurance limit for the materials.

2.2 DESCRIPTION - AS DESIGNED

2.2.1 The truck (Figure 2.2-1) is a three-piece unit consisting of quasi "T"-shaped sideframes (1) and a bolster (2). The sideframes are interconnected via self-aligning ball bushings (3) permitting wheel load equalization while limiting truck lozenging.

2.2.2 The sideframes connect to the axles (4) by wrapping around a rubber sleeve which surrounds the journal bearing. The motor and gearbox units (5) are supported by the sideframes through rubber-cushioned hangers and the axles.

2.2.3 The bolster (Figure 2.2-2) is supported by the sideframes on two double convoluted air springs (6). Its position with respect to the sideframes is controlled through lateral stops (7) and longitudinal rubber-mounted radius rods (8). In turn, the carbody is located by a centre pin (9) and supported by stainless steel/polymer side bearing pads (10).

2.2.4 The truck is equipped with a hydraulically actuated disk brake (11) at each wheel, with the discs attached to the axle end and the actuator mounted through four-piece articulated bracketry (12) to the sideframe.

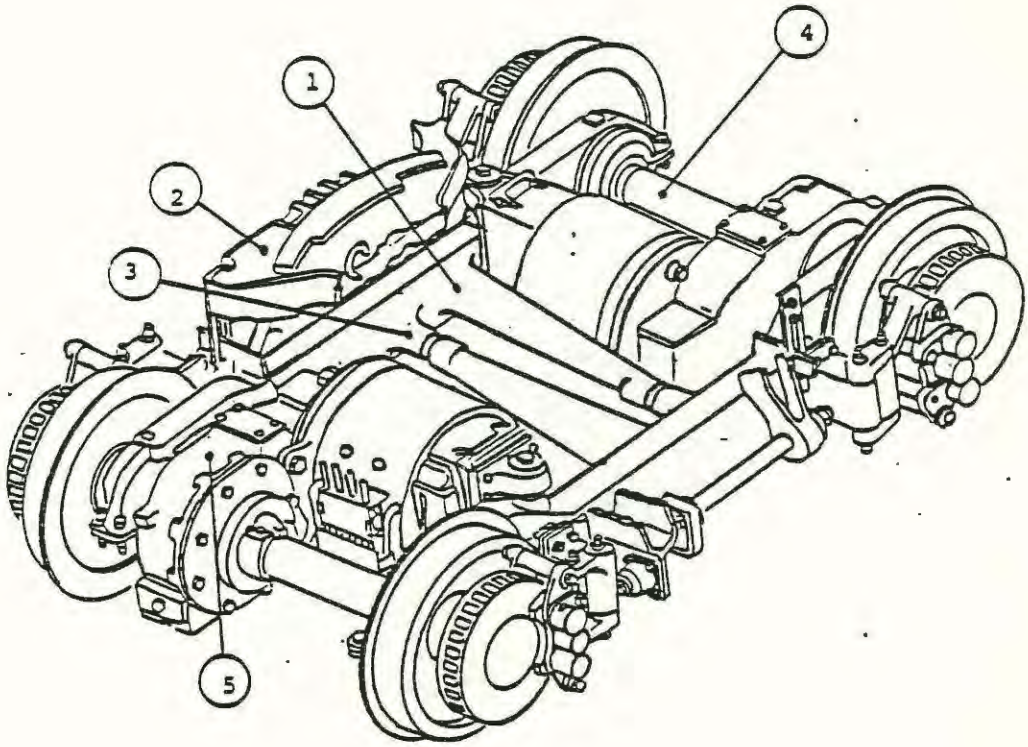

FIGURE 2.2-1 - WMATA ROCKWELL TRUCK

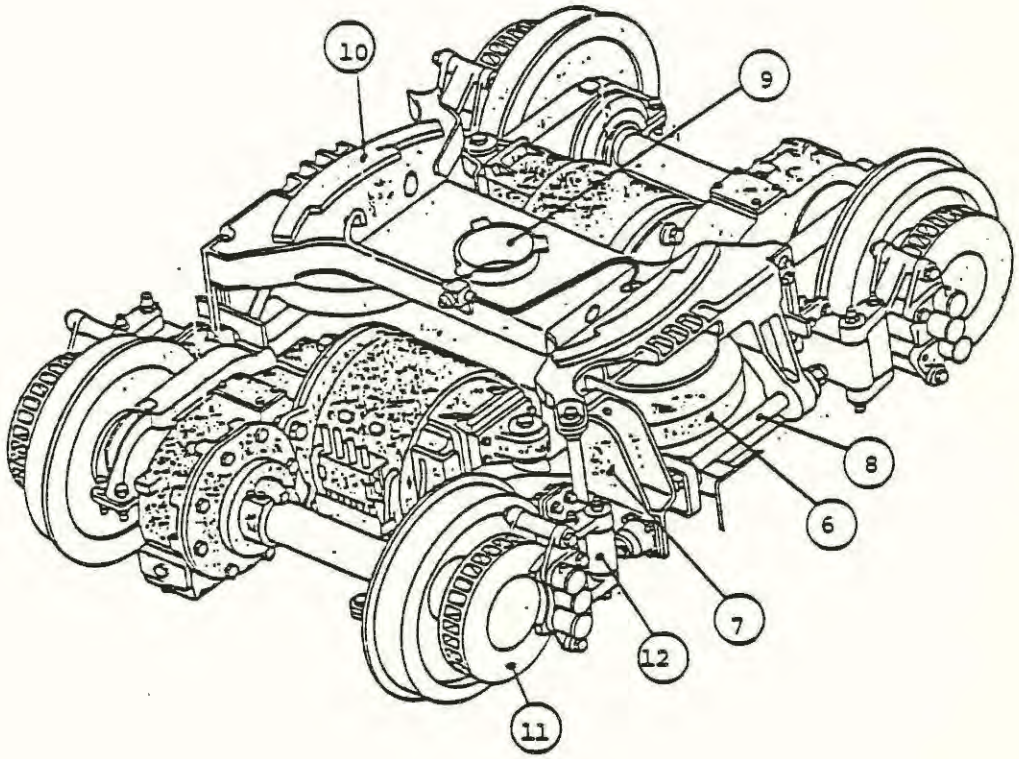

FIGURE 2.2-2 - WMATA TRUCK WITH BOLSTER

2.3 DESCRIPTION - STEERING RETROFIT

2.3.1 The design of the steering conversion (retrofit) affects the following vehicle elements:

a) primary suspension
b) disk brake actuator mountings
c) carbody underfloor
d) sideframes
e) air piping

2.3.2 The wrap-around rubber sleeve at each journal bearing is replaced by a cast journal bearing housing (2), angled steel/rubber pads (25) and cast top supports (7) to allow axle-to-sideframe yaw. (Figure 2.3-1).

2.3.3 The disc brake actuator mountings (Figure 2.3-2) become five-piece systems (26) to allow lateral and longitudinal pad-to-disc alignment.

2.3.4 The carbody underfloor has a pivot connector installed to provide the steering input.

2.3.5 The steering connection between the carbody and the journal housing (Figures 2.3-3 & 2.3-4) is provided by a horizontal push rod (11) connected to a vertical link (15, 16) pivoted on the top support which is connected to a connecting rod (27, 28) which is finally attached to the journal housing. All connections are terminated at rubber bushings.

2.3.6 A complete list of retrofit parts is contained in Appendix A.

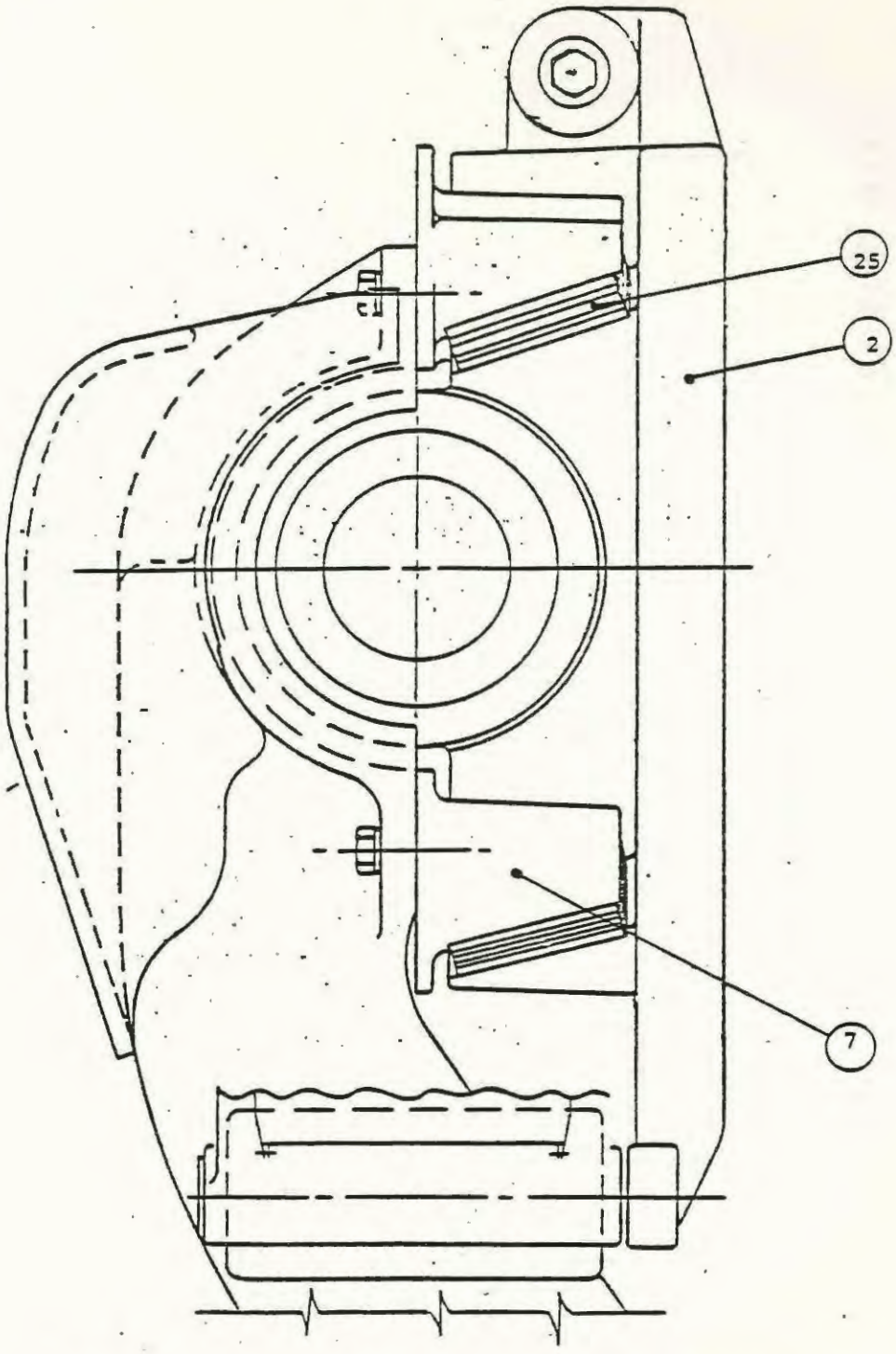

FIGURE 2.3-1 - PRIMARY SUSPENSION - UNSTEERED

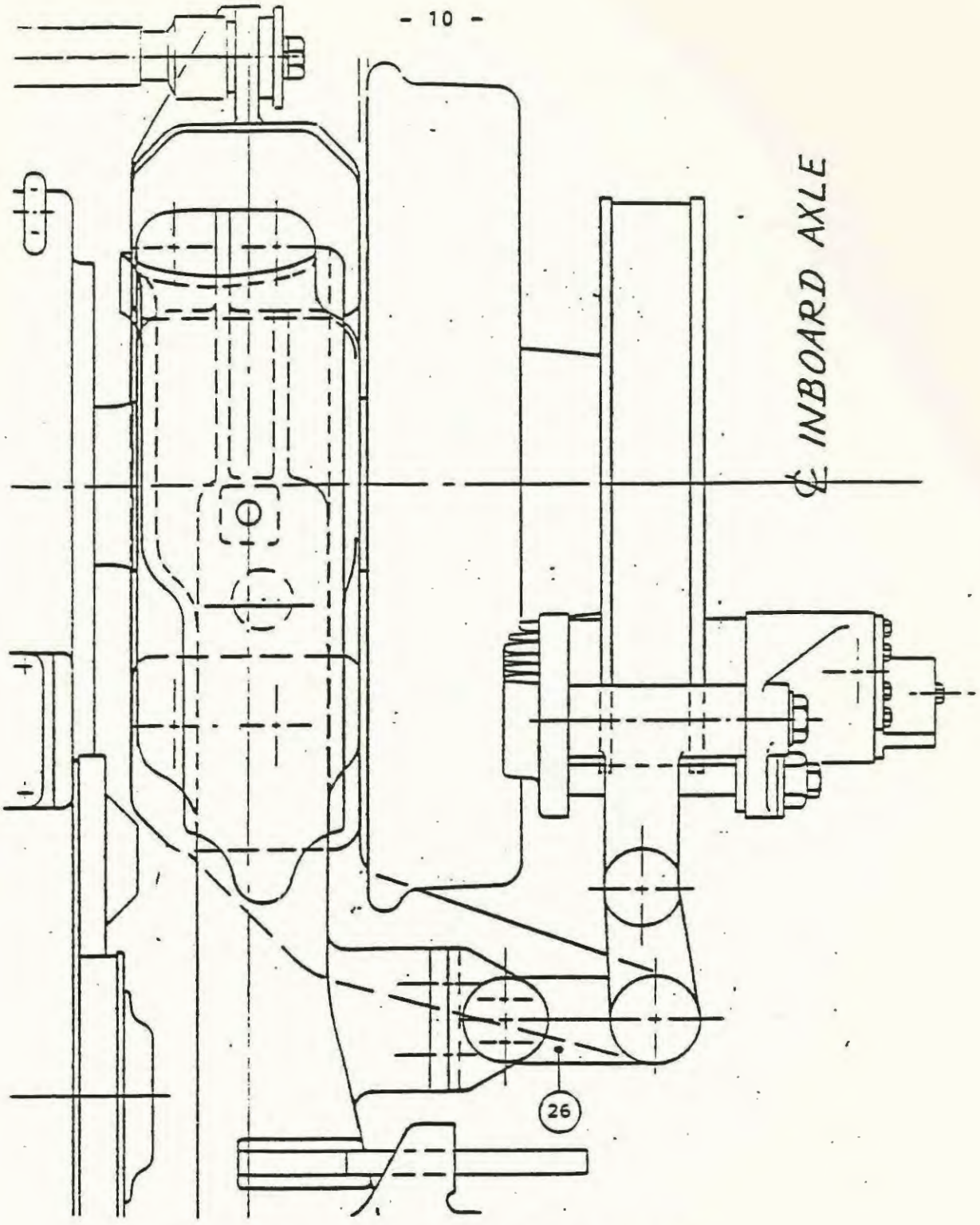

FIGURE 2.3-2 - DISC BRAKE ATTACHMENTS

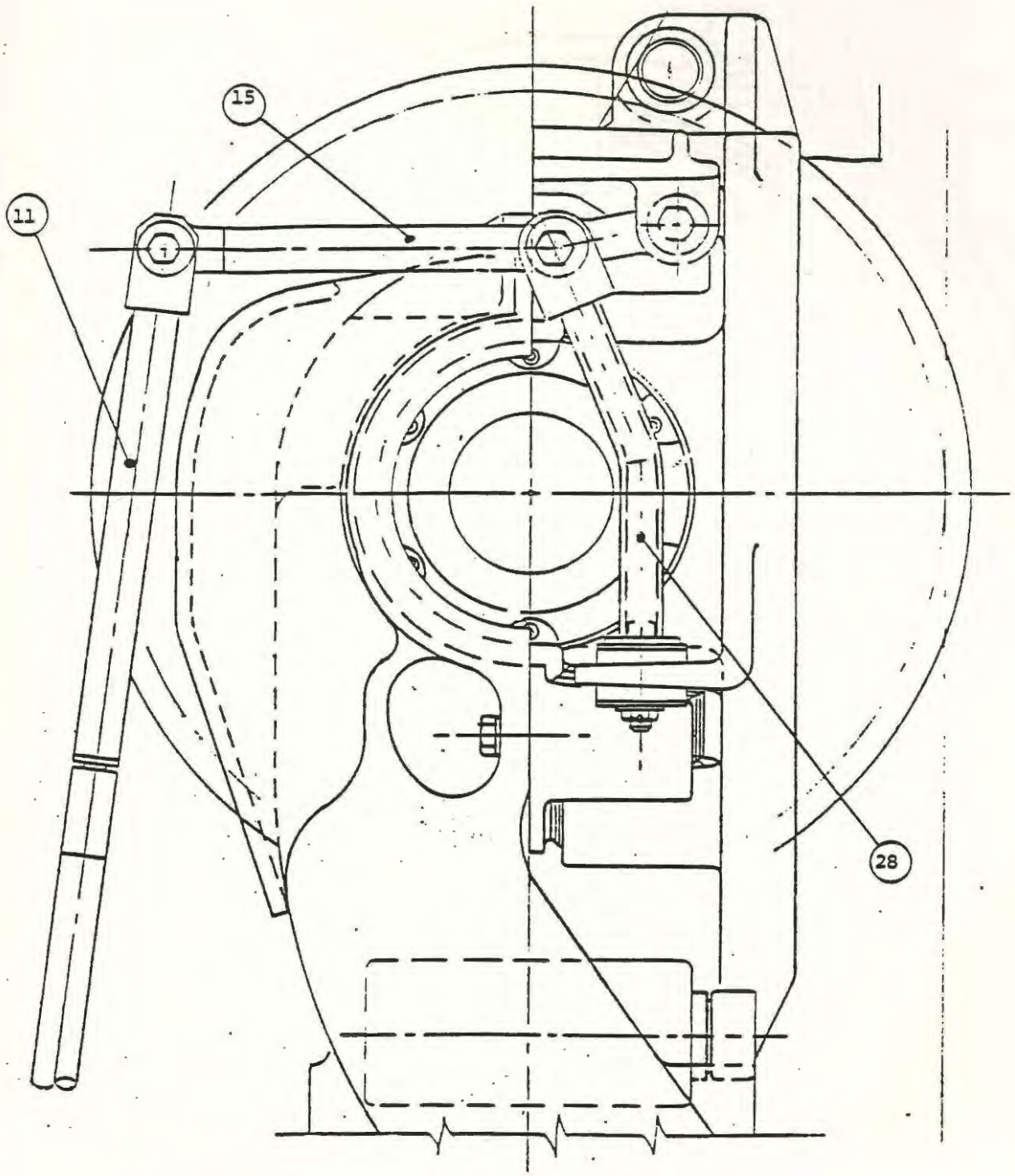

FIGURE 2.3-3 STEERING - FRONT TRUCK INBOARD

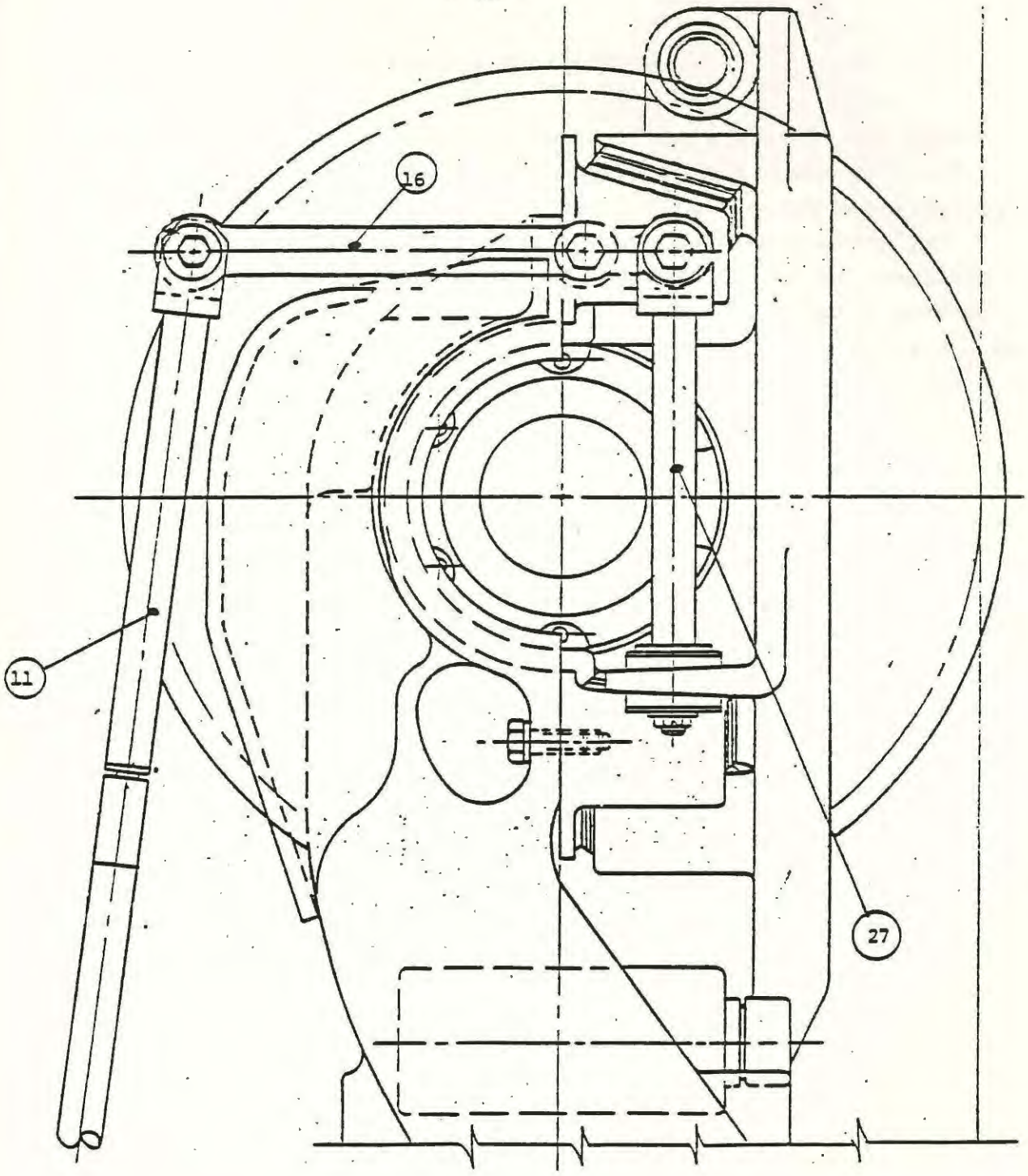

FIGURE 2.3-4 STEERING - FRONT TRUCK OUTBOARD

2.4 DESCRIPTION - STEERING OPERATION

2.4.1 As a vehicle enters a curve (Figure 2.4-1), the coned wheels are displaced laterally on the outer rail and initiate axle and truck yaw. With a truck semi-spacing of L and a curve radius R, the truck-to-carbody yaw angle becomes the inverse sine of L/R (AOB), assuming perfect steering. In addition, still assuming perfect steering with the axle radial, the steering angle of the axle to the truck is the inverse sine of L_1/R (COD). This results in an overall steering ratio L/L_1.

2.4.2 Employing the truck frame as the fulcrum (Figure 2.4-1), it remains necessary only to attach a lever between the carbody at A to the axle at B of such a ratio that the displacement $A-A^1$ between the carbody and the truck frame produces a displacement $B-B^1$ between the truck frame and the axle. It should be clear that on tangent track, A and A^1 coincide as do B and B^1.

2.4.3 It should be evident that any physical limitations on $B-B^1$ in turn limits how small the curve radius R can be before mechanical linkages fail. It should also be evident that a significant difference between $A-A^{11}$ (perfect displacement) and $A-A^1$ will affect the steering accuracy throughout the operating envelope.

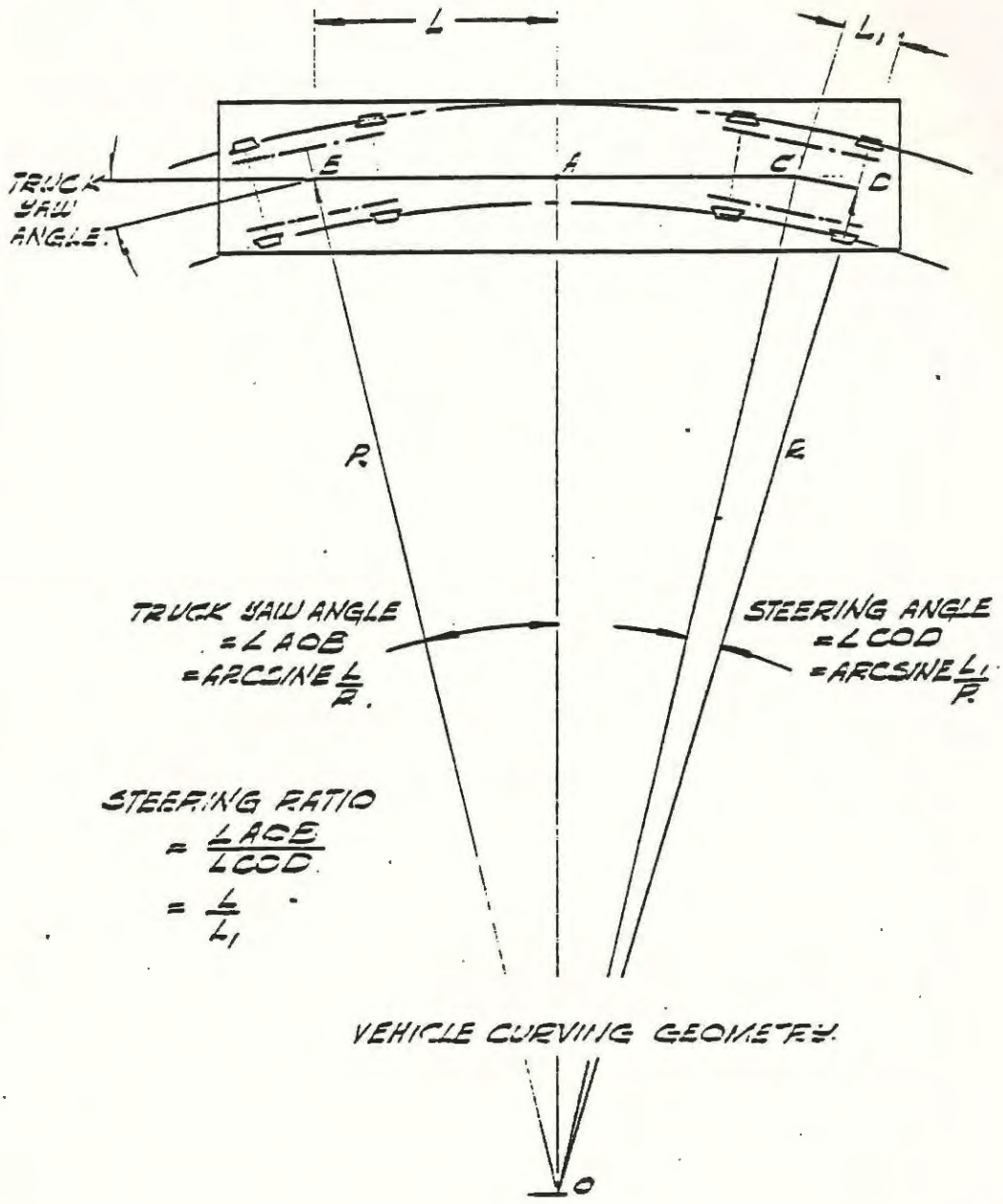

FIGURE 2.4-1 VEHICLE CURVING GEOMETRY

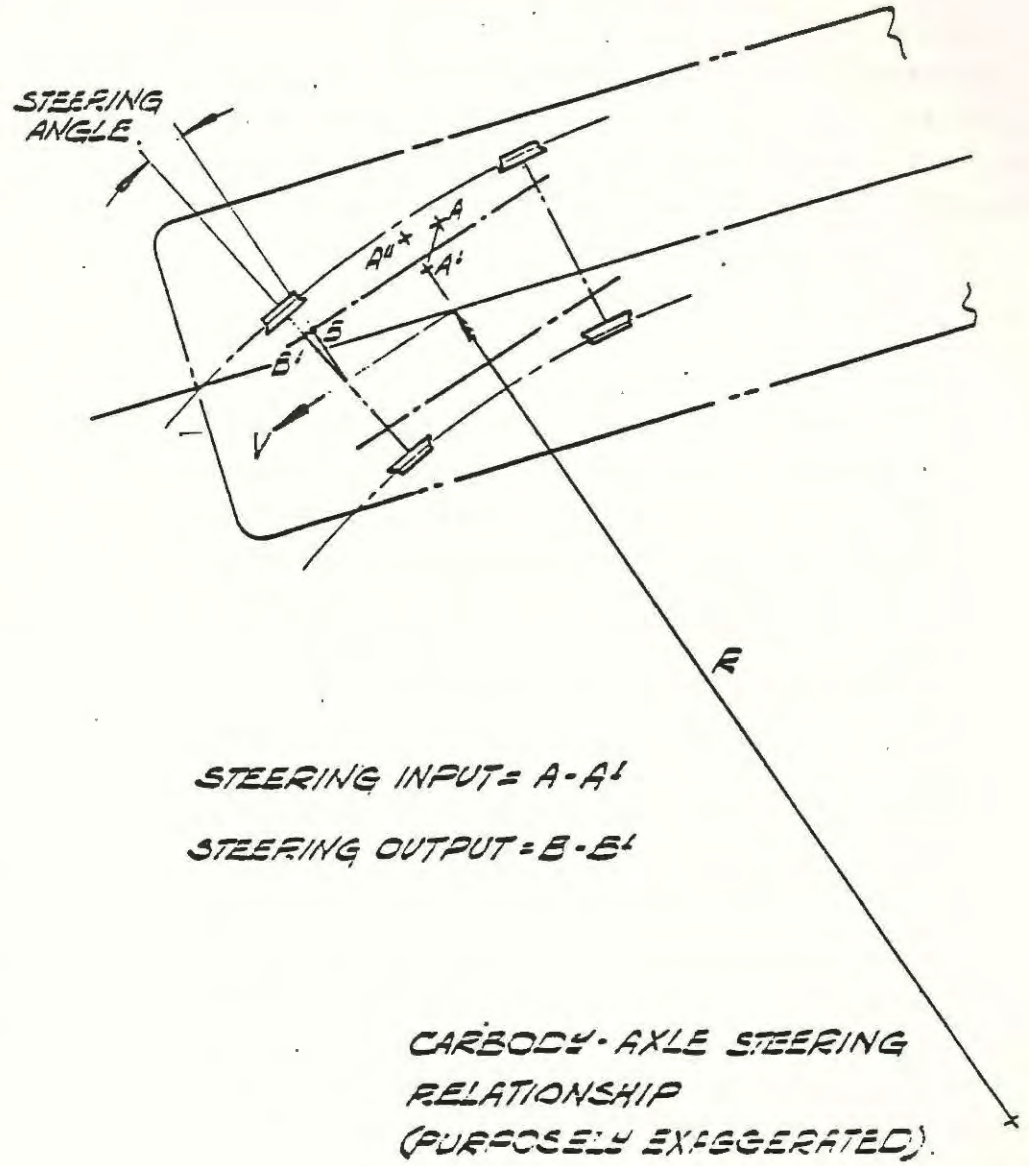

FIGURE 2.4-2 CARBODY - AXLE STEERING RELATIONSHIP (FIGURE PURPOSELY EXAGGERATED)

3.0 KINEMATIC ANALYSIS

A kinematic analysis of the proposed steering mechanism was carried out to ascertain overall steering ratios, steering lever lengths and the expected displacement of the axle while the vehicle negotiates a curve of known radius.

3.1 METHOD

Using the dimensions of the WMATA specification, Section 5.2 (corrected and/or validated) and the conceptual layout of the preferred steering mechanism, a graphical analysis was carried out. The results were then checked numerically using a hand calculator.

3.2 RESULTS

The complete results of the kinematic analysis appear as Appendix B. They show that for the preferred two-point steering system on a 230 ft. (70 m) radius curve the recommended steering lever lengths would produce a 0.61 % understeer in push (R trucks, right curve; F trucks, left curve) and a 1.49 % understeer in pull (R trucks, left curve; F trucks, right curve). The chosen lever ratios also ensure that no steering input exists on tangent track.

3.3 DISCUSSION

3.3.1 Because of the restrictions of space between the carbody and the truck frame, the limitation imposed by the gearbox/motor/sideframe mountings and the known flexibility of the motor/gearbox coupling, it became evident early in the program that two-point steering was a necessity. On that basis, it also became evident that analyzing more than one mechanism was unnecessary.

3.3.2 As shown in the results, a slight understeer has been preferred. Experience has shown that although an oversteer condition may be preferred for the leading axle of the leading truck, to compensate for rubber element strain and lever and pushrod flexibility, the trailing axle of that same truck would also achieve oversteer to the detriment of good steering, i.e., tending to flange on the outside rail. Consequently, perfect steering to slight understeer is preferred.

4.0 DYNAMIC STABILITY ANALYSIS

4.1 INTRODUCTION

4.1.1 For steerable trucks there are three groups of instabilities which can arise. These are represented schematically in Fig. 4.1-1.

4.1.2 Region I contains unstable modes which are similar to those found in conventional rail vehicles. Region II contain modes which are peculiar to steered axle vehicles. In these modes the direct coupling which exists between axle and body motions produces a situation in which the dynamic coupling is dependent upon frequency, a resonant coupling effect. In these instances an instability occurs at a relatively low frequency and velocity, but as velocity increases the frequency can eventually become high enough for decoupling to occur and the instability disappears. Similar modes can sometimes be seen in conventional vehicles, but they are not usually very pronounced and can be controlled quite easily through damping of the carbody. This is because the coupling which exists is indirect and rather weak. In the case of steered axle vehicles the coupling is direct mechanical and far stronger.

4.1.3 The third region of instability, region III, contains a mode which is entirely unique to steered axle vehicles. In this mode the action is not a periodic one; it is a monotonic divergence and only one truck is involved, the leading truck. It can be shown (see UTDC internal report "Some

Characteristics of Steered Railway Trucks" by R.E. Smith and R.J. Anderson) that below a certain conicity the leading truck of a steered axle vehicle will exhibit this divergence of its yaw position relative to the track. The effect of this phenomenon is that any yaw deflection of the truck will result in a moment being applied which increases the yaw deflection. This will continue until the wheels of the truck contact the rail flanges.

4.1.4 It can be seen from Figure 4.1-1 that this divergence occurs only at low conicities, and it can be shown that the limiting value of conicity is a function of a number of the truck design variables, including the steering mechanism stiffness and amplification ratio, truck geometry, wheel size and creep coefficients. In general, high stiffness increases the limiting conicity and high creep coefficients decrease it.

4.1.5 There is a fourth region of instability attributable to steered trucks, which is not shown in the figure. This is a divergence of the trailing truck, which occurs at and above certain high levels of conicity. This instability can only occur with very high levels of steering stiffness and usually for levels of conicity which are far beyond the range normally found in practice. For these reasons this fourth region will not be discussed.

4.1.6 The divergent instabilities of region III and IV have been named "The Weinstock Effect" in recognition of Dr. H. Weinstock of the U.S. D.O.T. who was instrumental in leading Dr. R.J. Anderson and R.E. Smith to discover the phenomenon while working on a program of analysis funded by the U.S. government.

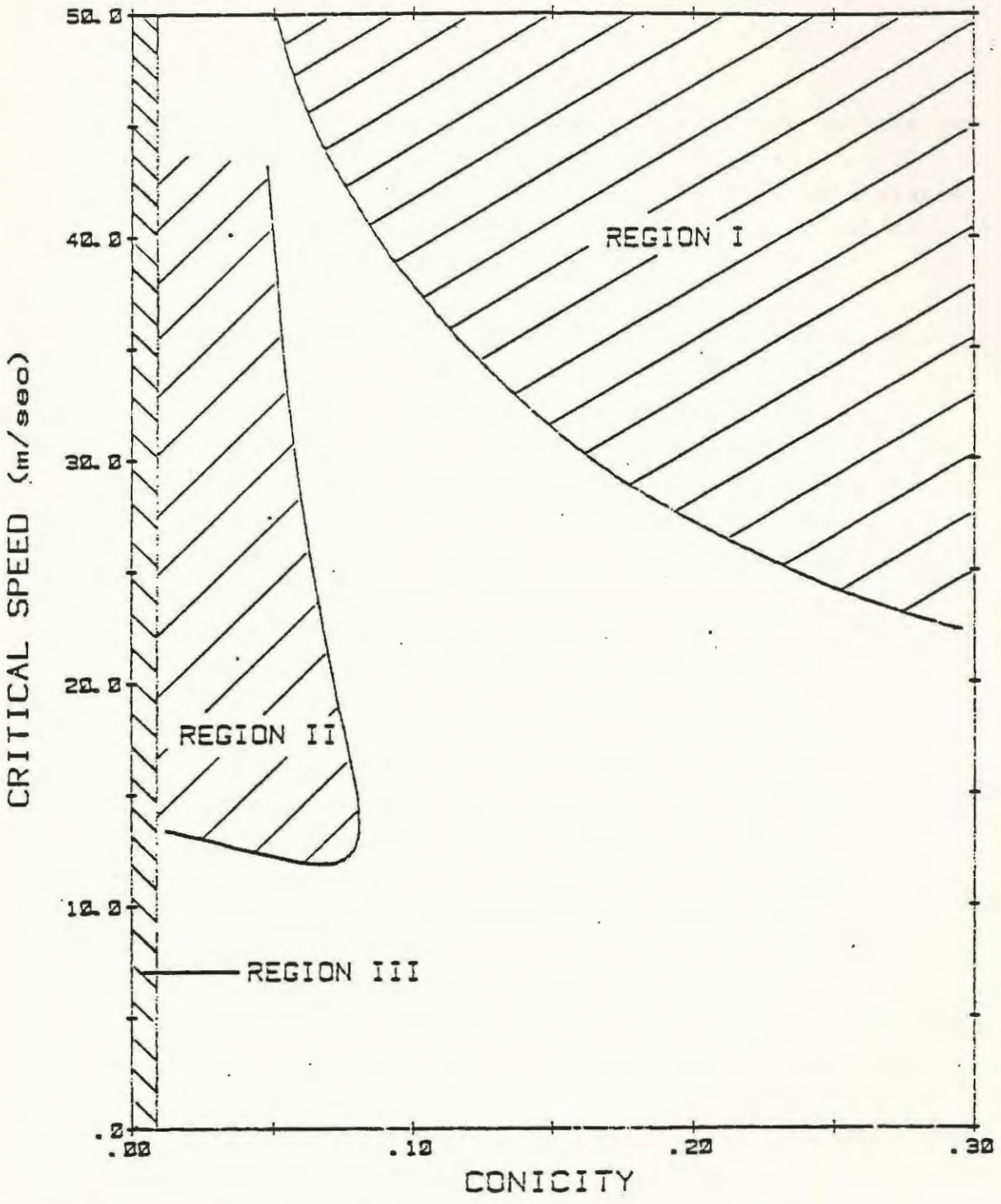

FIGURE 4.1-1 STABILITY CHARACTERISTICS - STEERED TRUCKS

4.2 METHOD

4.2.1 A linear mathematical model of the WMATA vehicle was formulated to provide stability information. The carbody and two trucks were represented as a system of rigid masses interconnected by parallel elastic and viscous elements.

4.2.2 The motions of the WMATA vehicle were described with 11 mass elements comprising a total of 33 degrees-of-freedom (q_i), as shown in Figure 4.2-1 Suspension components and interconnections between mass elements amounted to 98 linear and torsional springs with parallel viscous dampers. Creep forces arising from wheel and rail interaction were assumed to vary linearly with creepage, with no flange contact. A computer eigenvalue analysis was utilized to gather stability information regarding the system, for small amplitude motions.

4.2.3 The condition of lateral instability or hunting was considered in terms of the forward speed (or critical speed) at which damping in the least damped eigenvalue dropped to zero. The linear analysis predicts that the vehicle will oscillate with an amplitude dependent on the initial conditions at the critical speed while going unstable at higher speeds. The maximum operating speed of the vehicle should be kept somewhat below the critical speed.

4.2.4 The dynamic stability of the steered truck/empty car combination was examined for modes of interest and critical speed in the as-designed condition. All vehicle parameters were given their design values.

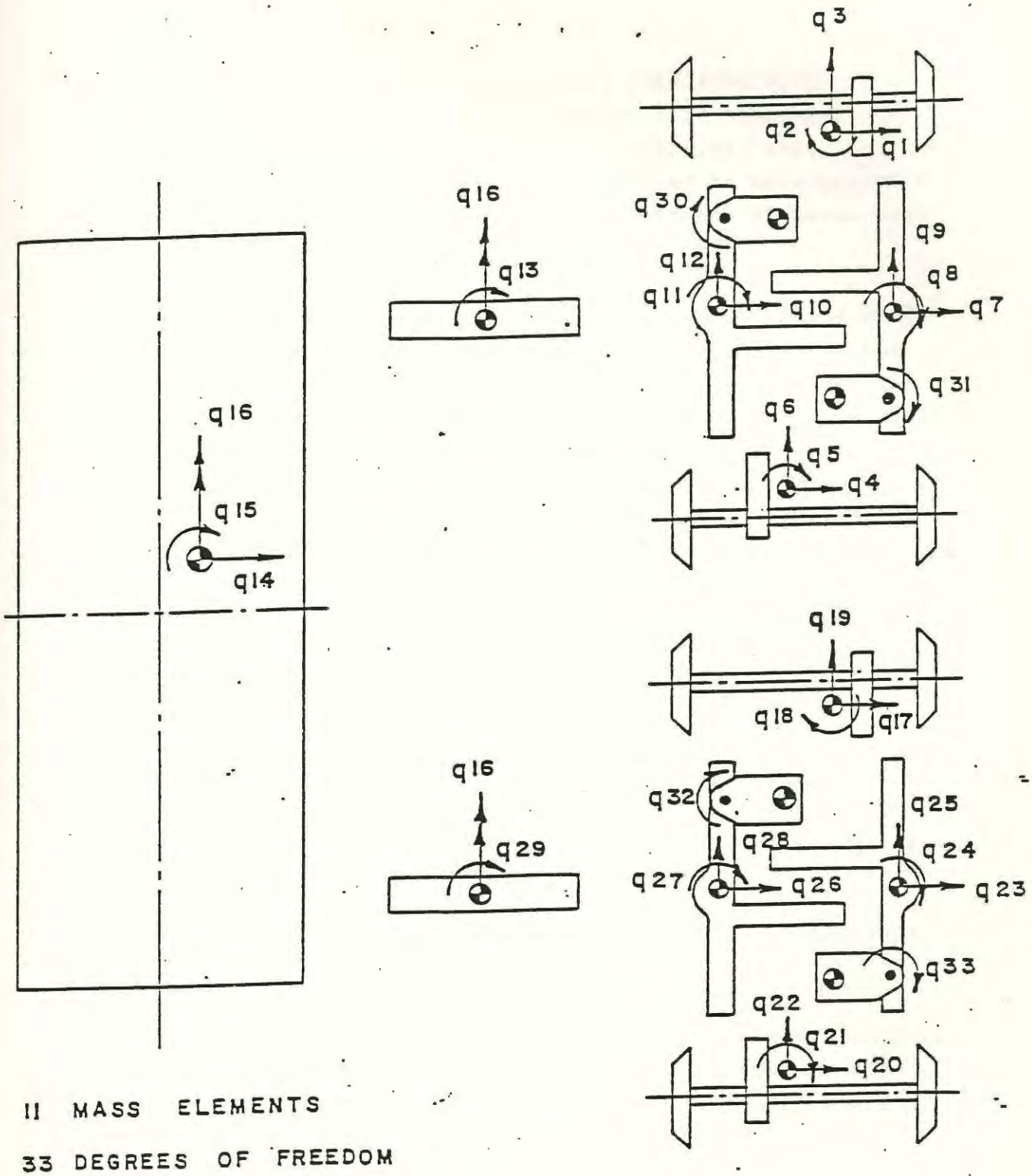

FIGURE 4.2-1 - VEHICLE MODEL

4.2.5 A crush loaded vehicle was simulated by increasing carbody weight by 36,300 lb. (220 passengers at 165 lb/passenger). Changes in inertias, axle load and creep coefficients were included in this analysis, while stiffnesses of load dependent elements were left unchanged.

4.2.6 At the request of WMATA Vehicle Engineering UTDC also ran out a few stability cases based on the stiffness parameters of the modified primary bushings as contained in Reference 1. In general, the modified bushings provided stiffer springing vertically and softer laterally and longitudinally. The numerical value are contained in Table 4.2.6-1. All other vehicles parameters remained unchanged.

PARAMETER	STANDARD BUSH	MODIFIED BUSH
Primary Vertical Stiffness (per wheel)	74,000 lb/in. 1.299 E 7 N/m	116,000 lb/in 2.036 E 7 N/m
Primary Lateral Stiffness (per wheel)	62,300 lb/in 1.093 E 7 N/m	32,000 lb/in 5.615 E 6 N/m
Primary Longitudinal Stiffness (per wheel)	115,000 lb/in 2.018 E 7 N/m	29,000 lb/in 5.089 E 6 N/m

Table 4.2.6-1: Modified Primary Bush Parameters (measured in Laboratory)

The vehicle critical speed was calculated for four conicities -- 0-05, 0-10, 0.15 and 0.20 -- and compared to the results obtained for the standard bushings.

4.3 RESULTS AND DISCUSSION

4.3.1 The examination indicated five principal modes of interest. Figure 4.3-1 shows the damping ratio for these modes as a function of speed, for full Kalker creep coefficients and a wheel conicity of 0.05 (1 in 20). Frequency variation with speed for these modes is also presented in Figure 4.3-2.

4.3.2 The mode which first becomes unstable does so at a speed of 137 mi/hr and involves motions within the trailing truck. It is characterized by lateral and yaw excursions of both the trailing truck axles, sideframes and bolster, combined with yaw motions of the steering levers. A similar mode associated with the leading truck becomes unstable at a higher speed of 156 mi/hr.

4.3.3 The remaining modes involve carbody motion and are substantially damped at all speeds considered with frequency being relatively insensitive to speed. They are:

(a) Carbody, upper center roll, frequency of 0.6 Hz
(b) Carbody, lower center roll, frequency of approximately 1.3 Hz
(c) Carbody, yaw, frequency of approximately 1.4 Hz.

4.3.4 These modes cause no concern in terms of stability or ride comfort. It is of interest to note the coupling of motions as the frequency of the truck and body modes approach each other.

4.3.5 A stability characteristic was produced in Figure 4.3-3 to show the behavior of the steered truck as a function of wheel conicity, for full Kalker creep coefficients. The empty car condition was again considered with all vehicle parameters having their design values. The critical speed (0% damping) produces the stability boundaries, with regions below the curve corresponding to the stable operating regime. Curves of 2%, 5% and 10% critical damping levels have also been included.

4.3.6 As wheel conicity increases from a value of 0.05, the critical speed decreases uniformly from a value of 137 mi/hr to 64 mi/hr at a conicity of 0.30. Over this region of conicity, the mode which first becomes unstable involves the lateral and yaw motions of the trailing truck as discussed previously. As wheel conicity decreases below 0.05, the critical speed decreases significantly to a value of 78 mi/hr at a conicity of 0.04, and finally falls to zero at a conicity of 0.015. In this region of conicity, the first unstable mode involves the lateral and yaw motions of the leading truck. Coupling of the truck and body modes does produce regions where the damping levels of both truck modes (leading and trailing) fall below the 10% level at a somewhat lower speed (45 mi/hr) and then increase as speed increases. This results in the "knee" for the 10% damping level shown in Figure 4.3-3 and can be seen in Figure 4.3-1.

4.3.7 With the axle-to-carbody connections on a steerable truck, disturbances other than curves also produce yawing motions between the truck and carbody. The axles will be steered in response to these perturbations, affecting stability of the vehicle on tangent track. Steering induced instabilities can exhibit a fluttering behavior and are known to be caused by low conicity and low creep coefficients. It is recommended that the wheel conicity be kept at 0.05 and above to avoid the low conicity effects on stability.

4.3.8 The actual creep coefficients experienced in rail vehicle operation can vary due to varying surface conditions and rail head shapes along the track length. Hence, a stability characteristic (Figure 4.3-4) was also produced for the steered truck/empty car design in which the creep coefficients were reduced to 50% of their theoretical values (half creep). As indicated, the design exhibits the desirable tendency of becoming more damped at conicities above 0.10, with the lower creep coefficients. The low conicity/low creep coefficient effect is demonstrated by the shift of the stability boundary to the right for a conicity less than 0.10.

4.3.9 The effect of increased mass on critical speed is shown in Figures 4.3-5 and 4.3-6 for conicities of 0.05 and 0.20, respectively. In both cases, the critical speed remains approximately the same, while the critical mode is slightly less damped at lower speeds. However, overall stability performance is not degraded to any significant degree as the carbody is loaded.

4.3.10 For the comparison of the standard unsteered truck to that of the truck with modified primary bushings, it can be seen in Figure 4.3.10-1 that at low conicities, the modified bushings provide greater stability than the standard units, but as the tread cone angle is increased, as would be experienced in normal wear, the characteristic curves cross until that of the modified bushes becomes less than the standard.

Damping of 10% critical is still present at the worst case (modified bushings, 0.2 conicity) at 65 mi/hr and the critical speed at that same conicity is predicted to be some 94 mi/hr.

4.3.11 It would appear then that the softer primary bushings could be used without any detrimental effects on the stability of the vehicle.

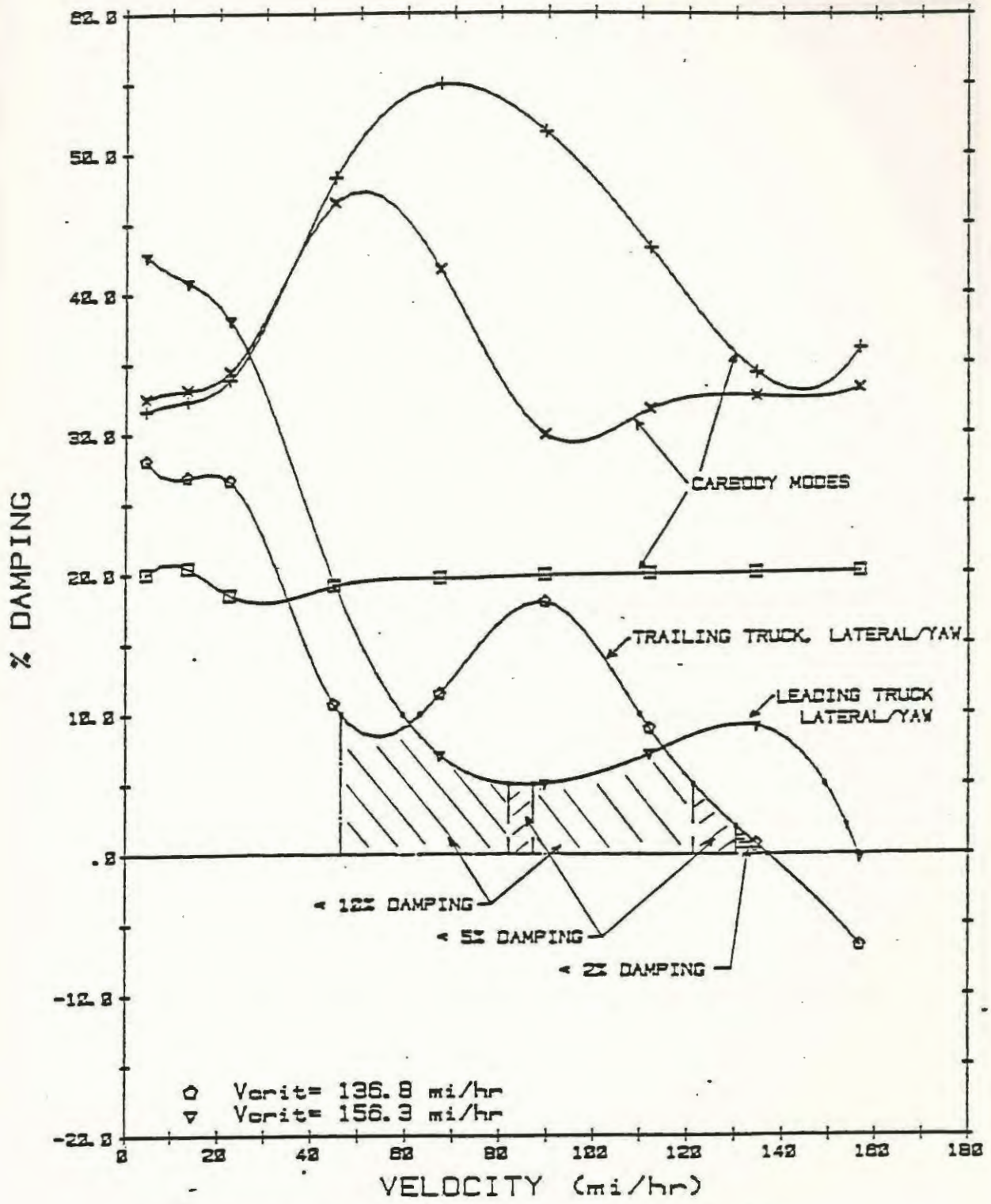

FIGURE 4.3.-1 - DAMPING OF MODES VS VELOCITY

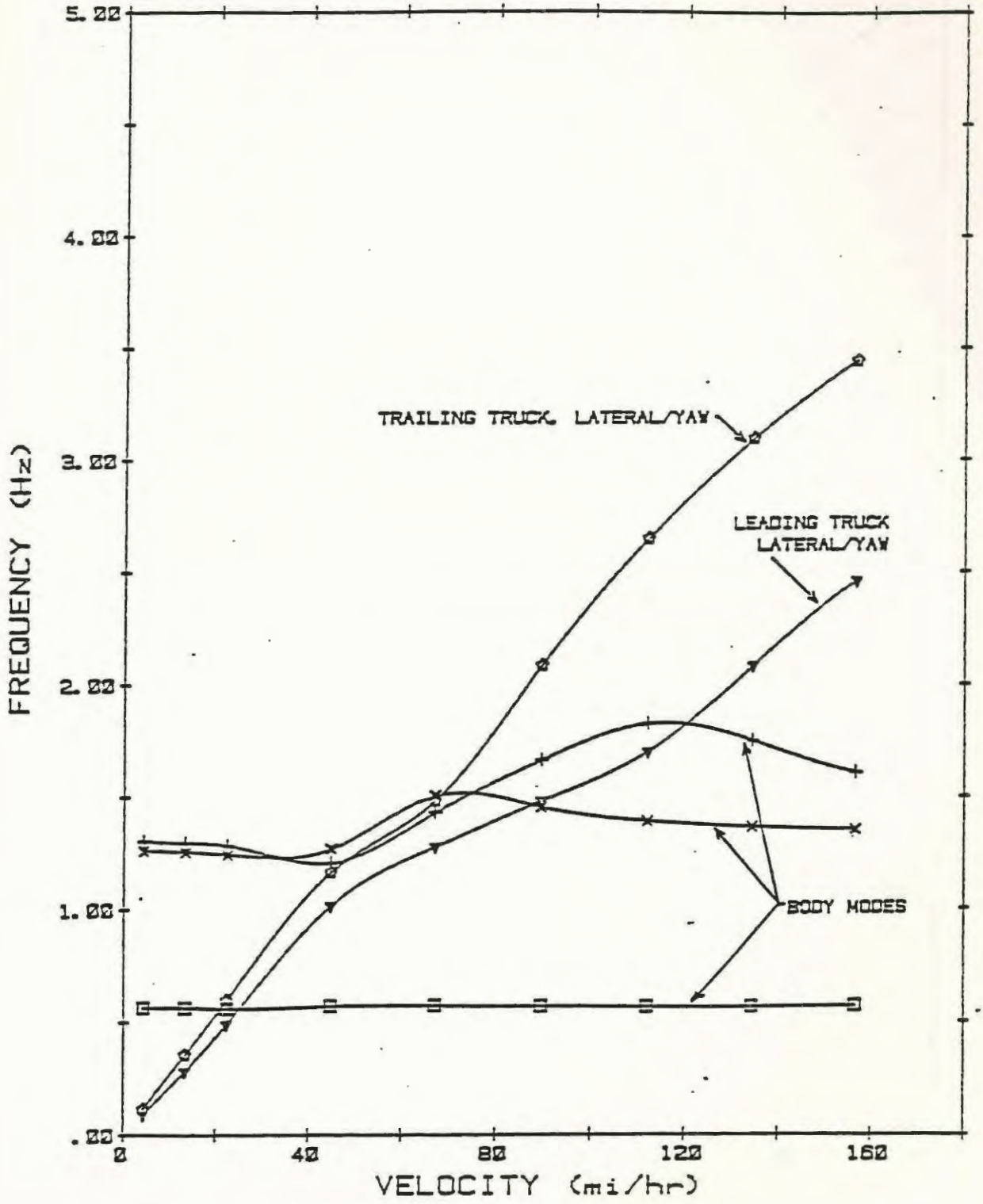

FIGURE 4.3-2 - FREQUENCY OF MODES VS VELOCITY

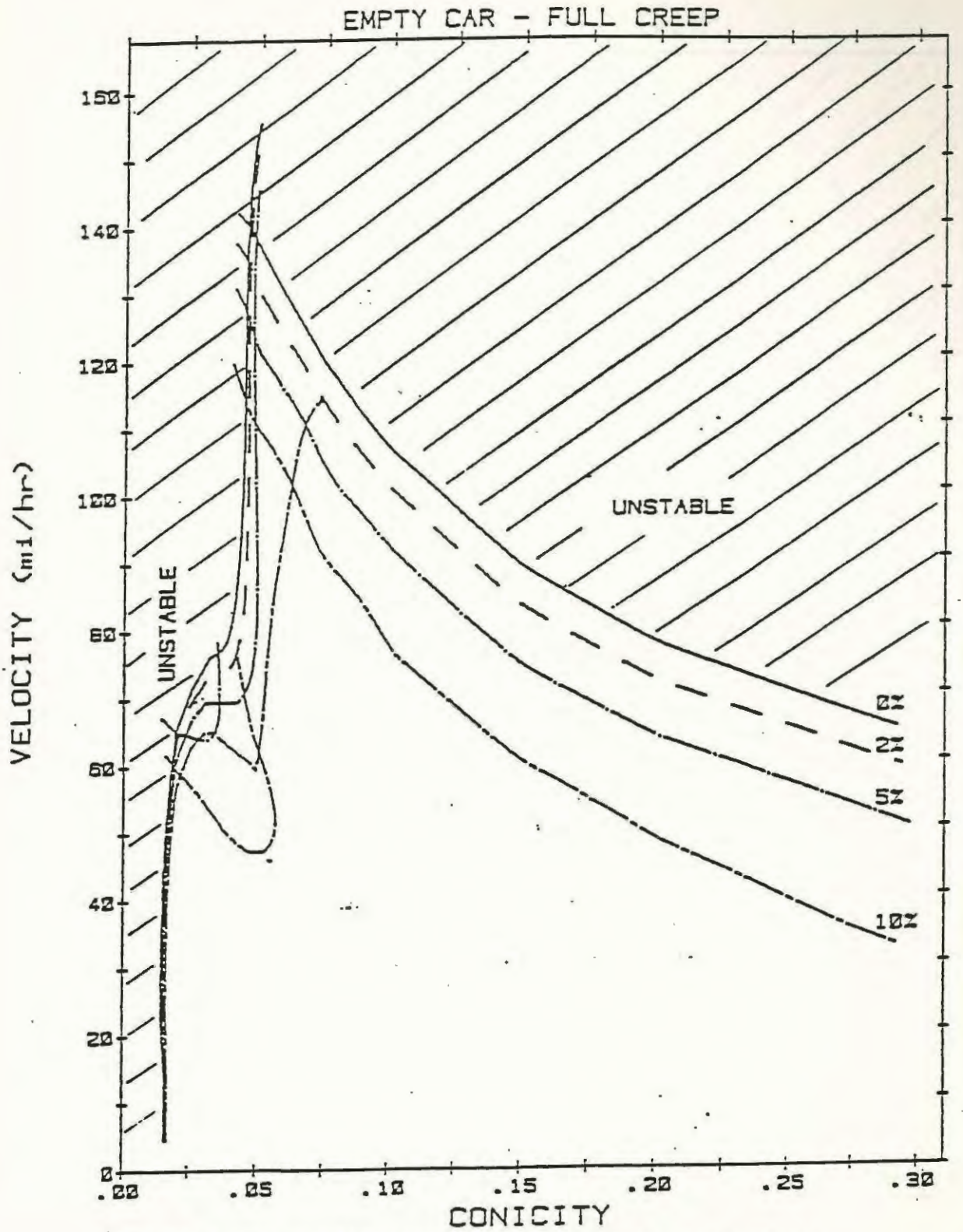

FIGURE 4.3-3 - STABILITY CHARACTERISTIC, FULL CREEP

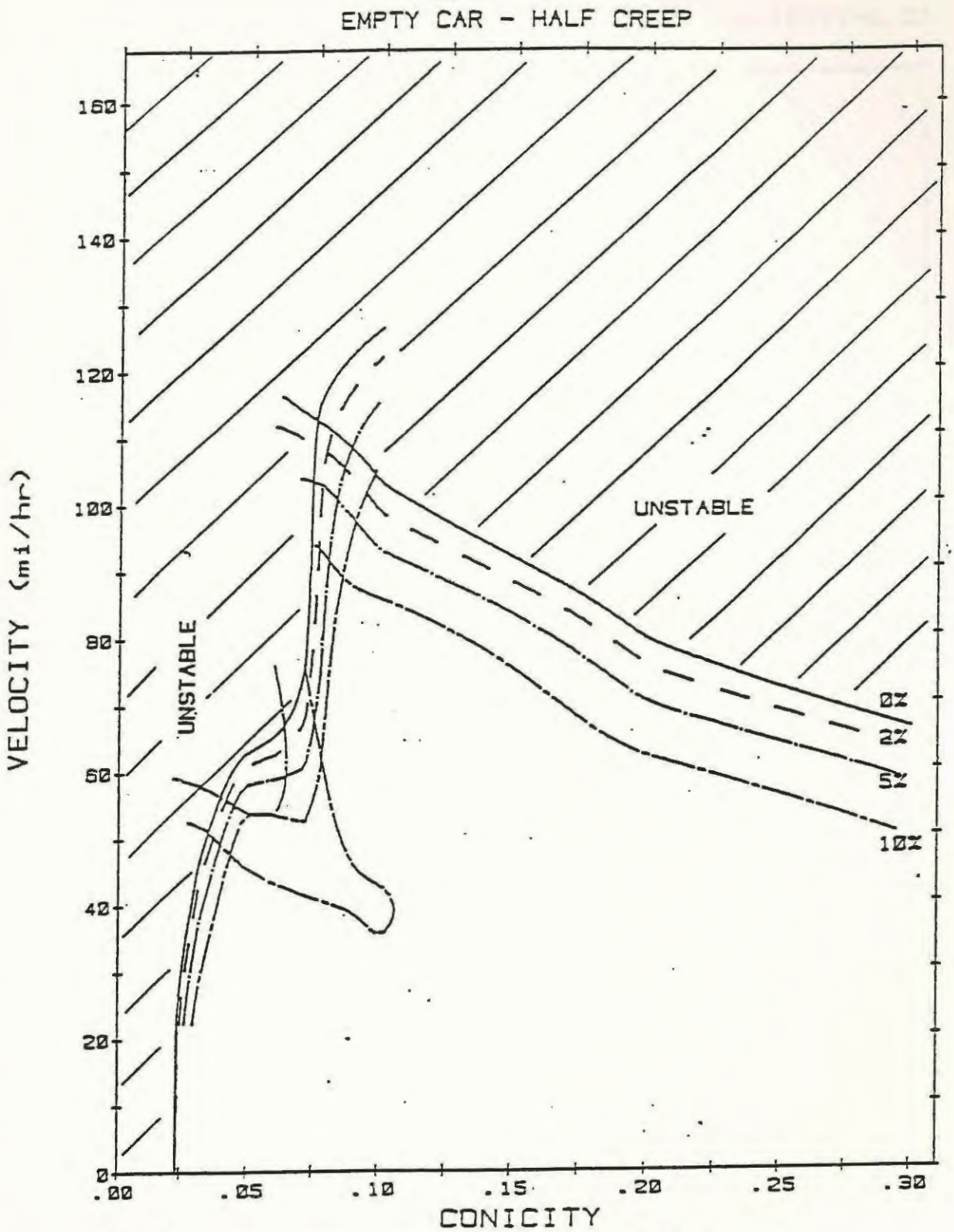

FIGURE 4.3-4 - STABILITY CHARACTERISTIC, HALF CREEP

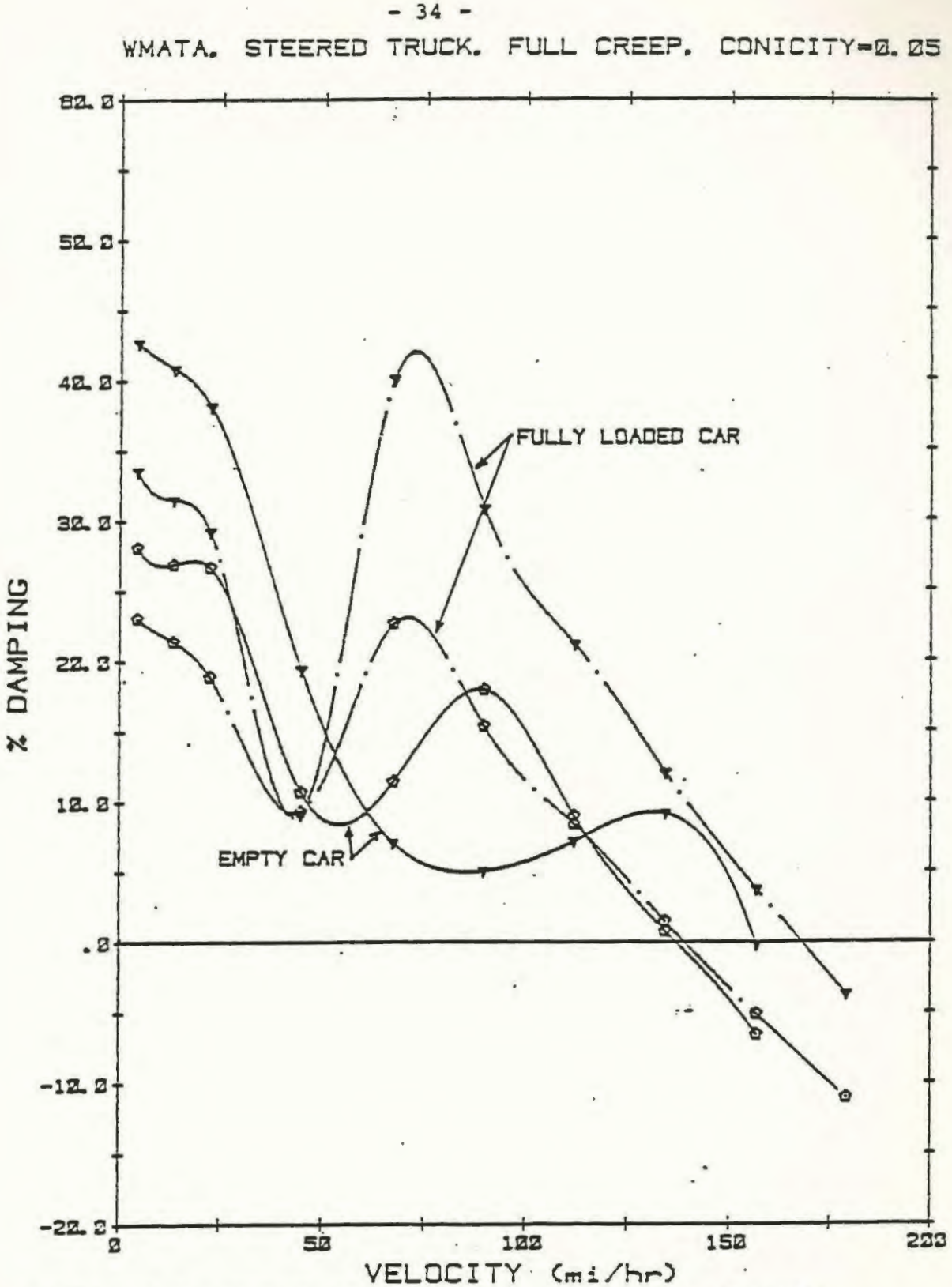

FIGURE 4.3-5 - EFFECT OF CAR LOADING ON DAMPING, CRITICAL MODES

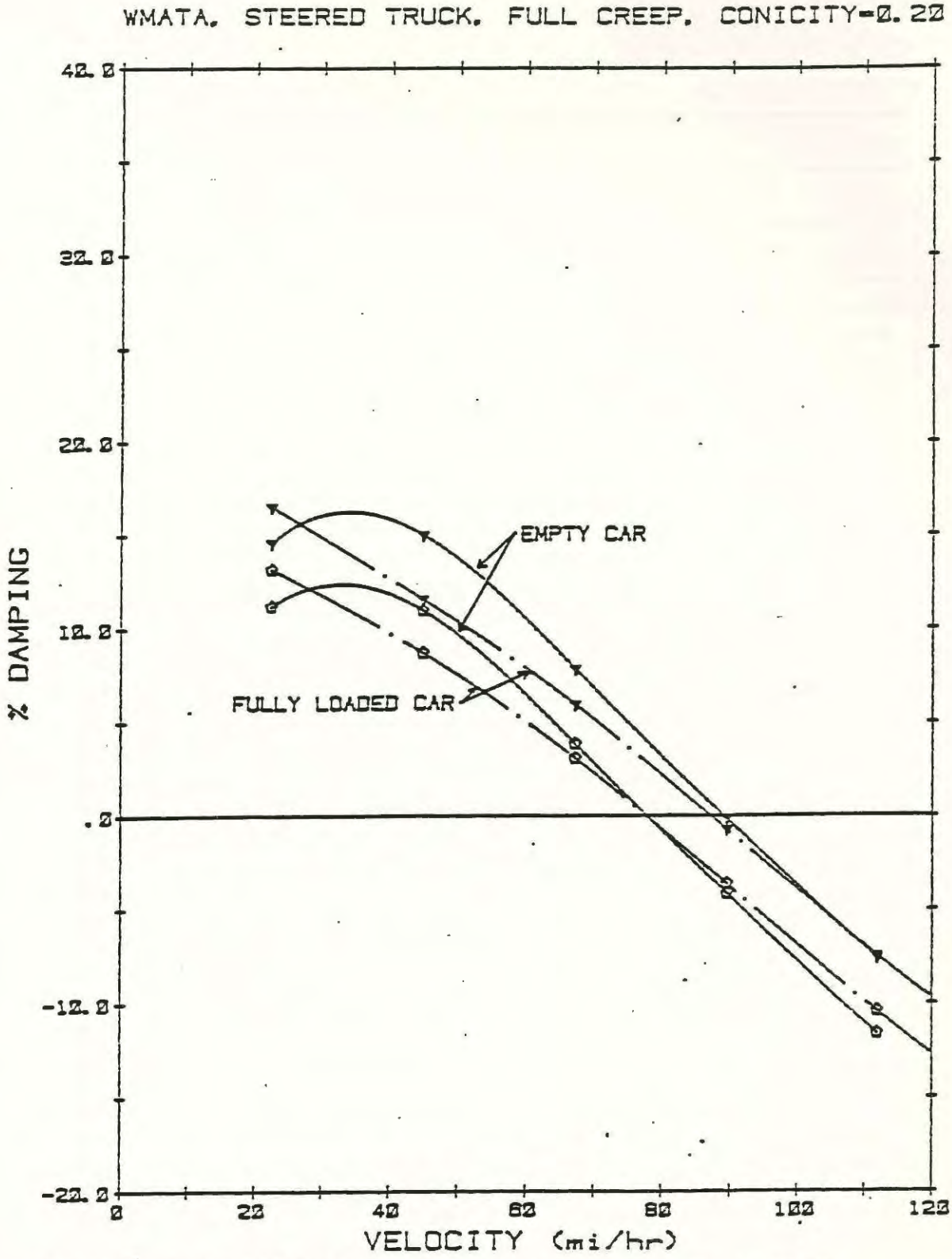

FIGURE 4.3-6 - EFFECT OF CAR LOADING ON DAMPING, CRITICAL MODES

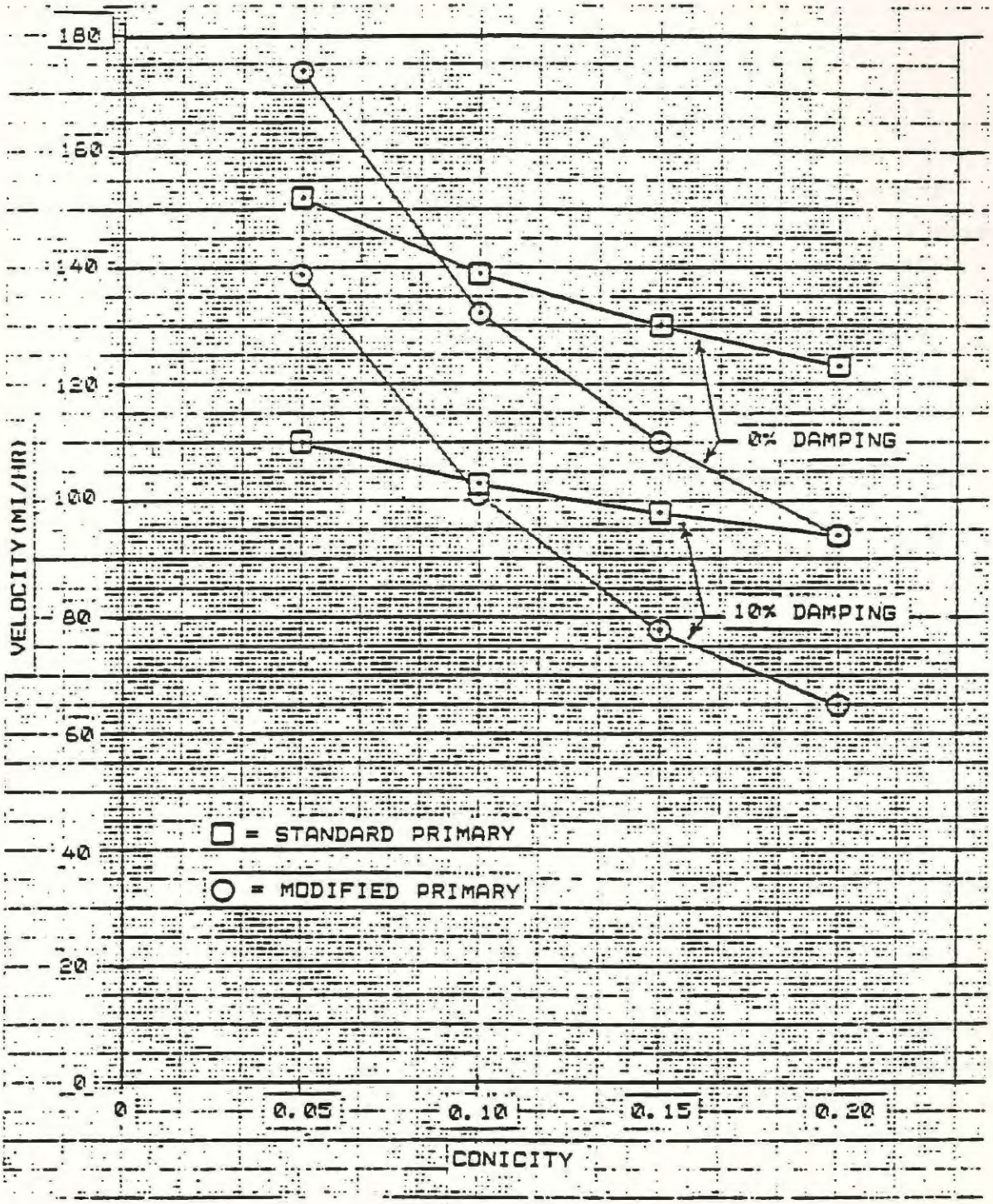

FIGURE 4.3.10-1 - COMPARISON OF VEHICLE STABILITY CHARACTERISTICS; STANDARD TO MODIFIED PRIMARY BUSHINGS

5.0 CURVING ANALYSIS

5.1 METHOD

5.1.1 Curving performance with both a steered and unsteered vehicle was examined using a computer simulation of each vehicle moving at constant speed on several constant radius curves (steady-state curve negotiation). The carbody and two trucks were modelled identically to the stability analysis (Figure 4.1-1), although viscous damping elements were not required for steady-state calculation. Using this multi degree-of-freedom model, the motions of the two trucks could be coupled, thus accounting for the transmission of wheel/rail interaction forces to the carbody through the steering linkage.

5.1.2 Inertial loads resulting from the curve negotiation were applied at the center of mass of each rigid body to represent the effect of mass distribution. The vehicle was moved in response to tread and flange forces arising from the wheel/rail interaction. A nonlinear formulation for creep forces was used, incorporating adhesion limits and flange contact. In each case, an overall force balance was obtained to predict angles of attack of each axle, lateral and longitudinal tread and flange forces on each wheel, positions of all rigid bodies and loads in each elastic element. The performance of both steered and unsteered vehicles was examined over a range of curve radii from 230 ft. to 3300 ft. This range embraces all curves representative of revenue track.

5.1.3 A direct comparison of curving performance was made between the steered and unsteered truck, each in its design condition. Flange clearance was taken to be 7/16 inch (11 mm), with the coefficient of adhesion held constant at 0.3. Wheel conicities of 0.05 and 0.20 were considered, with both an empty and fully loaded car.

5.1.4 In addition, as requested by H. Weinstock, the curving performance of the standard truck with modified axle bushings was calculated. The modified bushings showed an increase in vertical stiffness of 157%, a lateral stiffness decrease of 51% and a decrease in longitudinal stiffness to 25% of the standard bushing.

5.2 RESULTS AND DISCUSSION

5.2.1 The angle of attack of the leading axle (front truck) with respect to the track is shown in Figure 5.2-1, for a wheel conicity of 0.05. The large angles experienced by the unsteered truck are evident, particularly as the curve radius becomes smaller. The steered truck follows the track for curve radii above 1650 ft., and is understeered at lower radii by at most 0.15 degrees. Loading of the car has little effect on the unsteered truck but does induce a small degree of negative steering for the steered truck. For a wheel conicity of 0.20 (worn wheel), shown in Figure 5.2-2, the angles of attack for both the steered and unsteered trucks

become somewhat less, particularly as the curve radius increases. The steered truck follows the track for curve radii above 500 ft.

5.2.2 The average tread wear index for the front truck (4 wheels) is given in Figure 5.2-2, for a wheel conicity of 0.05. This index gives a measure of the work done per foot travelled against friction during sliding contact of the wheel treads with the rails. As indicated, the likely tread wear rate for the unsteered truck is more than two times that for the steered vehicle for all curve radii considered. Wear rate does increase in both cases, of course, as the vehicle is loaded. In Figure 5.2-4, the tread wear index is shown for a wheel conicity of 0.20. In this instance, the tread wear is about five times greater for the unsteered truck than for the steered truck at low curve radii. As curve radii increase, tread wear for the steered truck becomes negligible in comparison.

5.2.3 The average flange wear index for the front truck (2 axles) is shown in Figure 5.2-5, for a wheel conicity of 0.05. This index is used as an indicator of flange wear resulting from contact forces and slippage during flanging. Flange wear for the unsteered truck is substantially greater than that for the steered truck and increases the considerably as curve radius decreases. Flange wear for the steered truck remains almost constant for curve radii below 700 ft.

5.2.4 The curving behaviour of the trucks with the modified primary bushings is shown in Figures 5.2-11 to 5.2-20. These results were obtained using the modified bushing stiffness parameters, empty car (considered worst case), and wheel tread conicities of 0.05 (standard) and 0.2 (worn wheel).

5.2.5 In every case, the curving performance with the modified bushings was better than that with the standard units. At large curves in excess of 1,500 ft radius, the improvement in tread wear ranges from 22% with a 1:20 profile to more than 64% with a 1.5 profile. At the same time, the flange wear improvement ranges from near 9% using the 1.20 profile to 100% with the 1.5 profile. On curves of 500 ft and less, the difference between the standard primary performance and that of the modified bushings becomes less pronounced and in some cases the standard performs better.

5.2.6 When compared to the steerable truck, the effect on curving performance brought about by the modified bushings loses significance. The steered truck provides flange-free curving with a concity of 0.05 for all curve radii in excess of 1700 ft and with a coincity of 0.2 for all curves of radii in excess of 500 ft. The curving performance of the unsteered but modified truck approaches the steered only when the unsteered has the greater concity while the steered has the lesser.

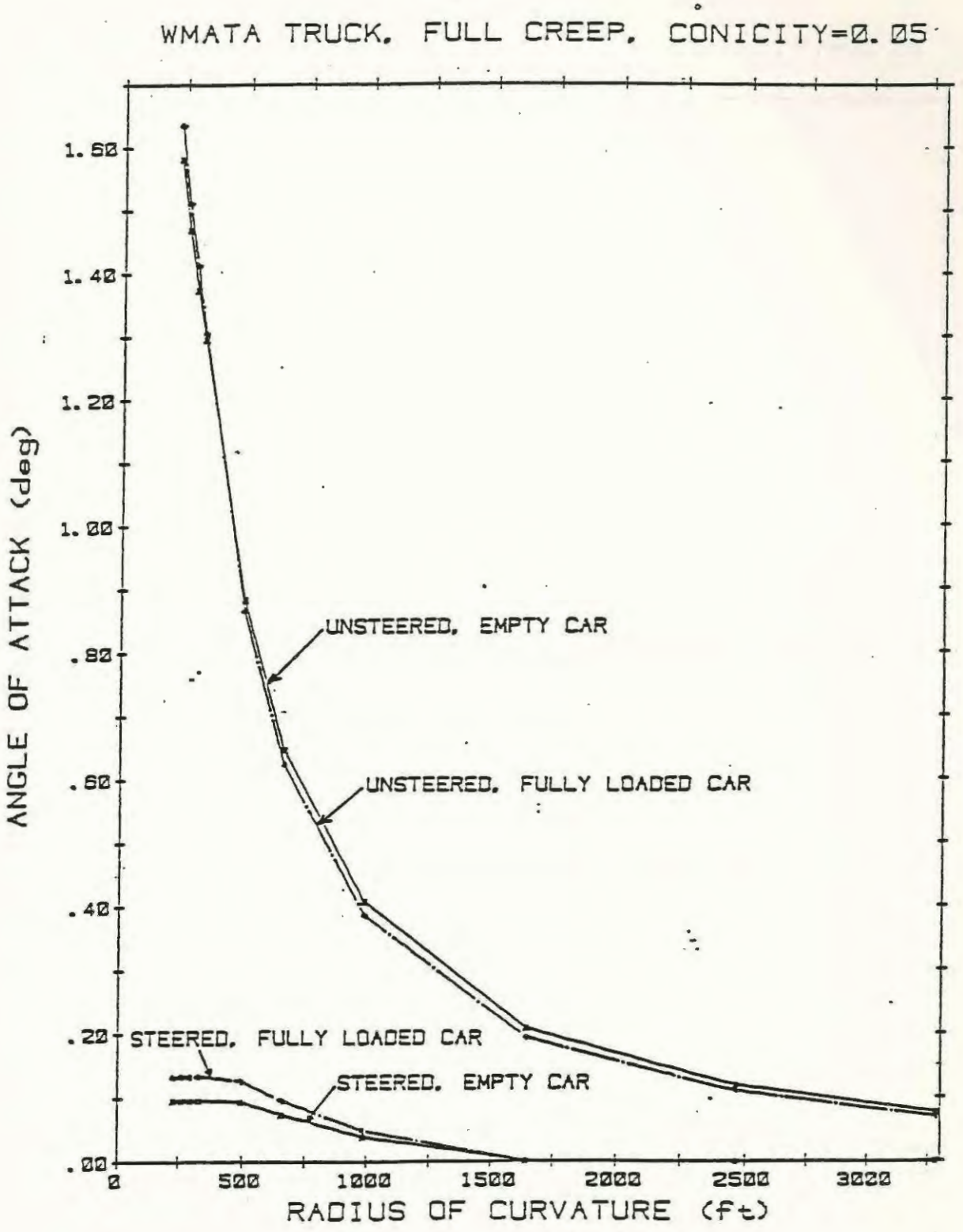

FIGURE 5.2-1 - ANGLE OF ATTACK, LEADING AXLE

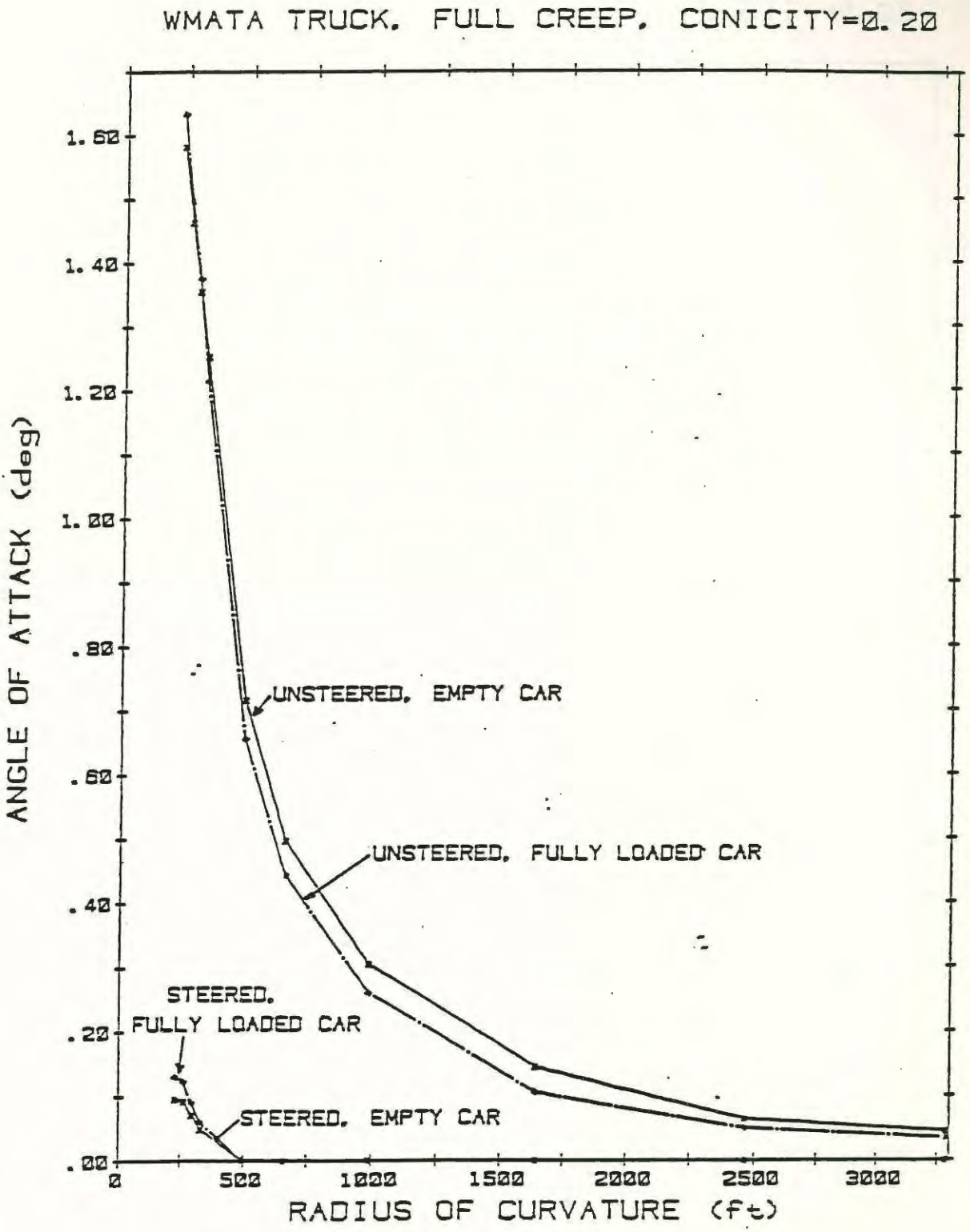

FIGURE 5.2-2 - ANGLE OF ATTACK, LEADING AXLE

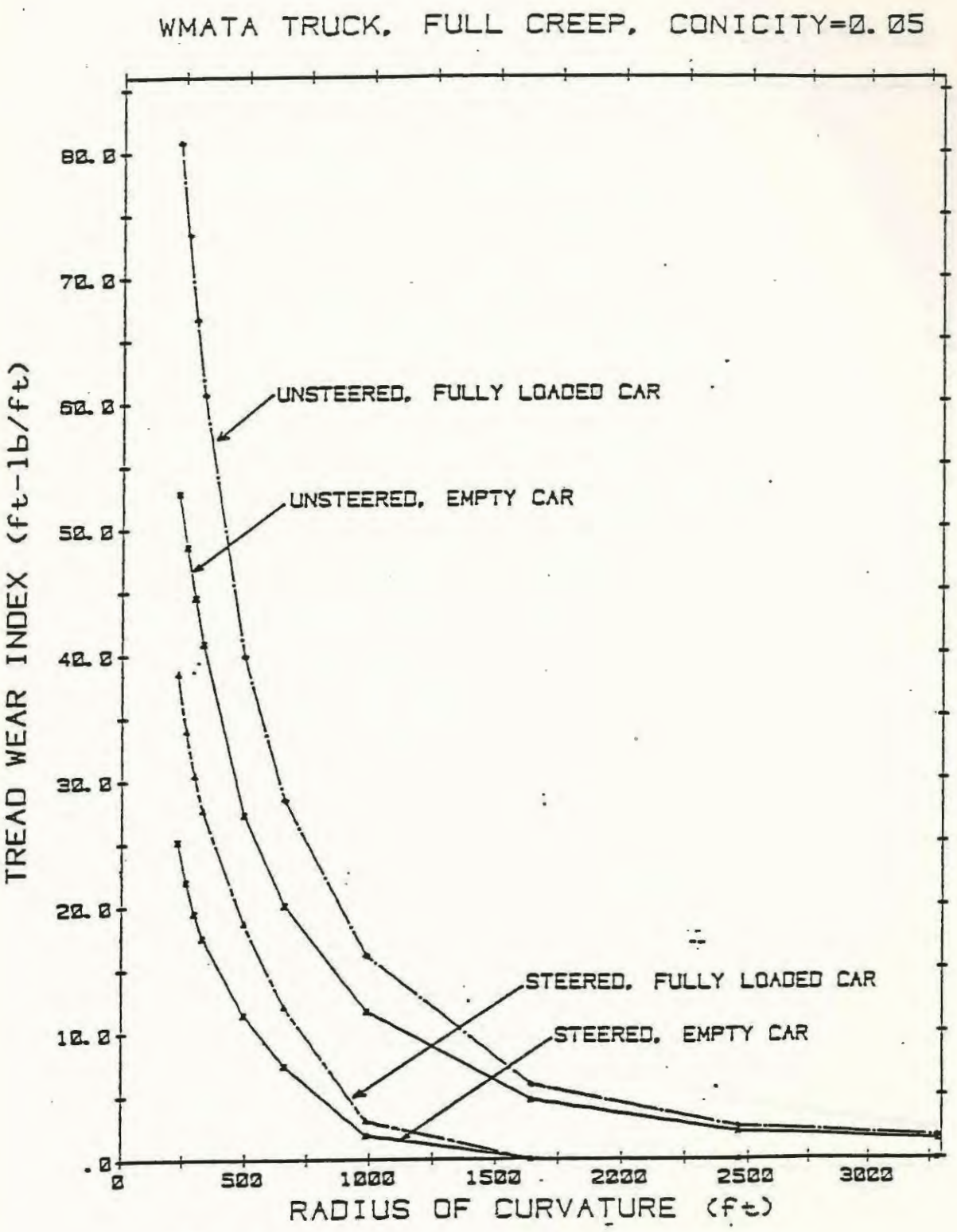

FIGURE 5.2-3 - TREAD WEAR INDEX, FRONT TRUCK

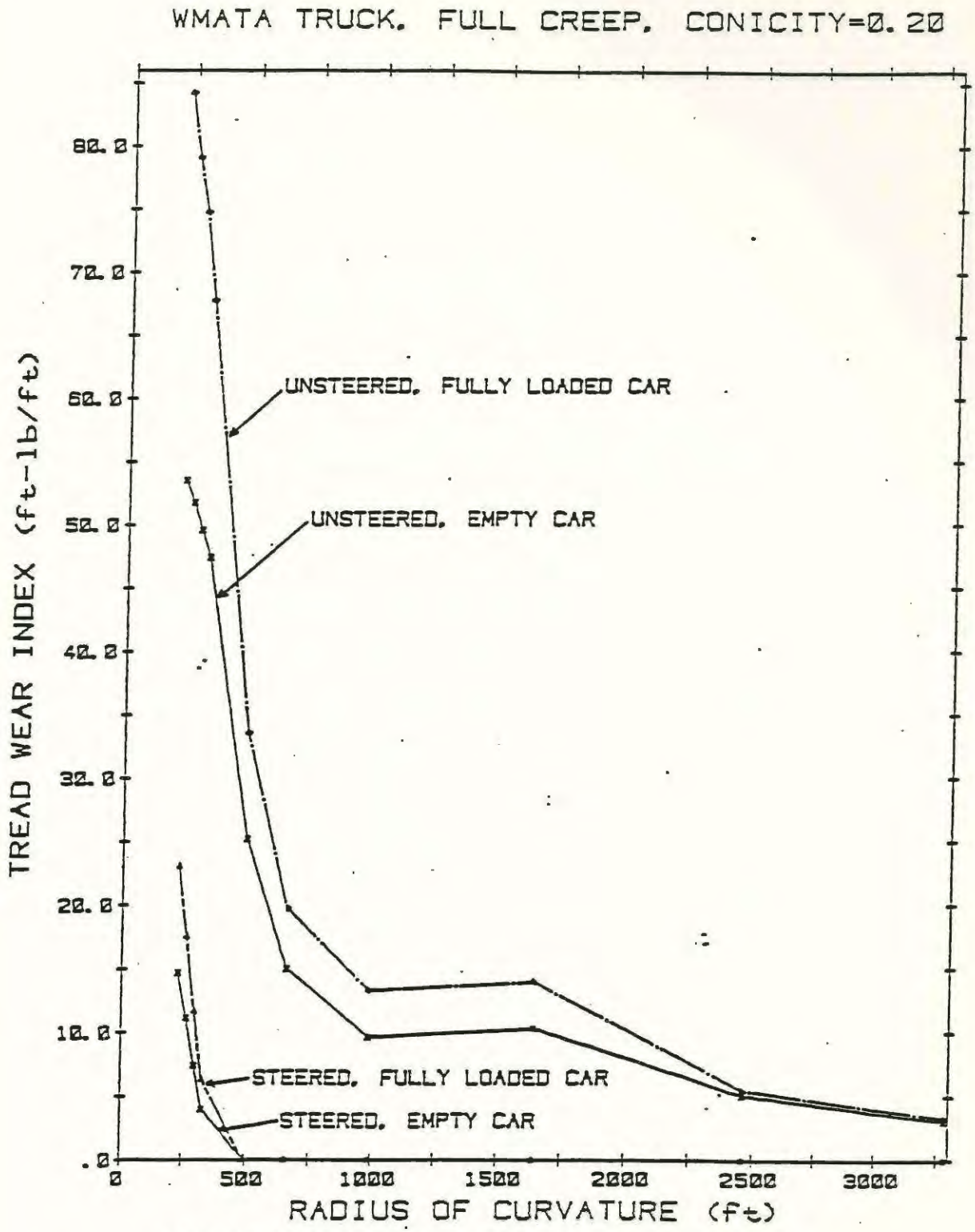

FIGURE 5.2-4 - TREAD WEAR INDEX, FRONT TRUCK

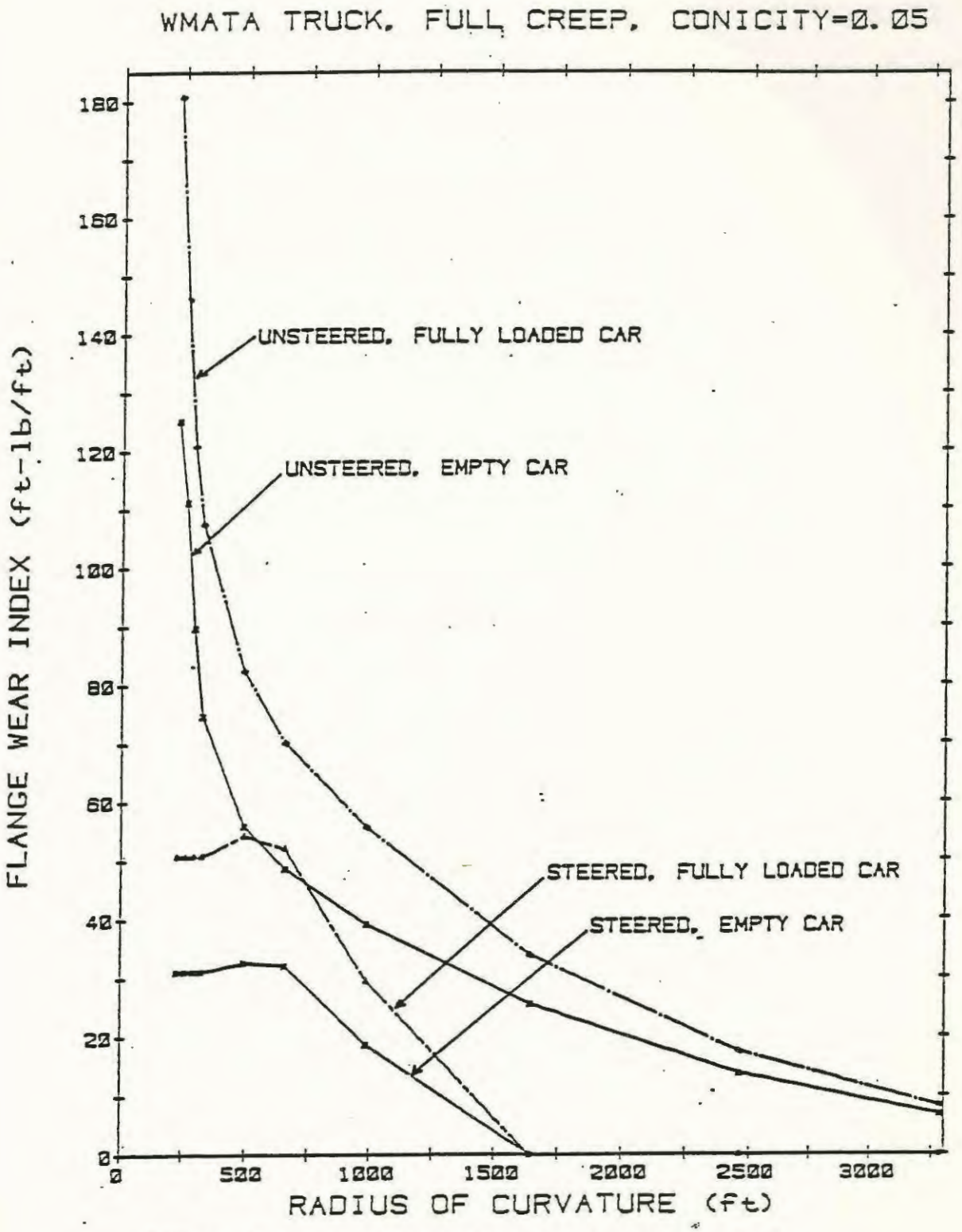

FIGURE 5.2-5 - FLANGE WEAR INDEX, FRONT TRUCK

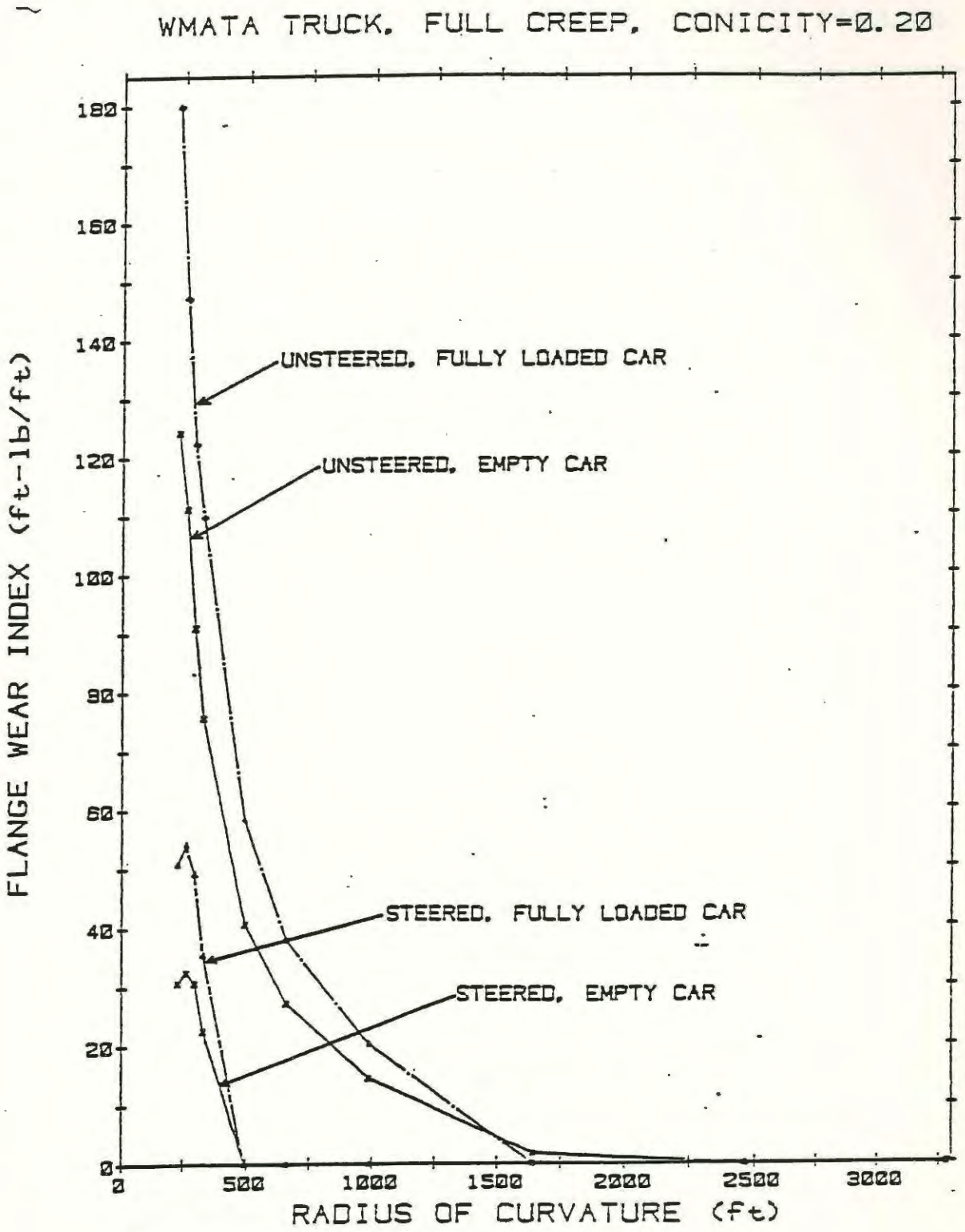

FIGURE 5.2-6 - FLANGE WEAR INDEX, FRONT TRUCK

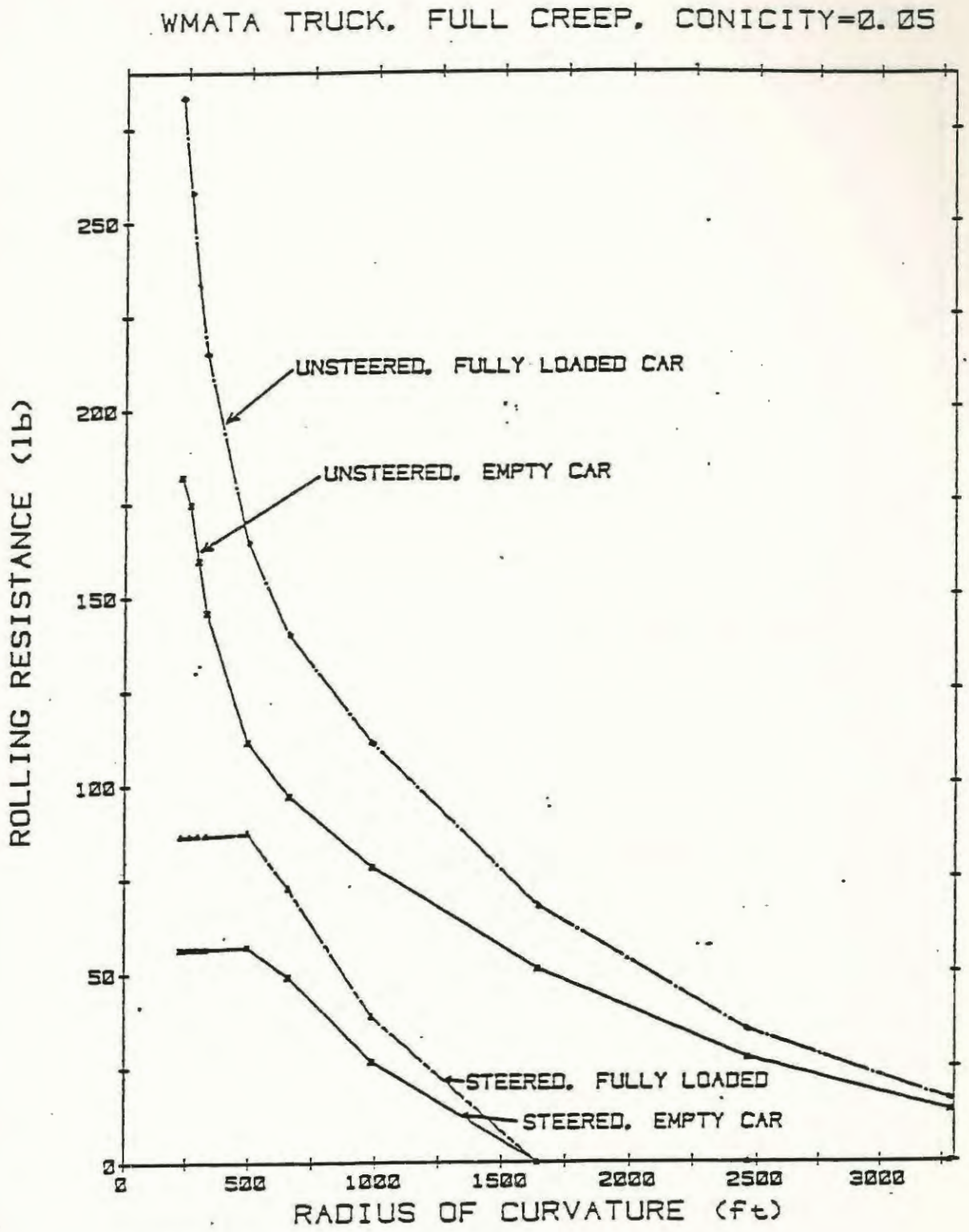

FIGURE 5.2-7 - ROLLING RESISTANCE, LEADING AXLE

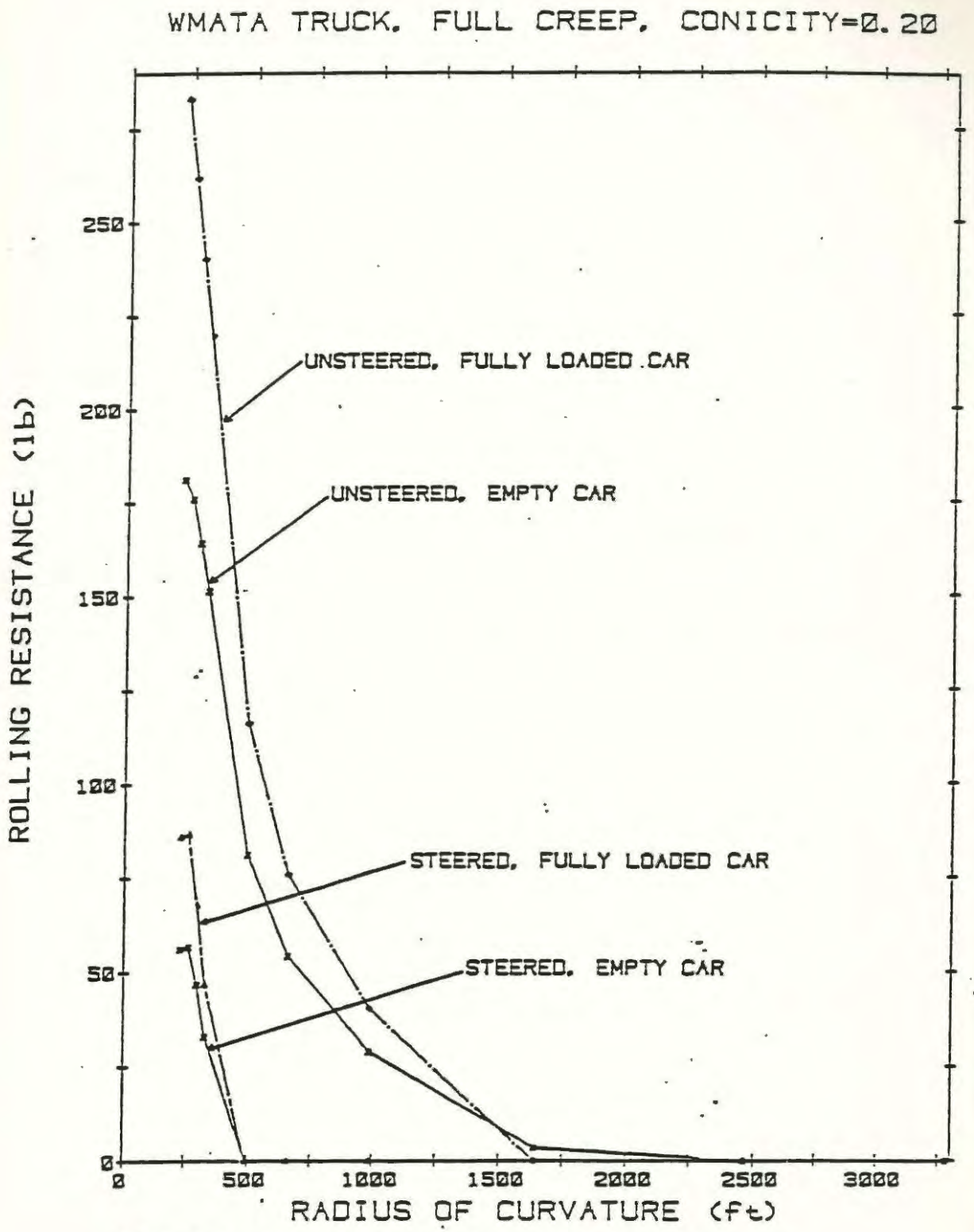

FIGURE 5.2-8 - ROLLING RESISTANCE, LEADING AXLE

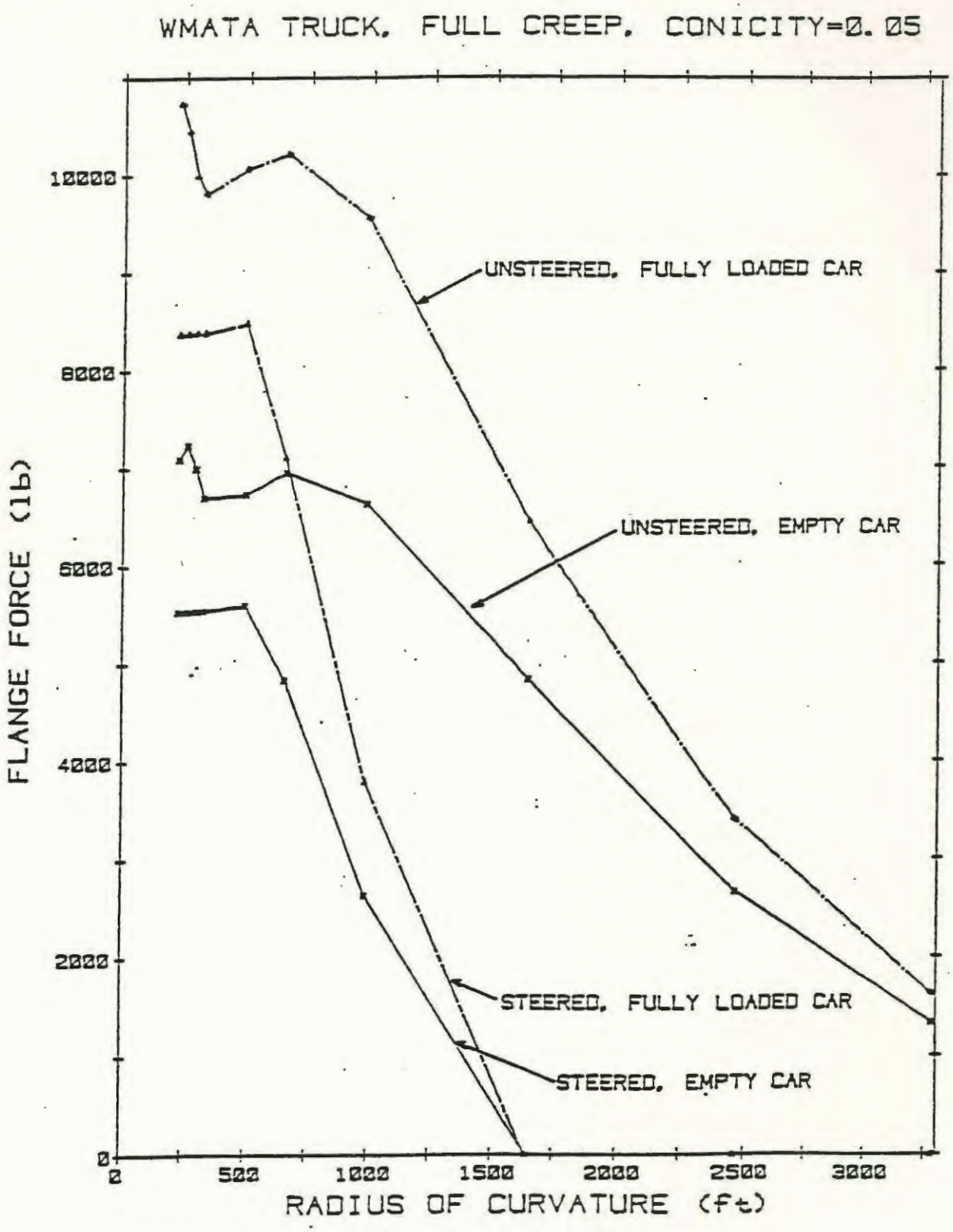

FIGURE 5.2-9 - FLANGE FORCE, LEADING AXLE

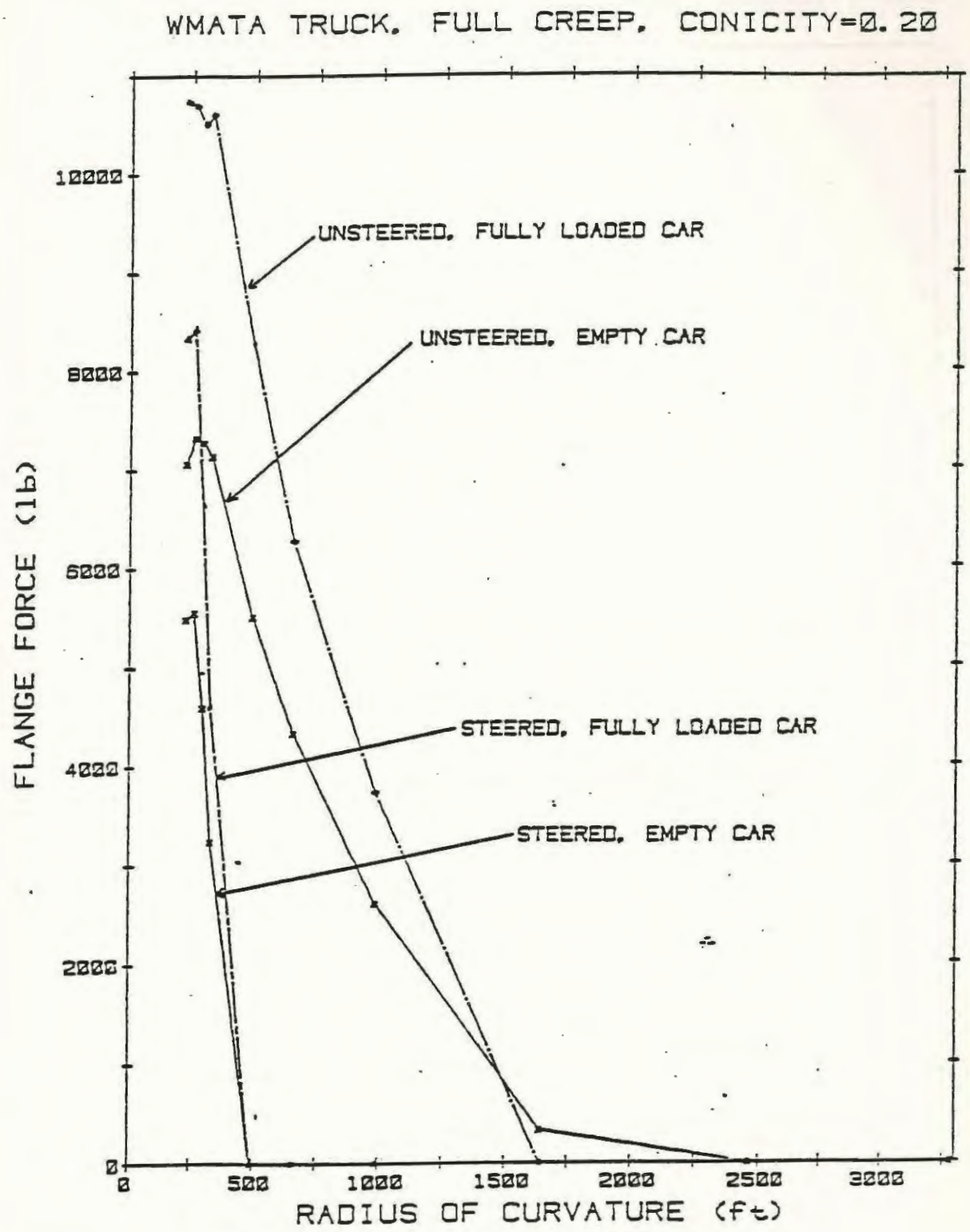

FIGURE 5.2-10 - FLANGE FORCE, LEADING AXLE

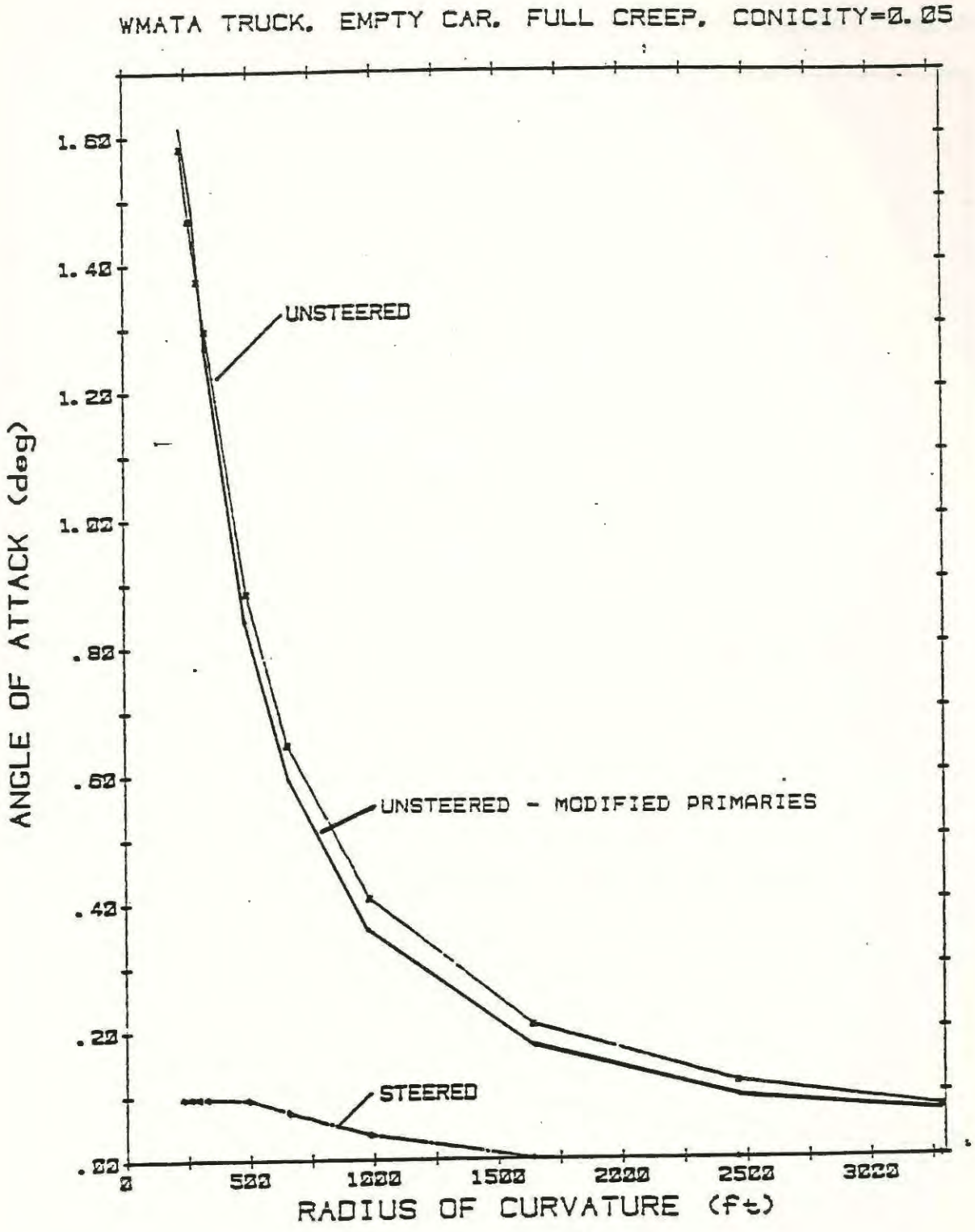

FIGURE 5.2-11 - ANGLE OF ATTACK, LEADING AXLE

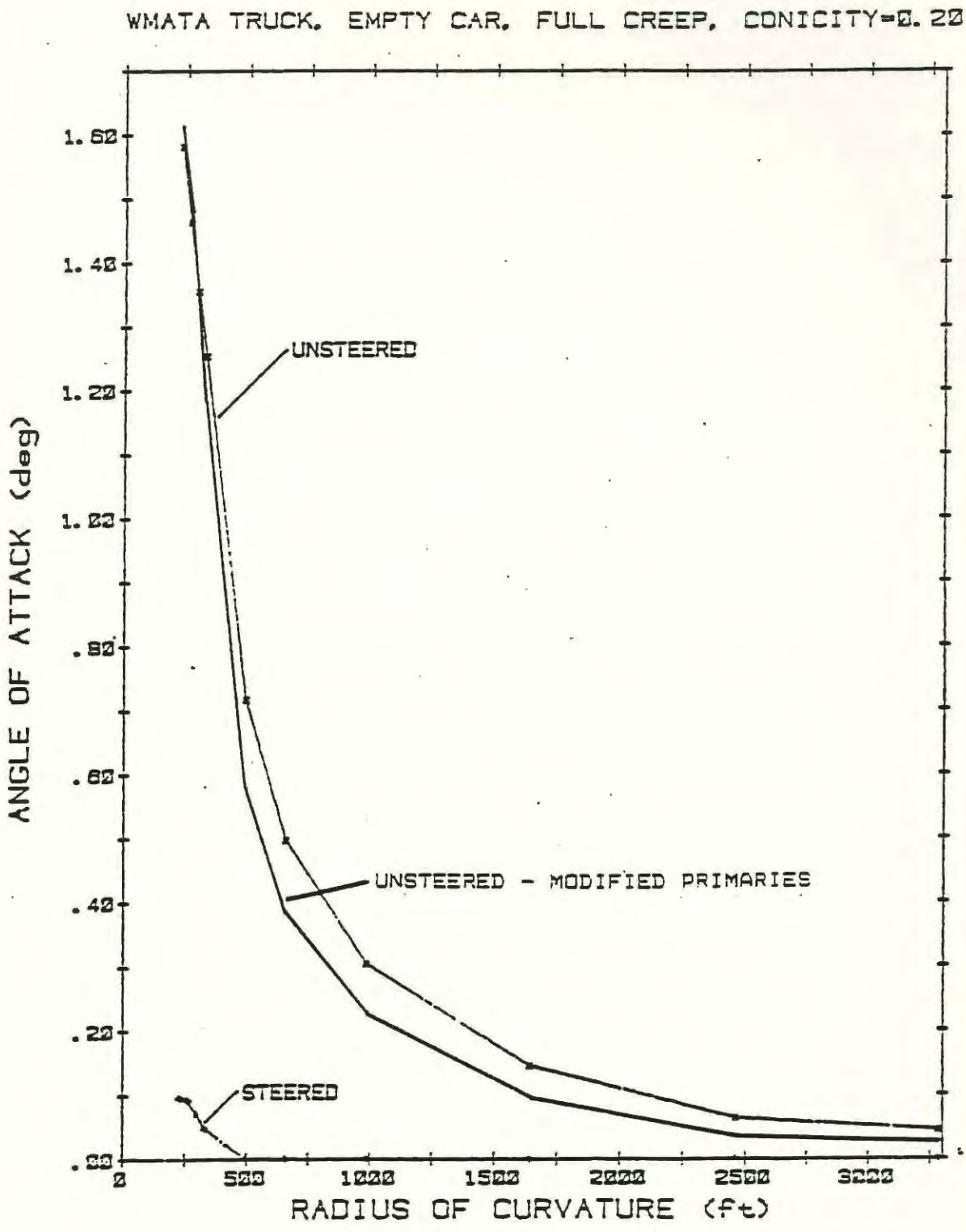

FIGURE 5.2-12 - ANGLE OF ATTACK, LEADING AXLE

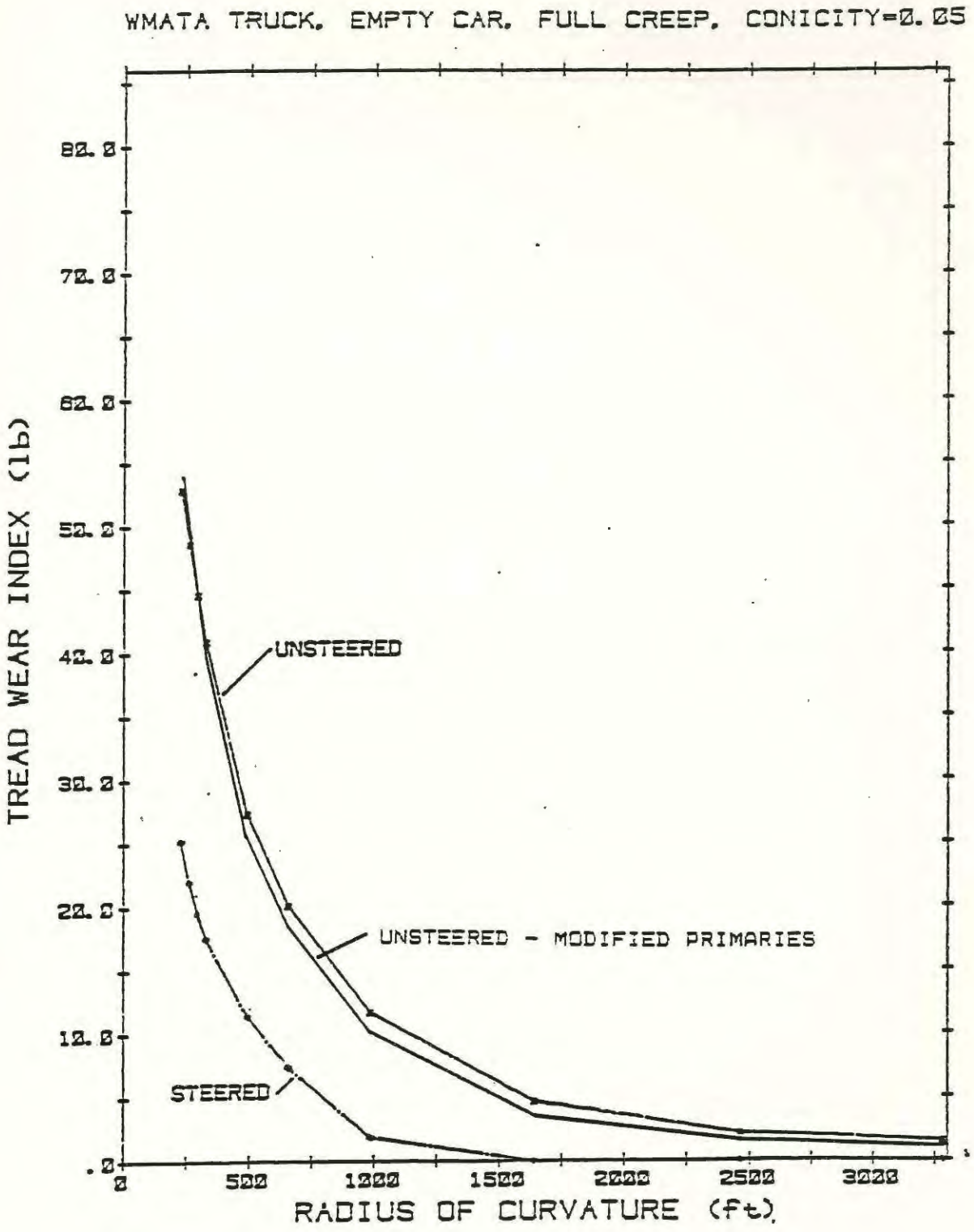

FIGURE 5.2.13 - TREAD WEAR VERSUS CURVE RADIUS

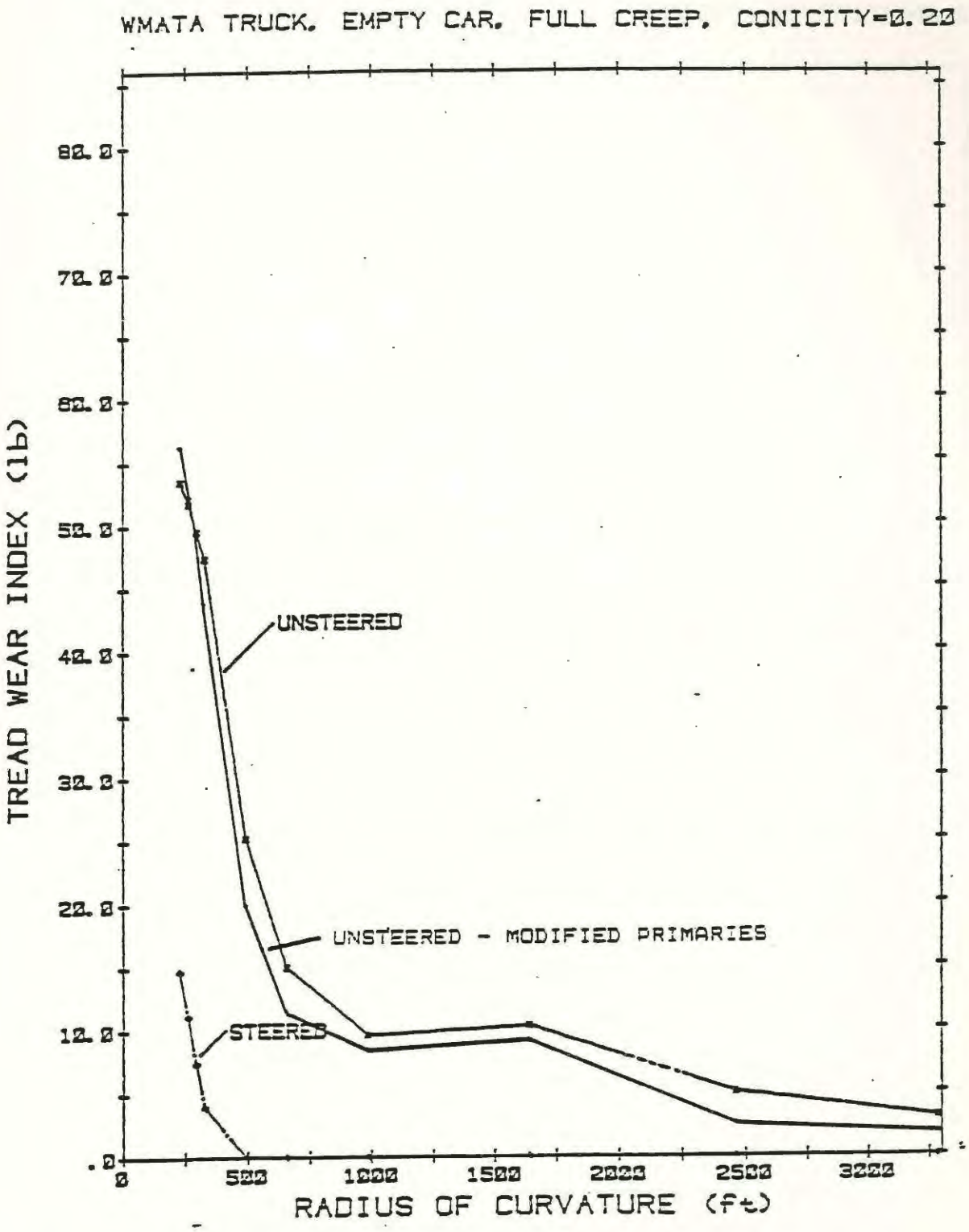

FIGURE 5.2-14 - TREAD WEAR VERSUS CURVE RADIUS

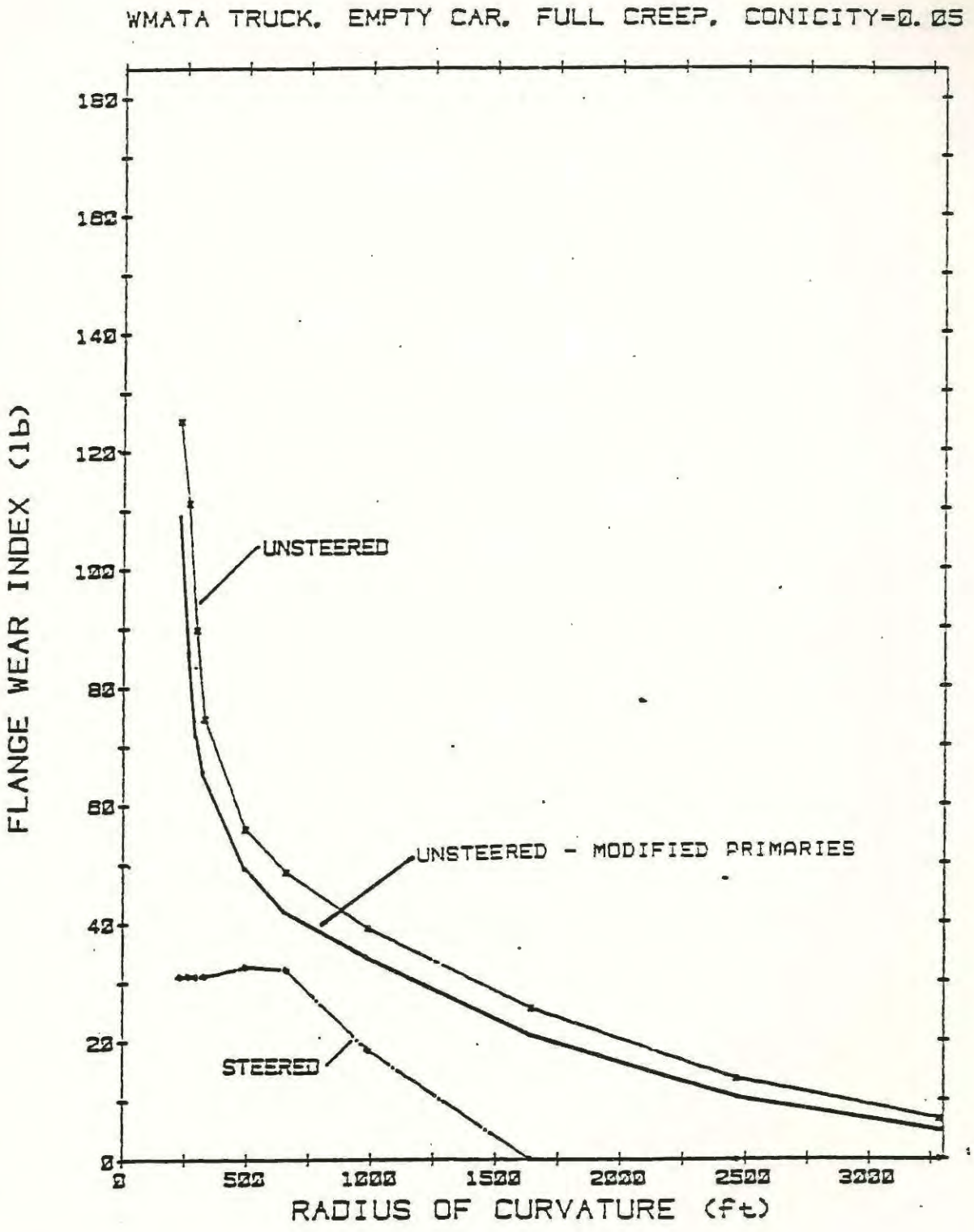

FIGURE 5.2-15 - FLANGE WEAR VERSUS CURVE RADIUS

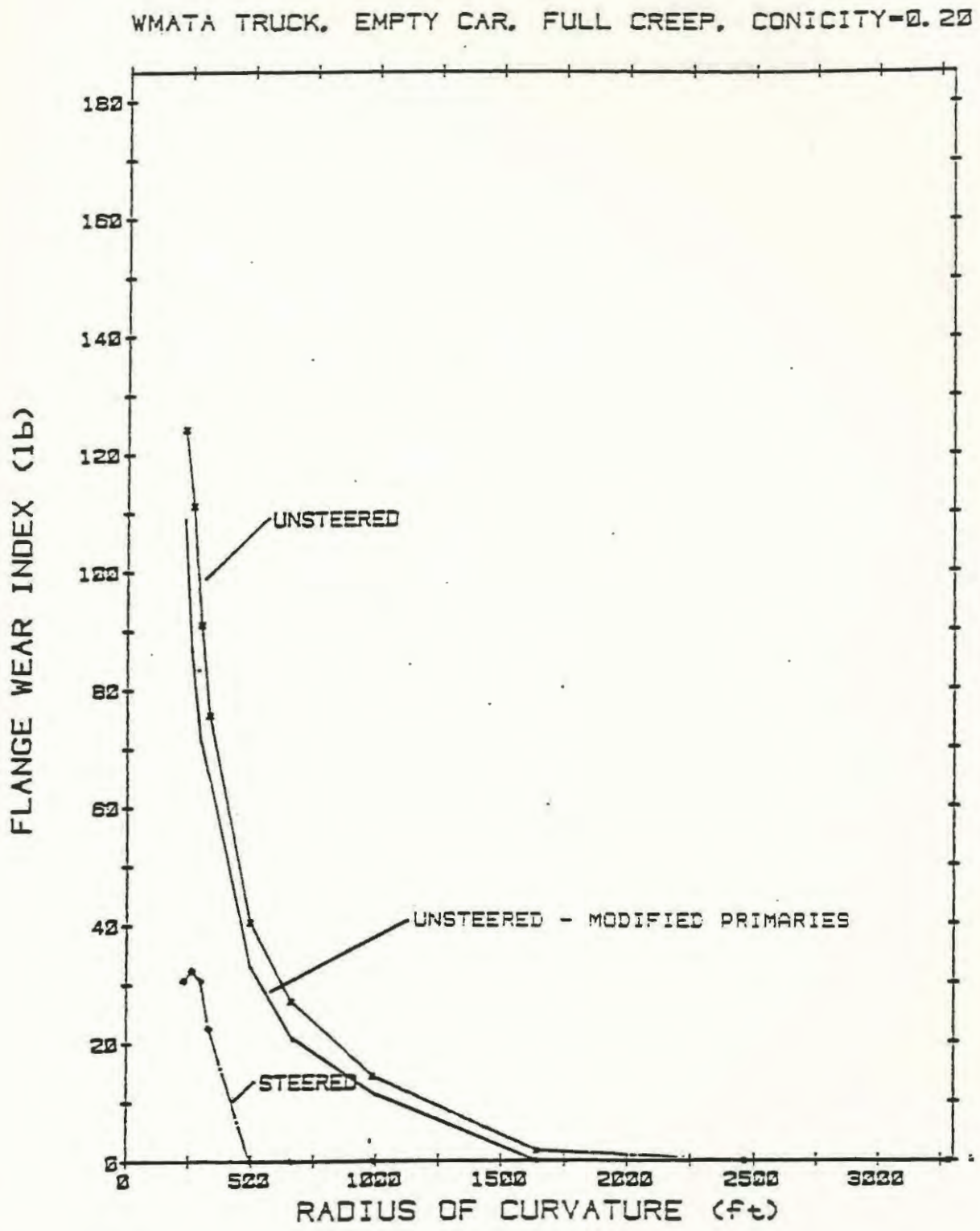

FIGURE 5.2-16 - FLANGE WEAR VERSUS CURVE RADIUS

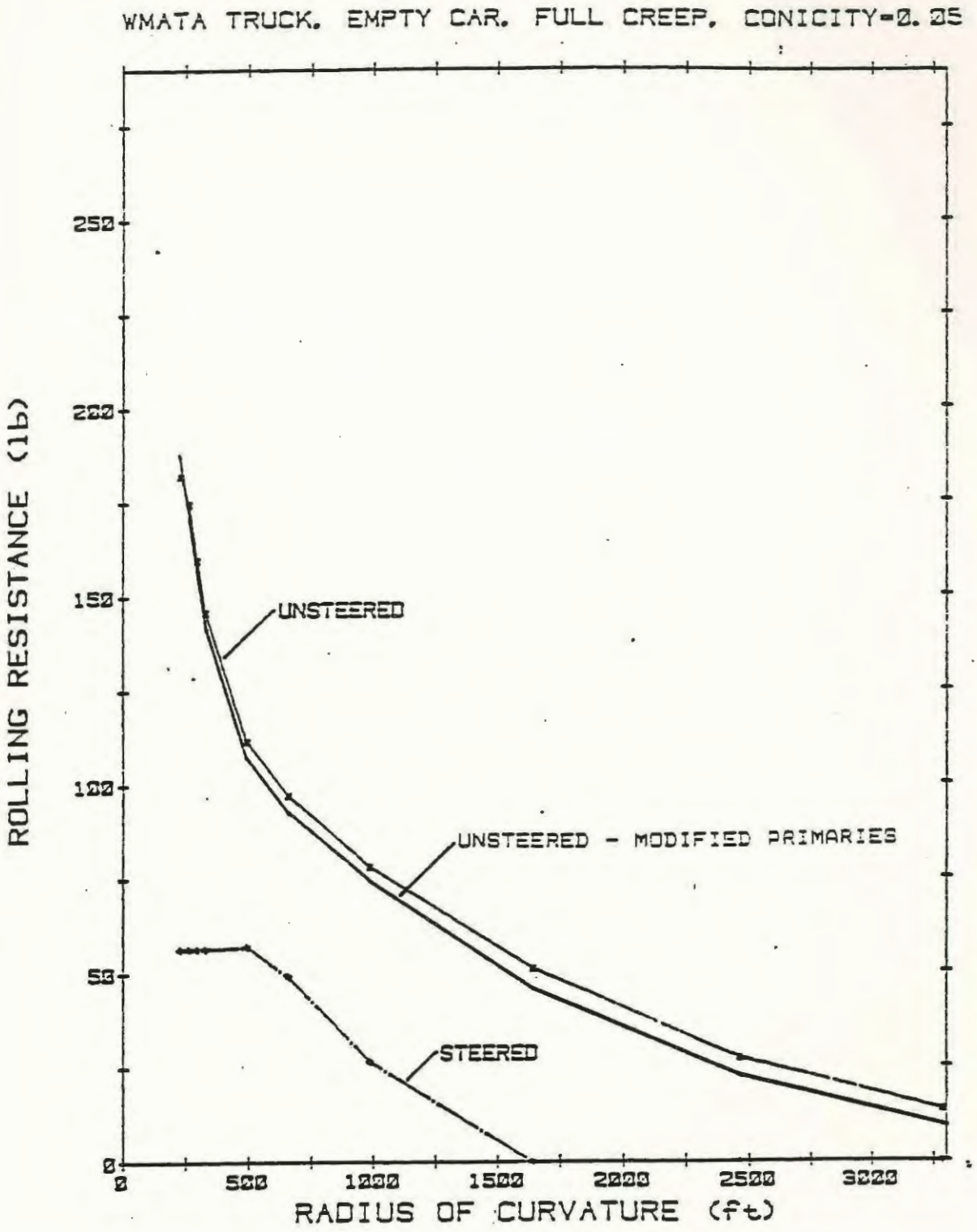

FIGURE 5.2-17 - ROLLING RESISTANCE VERSUS CURVE RADIUS

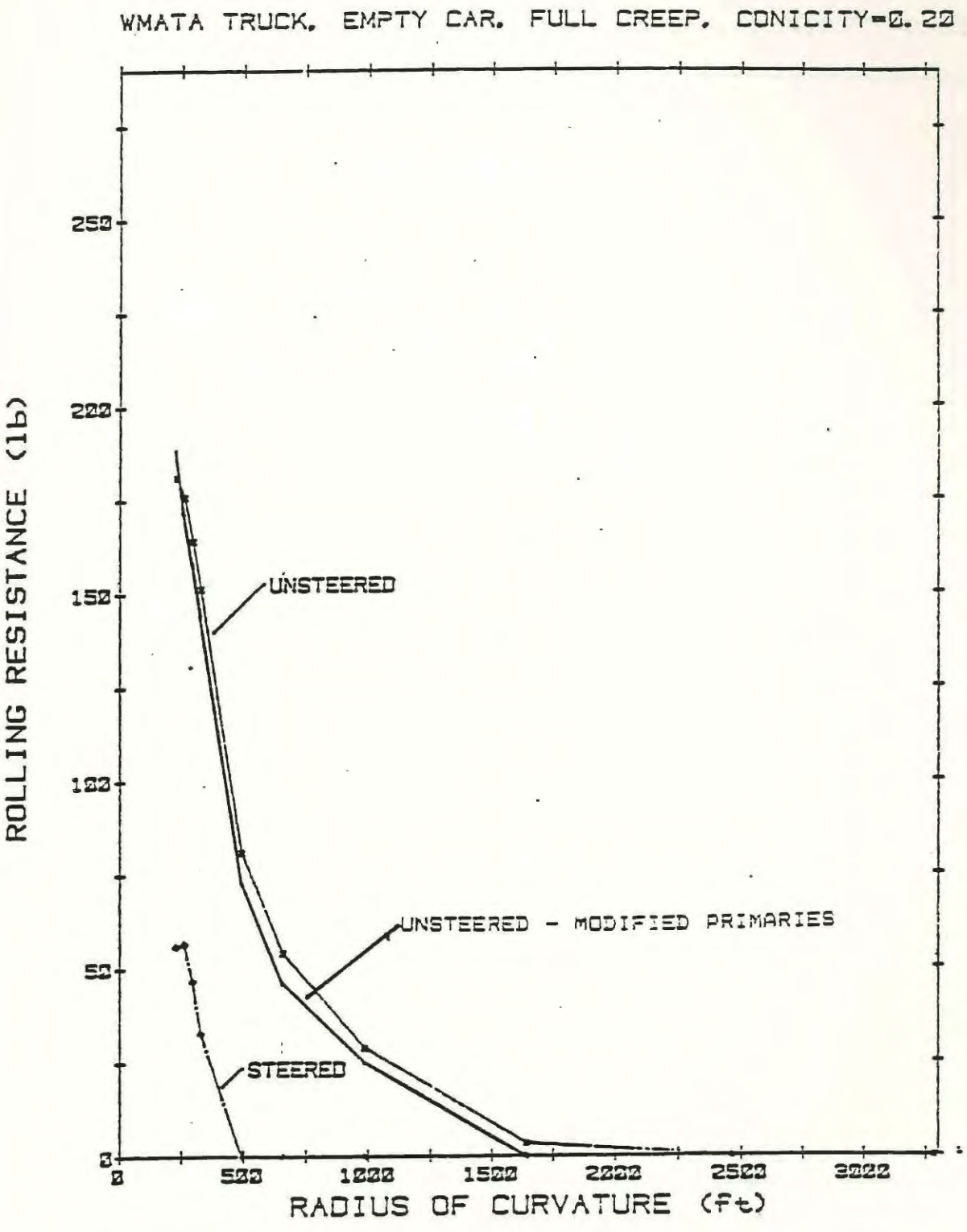

FIGURE 5.2-18 - ROLLING RESISTANCE VERSUS CURVE RADIUS

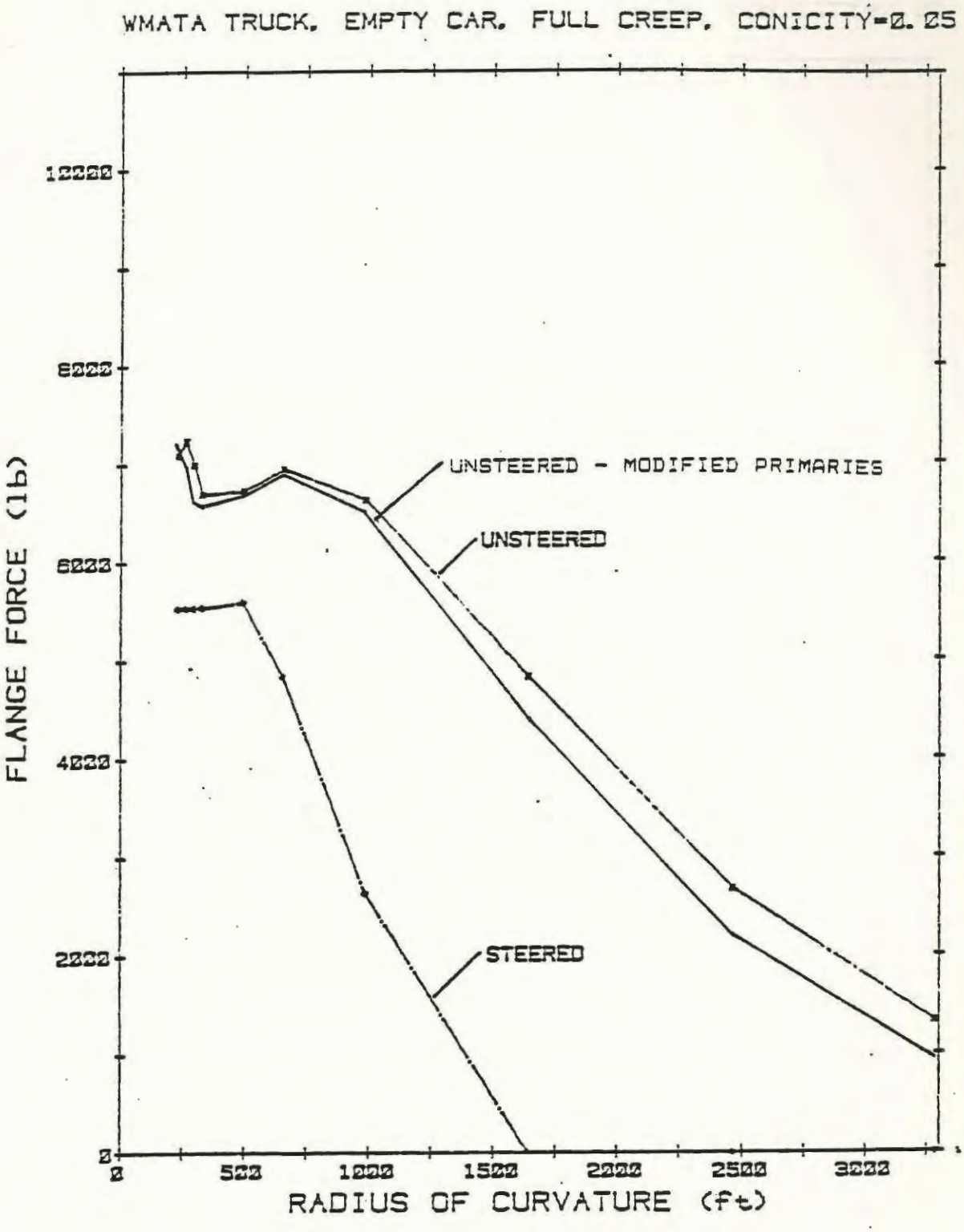

FIGURE 5.2-19 - FLANGE FORCE VERSUS CURVE RADIUS

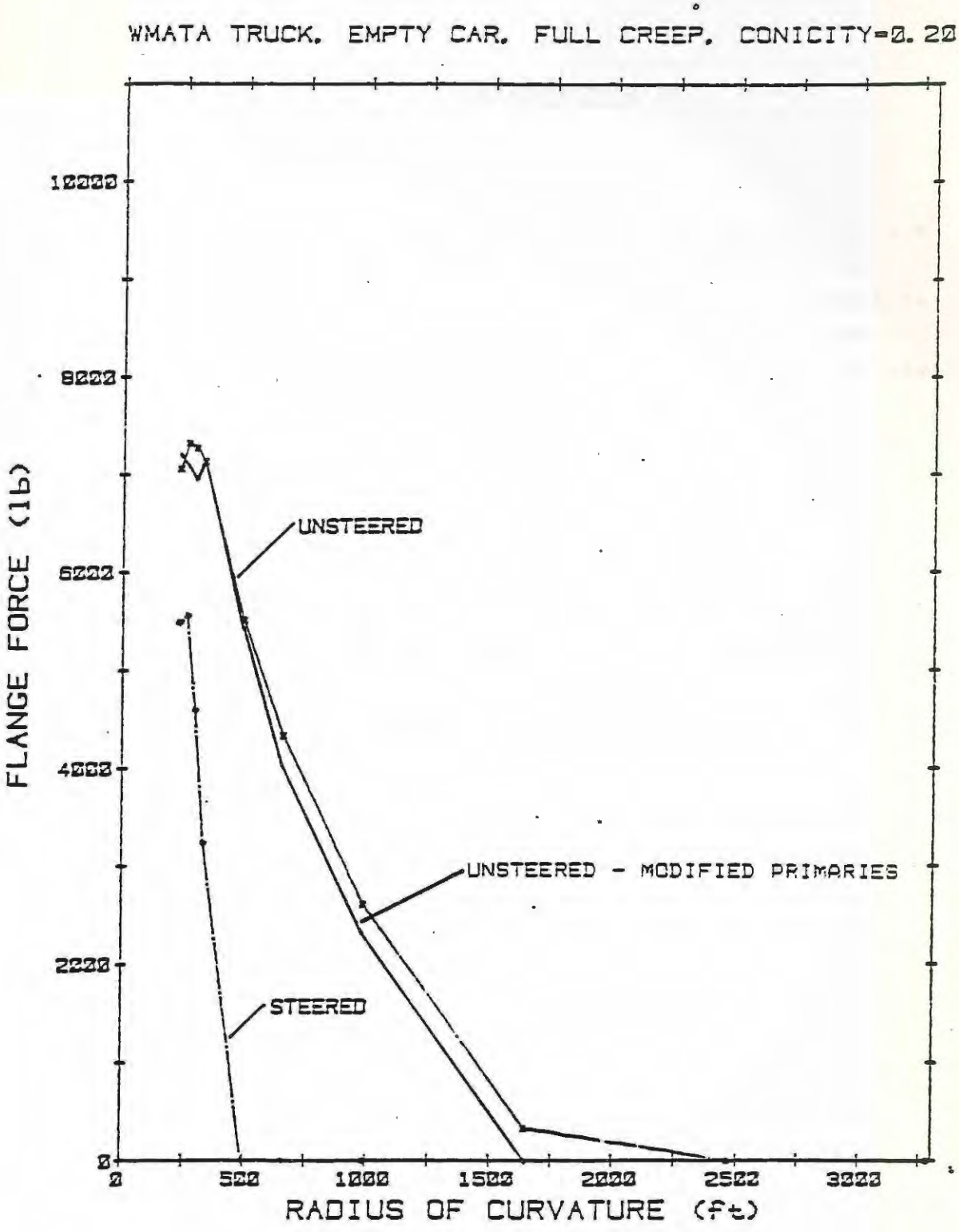

FIGURE 5.2-20 - FLANGE FORCE VERSUS CURVE RADIUS

6.0 FINITE ELEMENT STRESS ANALYSIS

6.1 INTRODUCTION

6.1.1 The finite element stress analysis was carried out on the WMATA Rockwell truck sideframe with the proposed steering retrofit. The primary objective was to determine the principal stresses in the sideframe produced by various wheel loads. It was also required to determine the axle stresses, steering link forces, deflections of the various components, and in the event that any of those results exceeded normal rail engineering practices, to recommend corrective measures.

6.1.2 Based on the results of the first analysis, two more were carried out incorporating the proposed corrective measures. A complete set of the reports appears as Appendix C.

6.2 METHOD

6.2.1 The initial model consisted of the following interconnected components:

a) sideframe (steering link side);

b) journal housing;

c) top support;

d) steering linkage;

e) primary springs;

f) journal housing (non-steering side);

g) primary spring; and

h) axle.

6.2.2 Four load cases were examined as follows:

a) load case 1;

i) vertically equivalent to loaded car,

ii) longitudinally equivalent to maximum braking force, and

iii) laterally equivalent to 0.13 lateral acceleration of the vehicles in a left curve.

b) load case 2 - braking only;

c) load case 3 - laterally only; and

d) load case 4 - vertically only.

6.2.3 The load cases were rerun after a sideframe reinforcement was designed and modelled.

6.2.4 The load cases were rerun for a change in primary spring pad orientation.

6.3 RESULTS

6.3.1 The maximum stress in the sideframe was found at the underside of the arch, as shown in Figure 6.3-1. Its value was 46,400 psi from load case 1. At the same time, the maximum deflection of the sideframe occurred at the extreme end, quantitatively 0.065 in (Figure 6.3-2).

6.3.2 The maximum force in the steering linkage results from load case 2 (braking) of magnitude 234 lb.

6.3.3 For the axle, the maximum vertical deflection was found to be 0.17 in. at the steered side. The maximum bending stress was 6,740 psi (all results from load case 1).

6.3.4 As a result of the high stress (46,400 psi) in the sideframe, the reinforcing cap (Figure 6.3-3) was designed and the analysis repeated. THe results showed a signiticant decrease in the stresses at the sideframe arch but high forces were found at the primary pads and pad supports. In essence the stresses had moved to the end of the arch as a result of the reinforcement (Figure 6.3-4).

6.3.5 As a result of the high forces on the primary pads, the pad orientation was changed and the cases rerun. The results showed that although the forces were reduced, no significant changes were experienced in the magnitude of the stresses. The analysis were terminated.

6.4 DISCUSSION

6.4.1 This analysis showed high stress concentrations in areas of the sideframe never designed to sustain them. The loads that produced those stresses were, from experience, typical and reasonable for normal track operations.

6.4.2 It can be seen, from the results, that the addition of the reinforcing cap moves the stress concentrations and ultimately, with further design work, should reduce the stresses to acceptable levels. The cost of this addition is estimated to be 400-600 pounds per truck in additional weight.

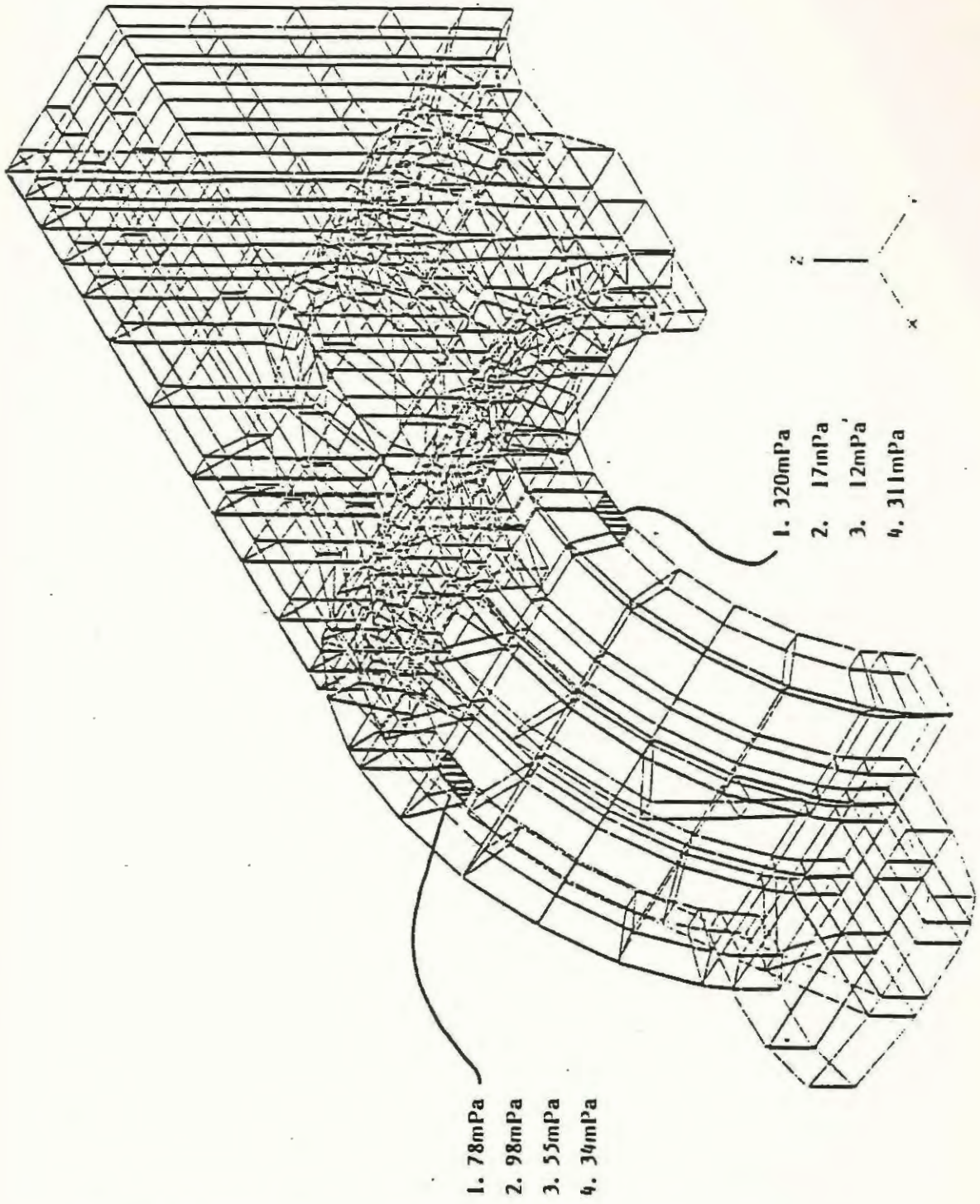

FIGURE 6.3-1 - MAXIMUM STRESS LOCATIONS - SIDEFRAME

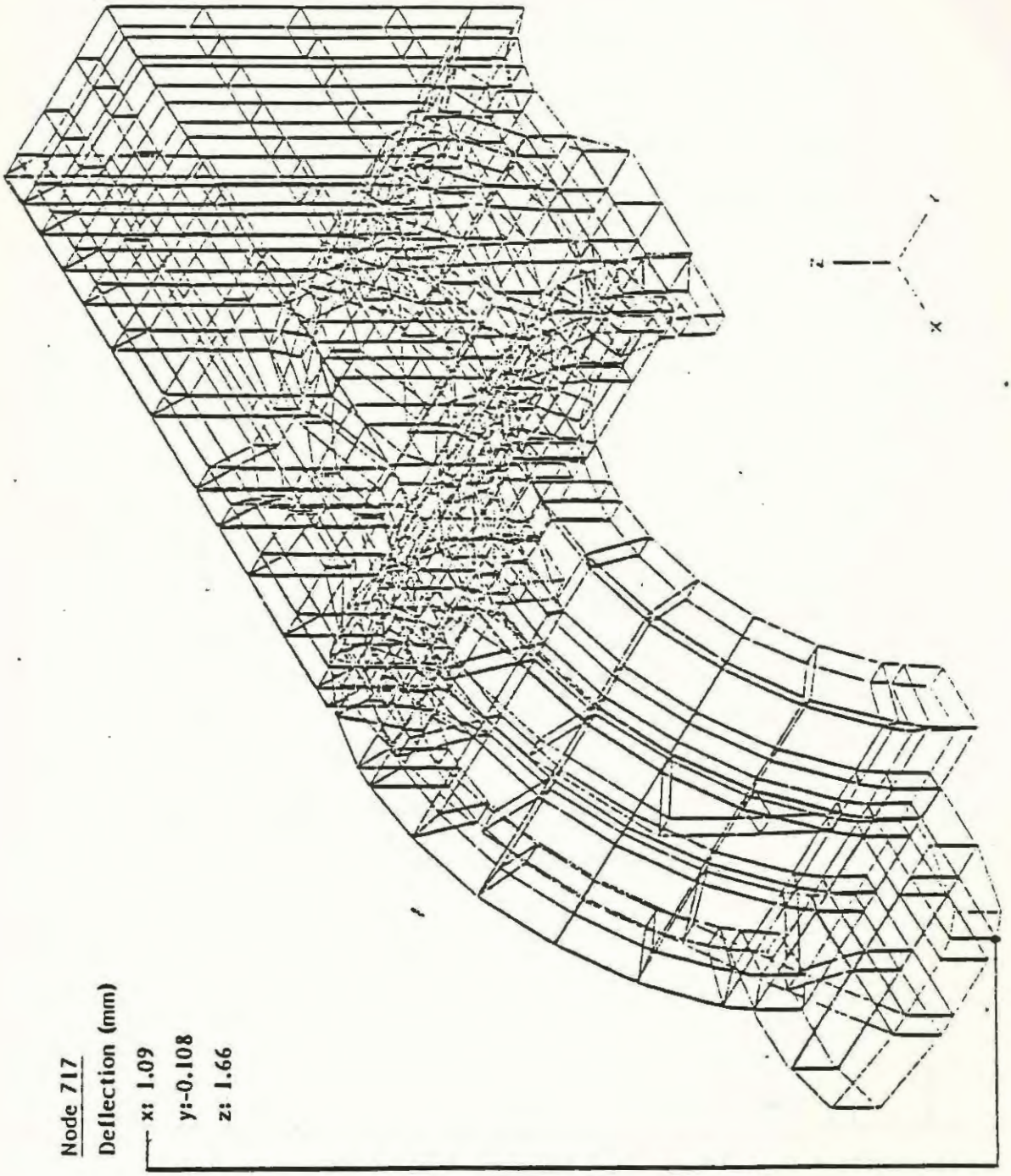

FIGURE 6.3-2 - POINT OF MAXIMUM DEFLECTION - SIDEFRAME

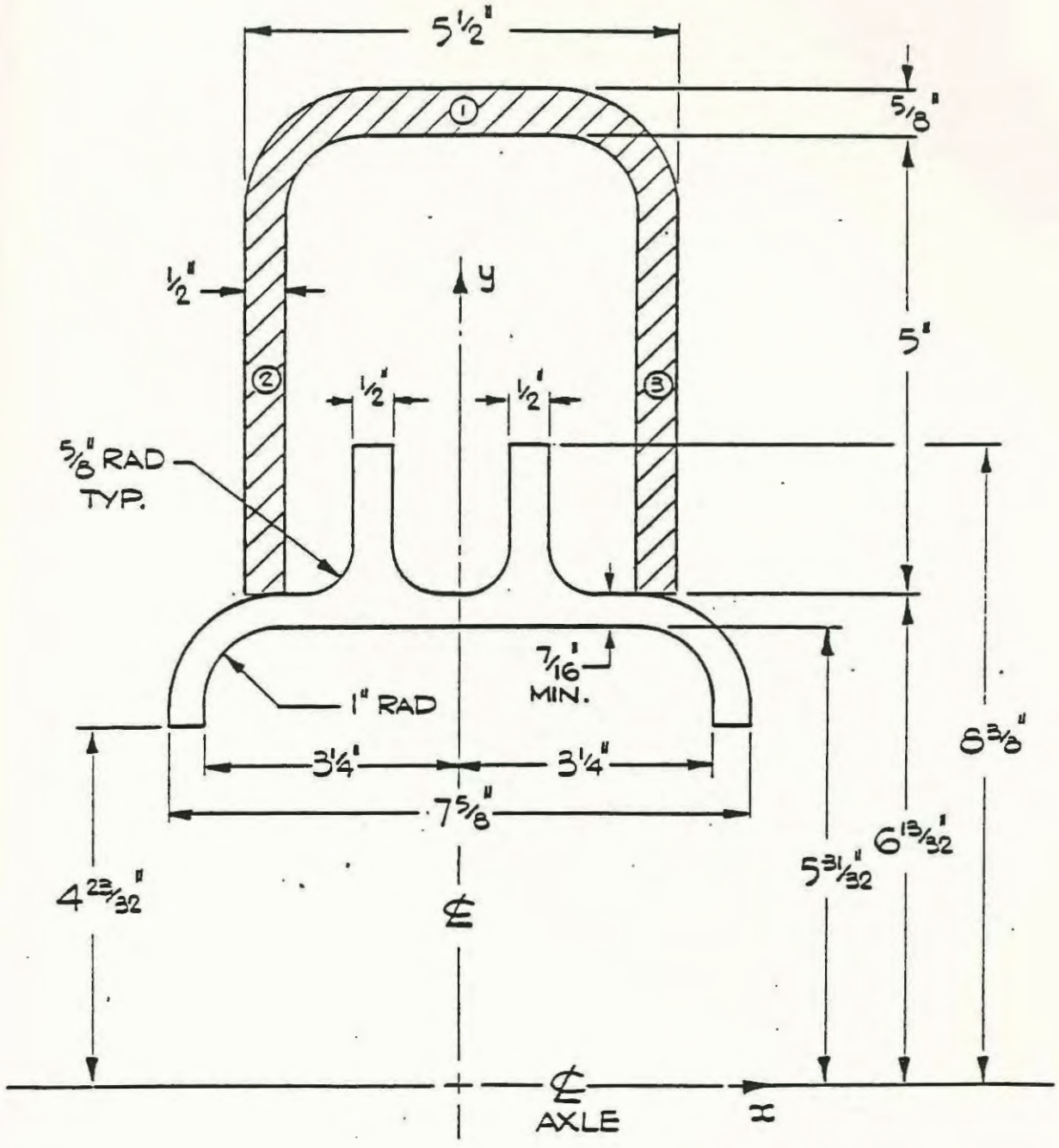

FIGURE 6.3-3 - REINFORCING CAP - CROSS SECTIONAL END VIEW

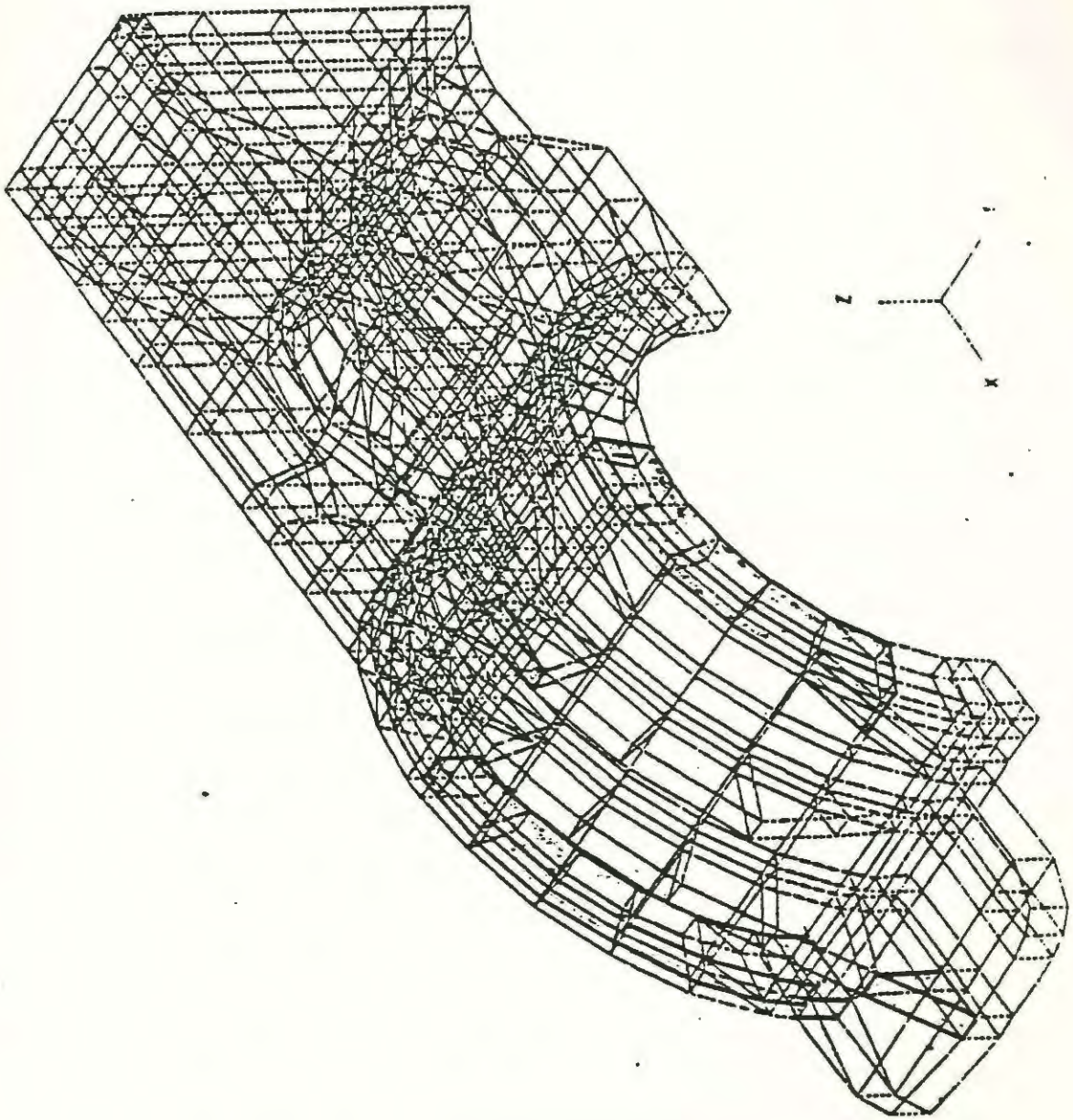

FIGURE 6.3-4 - SIDEFRAME STRESSES EXCEEDING 6000 PSI - MODIFIED

7.0 DISCUSSION - OVERALL

7.1 This section summarizes Sections 2 through 6 and illustrates their relationship.

7.2 The hardware design of the retrofit was by necessity a two point steering configuration to take advantage of the large allowable motor/gearbox coupling angle while eliminating any coupling longitudinal shear. The retrofit kit will add some weight to the truck mainly in the axle bearing box (estimated at 100 lb) and the reinforcement cap (estimated at 100 - 150 lb).

7.3 It should be clear that a vehicle stability and curving ability are trade-offs. High stable speeds are normally brought about through very stiff primary suspensions both longitudinally and laterally. The retrofit design, by necessity, requires reasonably soft axle yaw stiffness to allow steering. Irrespective of these compromises, the results of the analyses show that the truck is stable over the complete range of operating speeds at which coincities up to the worn wheel 1/5 (0.2), and the curving ability is excellent on all curves of radii above 700 ft., the smallest curve on the WMATA revenue lines.

7.4 In addition to the ability to steer resulting from the truck modifications, it should be clear that tread wear, flange wear and tread and flange forces have been reduced significantly compared to the standard truck. The benefits of these reductions would be seen in reduced track and rail tie-down maintenance, as well as reduced wheel wear.

7.5 The finite element stress analysis results clearly showed the need for a sideframe reinforcing cap and an axle bearing box spreader bar. These results also showed the need for further design work on the cap.

8.0 SCHEDULE

The program schedule is shown as Tables 8.1-1 and 8.1-2. The program was originally planned for a ten-month duration. Problems were experienced in getting accurate up-to-date vehicle and track information. This was resolved near the end of the second month. The bulk of the program was completed in July 1983 whereby a design review meeting was planned. The meeting took place 23 September 1983 at which the task of investigating the dynamic and curving behaviour of the Rockwell truck with modified primary bushings was requested.

At the meeting of 2 December 1983, it was agreed that the completion and submission of the Phase 1A, report would occur early in 1984.

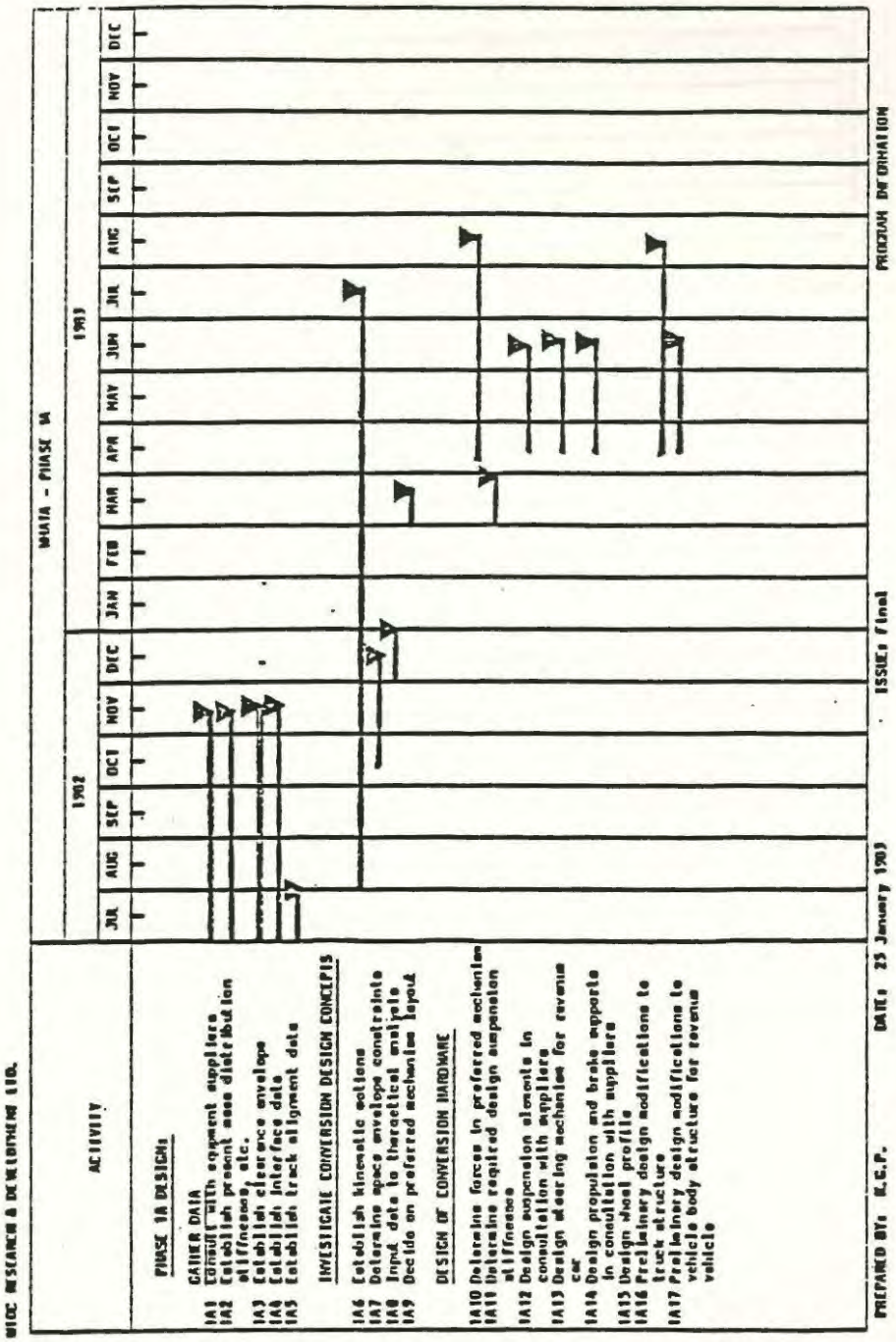

FIGURE 8.1-1: PROJECT SCHEDULE (PAGE 1 OF 2)

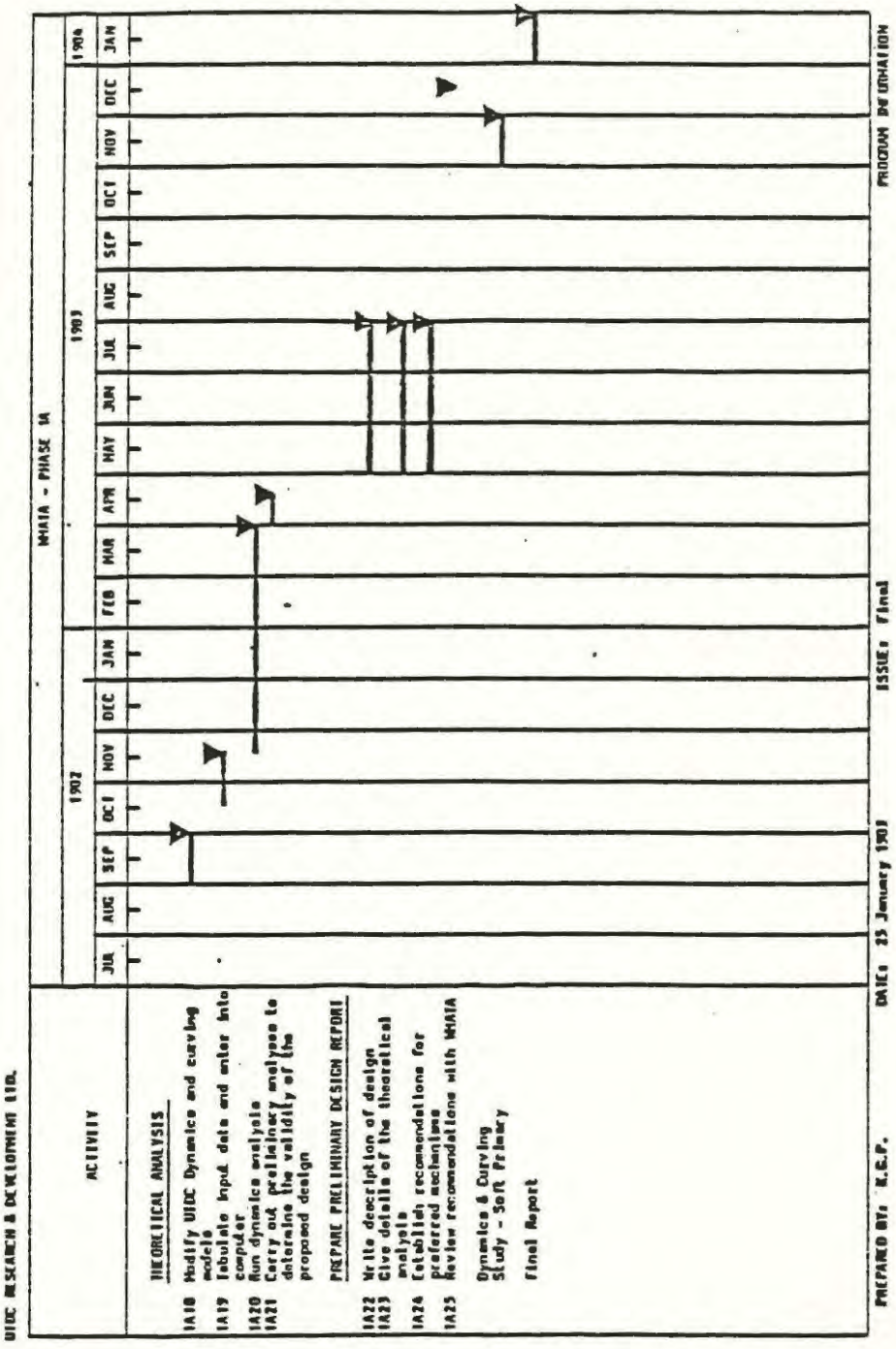

FIGURE 8.1-2: PROJECT SCHEDULE (PAGE 2 OF 2)

9.0 CONCLUSIONS

9.1 It is concluded that this program has produced a steering retrofit to the WMATA Rockwell truck that:

- o adds 45 major parts and approximately 1,000 lb to each truck;
- o provides steering within 0.61 percent; of theoretically perfect on all curved track of 230 ft radius or greater;
- o is dynamically stable within the WMATA operating envelope with a stable worn wheel profile;
- o will provide flangeless curving on the system revenue track (700 ft radius or greater);
- o requires further structural design work at the primary suspension area of the sideframe (reinforcing cap).

9.2 It is also concluded that:

the program has been completed within an admissible time period; and within the constrained budget.

10.0 RECOMMENDATIONS

10.1 It is recommended that WMATA take the following actions:

- o initiate a new program of work to include the final design of the retrofit kit including the sideframe reinforcing cap;
- o install and test the retrofit kit on two ROHR cars;
- o include in further work, the retrofitting and testing of the Breda trucks; and if all successful, retrofit the complete fleet of WMATA cars with steerable trucks.

REFERENCES

1. Elkins, J.A. Wheel Rail Force Measurement of the Washington Metropolitan Area Transit Authority, U.S. D.O.T. Report. DOT-TSC-UMTA-82-28, June 1983.

2. Cross, Mary E., Preliminary Cost-Benefit Analysis of Steerable Trucks in Heavy Rail Transit; U.S. D.O.T Report No. PM-732-U-30-020; September, 1980.

ABBREVIATIONS

AAR	-	Association of American Railroads
AREA	-	American Railway Engineering Association
CTA	-	Chicago Transit Authority
F	-	front
LH	-	left hand
R	-	rear
RE	-	Railway Engineering
RH	-	right hand
R&D	-	Research and Development
TSC	-	Transportation System Centre
UMTA	-	Urban Mass Transportation Administration
US	-	United States (of America)
US DOT	-	United States Department of Transportation
UTDC	-	Urban Transportation Development Corporation
UTDC R&D	-	UTDC Research and Development Company Ltd.
WMATA	-	Washington Metropolitan Area Transit Authority
CWT	-	hundredweight (100 lb.)
ft	-	foot
in	-	inch
lb	-	pound
m	-	meter (metre)
mi	-	mile
mph	-	miles per hour
psi	-	pound force per square inch

APPENDIX A

LIST OF RETROFIT PARTS

PARTS LIST - WMATA TRUCK STEERING RETROKIT

ITEM	PART NO.	DESCRIPTION	QUANTITY PER HIGHER ASSY.
	42-8000-003	Truck Assembly	1
1	42-8000-027	- Housing	2
2	42-8000-025	- Housing	2
3	42-8000-033	- Support, Top, non-steered side, 17-24 degree	2
4	42-8000-037	- Support, Top, lever pivot end, 41-46 degree, inboard	1
5	42-8000-035	- Support, Top, lever pivot end, 41-46 degree, outboard	1
6	42-8000-039	- Support, Top, steered side 62-69 degree	2
7	42-8000-041	- Support, Top, non-steerd side, 36-48 degree	2
8	42-8000-029	- Ring, Retaining	4
9	42-8000-030	- Screw, Socket Head, Modified 3/8-16 UNC-2A x 1 1/4	24
10		- Wire (B.W. 18 GA (.042) DIA)	A/R
11	42-8000-024	- Rod, Push, Steering	2
11-1		- Flat Bar HRS SAE 1018 2 1/4 x 2 1/2 x 3 1/4	
11-2		- Flat Bar HRS SAE 1018 3/4 x 2 1/2 x 10 1/4	
11-3		- Round Bar HRS SAE 1018 1 1/2 O x 3 1/2	
11-4		- Mech Tubing SAE 1015/1018 1 1/2 OD x .120 Wall x 13.6	
11-5		- Mech Tubing SAE 1015/1018 1 1/2 OD x .120 Wall x 28.7	
11-6	SPAE NAUR HC 243	- Screw, Hex Head GR5 3/4-16 UNF x 3" LG	
12	42-8000-021	- Connector, Pivot	2
12-1	42-8000-022	- Screw Assy	1
12-1-1		- Bar HRS SAE 1018 3"O x.62	

PARTS LIST - WMATA TRUCK STEERING RETROKIT

ITEM	PART NO.	DESCRIPTION	QUANTITY PER HIGHER ASSY.
12-1-2	01-217-11-1020	- Screw, Cap, Hex Socket·GR5, 5/8-11 UNC x 2 1/2	
12-2	42-8000-031	- Washer, Rubber/Steel 1/8" THK	1
12-2-1		- Tube MT 1018 7/8 OD 5/8 ID x .125 THK	
12-2-2		- Rubber 1 1/2 7/8 ID x .125 THK	
12-3	W158	- Washer, SPAE NAUR 41/64 Bore 2 1/2 OD x 3/16	1
12-4	01-412-17-1000	- NUT, Hex Slotted 5/8-11 UNC-2B GR5	1
12-5	01-301-01-08-12	- Pin, Cotter 1/8 0 x 1 1/2 REF	
12-6	BCT 13/935	- Bush, Rubber 1.50D, .625 Bore Metalastik	
13	01-101-17-1418	- Screw, Hex 7/8 -9 UNC-2A x 2 1/4 GR 8	16
14	01-511-01-1400	- Washer, Lock 7/8 NOM	16
15	42-8000-043	- Link, Inboard	1
16	42-8000-042	- Link, Outboard	1
17	42-8000-044	- Washer, Flanged	2
17-1		- Bar, 2" DIA x 9/16 LG Stress Proof	
18	42-8000-045	- Washer, Flanged	4
18-1		- Bar, 2 1/4 DIA x 11/16 Stress Proof	
19	01-101-17-1028	- Screw, Hex 5/8-11 UNC-2B GR 5	2
20	01-101-17-1232	- Screw, Hex 3/4-10 UNC-2A x 4	4
21	01-431-27-1000	- Nut, 5/8-11 UNC-2B GR5	2
22	01-431-27-1200	- Nut, 3/4-10 UNC-2B GR5	4
23	01-511-01-1000	- Washer, Lock 5/8 Nom	2

PARTS LIST - WHATA TRUCK STEERING RETROKIT

ITEM	PART NO.	DESCRIPTION	QUANTITY PER HIGHER ASSY.
24	01-511-01-1200	- Washer, Lock 3/4 Nom	4
25	42-8000-020	- Spring, Primary	16
26	42-8000-055	- Hinge Assy	4
26-1	42-8000-046	- Support, Swing	1
26-1-1		- Lug HRS A36 1.75 PL 5 x 3.63	2
26-1-2		- Plate HRS A36 3/8 PL 5 x 6.75	1
26-2	TWL-104-28	- Bushing HD Less liner 1 1/4 ID x 1 5/8 OD	2
26-3	42-8000-047	- CAP	2
26-4	2-127	- Seal, O-Ring 1.424 ID x .103 W	2
26-5	GF-611	- Fitting, Grease 1/8 NPT	4
26-6	TT-2800	- Bearing, Thrust (modified) 1" ID x 2 7/9 OD x 1/8	2
26-7	TWL-104-24	- Bushing, HD Less liner 1 1/4 ID x 1 5/6 OD	4
26-8	42-8000-048	- Arm Swing	1
26-9	42-8000-053	- Pin Hinge 1 1/4 DIA	1
26-10	42-8000-054	- Pin Hinge 1 1/4 DIA	1
26-11	TT-230401	- Bearing, Thrust 1 1/4 ID x 2 3/8 OD x 1/16	8
26-12	01-503-00-1800	- Washer, Style AA 1 1/4 ID x 2 3/4 OD	2
26-13	680-111	- Spring, Steel Disc - for 1 1/4 bolt	6
26-14	01-412-17-2000	- Nut 1 1/4 -7 UNC GR5	1
26-15	01-103-28-1416	- Bolt 7/8 -14 UNF x 2 LG Drilled Head	4
26-16	01-501-00-1400	- Washer 7/8 DIA	4

PARTS LIST - WMATA TRUCK STEERING RETROKIT

ITEM	PART NO.	DESCRIPTION	QUANTITY PER HIGHER ASSY.
26-17	01-103-18-0610	- Bolt 3/8 -16 UNC x 1.25 Drilled Head	4
26-18	01-501-00-0600	- Washer 3/8 DIA	4
26-19	01-301-01-1622	- Pin, Cotter 1/4 DIA x 2.75 LG	1
27	42-8000-050	- Connecting Rod Assy	1
27-1	42-8000-049	- Connecting Rod	1
27-2	5533-1000-4	- Mount Kit, Lord	1
27-3	01-431-27-1200	- Nut, Hex, Slotted 3/4-11 UNC-2B GR5	1
27-4	01-301-01-810	- Pin Cotter 1/8 DIA x 1 1/4 LG	1
28	42-8000-052	- Connecting Rod Assy	1
28-1	42-8000-051	- Connecting Rod	1
28-2	5533-1000-4	- Mount Kit, Lord	1
28-3	01-431-27-1200	- Nut, Hex Slotted 3/4-11 UNC-2B GR5	1
28-4	01-301-01-810	- Pin, Cotter, 1/8 DIA x 1 1/4 LG	1
29	BC 131903	- Bushing Rubber/Metal	12

APPENDIX B

STEERING KINEMATIC ANALYSIS

REVISIONS

ISSUE	DATE	REVISIONS	PAGES AFFECTED
2	15/11/88	Spelling corrections of word "labelled".	2
		Linkage ratio calculations corrected.	4 & 5
		99.0 mm changed to 104 mm	7

WMATA Steering Linkage
Kinematic Analysis

R.v.H.

SUMMARY

The W.M.A.T.A. steerable truck was analysed using classical graphical methods. The outboard steering linkage was found to give perfect steering while the inboard steering linkage, as designed, featured an oversteer. A design change is recommended such that the inboard steering linkage gives perfect steering as well.

CONTENTS

83.07.14 1 1 9

WMATA Steering Linkage
Kinematic Analysis

R.v.H.

1.0 INTRODUCTION

This report describes the graphical kinematic analysis of the inboard and outboard steering linkages on the W.M.A.T.A. steerable truck. The analysis and subsequent re-design are based on a perfect steering condition on a 70 metre radius curve.

Curves having a 70 metre radius are the tightest curves in the W.M.A.T.A. system.

2.0 GENERAL DISCUSSION

2.1 KINEMATIC MODEL

The model assumes a fixed carbody and the truck is assumed to rotate about the center pin, shown as (1,5) on all drawings.

The numbering convention used for the links and pivots is shown on drawing 42-8000-003, where a pivot between two links X and Y is labelled: point (X,Y).

Three points on the truck were isolated: the truck center (1,5), the fixed pivot on the steering link 3, (3,5), and the axle center rotation, (R). The point R was assumed to remain fixed (with reference to the truck) for the graphical analysis.

Misalignment and movement of link 3, with respect to the side frame (because of the rubber bushing in the fixed pivot point, (3,5)) was ignored and the link assumed to move parallel to the side frame. The small effect of the rubber bushings at all joints was also ignored.

The graphical analysis method consists of tracing the linkage movements resulting from a steering input (truck rotation) through the model to the steering output. The angular rotation of the axle about the axle center of rotation is measured from the resulting graphical layout. This is the steering output angle, which can be compared to the angle required for perfect steering.

2.2 RESULTS AND DISCUSSION

2.2.1 Results

The steering input angle resulting from a 70 metre radius curve is: $\theta = 6.50$ degrees, and the steering output angle required for perfect steering is: $\theta = 0.9045$ degrees. These angles are illustrated on drawing 42-8000-KIN-01.

Drawing 42-8000-KIN-02 shows the analysis of the outboard steering linkage. The analysis indicates that the steering on a 70 metre radius curve is virtually perfect

i.e. $\theta_{actual} = 0.904$ degrees

The analysis of the inboard steering linkage, as originally designed, indicated an oversteer of 11% (see drawing 42-8000-KIN-03). Since an oversteer can not be tolerated the steering link was re-designed to achieve perfect steering.

A re-designed inboard steering linkage was analysed for both push and pull (see drawing 42-8000-KIN-04). The steering output was found to be $\theta = 0.899°$ and $0.891°$ for push and pull respectively. Since $\theta = 0.9045°$ yields perfect steering, there is 0.61% understeer in push, and 1.49% understeer in pull.

2.2.2 Inboard Linkage Re-design

Since the outboard steering linkage was shown to feature "perfect" steering, the steering link ratio of the outboard linkage can be used to re-design the inboard. Noting that the connecting link for the outboard linkage is perpendicular to the steering link and horizontal, the link ratio is the ratio of the link lengths (see figure A):

$$r = \frac{L_{output}}{L_{input}} = \frac{80 \text{ mm}}{337.7 \text{ mm}} = 0.23689$$

With the inboard linkage (see Figure B), however, since the net link ratio must still be 0.23689 (for perfect steering) and the bottom connection is fixed to the frame while the centre one is connected to the link, we get:

$$\frac{\ell}{L_{input}} = 0.23689$$

Where ℓ = vertical projection of (3,5) to (3,4). (See figure B)

$$L_{input} = (337.7 + \ell)$$

Thus:

$$\frac{\ell}{337.7 + \ell} = 0.23689$$

$$0.76311\,\ell = 0.23689 \times 337.7$$

$$\therefore \quad \ell = 104.83 \text{ mm}$$

3.0 CONCLUSIONS

The outboard steering linkage, as designed, gave virtually perfect steering on a 70 metre radius curve. The inboard steering linkage, as designed, gave an 11% oversteer. The recommended inboard linkage re-design features a 0.61% understeer, in push, and a 1.49% understeer in pull.

4.0 RECOMMENDATIONS

Based on the above calculation and the previously presented analysis, it is recommended that the inboard steering linkage be re-designed with an "ℓ" value of 104.0 mm (see Figure B). (The slightly reduced value of "ℓ" was chosen to ensure a slight understeer.)

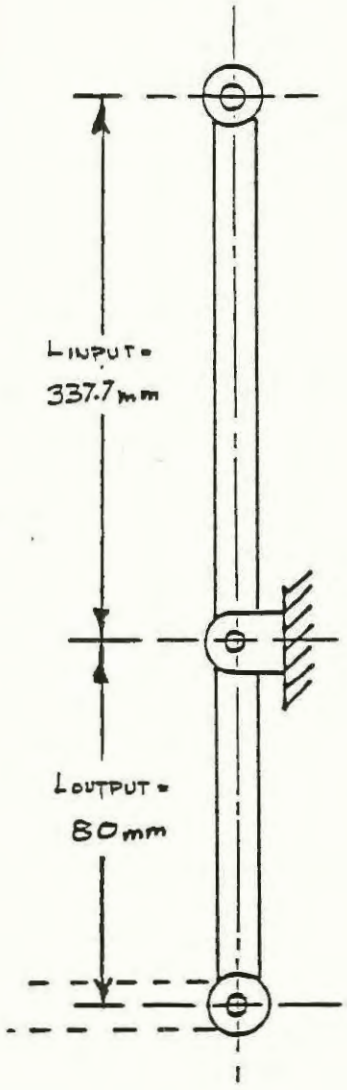

FIGURE A:
Outboard Steering Linkage

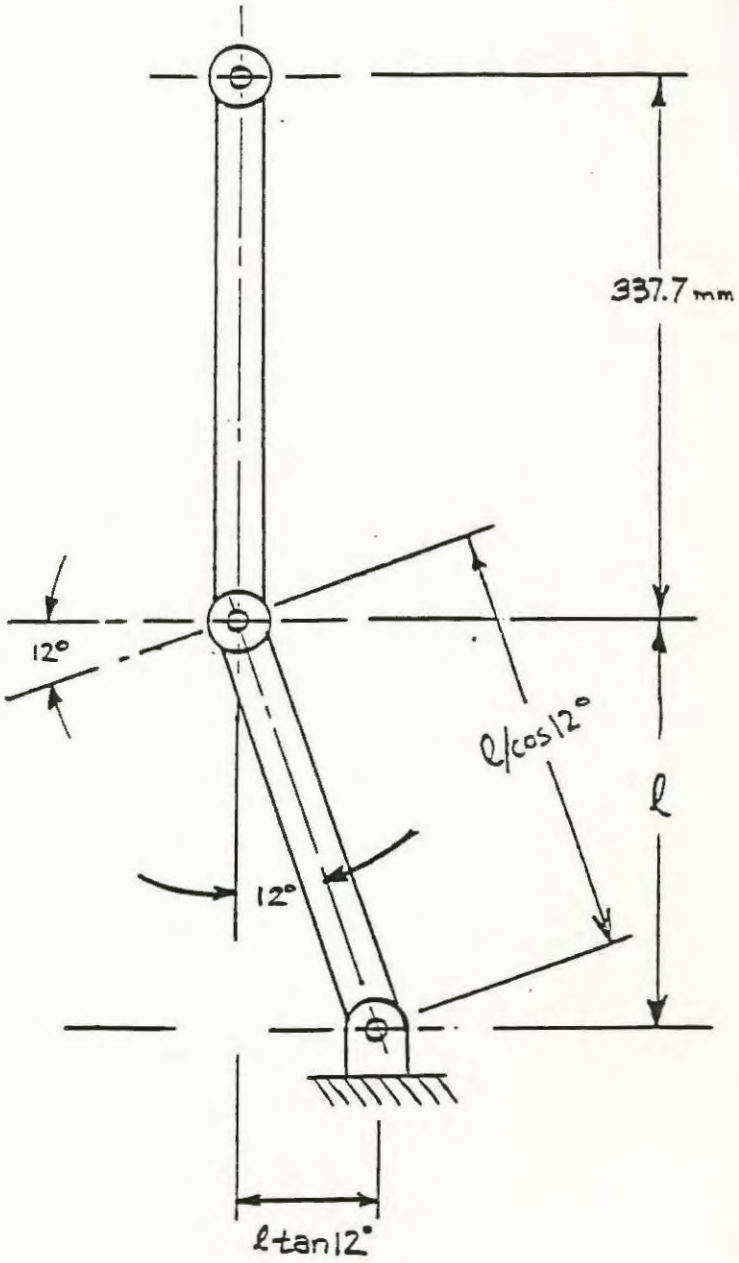

FIGURE B:
Inboard Steering Linkage

83.07.14 1 9 9

WMATA Steering Linkage
Kinematic Analysis

R.v.H.

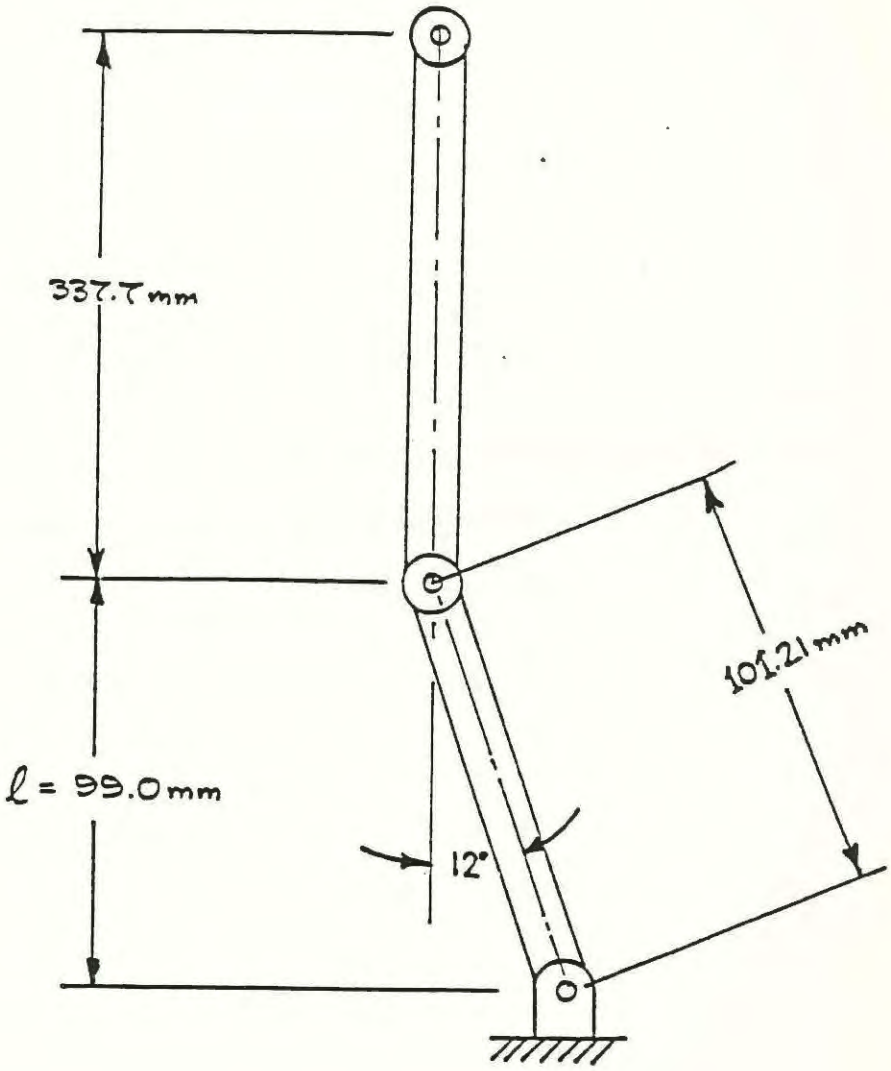

FIGURE C:
Redesigned Inboard Steering Link

APPENDIX C

REPORTS OF THE SIDEFRAME FINITE ELEMENT ANALYSIS

Part One	The Analysis and Findings
Part Two	Sideframe Reinforcement
Part Three	Revised Spring Pads

Chadwick
Engineering Ltd

APPENDIX C

Part One The Analysis and Findings

WMATA SIDEFRAME

Finite Element Analysis

Approved by: D. Chadwick

D. Chadwick, P. Eng.,
President,
Chadwick Engineering.

Date: 22 July 1983

12D Sherwood Avenue, Amherstview, Ontario K7N 1N2 (613) 384 2866

TABLE OF CONTENTS

WMATA SIDEFRAME FINITE ELEMENT MODEL

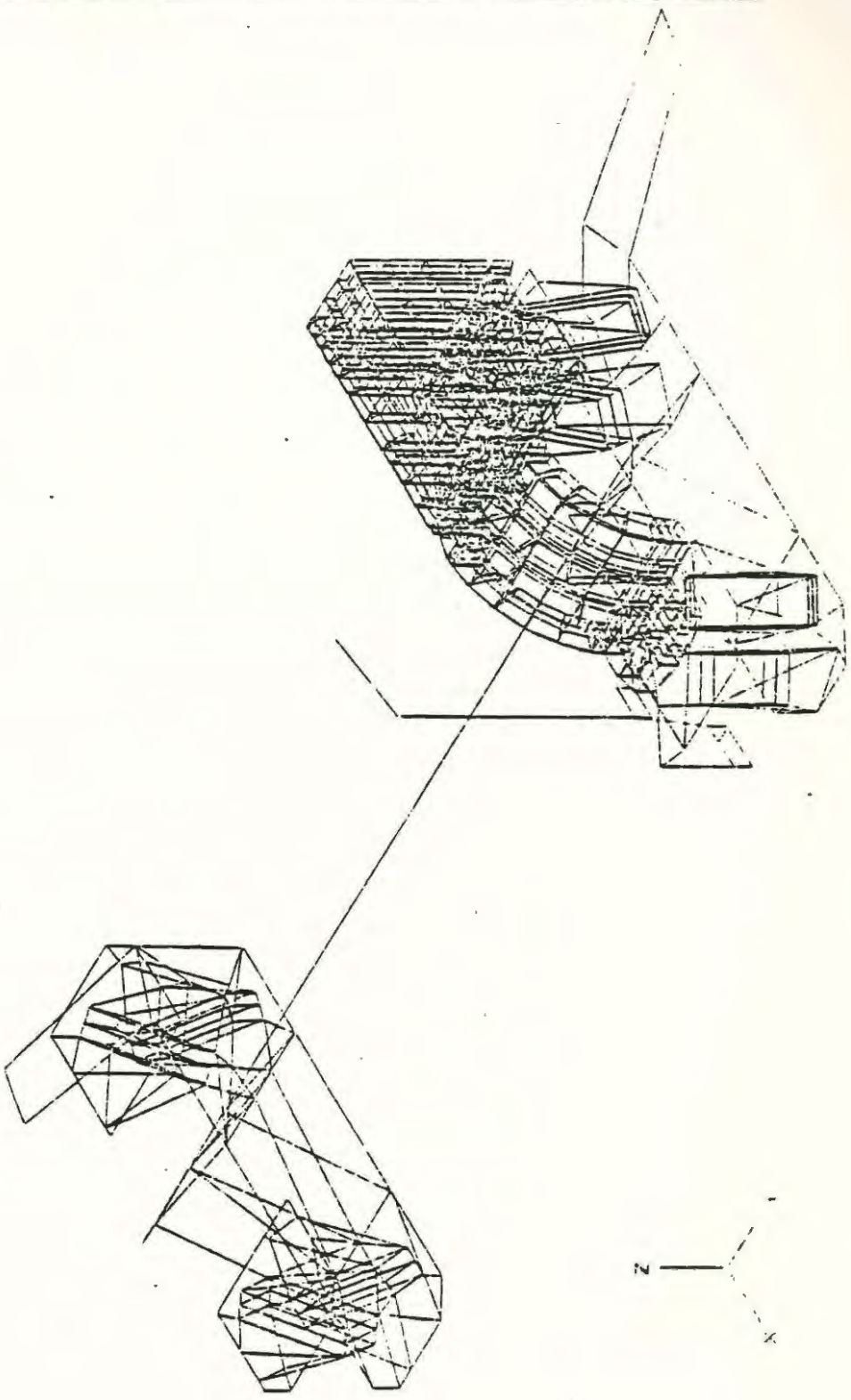

1. GENERAL DESCRIPTION of WMATA SIDEFRAME.

A finite element analysis was carried out on the WMATA Sideframe shown in Figure 1 (Appendix I). The following interconnected components of a front truck at the inboard axle (Dwg.# 42-8000-003) were modelled:

COMPONENT	DWG. #	FIGURE (See Subpart A)
A) Steering Link Side:		
1 - Sideframe	42-8000-017	2
2 - Journal Housing & Primary Spring Pads	42-8000-015	15,16
3 - Top Support, Primary Spring Pads	42-8000-011	17
4 - Steering Linkage	42-8000-003	19
	42-8000-016	
B) Non-Steering Link Side		
5 - Journal Housing and Primary Spring Pads	42-8000-014	20,21
6 - Top Support Primary Spring Pads;		22
inboard	42-8000-041	
outboard	42-8000-039	
C) General		
7 - "LK" Primary Spring Pad	42-8000-007	
8 - Axle		23

2. OBJECTIVES OF ANALYSIS

The primary objective was to determine the principal stresses in the sideframe. It was also required to determine the axle stresses, steering link forces and deflections of the various components.

3. DESCRIPTION of FINITE ELEMENT MODEL

The finite element model was developed with sufficient detail at the sideframe, springpads and steering linkage to ensure that a proper overall response to the applied loads would be obtained. The final model contained 907 elements which resulted in over 3500 equations being solved.

3(i) Components

Specifically the physical problem was discretized into 16 finite element groups:

GROUP	COMPONENT	No OF ELEMENTS	FIGURE(S)
1	Sideframe Webs	16	3
2	Sideframe Front Section	136	4,5,6,7
3	Sideframe Rear Section	209	8
	Section 1		9
	Section 2		10,11,12
	Section 3		13
4	Journal Housing and Axle Steering Side	90	16
5	Rear Primary Spring Pad - Steering Side	30	17
6	Forward Primary Spring Pad - Steering Side	32	17
7	Spring Pad Truss Elements - Steering Side	48	17
8	Spring Pad Three Dimensional Elements - Steering Side	8	17

9	Interfacing between Journal Housing and Side Frame	102	18
10	Steering Linkage-Beam Elements	16	19
11	Steering Linkage-Truss Elements	7	19
12	Journal Housing and Axle - Non-steering Side	89	21
13	Rear Primary Spring Pad - Non-steering Side	32	22
14	Forward Primary Spring Pad - Non-steering Side	36	22
15	Spring Pad Three Dimensional Elements - Non-steering Side	8	22
16	Spring Pad Truss Elements - Non-steering Side	48	22

The following comments should be made with respect to each fundamental component.

(a) Sideframe (Figure 2)

- the sideframe was modeled using 361 three dimensional elements.
- modules of elasticity (E) was 190,000. MPa
- poissons ratio (μ) was 0.27

(b) Journal Housing and Axle (Figure 14)

- the journal housings were modelled using three-dimensional beam elements.
- the modulus of elasticity and poissons ratio were assumed to be the same as the sideframe
- the section properties were selected such that the housings behaved in a rigid manner while still providing the proper load path.
- the axle, on the other hand, was given the appropriate section properties of a 5 1/2 inch diameter solid section

(see Subpart B)

- the spring or shear pads were modelled using three-dimensional beam and truss elements such that the provided compressive and shear stiffnesses could be obtained

(see Subpart C)

(c) Steering Linkage (Figure 19)

- the steering linkage was modified using three dimensional beam and truss elements such that the provided bushing stiffnesses could be obtained

(see Subpart D)

3(ii) Load Cases.

The following Load Cases were examined:

LOAD CASE 1

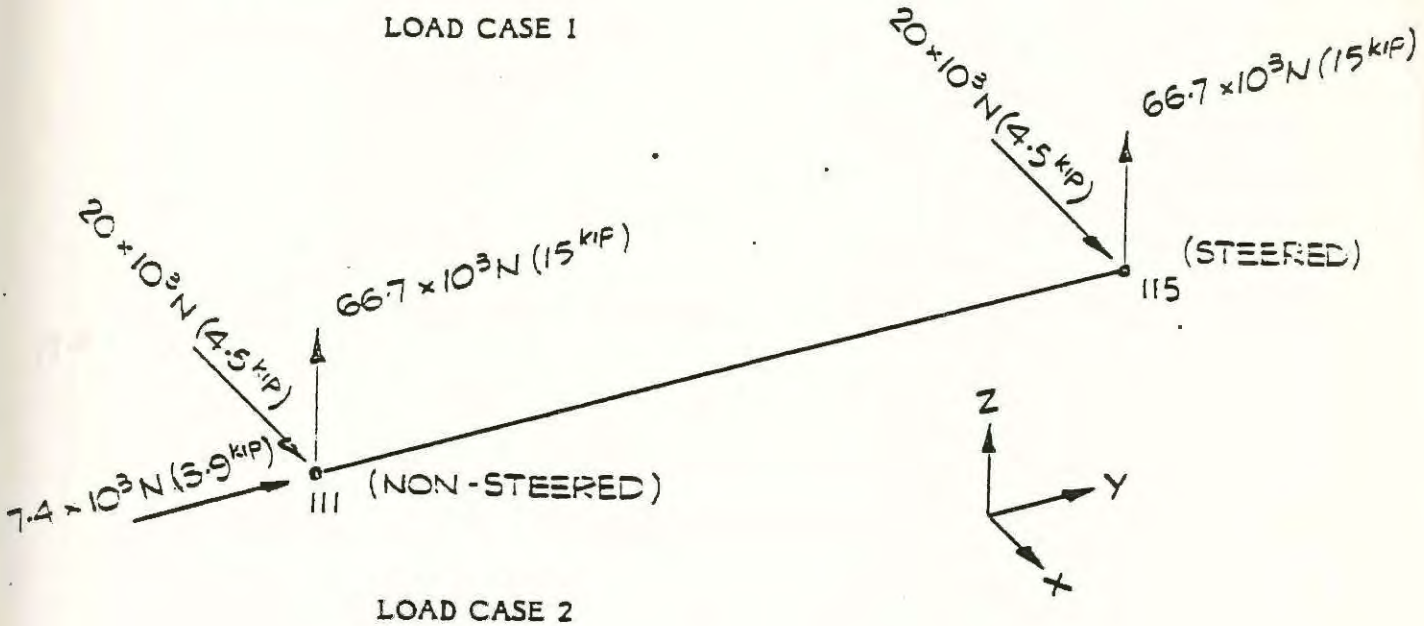

LOAD CASE 2

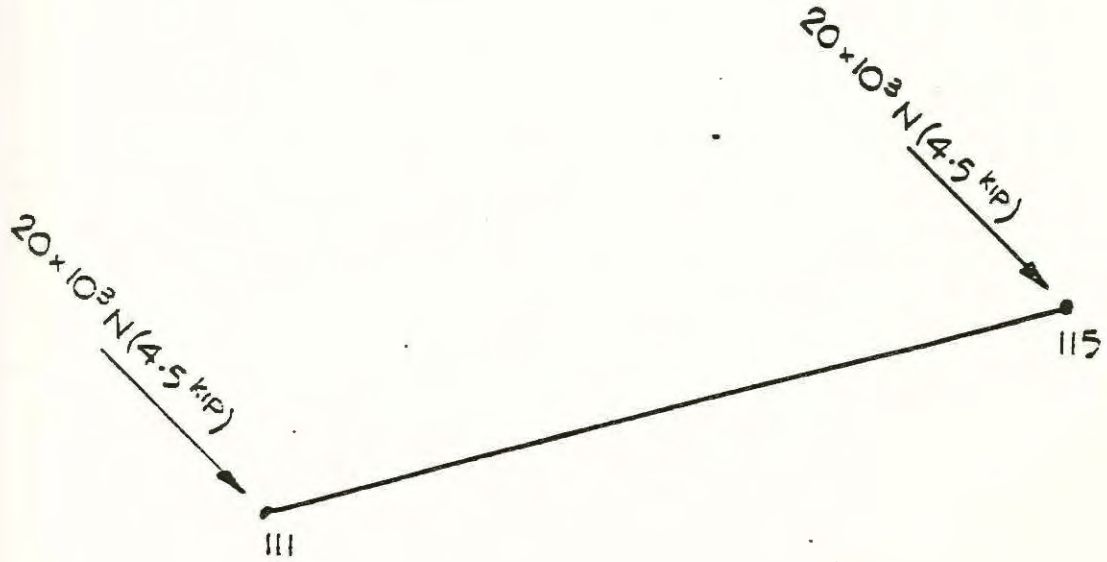

LOAD CASE 3

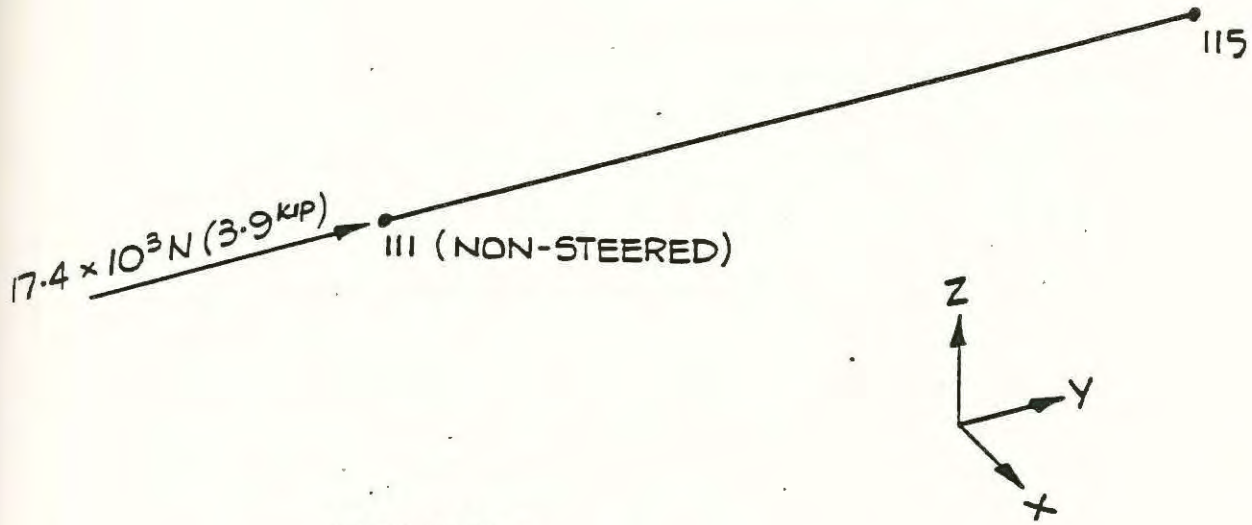

LOAD CASE 4

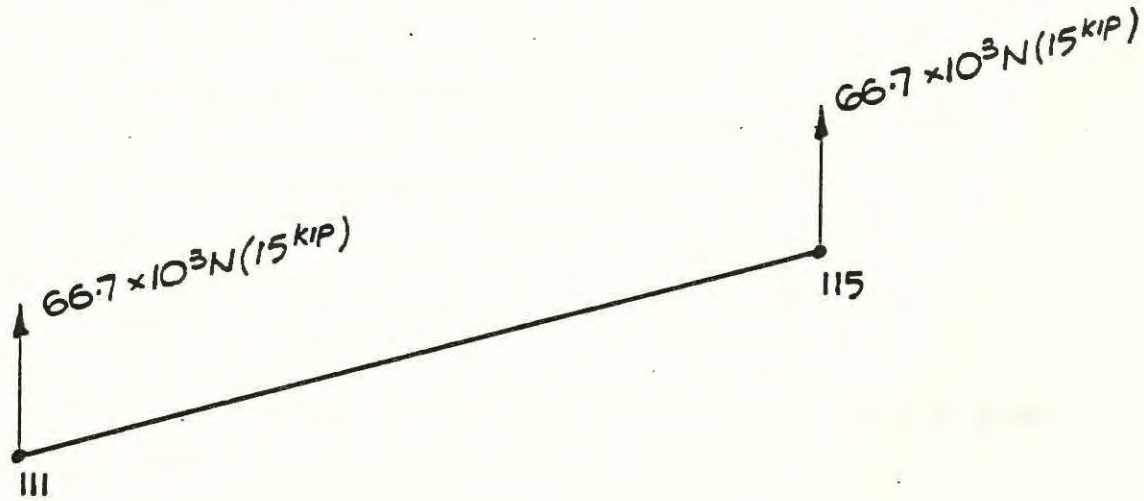

3(iii) Boundary Conditions.

The following components were restrained from moving at specific locations as shown in Figure 24 and noted below.

(a) the rear of the side frame
(b) the upper end of the steering linkage
(c) the top of the forward and rear brackets at the non-steering side.

3(iv) Input and Output

The input and output is given in Appendix V. The input consists of the following sections:

(a) nodal coordinates and boundary conditions
(b) definition of the 16 element groups.(material and geometric properties.
(c) loading.

The output consists of the following sections;

(a) nodal displacements and rotations for each load case
(b) stresses in each element for all 16 element groups and all four load cases.
(c) overall equilibrium check and the strain energy density levels.

4. RESULTS OF ANALYSIS

The entire model as shown in Figure 1 was subjected to the load cases as given earlier. The following results were obtained:

(a) Sideframe - Stresses/Deflections

- the maximum von Mises stress was found to be 320 MPa (46,400psi) as shown in Figure 25 due to load case 1. Other stresses are illustrated at selected points of interest in Figures 25 and 26.

- the maximum deflection in the sideframe was found to be 1.66 mm (.065 inches) in the vertical direction as shown in figure 27 due to load case 1. It should be noted that the sideframe underwent severe twisting as displayed in Figures 28,29 and 30.

(b) Steering Linkage - Forces

-the steering linkage forces are shown in Figure 31, with a maximum value of 1040 N (234 lb) being obtained due to load case 2.

(c) Axle - Deflections/Moments/Stresses

-the deflections in the x,y and z directions for load case 1 are shown in Figure 32. A maximum vertical deflection of 4.33 mm (.17 inches) was obtained at the steered side.

-the axle moment diagram was plotted for the combination of horizontal and vertical moments in Figure 33.

-the maximum bending stress was 46.5MPa (6740psi) due to load case 1.

APPENDIX C

Part One The Analysis and Findings

Subpart A Figures

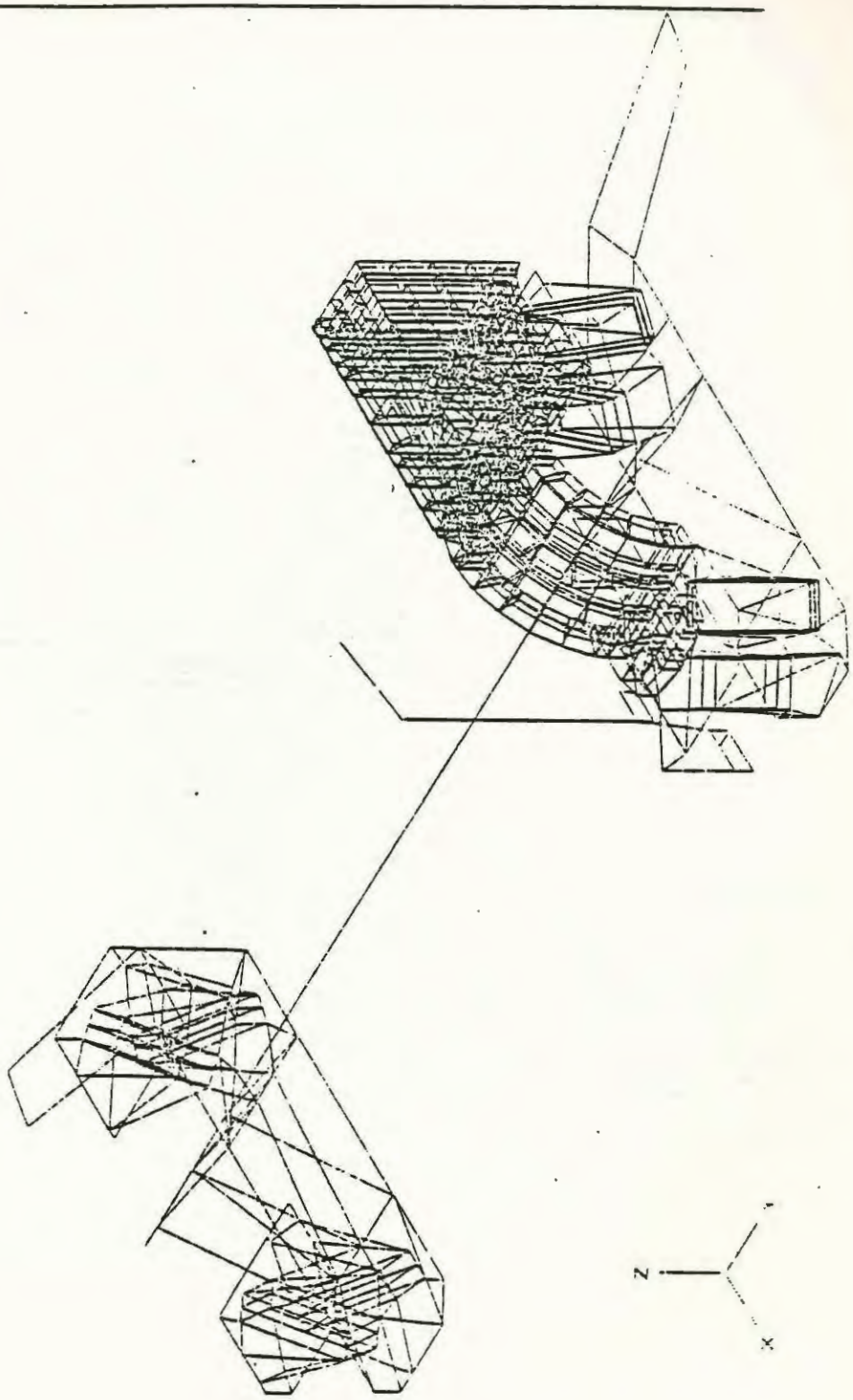

Figure 1 - TRUCK SIDEFRAME ANALYSIS

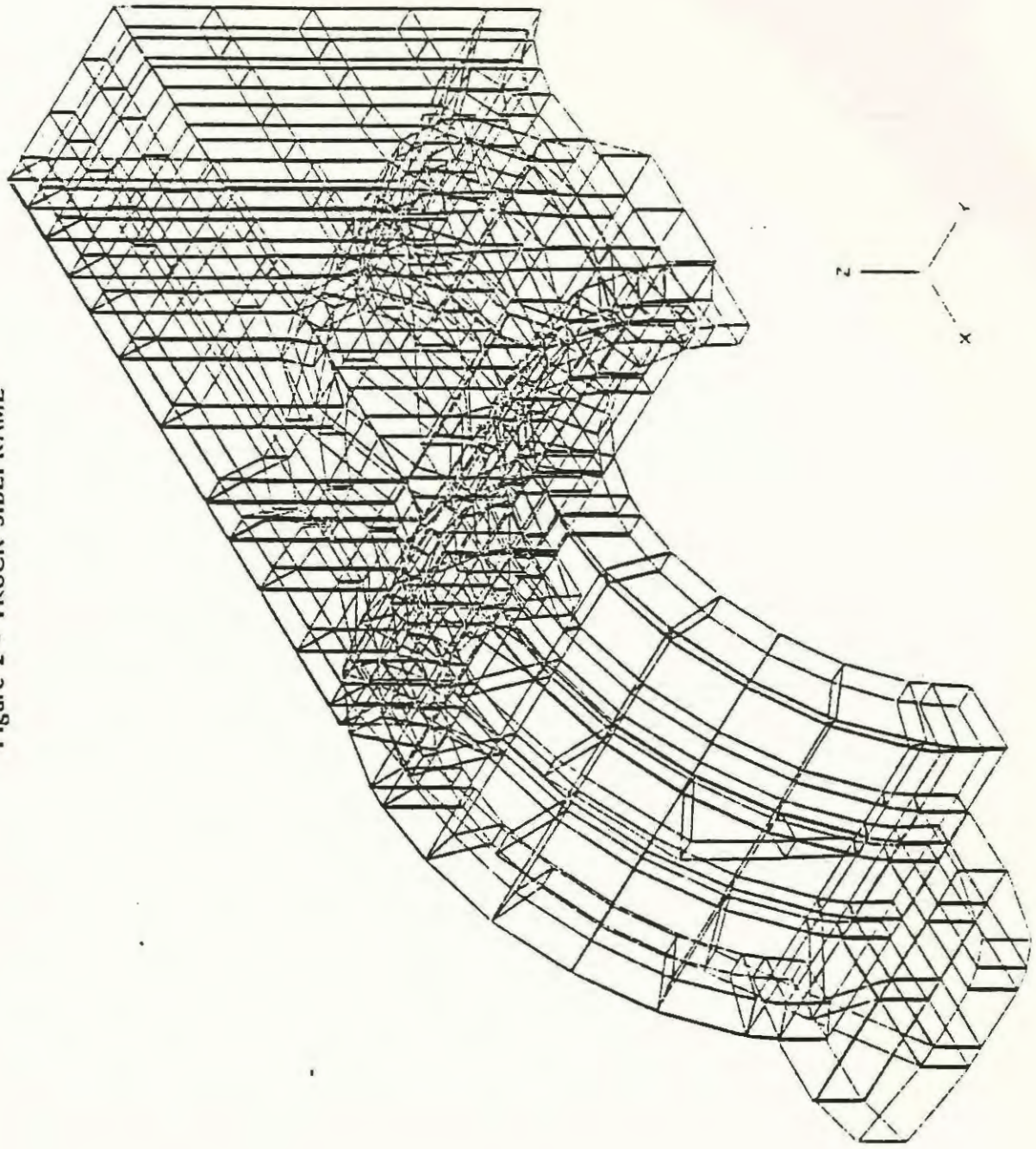

Figure 2 - TRUCK SIDEFRAME

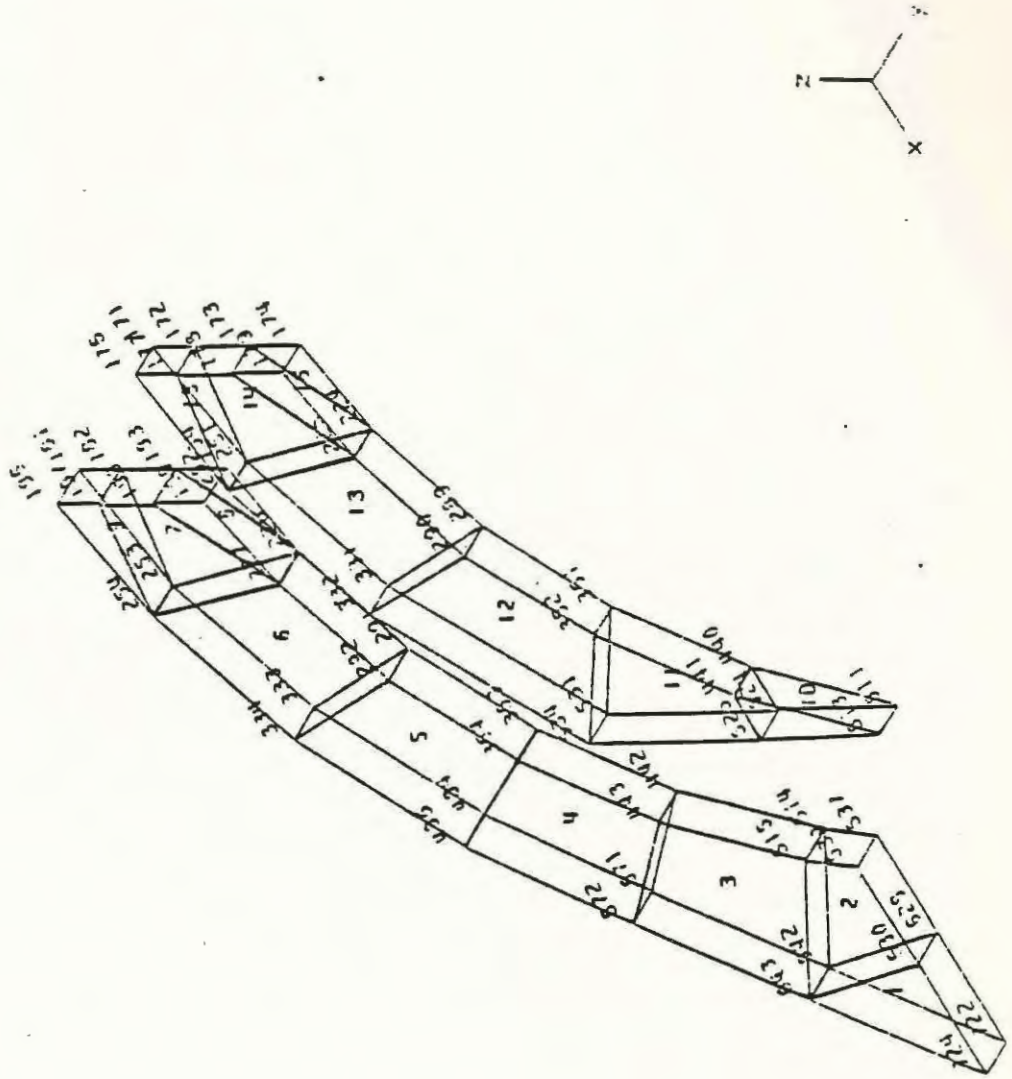

Figure 3 - SIDEFRAME WEBS - Element Group 1

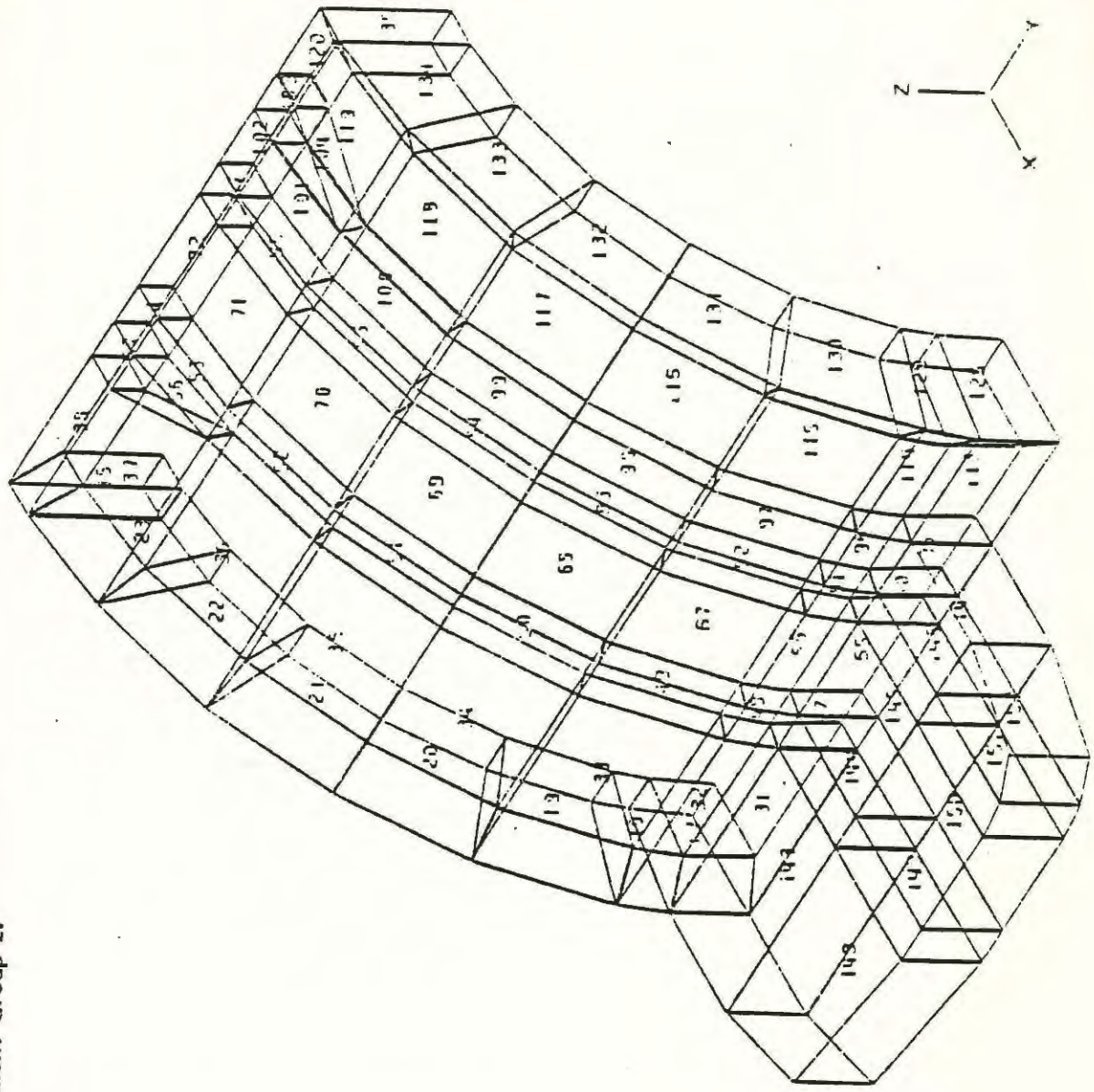

Figure 4 - SIDEFRAME FORWARD SECTION
- Element Group 2.

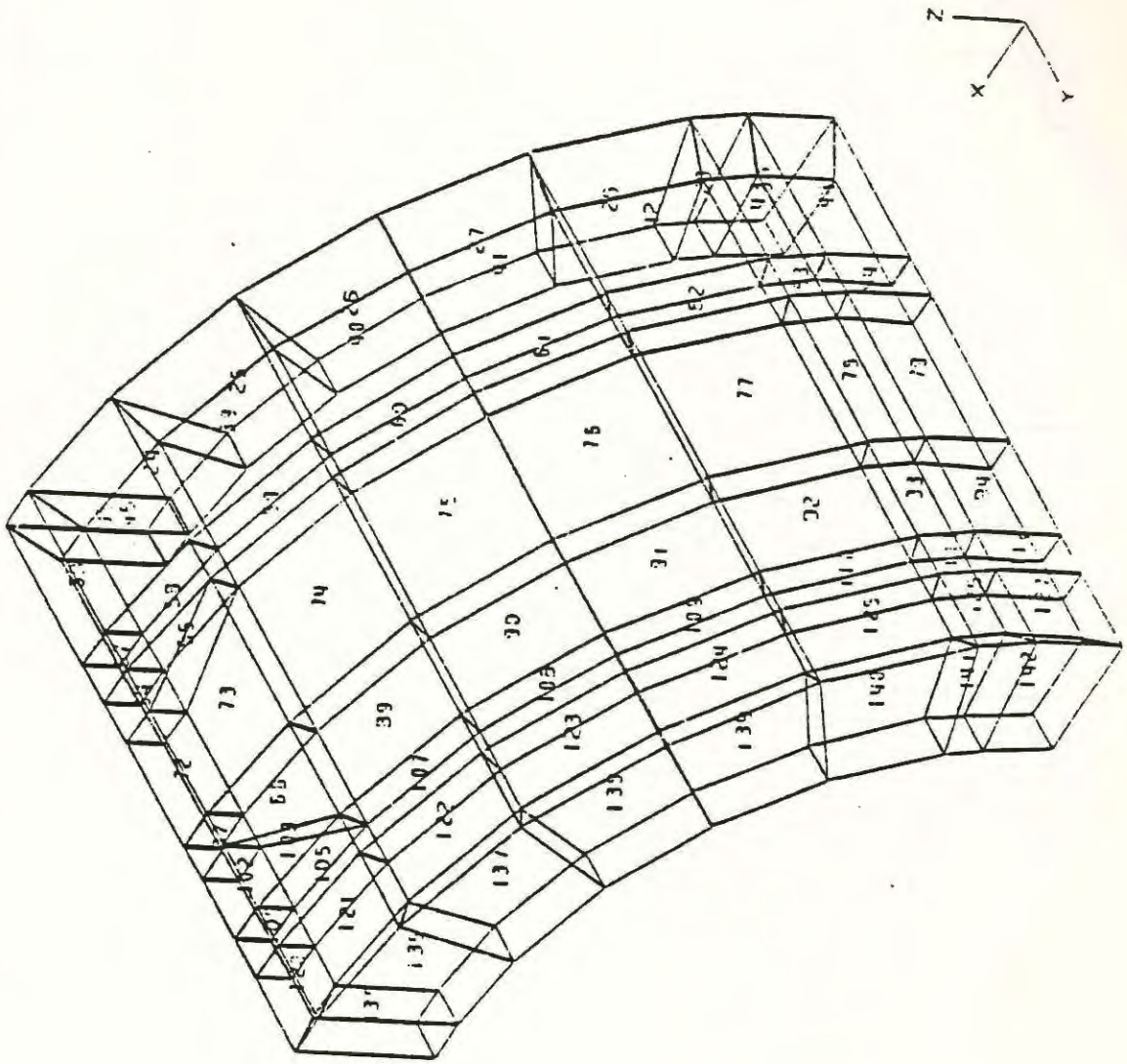

Figure 5 - SIDEFRAME FORWARD SECTION - Element Group 2; View from Rear.

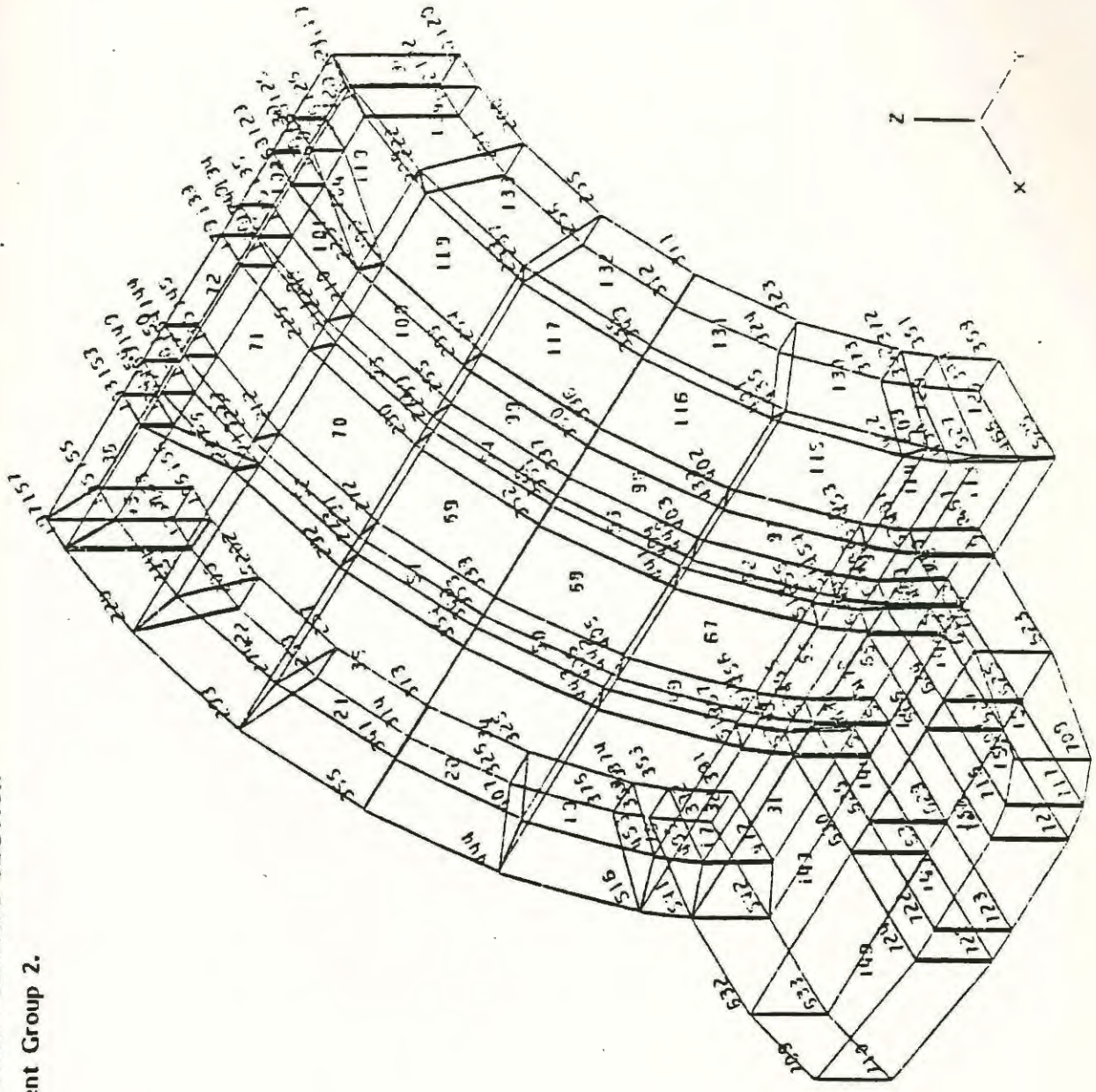

Figure 6 - SIDEFRAME FORWARD SECTION
- Element Group 2.

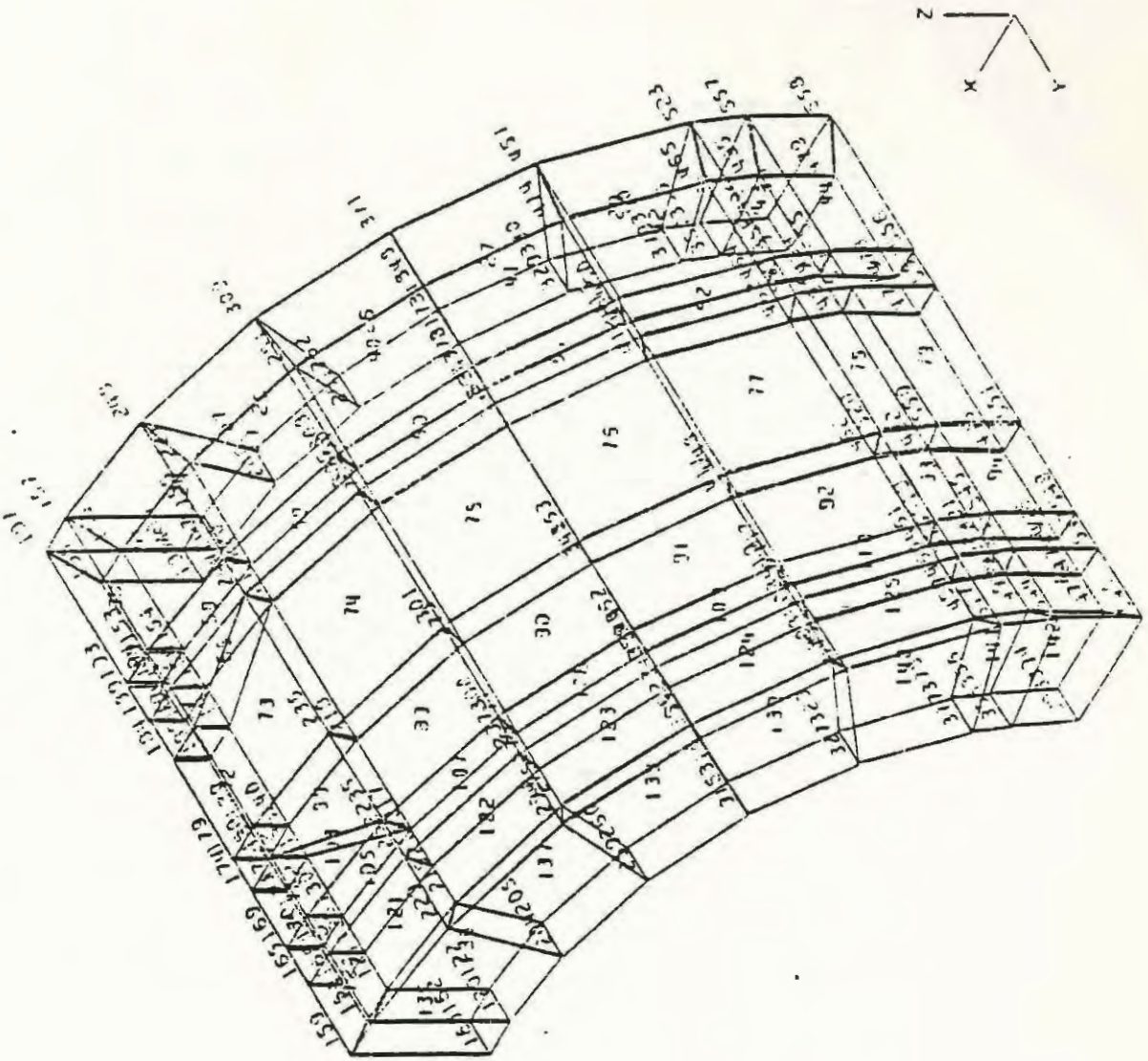

Figure 7 - SIDEFRAME FORWARD SECTION - Element Group 2; View from Rear.

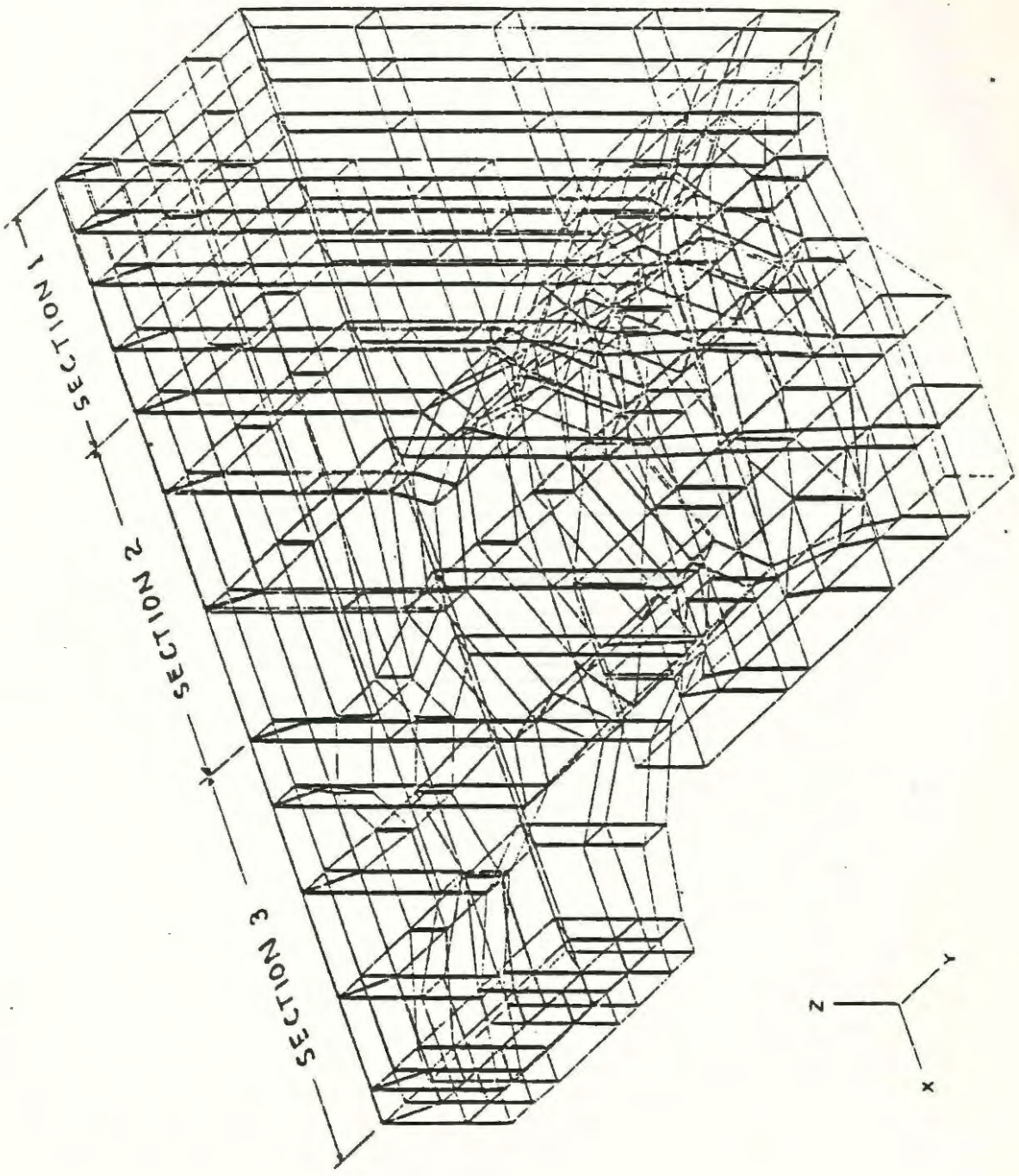

Figure 8 - SIDEFRAME REAR SECTION - Element Group 3.

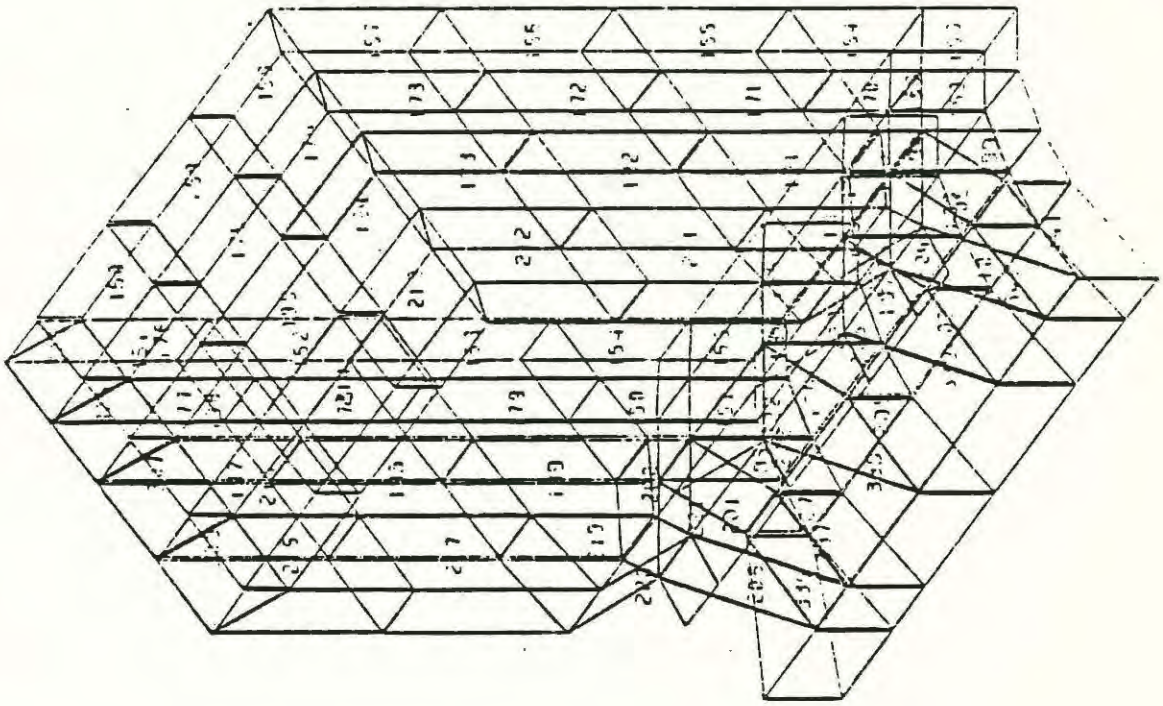

Figure 9 - SIDEFRAME REAR
- Section 1

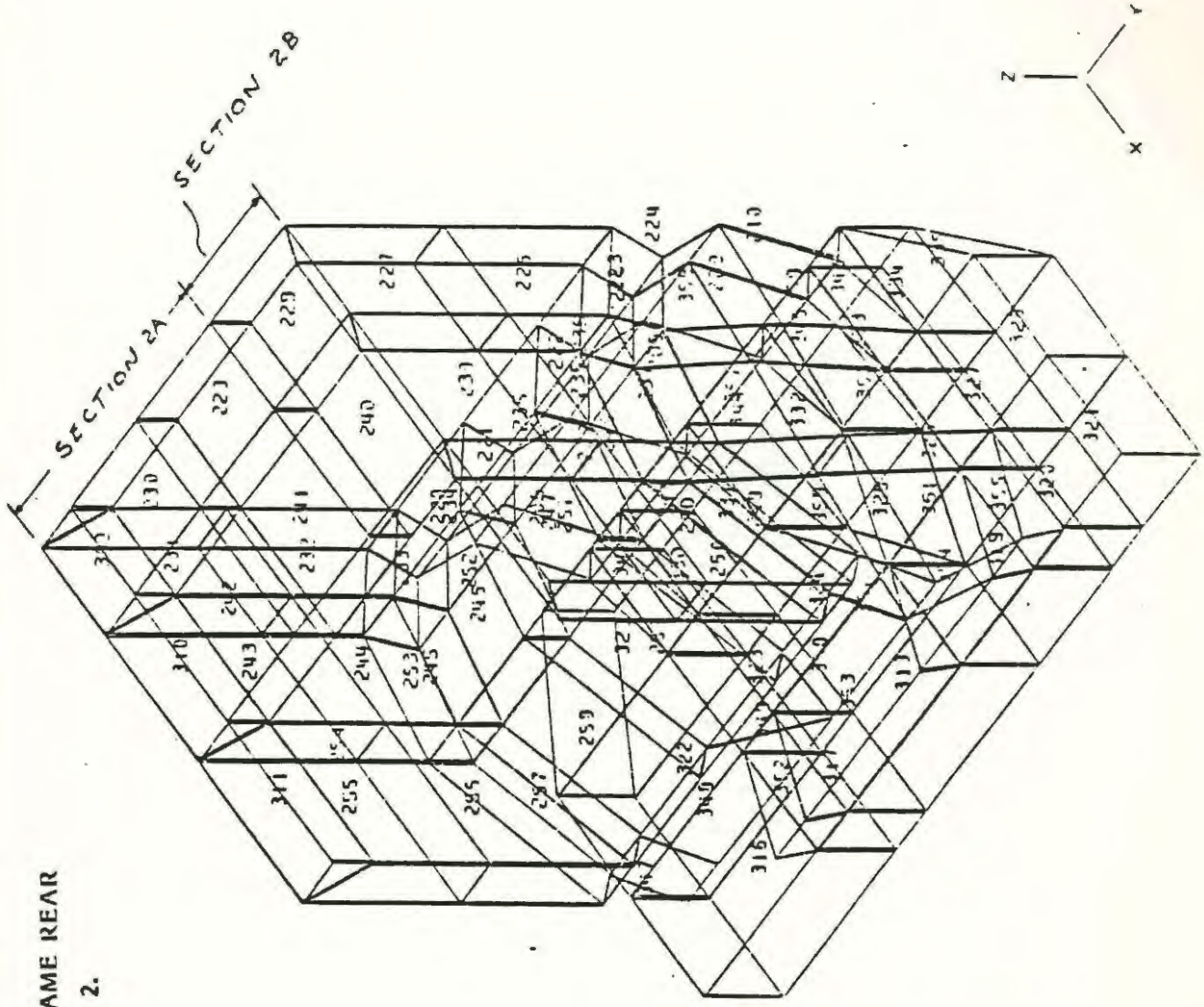

Figure 10 - SIDEFRAME REAR
Section 2.

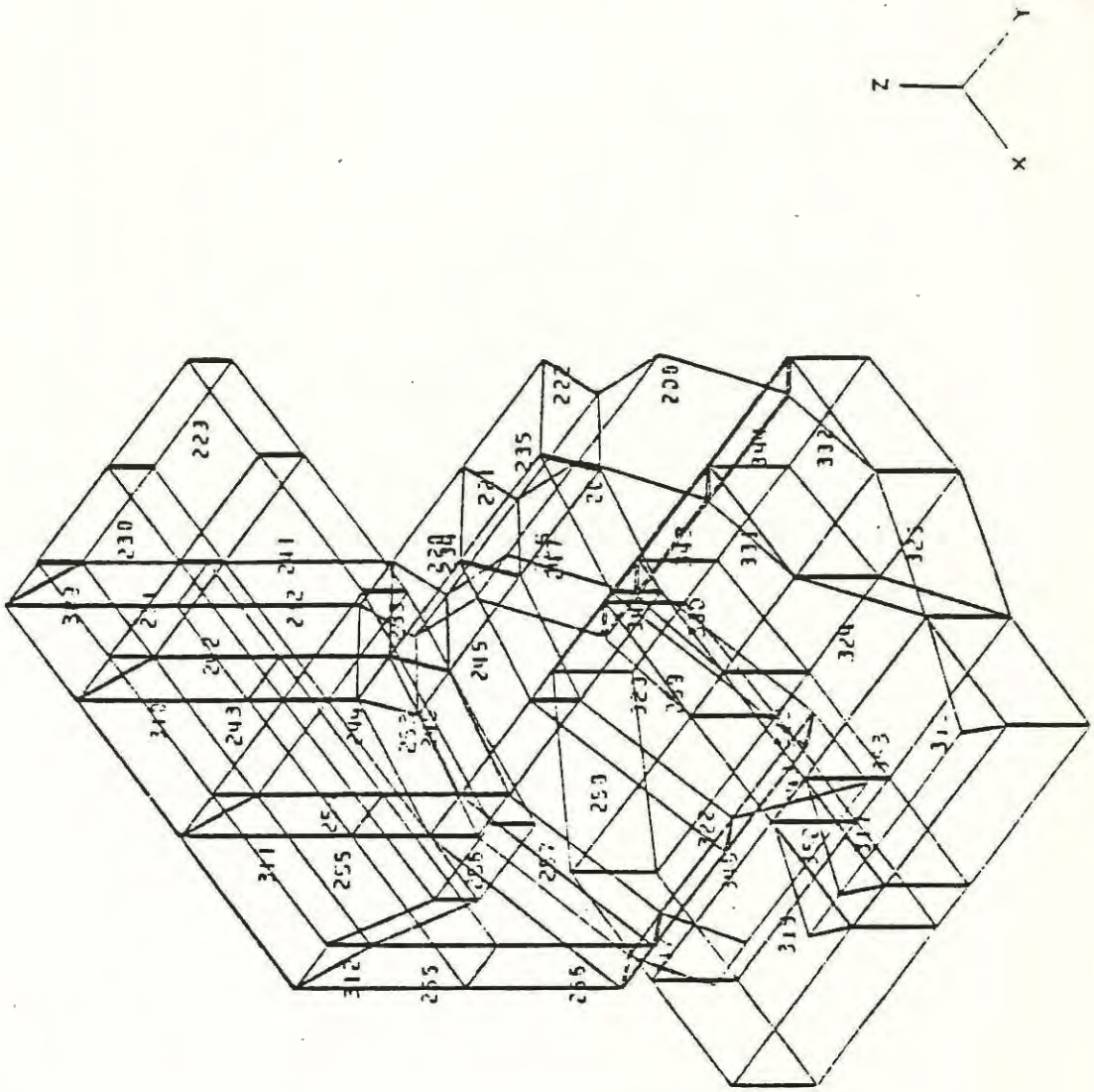

Figure 11 - SIDEFRAME REAR
Section 2A

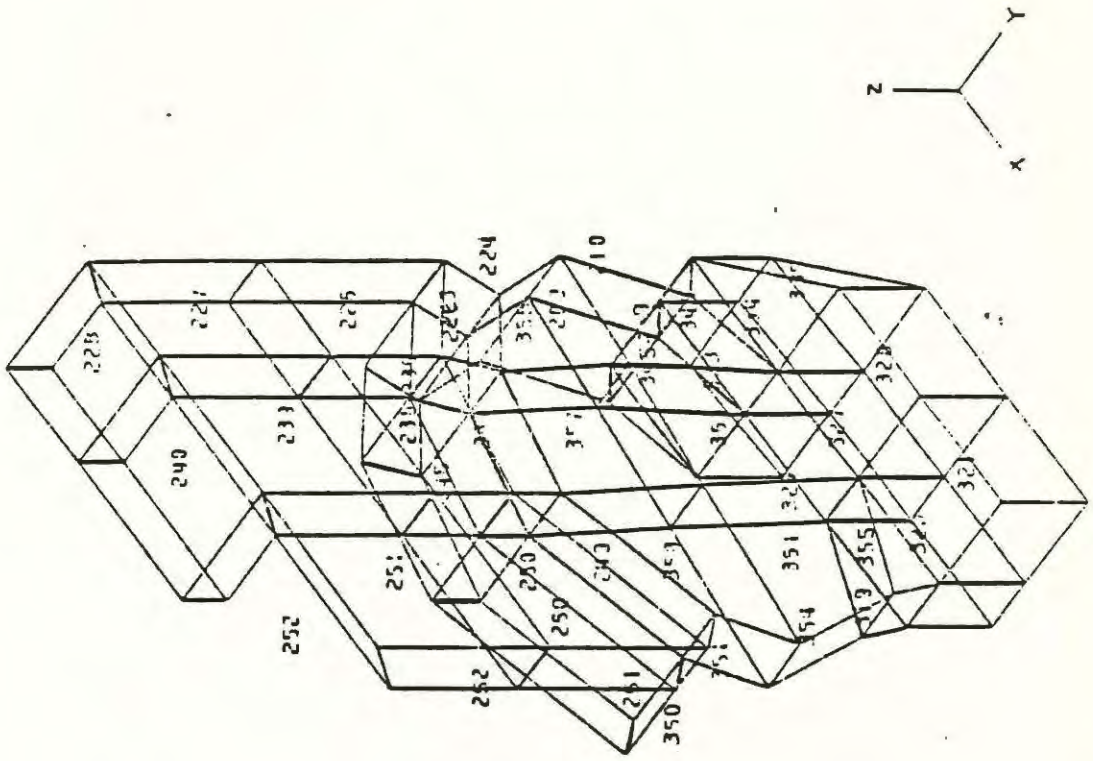

Figure 12 - SIDEFRAME REAR
Section 2B

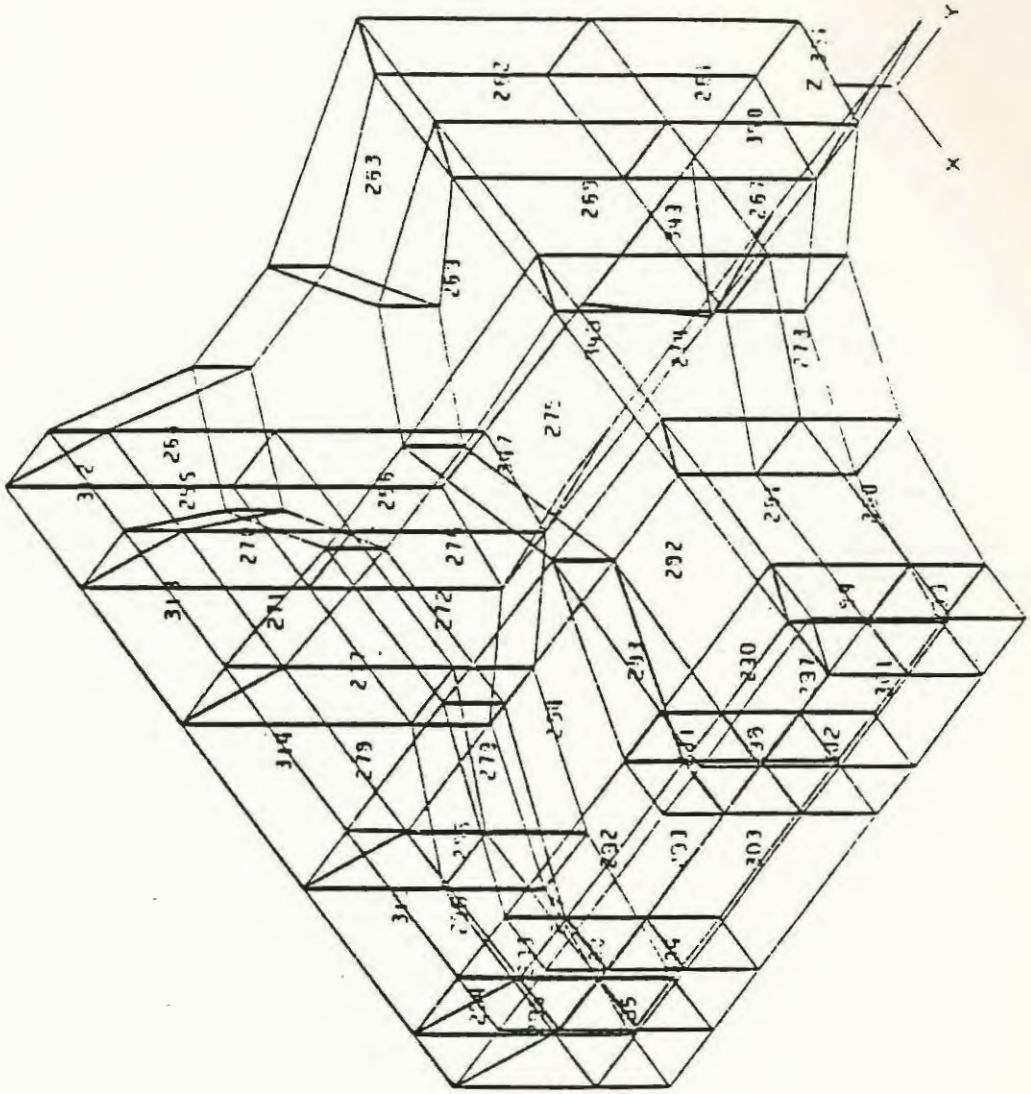

Figure 13 - SIDEFRAME REAR - Section 3

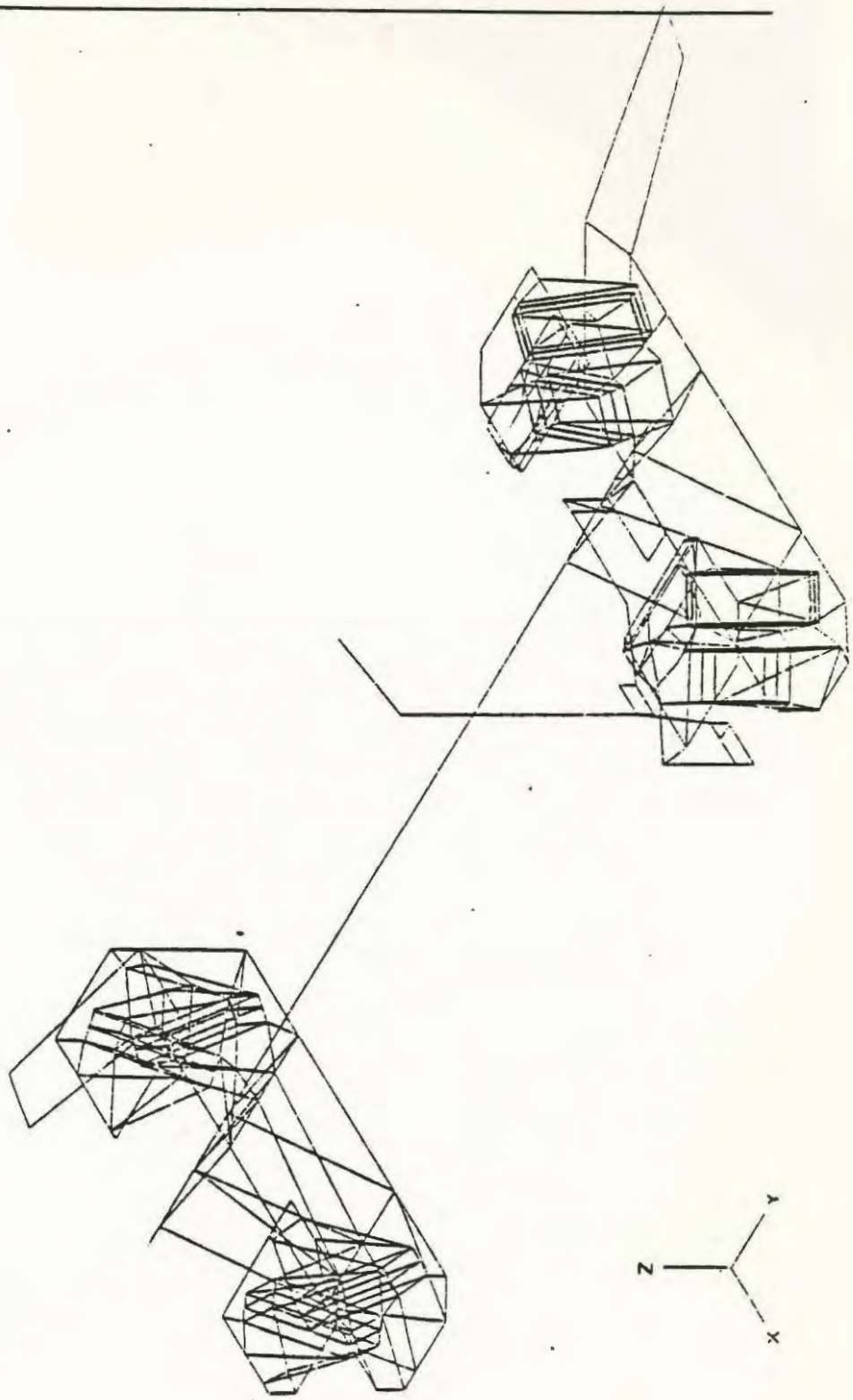

Figure 14 - TRUCK JOURNAL HOUSINGS

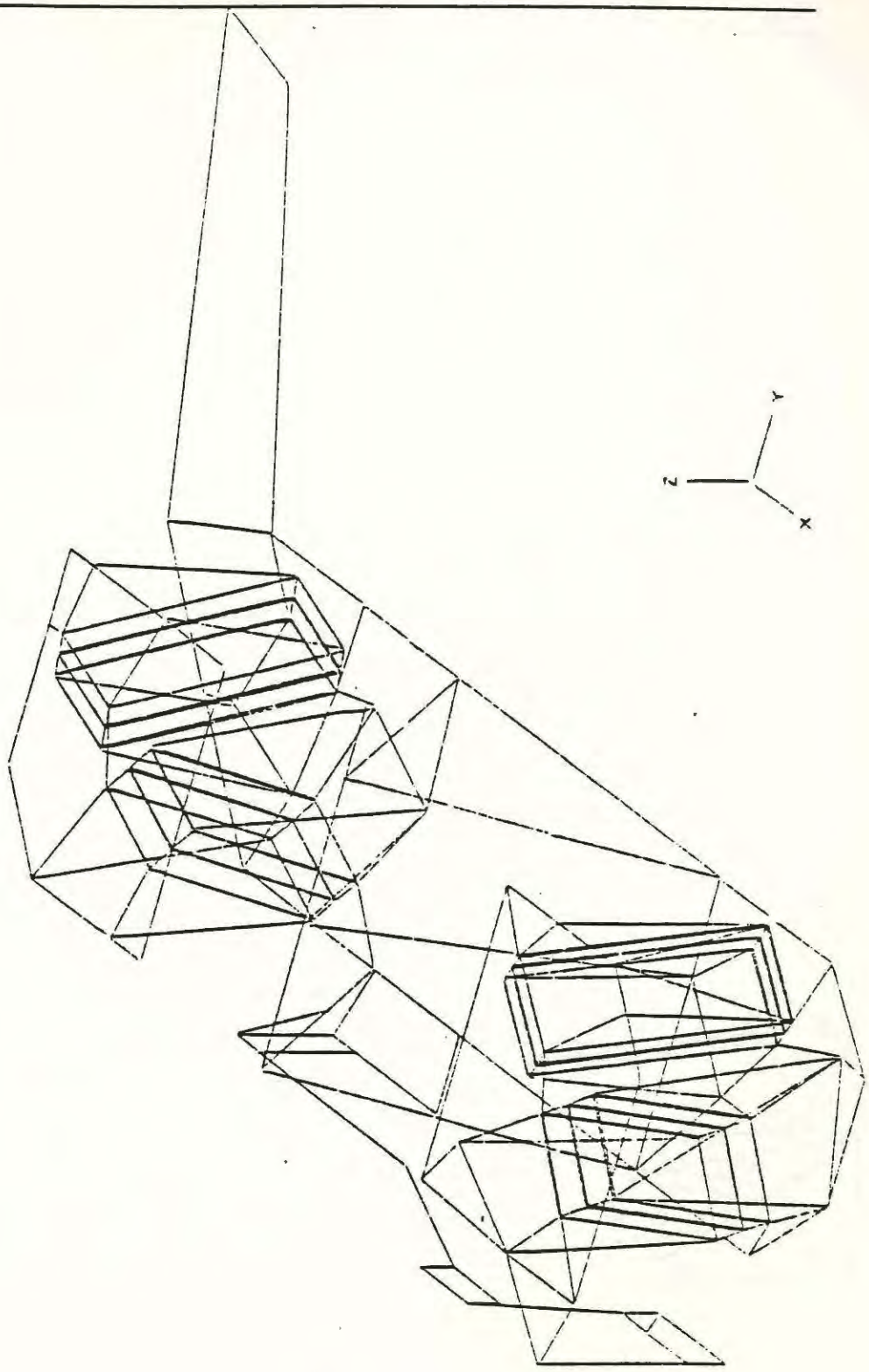

Figure 15 - JOURNAL HOUSING - Steering Side.

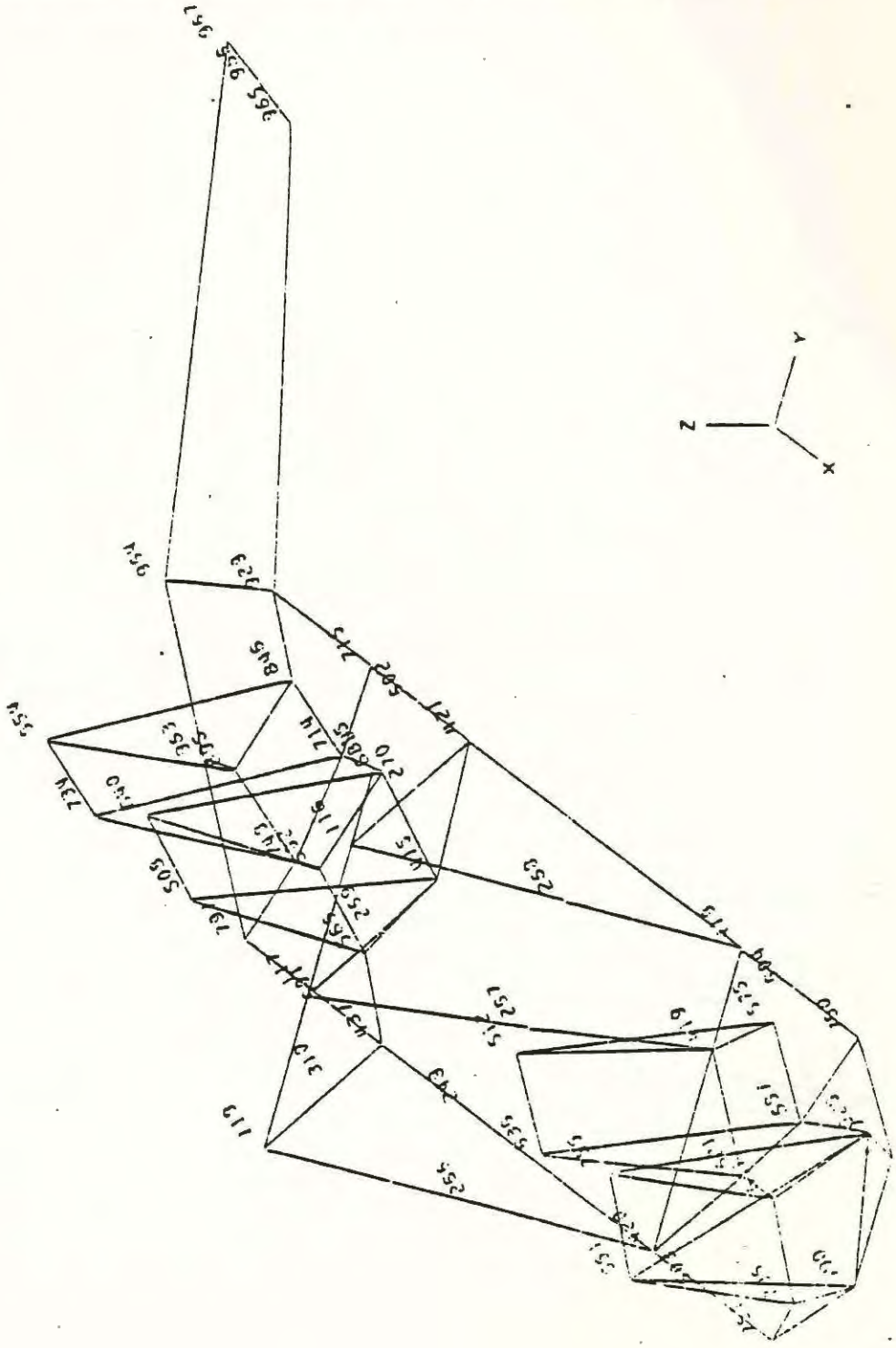

Figure 16 - JOURNAL HOUSING - Steering Side; Element Group 4.

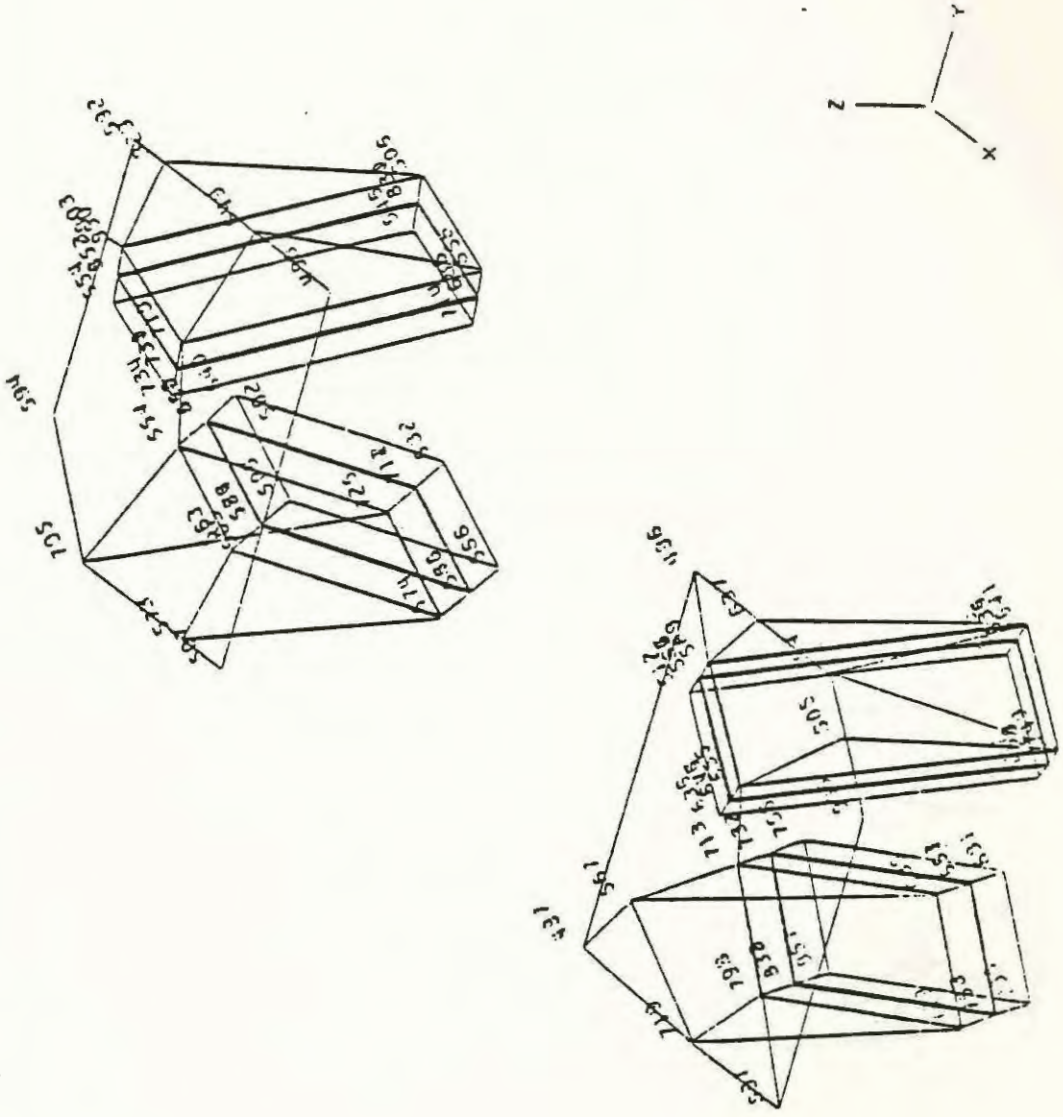

Figure 17 - PRIMARY SPRING PADS - Steering Side; Element Groups 5,6,7,8.

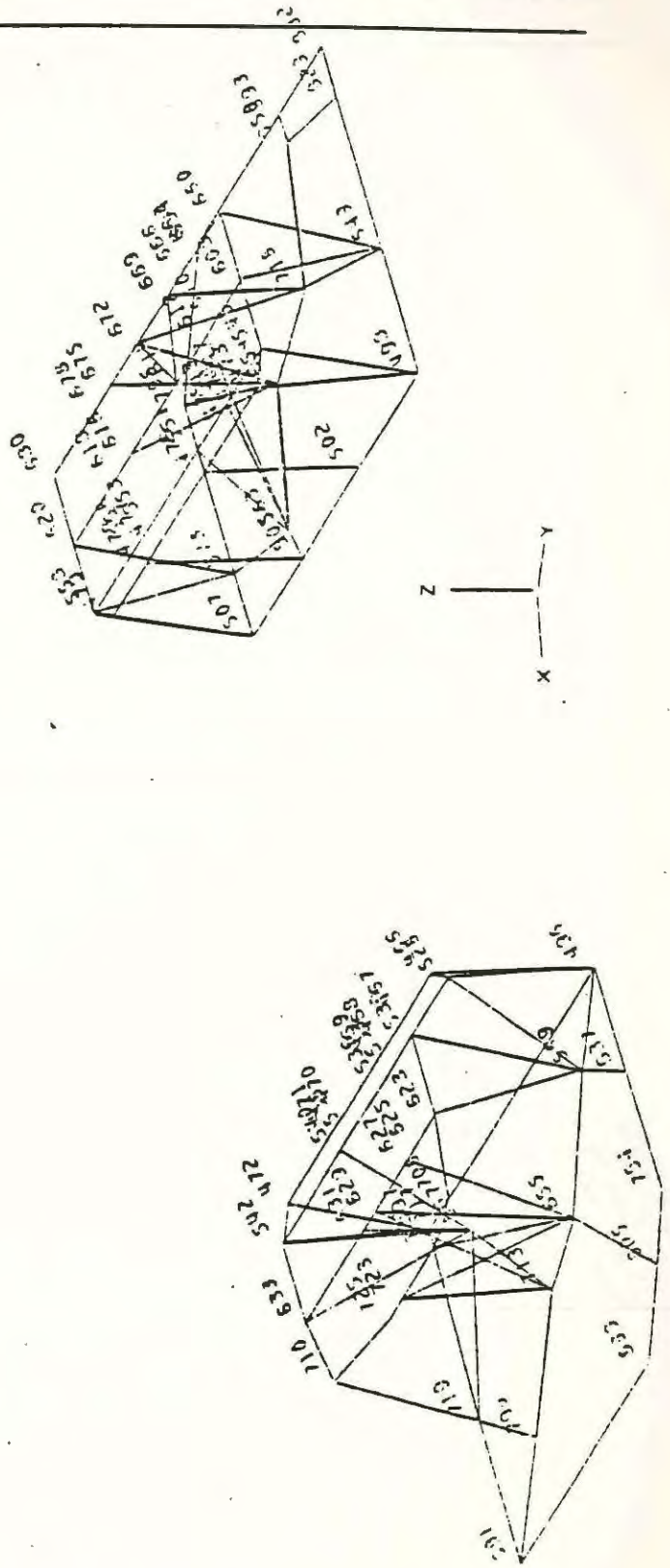

Figure 18 - INTERFACING BETWEEN HOUSING AND SIDEFRAME - Element Group 9.

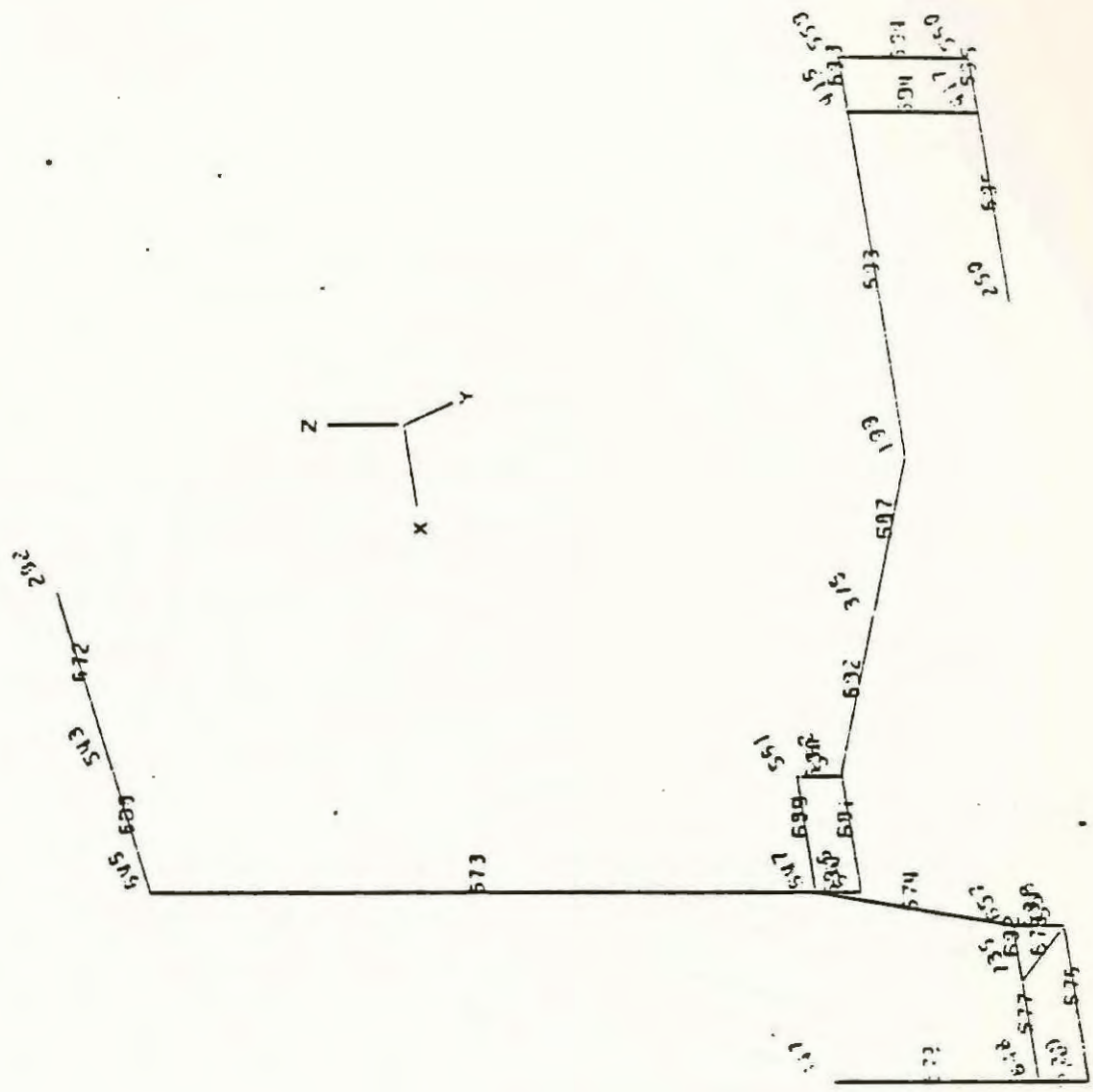

Figure 19 - STEERING LINKAGE - Element Groups 10,11.

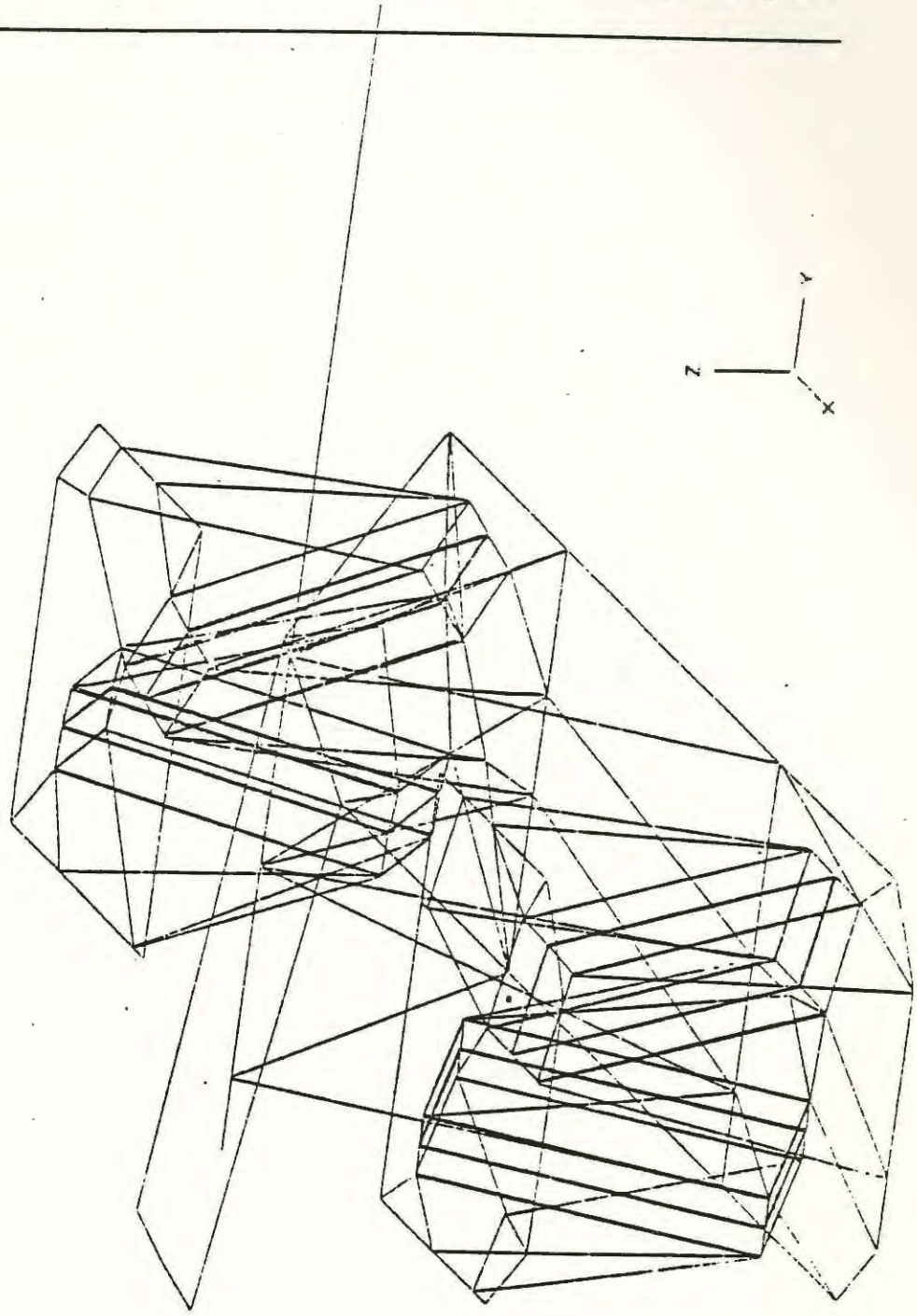

Figure 20 - JOURNAL HOUSING - Non-steering Side.

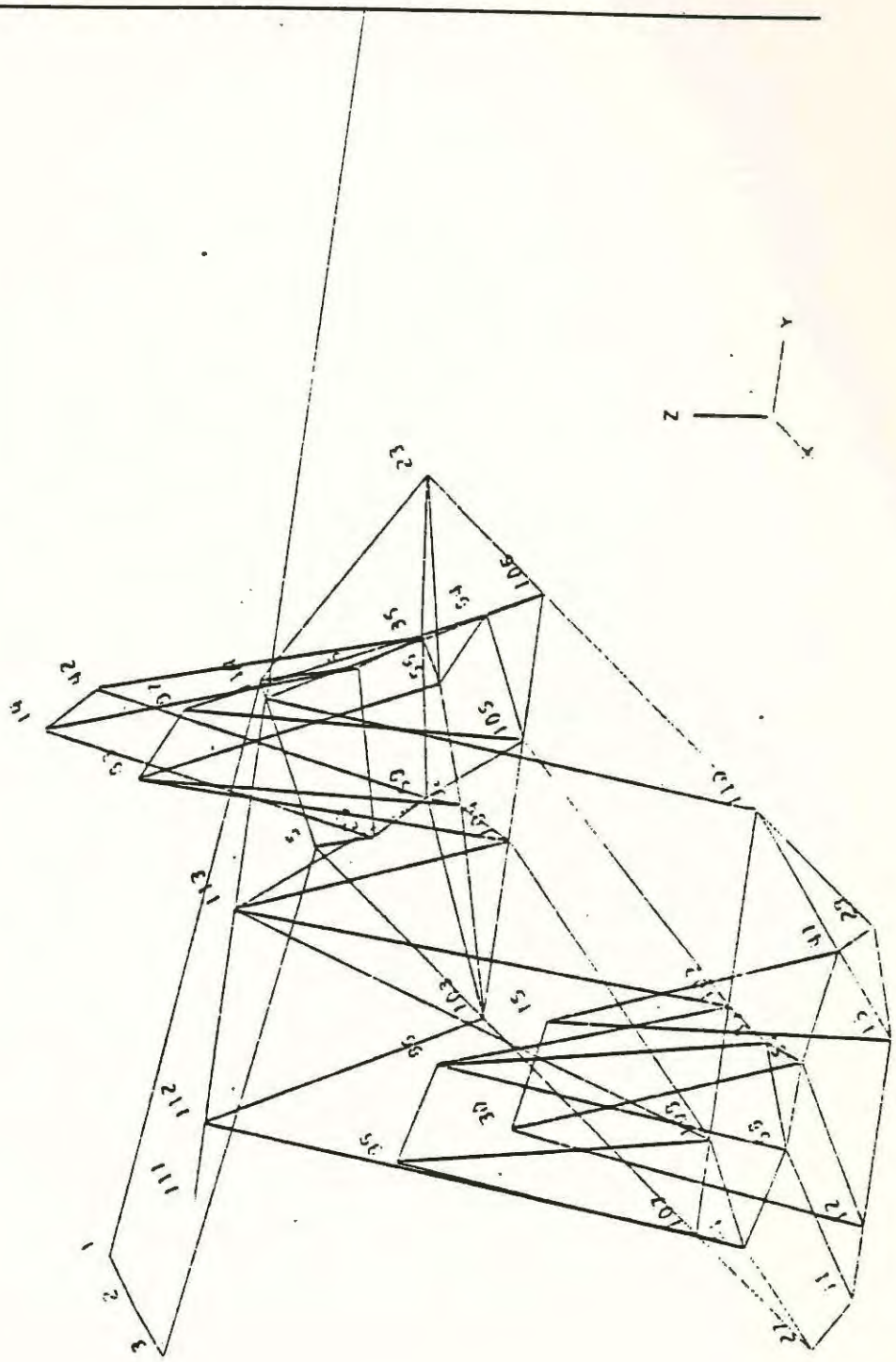

Figure 21 - JOURNAL HOUSING, NON-STEERING SIDE - Element Group 12.

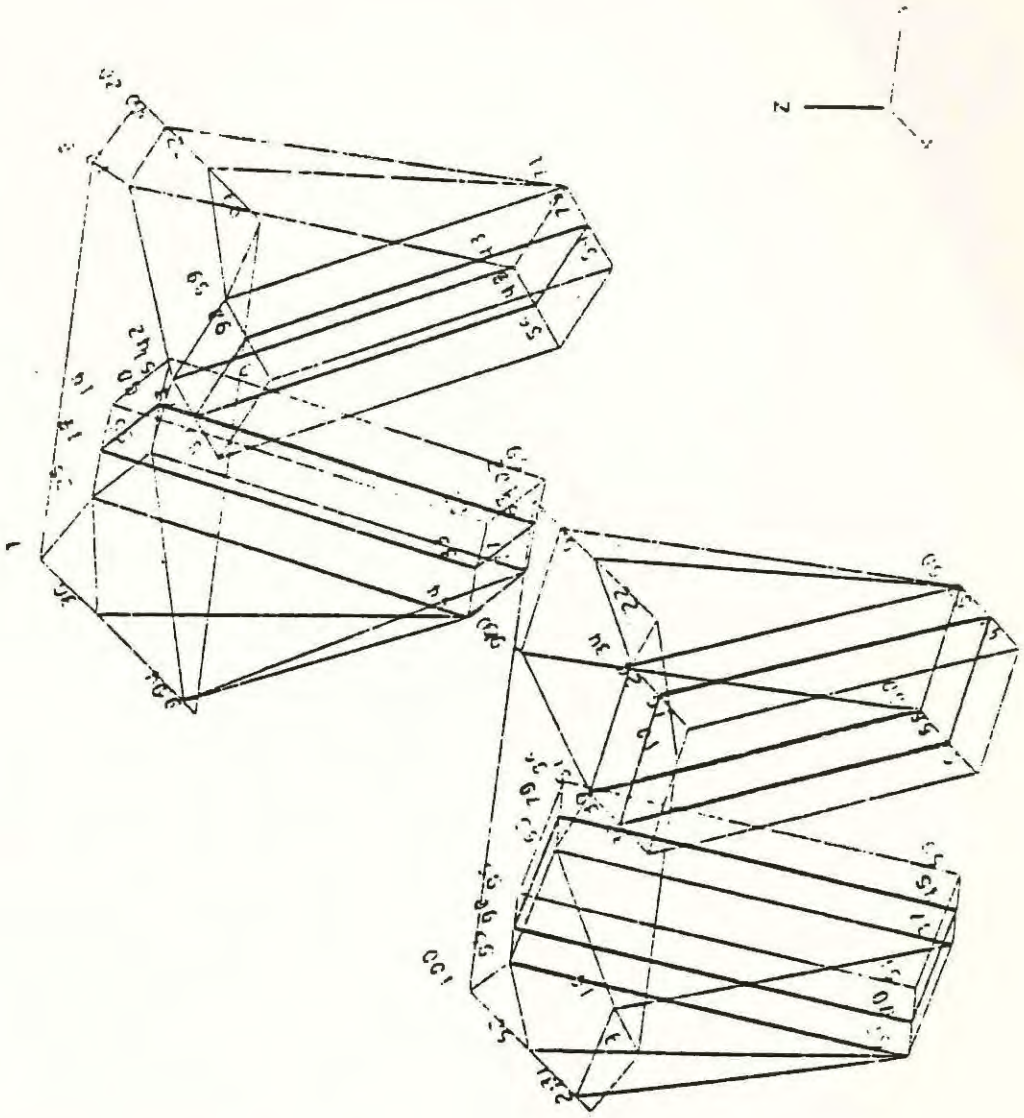

Figure 22 - PRIMARY SPRING PADS, NON-STEERING SIDE - Groups 13,14,15,16.

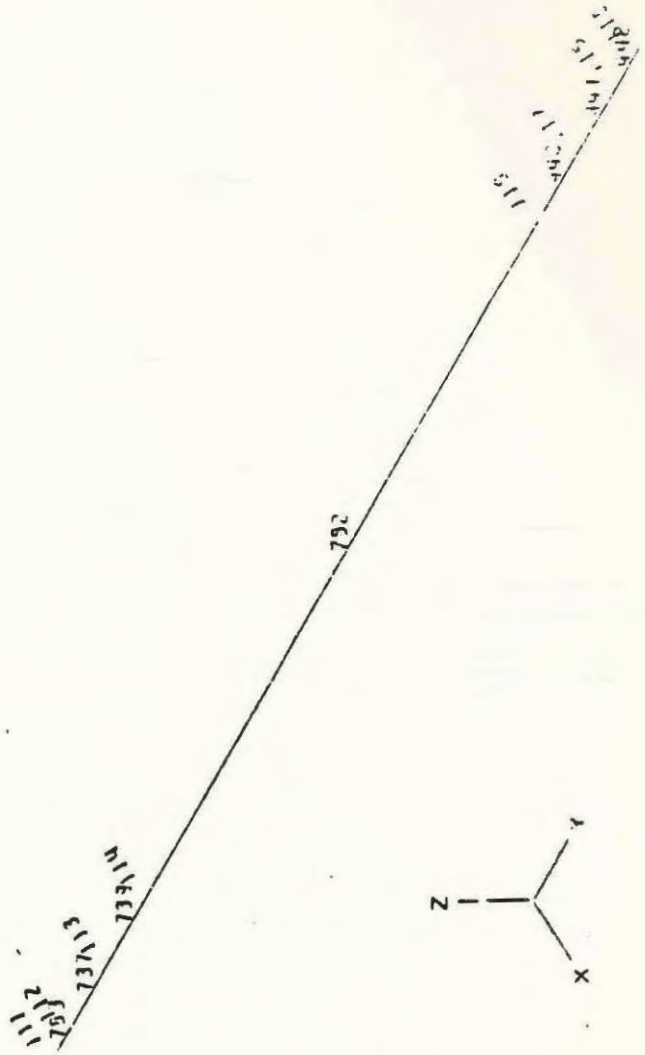

Figure 23 - TRUCK AXLE.

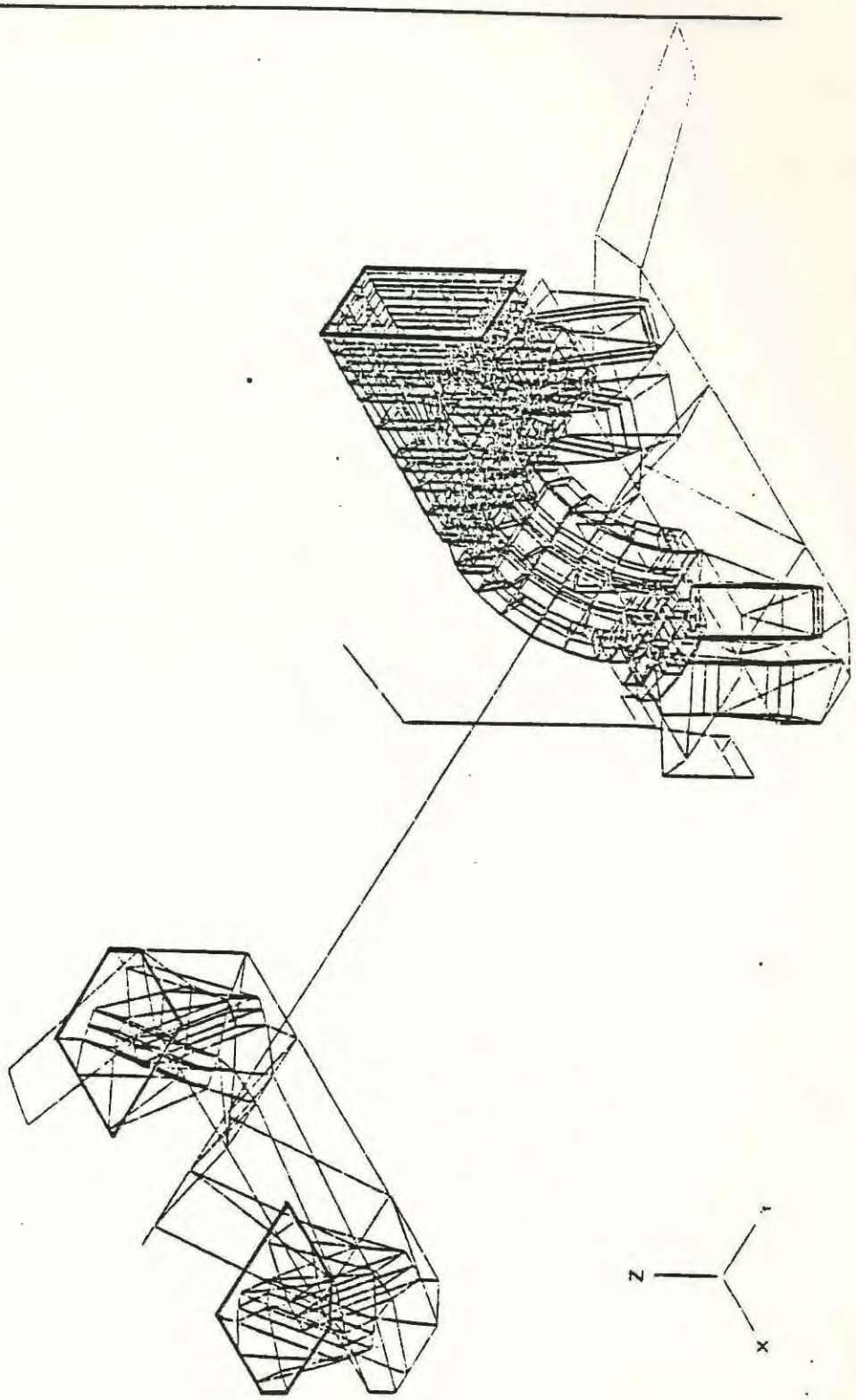

Figure 24 - MODEL BOUNDARY CONDITIONS
- All fixed boundary conditions
shown with heavy lines.

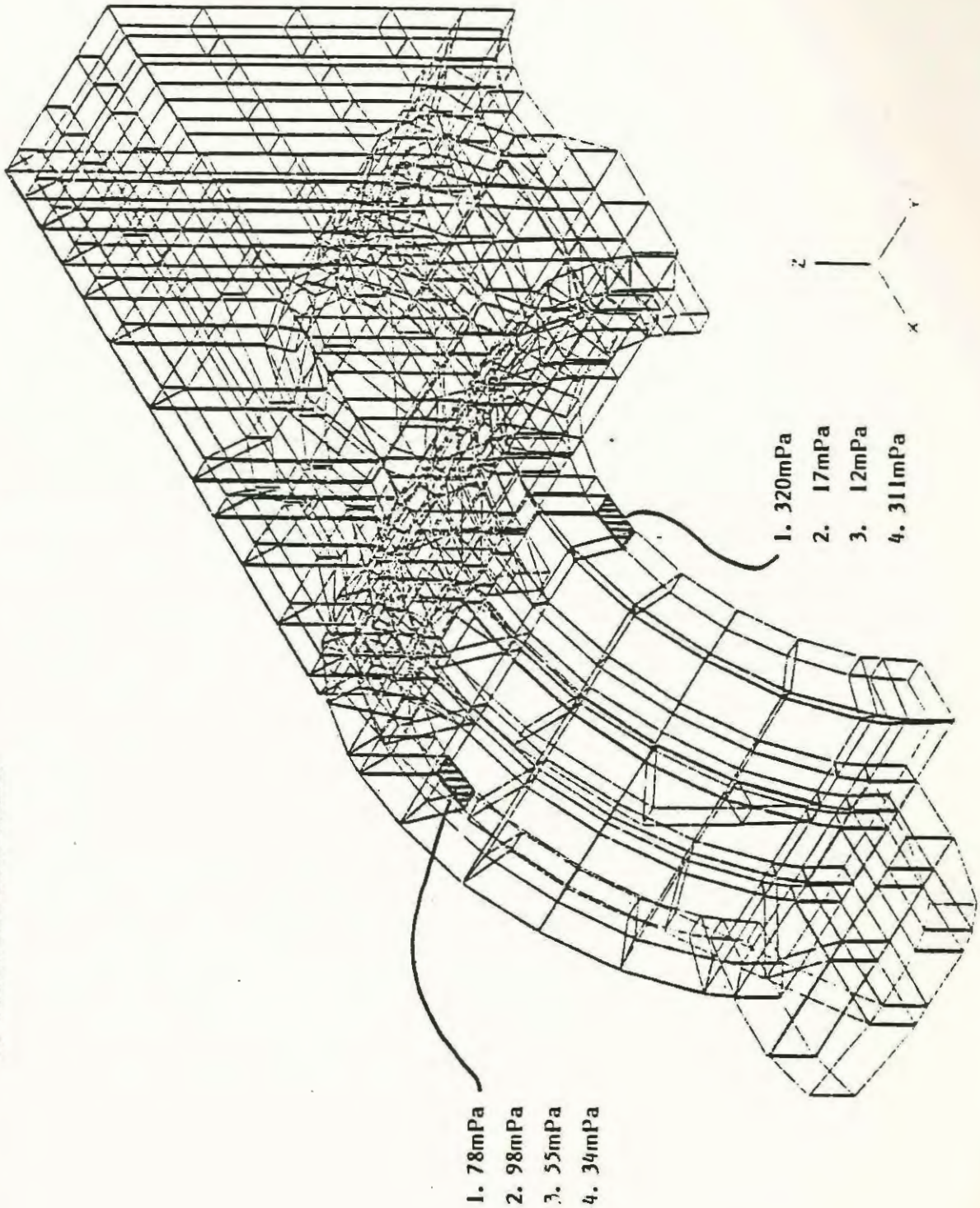

Figure 25 - VON MISES STRESSES FOR THE FOUR LOAD CASES ON SELECTED SURFACES.

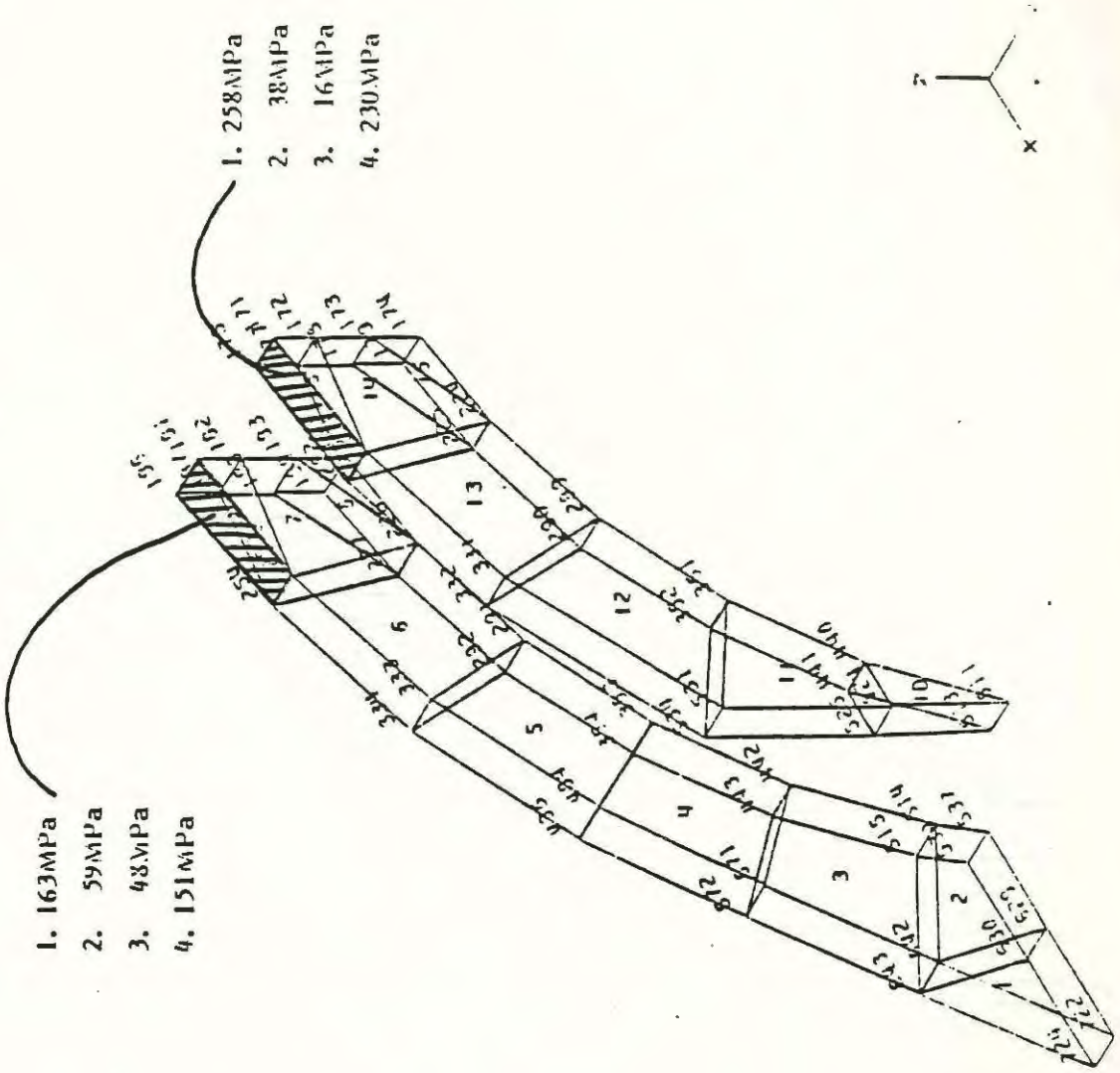

Figure 26 - VON MISES STRESSES FOR THE FOUR LOAD CASES.

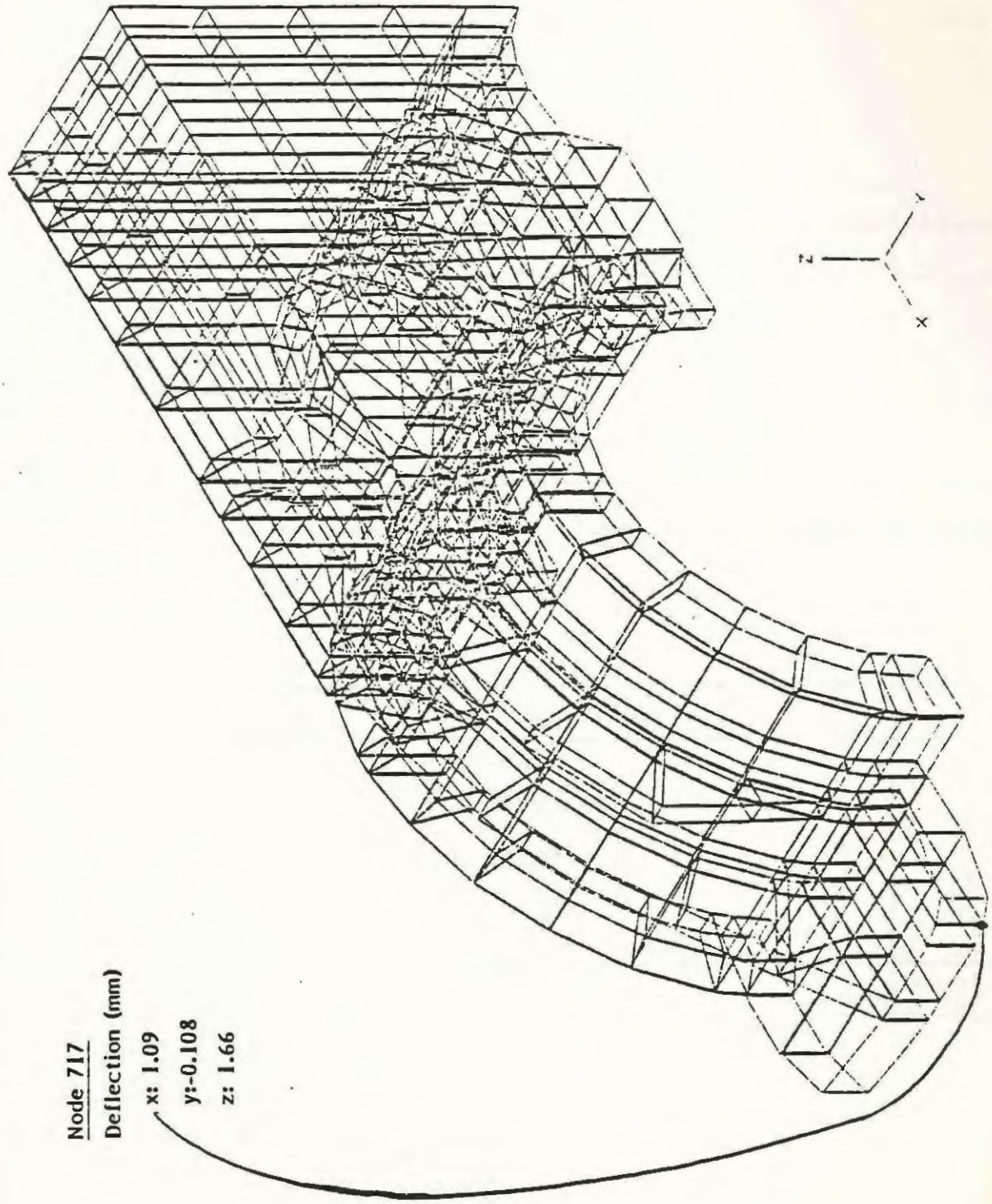

Figure 27 - MAXIMUM SIDEFRAME DEFLECTION.

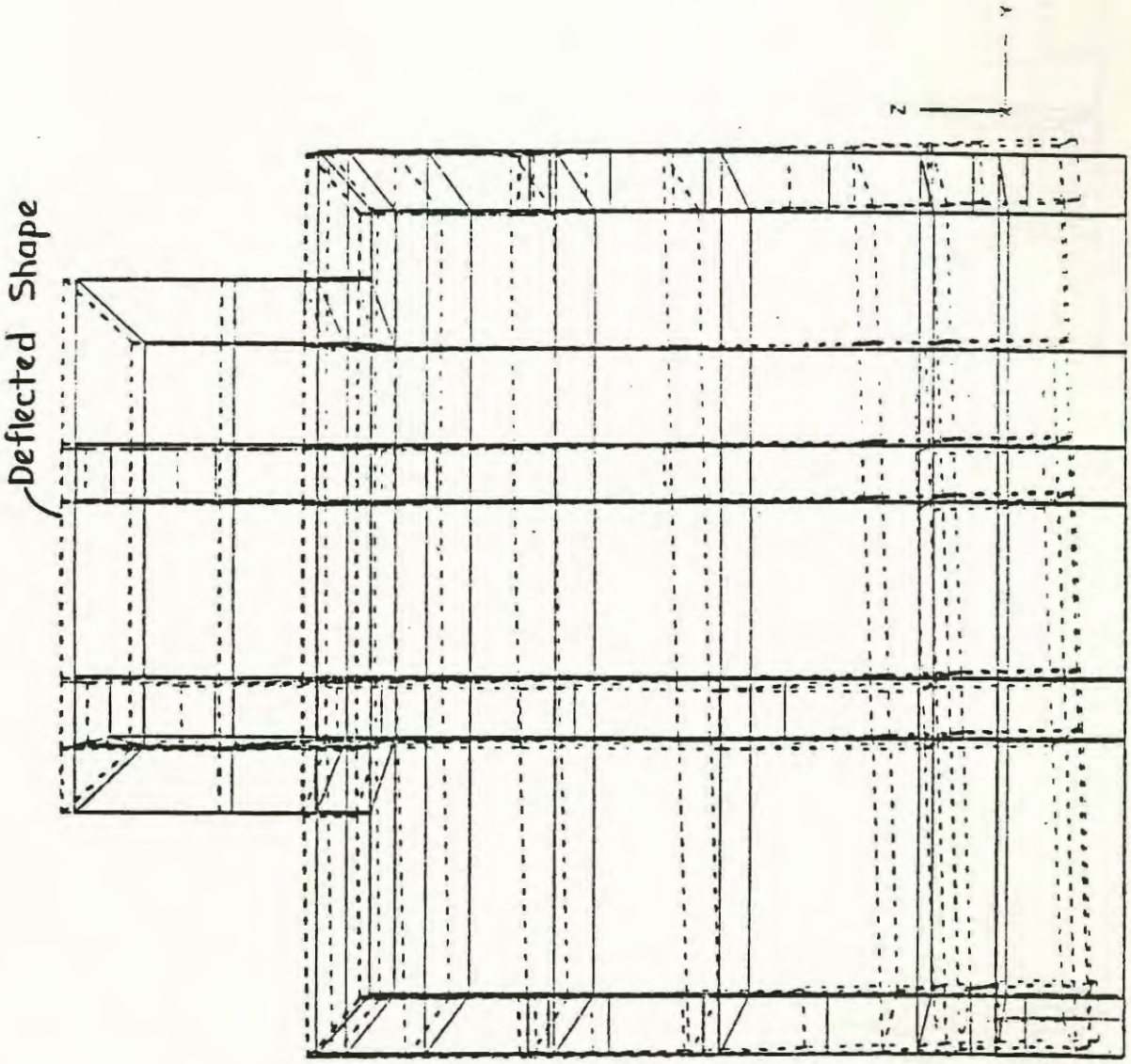

Figure 28

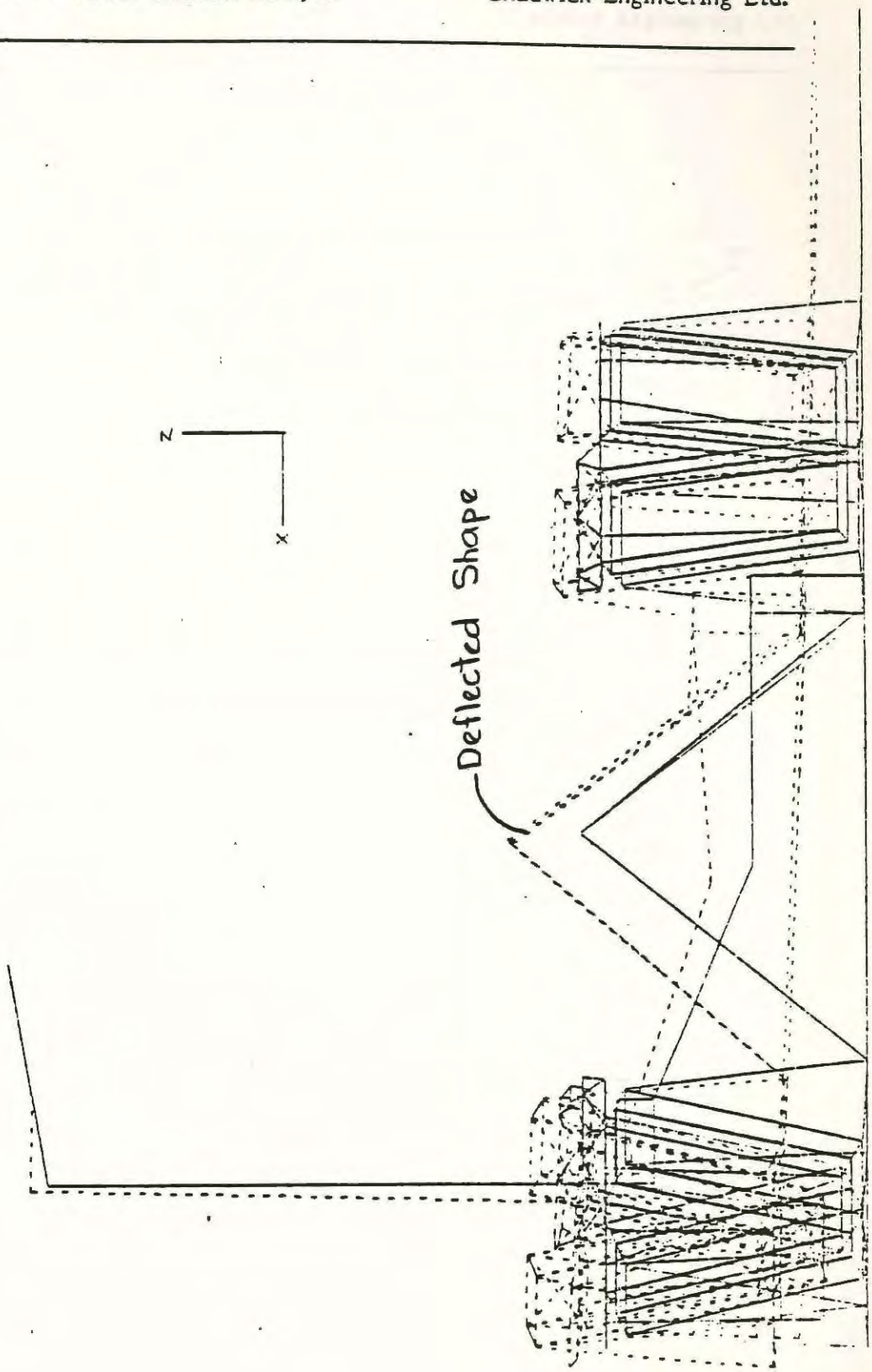

Figure 29

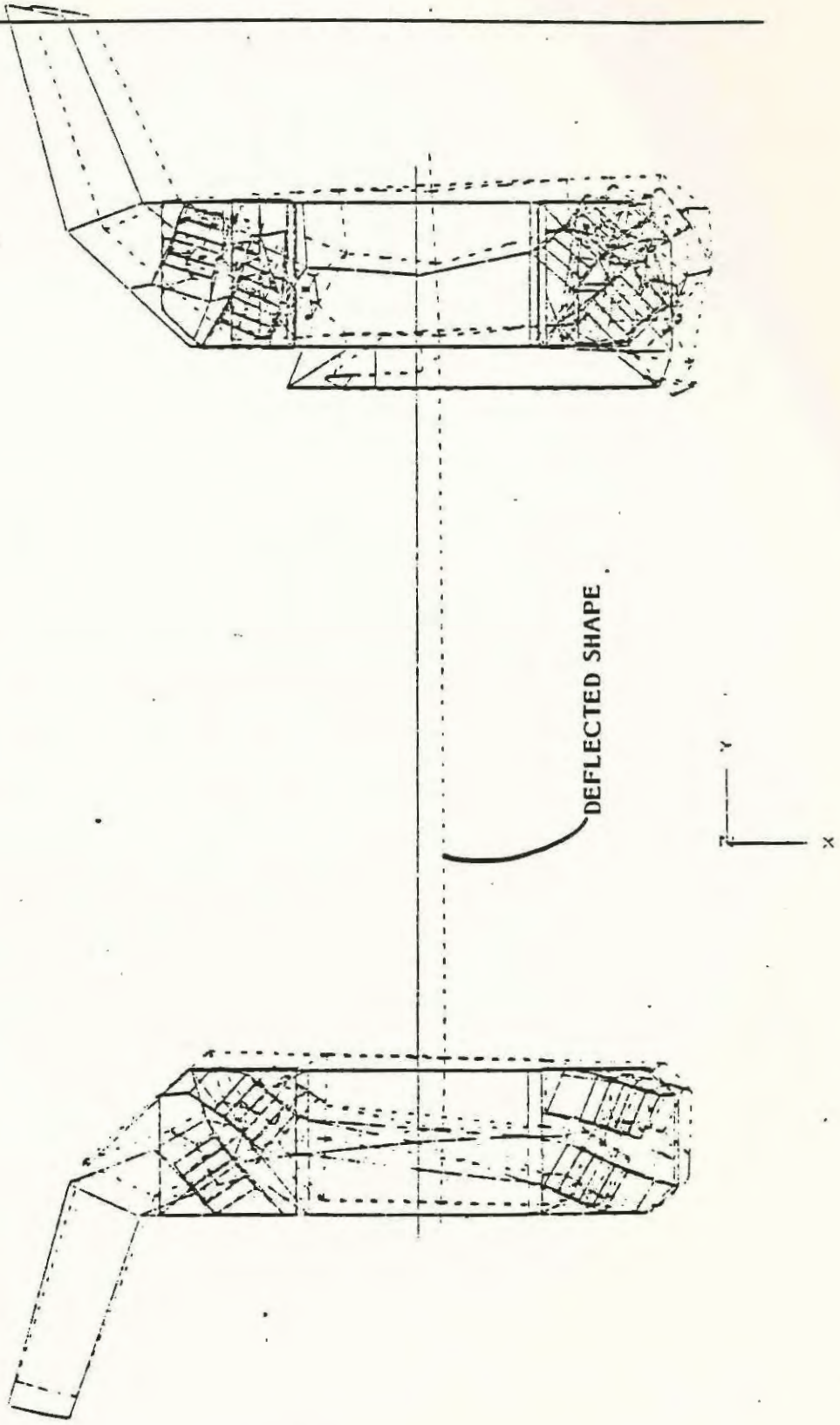

Figure 30

Figure 31 - STEERING LINKAGE FORCES FOR THE FOUR LOAD CASES

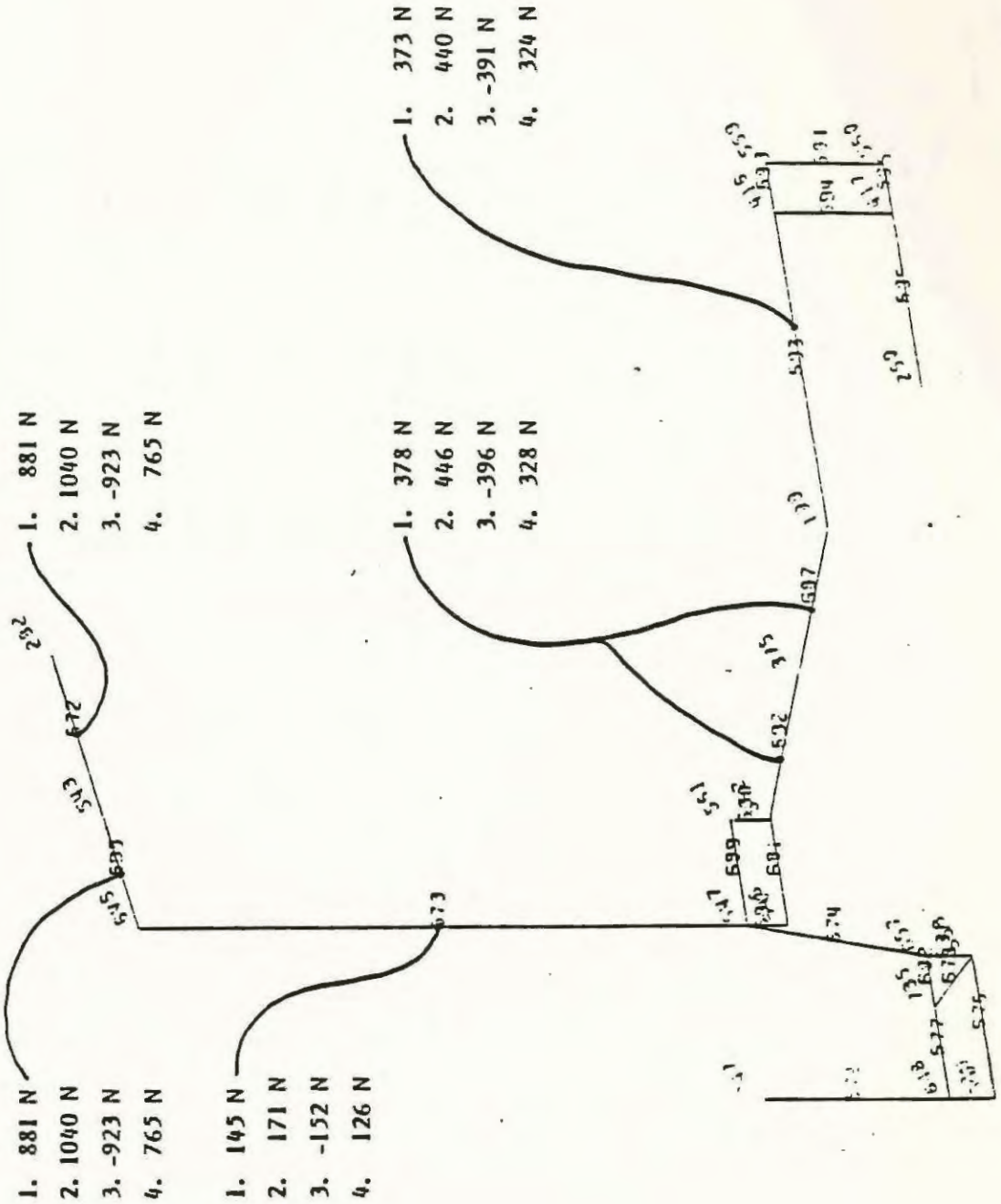

NODE	DEFLECTION (mm)		
	x	y	z
111	0.646	0.442	3.43
112	0.672	0.442	3.42
113	0.743	0.442	3.41
114	0.814	0.441	3.39
118	0.687	0.427	3.40
117	0.561	0.426	4.13
116	0.436	0.426	4.26
115	0.372	0.426	4.33

Figure 32 - AXLE DEFLECTIONS - Load Case 1.

Figure 33 - AXLE BENDING MOMENTS - Load Case 1
Vertical & Horizontal moments combined.

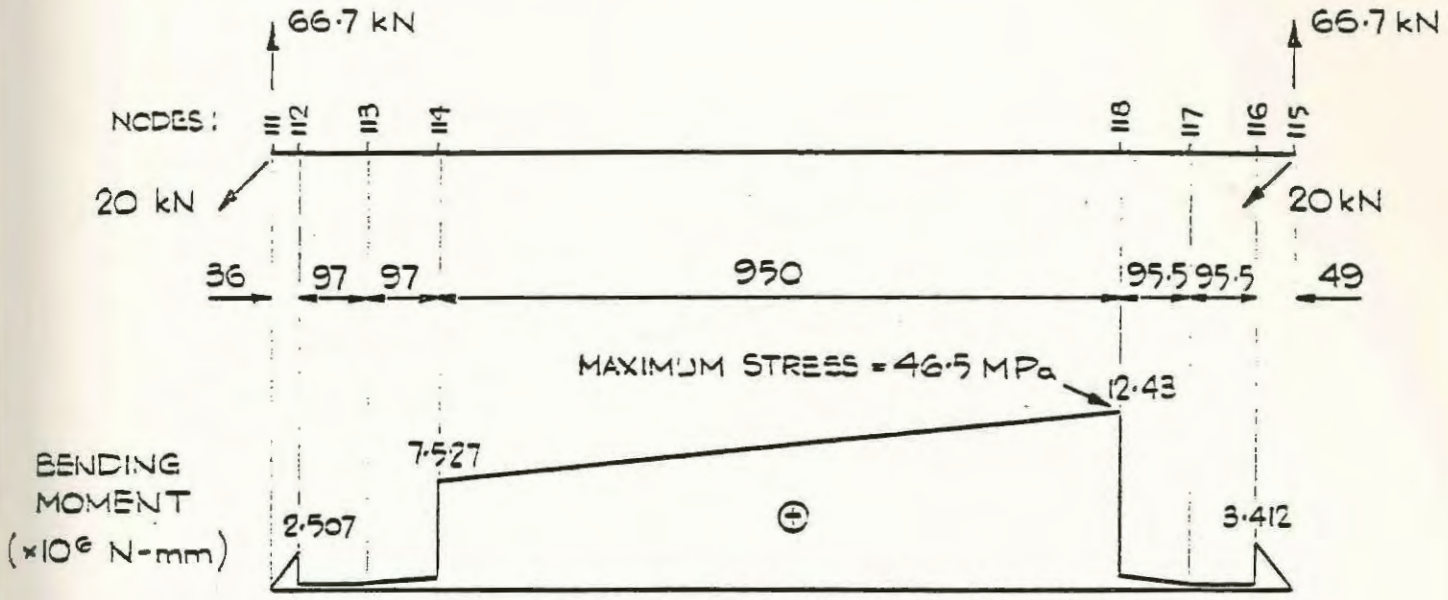

Consider as a simply supported beam:

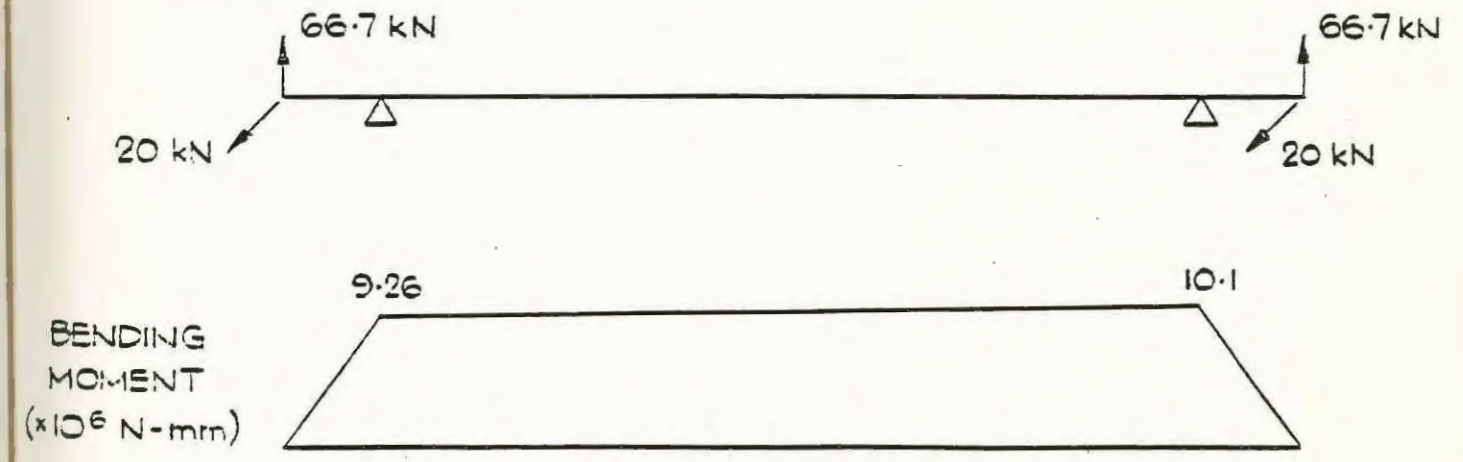

APPENDIX C

Part One The Analysis and Findings

Subpart B Axle

AXLE

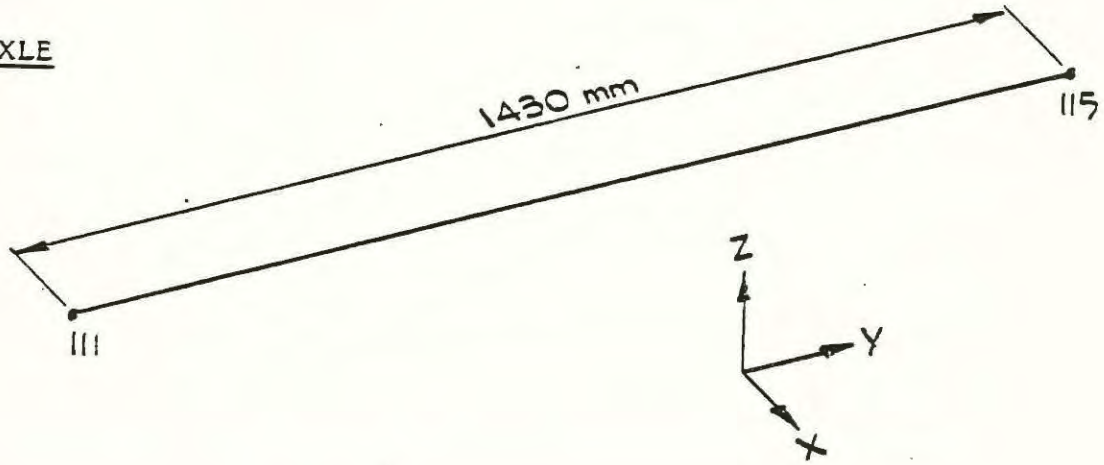

Area (5.5 inch dia) $= \pi r^2 = 15.39 \times 10^3$ mm^2
(140mm)

$I_{xx} = I_{zz} = \frac{\pi r^4}{4} = 18.86 \times 10^6$ mm^4

$I_{yy} = J = 2I_{xx} = 37.71 \times 10^6$ mm^4

: However, J was chosen to be relatively small, such that the proper behaviour between the housing and the axle could be modelled.

$J = 100$mm^4

APPENDIX C

Part One The Analysis and Findings

Subpart C Spring Pads

SPRING PADS.

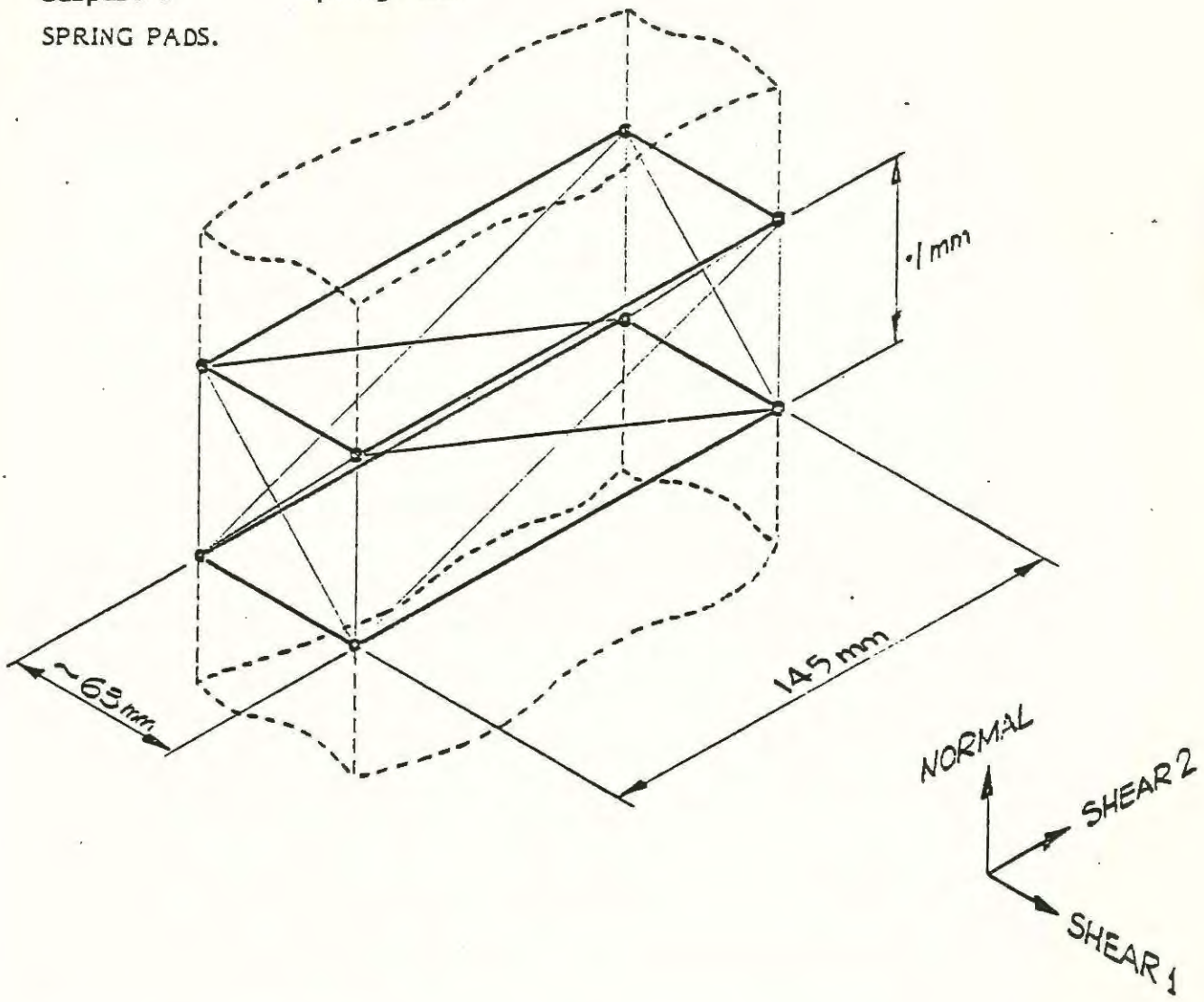

Given spring pad stiffnesses

normal	280,000 lb/in	= 49033 N/mm
shear	2,600 lb/in	= 455 N/mm

Calculation of Equivalent Truss Element Stiffnesses

All elements act within .1mm of the centre line of the pad.

NORMAL

$$K_N = \frac{49033}{4} = \frac{AE}{L} = \frac{AE}{.1}$$

Therefore $AE = 1226.N$

with $E = 1000\ N/mm^2$ Therefore $A = 1.226mm^2$/per element

SHEAR 1

$$K_{SI} = \frac{455}{4} = \frac{AE}{L} = \frac{AE}{63.25}$$

Therefore $AE = 7195.N$

with $E = 1000\ N/mm^2$ Therefore $A = 7.195mm^2$/per element

SHEAR 2

$$K_{S2} = \frac{455}{4} = \frac{AE}{L} = \frac{AE}{145}$$

Therefore $AE = 16494.N$

with $E = 1000\ N/mm^2$ Therefore $A = 16.494mm^2$/per element

A number of sample test runs were carried out to ensure that the pads behaved properly.

APPENDIX C

Part One The Analysis and Findings

Subpart D Steering Linkage

STEERING LINKAGE

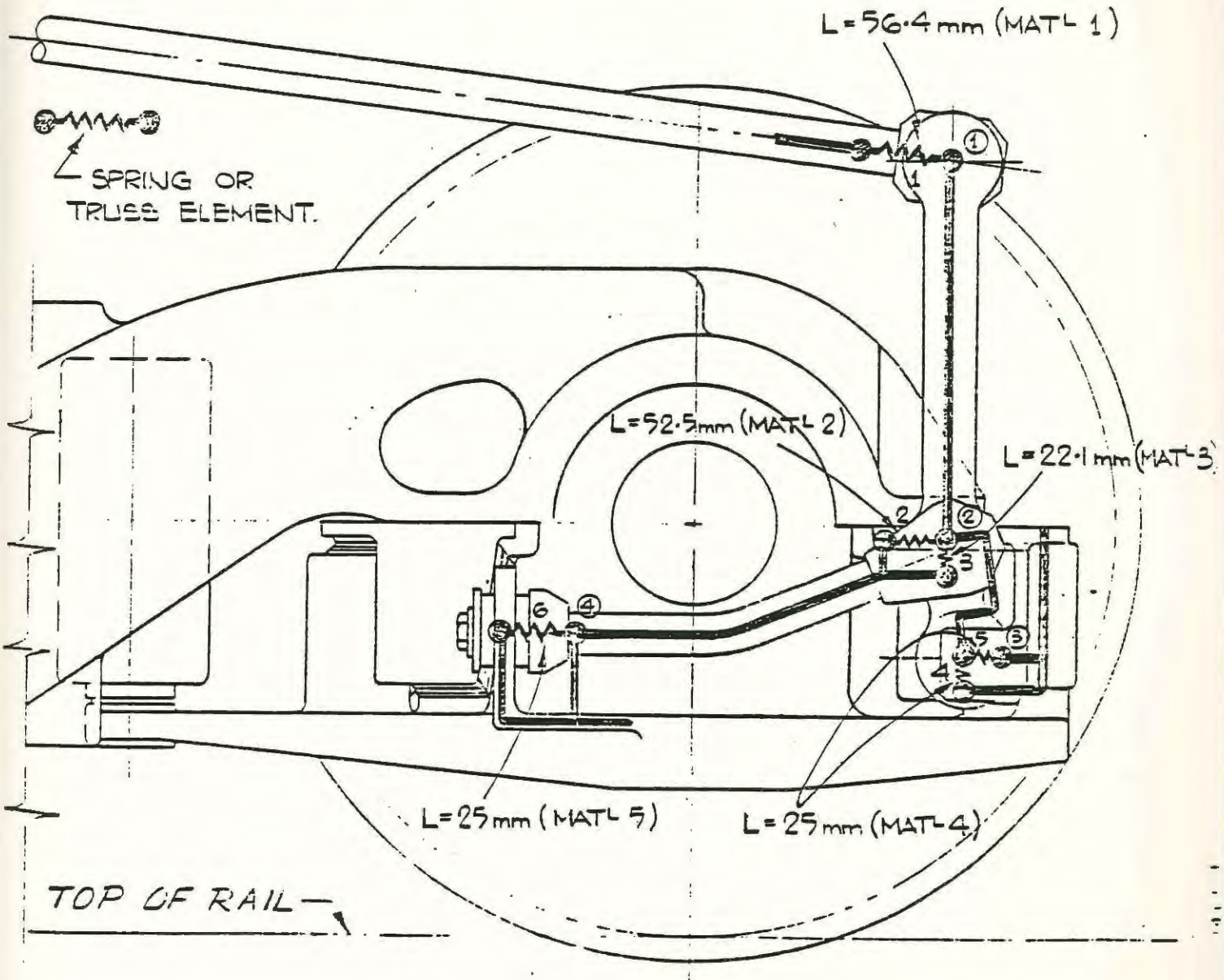

Given radial stiffnesses at

①	24,500 lb/in
②	49,000 lb/in
③	49,000 lb/in
④	490,000 lb/in

Calculation of equivalent spring or truss stiffnesses

These calculations were carried out in a similar manner to the pad calculations using K = AE/L and E = 1000.

Consequently the following areas were input to achieve the proper bushing stiffnesses;

Truss Element	Length(mm)	K(N/mm)	A(mm^2)
1	56.4	4290.	242.
2	52.5	8581.	450.5
3	22.1	8581.	189.6
4	25.0	8581.	214.5
5	25.0	8581.	214.5
6	25.0	85807.	2145.0

Chadwick
Engineering Ltd

:D Sherwood Avenue, Amherstview, Ontario K7N 1N2 (613) 384 2866

APPENDIX C

Part Two Sideframe and Reinforcement

WMATA SIDEFRAME
FINITE ELEMENT ANALYSIS

Approved by: D. Chadwick

D. Chadwick, P. Eng.,
President,
Chadwick Engineering Ltd.

Date: 14 Oct 83

TABLE OF CONTENTS

1. REVIEW OF EXISTING WMATA SIDEFRAME ANALYSIS.

A finite element analysis was carried out and presented in a report entitled 'WMATA SIDEFRAME - Finite Element Analysis', dated July 22, 1983. The results of this analysis indicated that the sideframe and journal housings underwent excessive twisting and the entire sideframe experienced maximum von Mises stresses in the order of 46,000 psi.

Consequently it was decided to reinforce the existing sideframe and add a tie bar with bushings at each end between the journal housings in an attempt to reduce the twisting and high stresses.

2. OBJECTIVE OF ANALYSIS.

The objective of this analysis was to determine the effect on the stresses of reinforcing the existing sideframe and adding the tie bar.

3. MODIFICATIONS.

3(i) Sideframe

From the first analysis, the maximum stress locations and values were determined as shown in Figure 1, consequently attention was primarily focused on increasing the cross-sectional properties in this region. In an attempt to choose an appropriate section, a series of hand calculations were carried out for two possible modifications shown in Subpart B in Figure A2-1 and Figure A2-2. Modification 1 consisted of a 5.625 in. by 5.5 in. cast section while Modification 2 had overall dimensions of 6.625 in. by 5.5 in.

Based on these initial, approximate calculations, either modification appeared satisfactory in reducing the stresses to an acceptable level. It was decided to use modification 1 consequently a modified sideframe drawing was prepared from which

the current finite element model illustrated in Figure 2 was changed as shown in Figures 3a, 3b and 3c.

3(ii) Tie Bar

The initial analysis indicated that the sideframe underwent severe twisting about the longitudial axis and the journal housing toed out under a vertical load. (Figure 8). As a result, a tie bar was added between the journal housings with bushings at each end having a stiffness of 600,000 lb/in: This change was accomplished by adding a bar or truss element with an equivalent stiffness of 300,000 lb/in as shown in Figure 4.

4. RESULTS OF ANALYSIS

It is important to note that the initial investigation of the journal housing and sideframe was carried out in one analysis. Due to the size and complexity of the modified sideframe problem and resulting computational costs it was decided that the analysis would be split into two parts. The first part was an analysis of the journal housing subjected to the wheel loads with the top pad plates, interfacing the sideframes on both sides, being completely fixed out. The second part consisted of an analysis of the sideframe on the steered side subjected to the opposite of the reactions on the top pads obtained from the first analysis. This approach was felt to be conservative since higher forces would be atracted to the stiffer outboard pad areas on both sides due to the rigidity of the support conditions compared to the stiffness of the sideframes.

4(1) Comparison of Deflections

The same load cases were applied as in the initial analysis and the resulting movement for each load case of the modified journal housing (with tie bar) and original journal housing can be compared by examining the following figures.

Load Case	Original housing	Modified housing
1. (combined)	Figure 5	Figure 9
2. (Longitudinal)	Figure 6	Figure 10
3. (Lateral)	Figure 7	Figure 11
4. (Vertical)	Figure 8	Figure 12

In comparing these genral motions little change is noted except as is evident in load case 4 where the toeing out was removed due to the tie bar. It was also observed that there was a slight overall increase in stiffness of the system and reduction in the twist of the journal housing.

4(ii) Comparison of Stresses

In order to examine the effect of the sideframe modification, a comparison was made between those regions in the original and modified sideframe that had stresses exceeding 55 MPa (8,000 psi). Figures 13 to 19 illustrate these high stress areas. It can be seen that a significant change has occurred with the critical stresses moving away from the largest, overstressed region at the centre of the original sideframe (Figures 13 to 17) to the outside of the sideframe flanges towards the outboard pad (Figure 18). Similarly high stresses occurred in the forward portion of the webs of the reinforcement (Figure 19).

In additiion to the above comparison, selected areas of the sideframe have been identified in Figures 20 and 21 on which principal stress values have been noted for the modified and original sideframe (bracketed numbers). From these numbers it is evident that all the significant stresses have been reduced however there are still regions on the modified sideframe within which the stresses are well in excess of 55 MPa.

It must be noted that the stresses were not reduced to the level that was anticipated. This fact lead to an examination of the individual pad normal forces and the resulting lateral and longitudinal forces from a pair of pads. It was found that the total normal force was extremely high as borne out by approximate hand calculations. Consequently, the individual pad orientation, although slightly different for each pad within a pair created relatively large lateral and longtudinal forces. This, in turn produced large unaccounted for torsional and additional bending stresses in the modified sideframe which were not employed in selecting the reinforcement size. Typical normal forces for each pad and reaction forces for each pair of pads are shown in figures 22 and 23 respectively.

5. CONCLUSIONS

The effect of reinforcing the sideframe and adding the tie bar reduced the stresses by approximately one-third in the initial regions of high stress. However they are still in excess of the 55 MPa maximum stress requirement of UTDC. In addition other areas became more highly stressed as a result of the change in the load path due to the reinforcement.

It should also be noted that during this analysis it was revealed that there are relatively high normal pad forces and consequently high resultant lateral and lontitudinal forces acting on the pad supports and sideframe respectively.

APPENDIX C

Part Two Sideframe and Reinforcement

Subpart A Figures

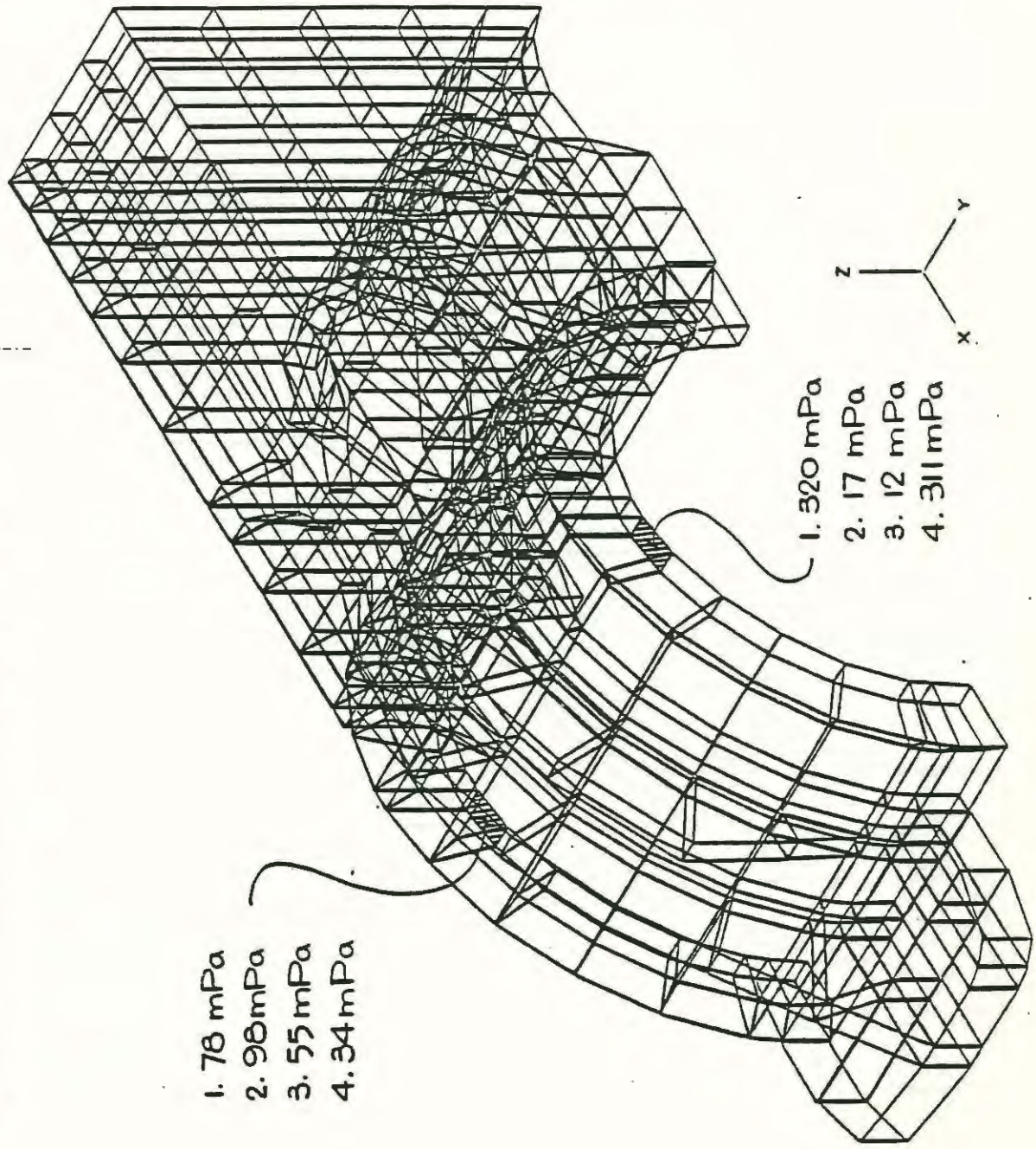

Figure 1 - VON MISES STRESSES FOR THE FOUR LOAD CASES ON SELECTED SURFACES - ORIGINAL SIDEFRAME

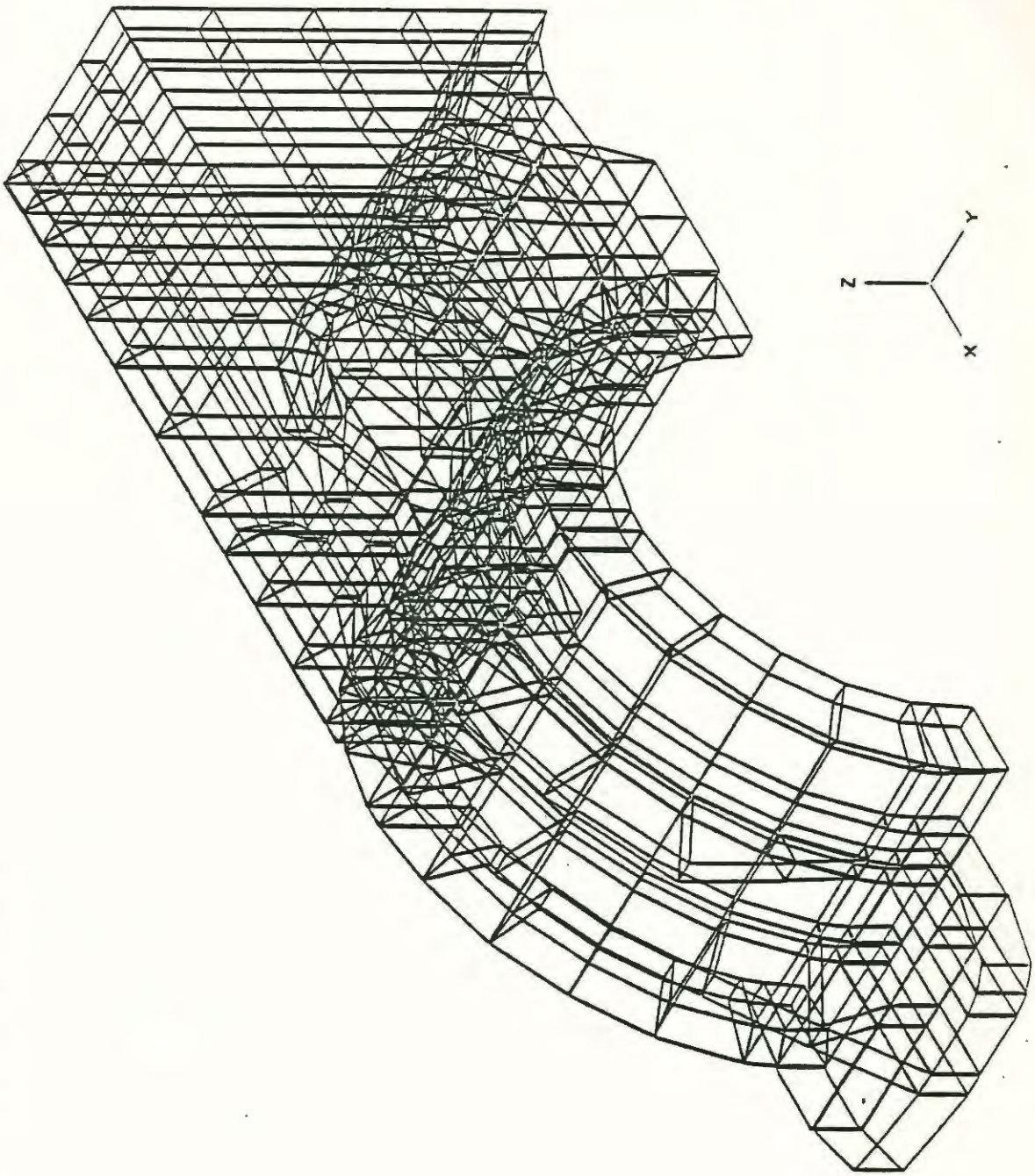

Figure 2 - ORIGINAL SIDEFRAME

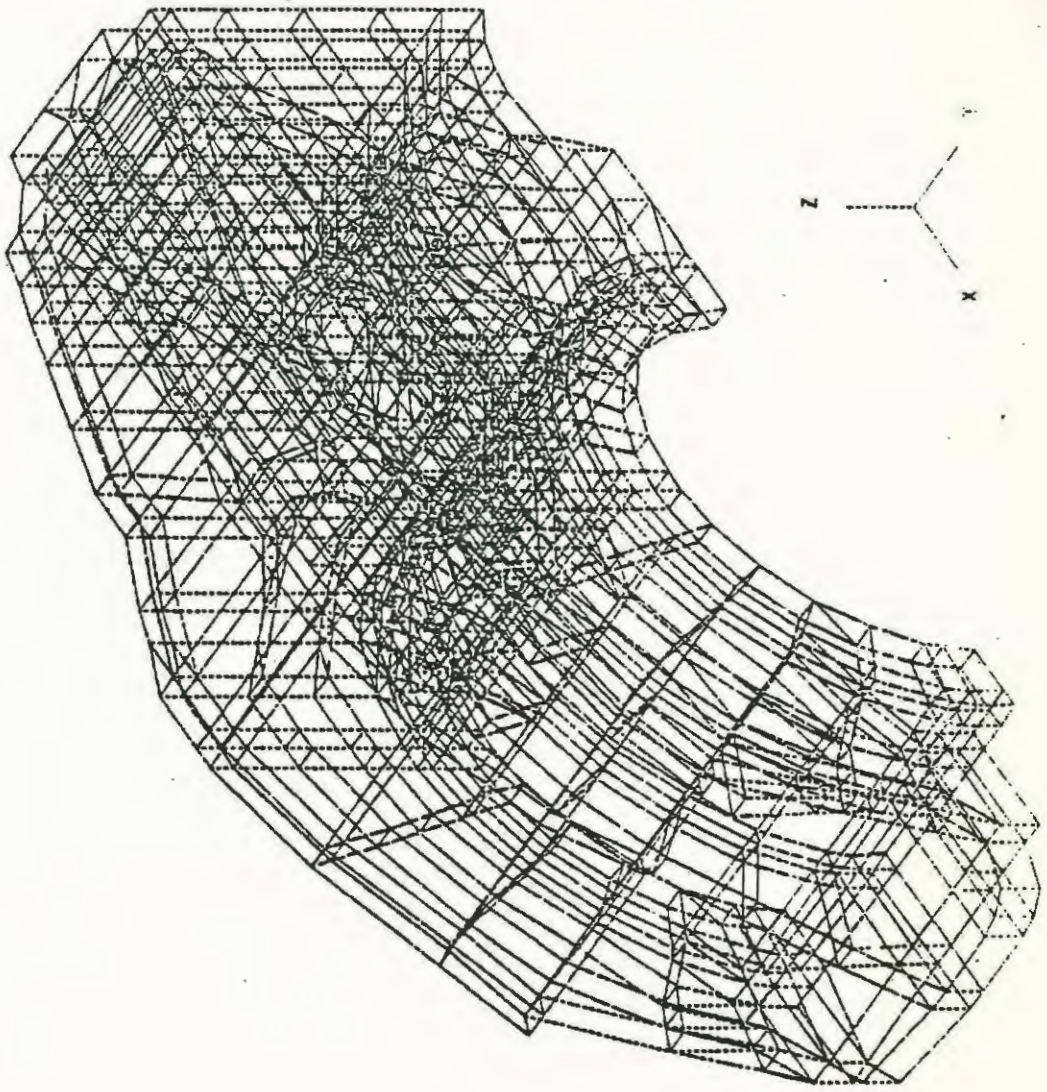

Figure 3a - MODIFIED SIDEFRAME

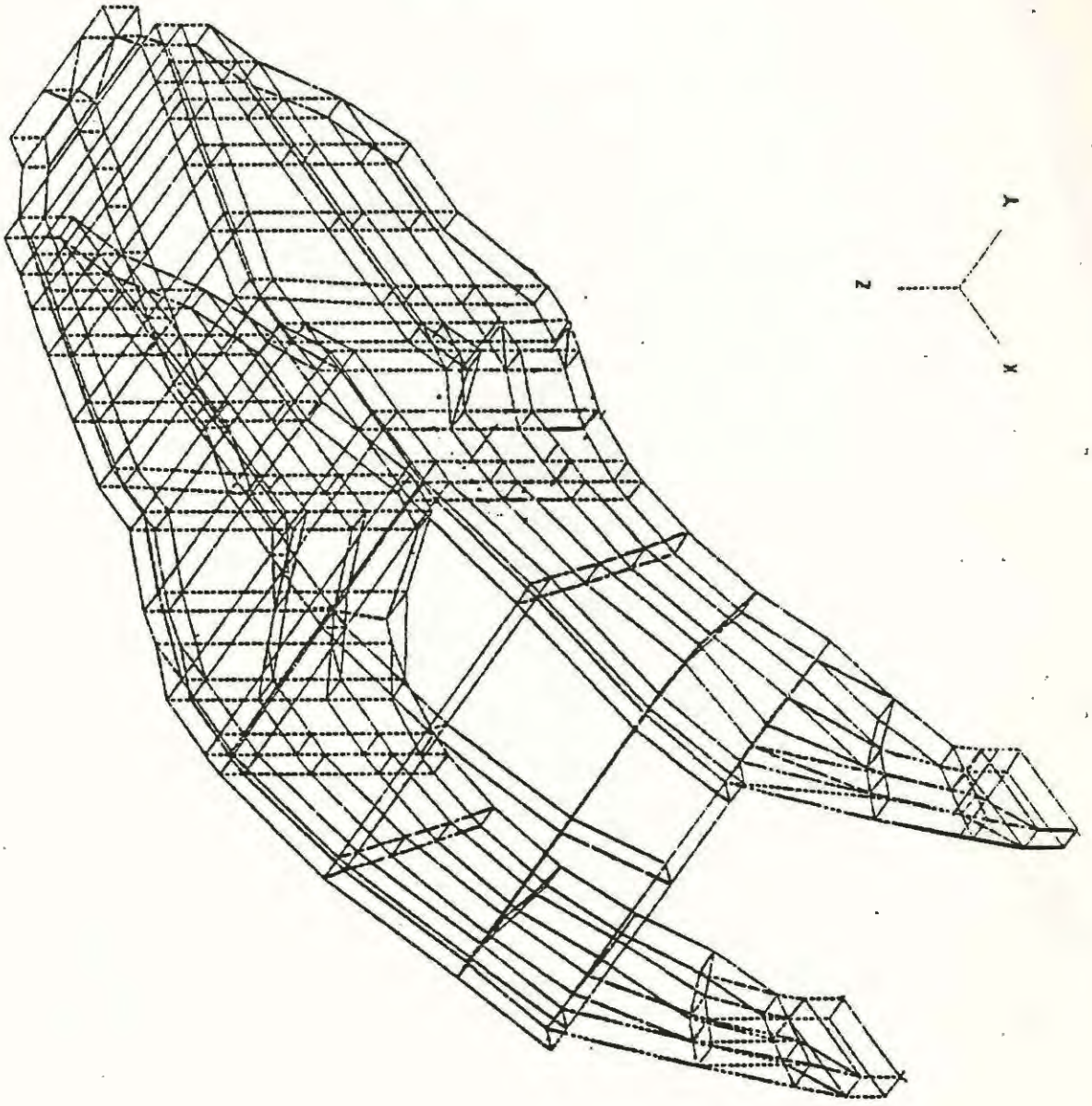

Figure 3b - SIDEFRAME REINFORCEMENT

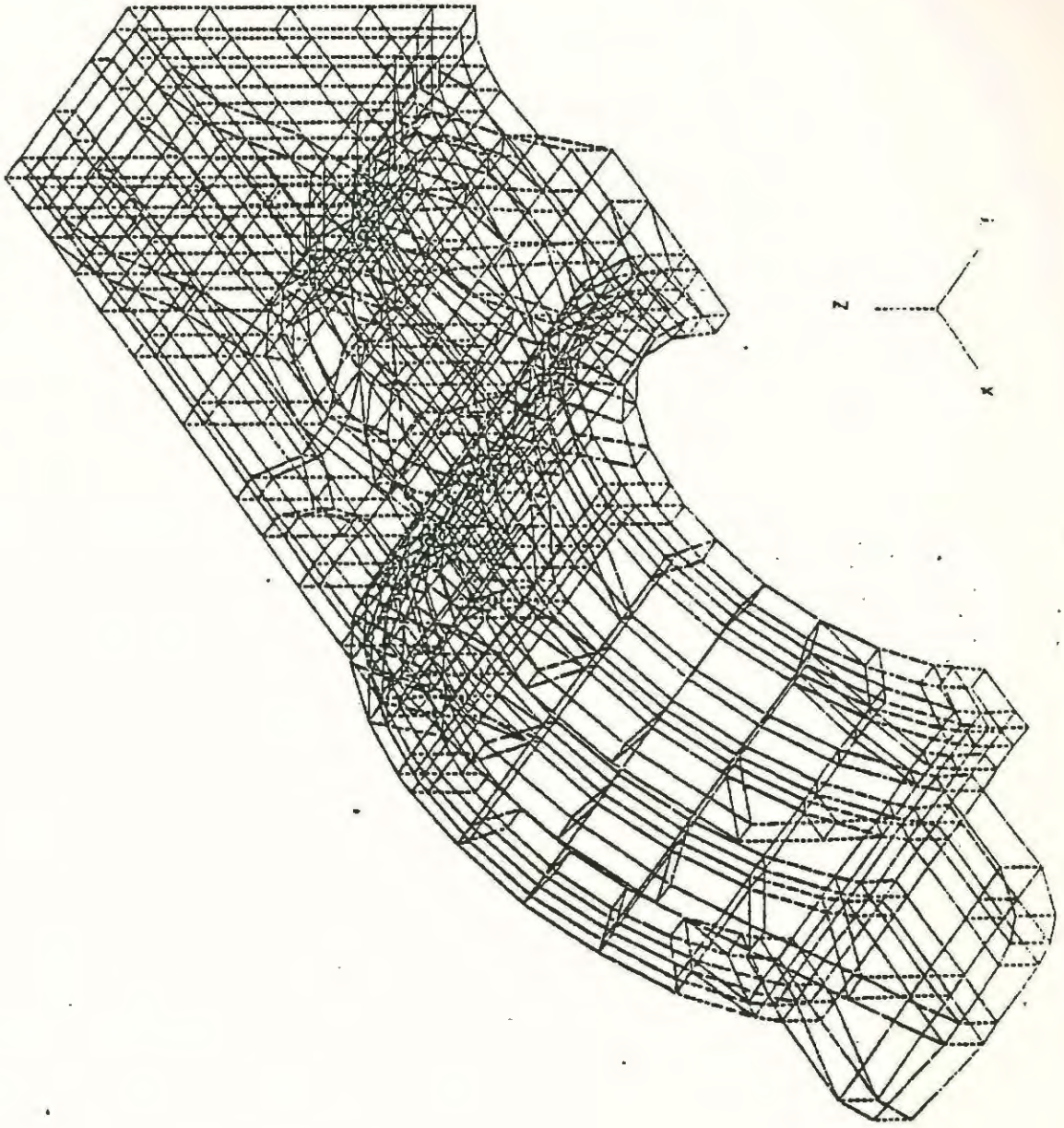

Figure 3c - REFINED MESH OF ORIGINAL SIDEFRAME

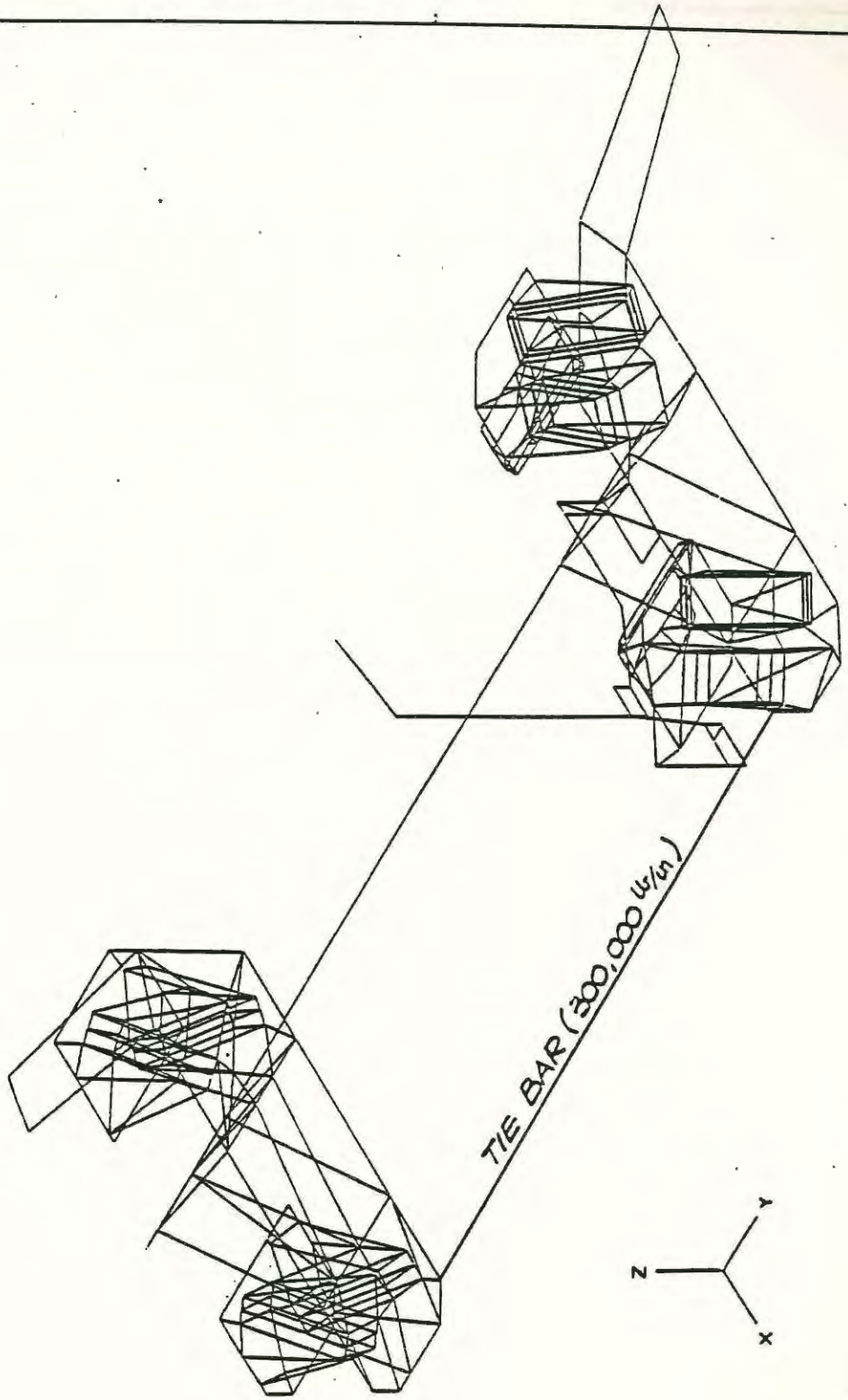

Figure 4 - TIE BAR MODIFICATION TO JOURNAL HOUSINGS.

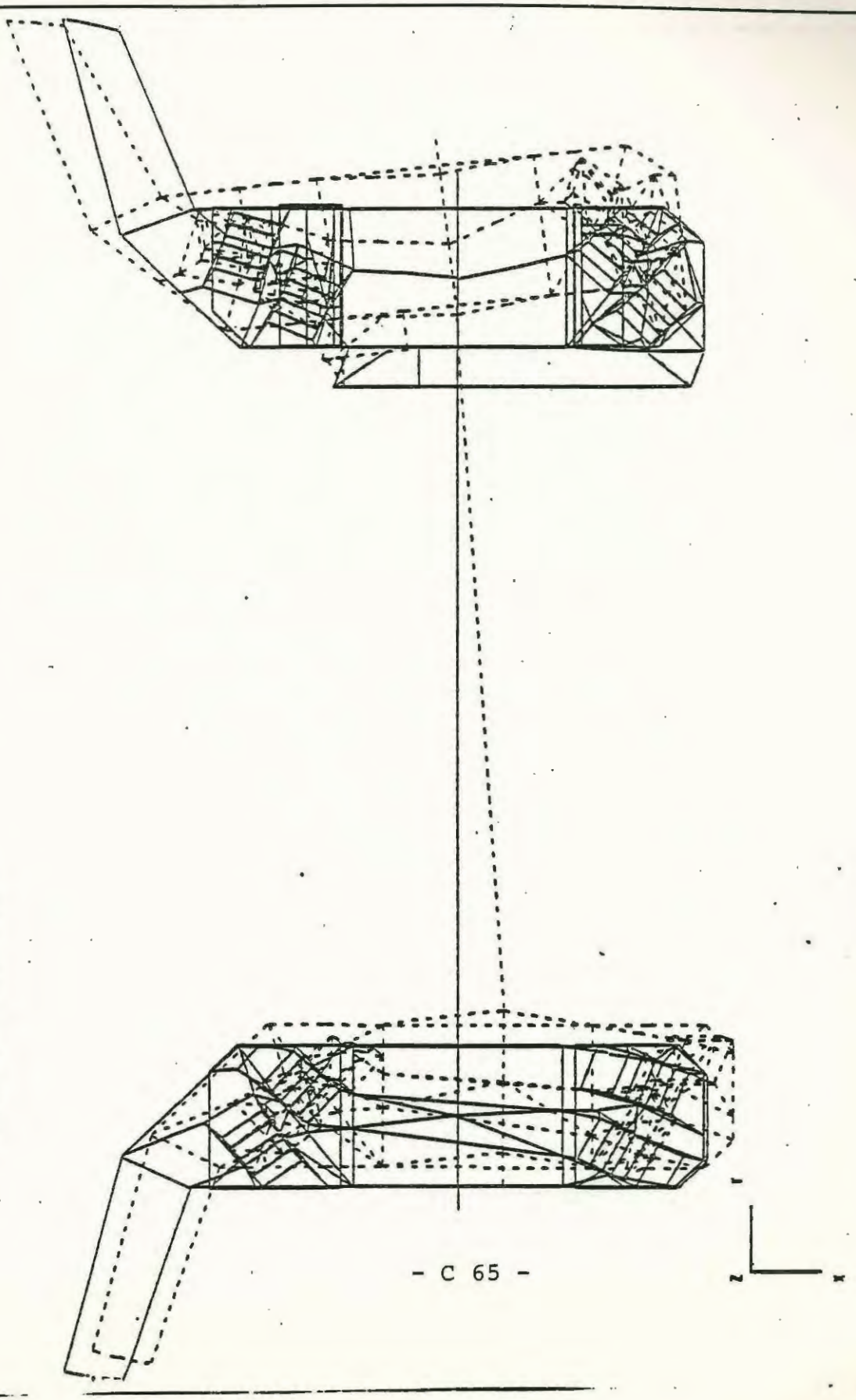

Figure 5 - ORIGINAL SIDEFRAME - DISPLACEMENTS DUE TO COMBINED LOAD-CASE 1

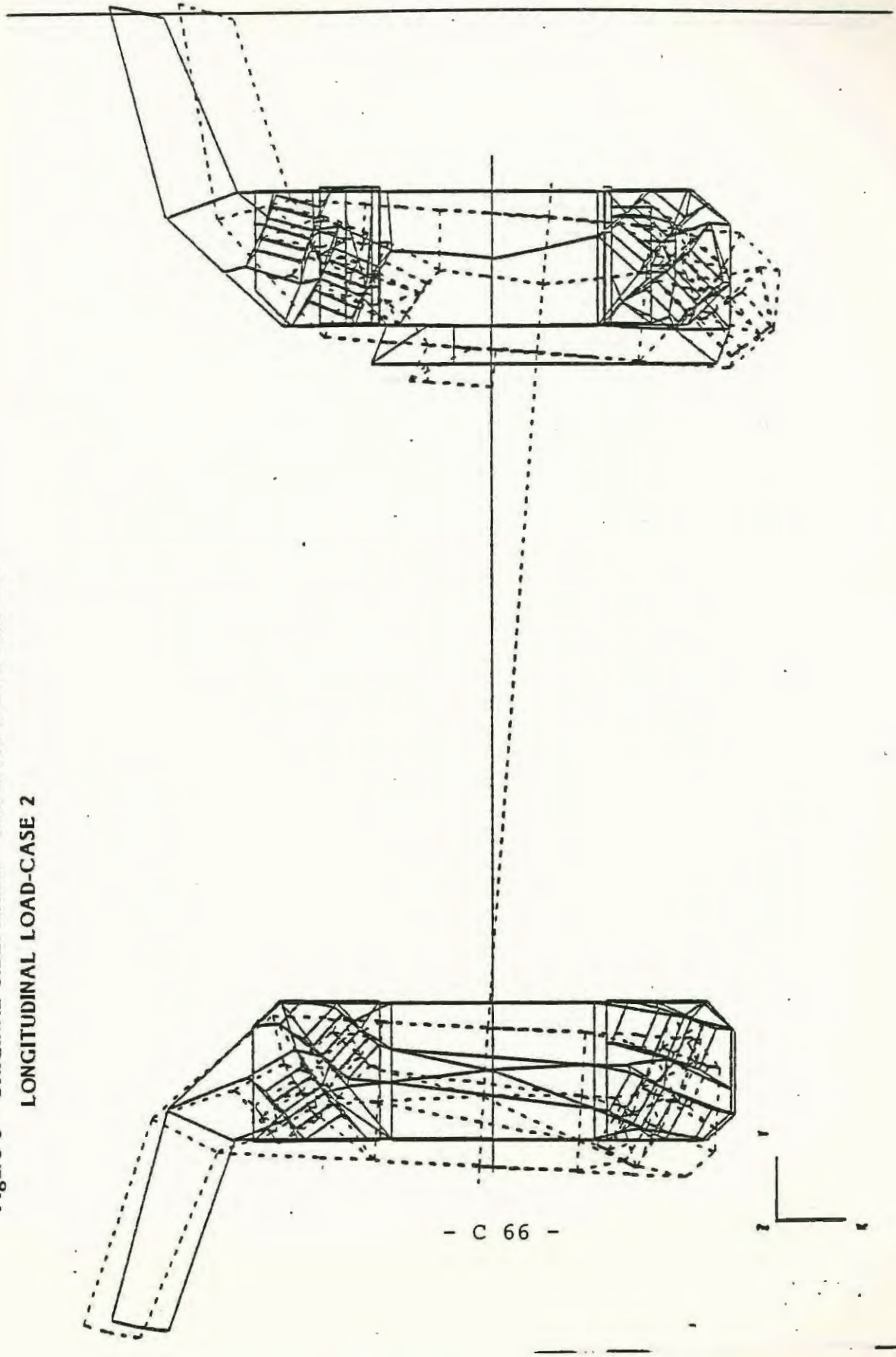

Figure 6 - ORIGINAL SIDEFRAME - DISPLACEMENTS DUE TO LONGITUDINAL LOAD-CASE 2

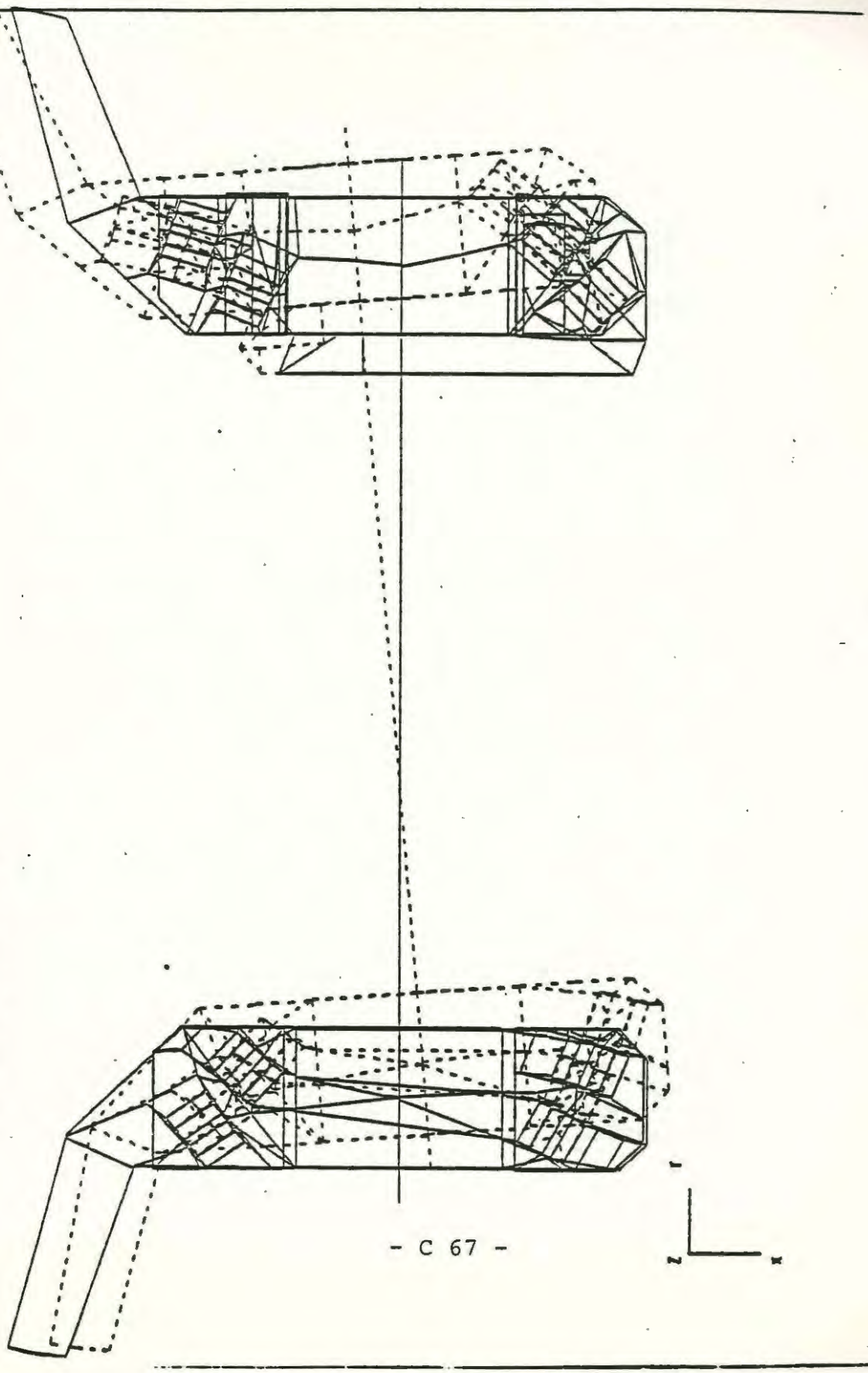

Figure 7 - ORIGINAL SIDEFRAME - DISPLACEMENTS DUE TO LATERAL LOAD-CASE 3

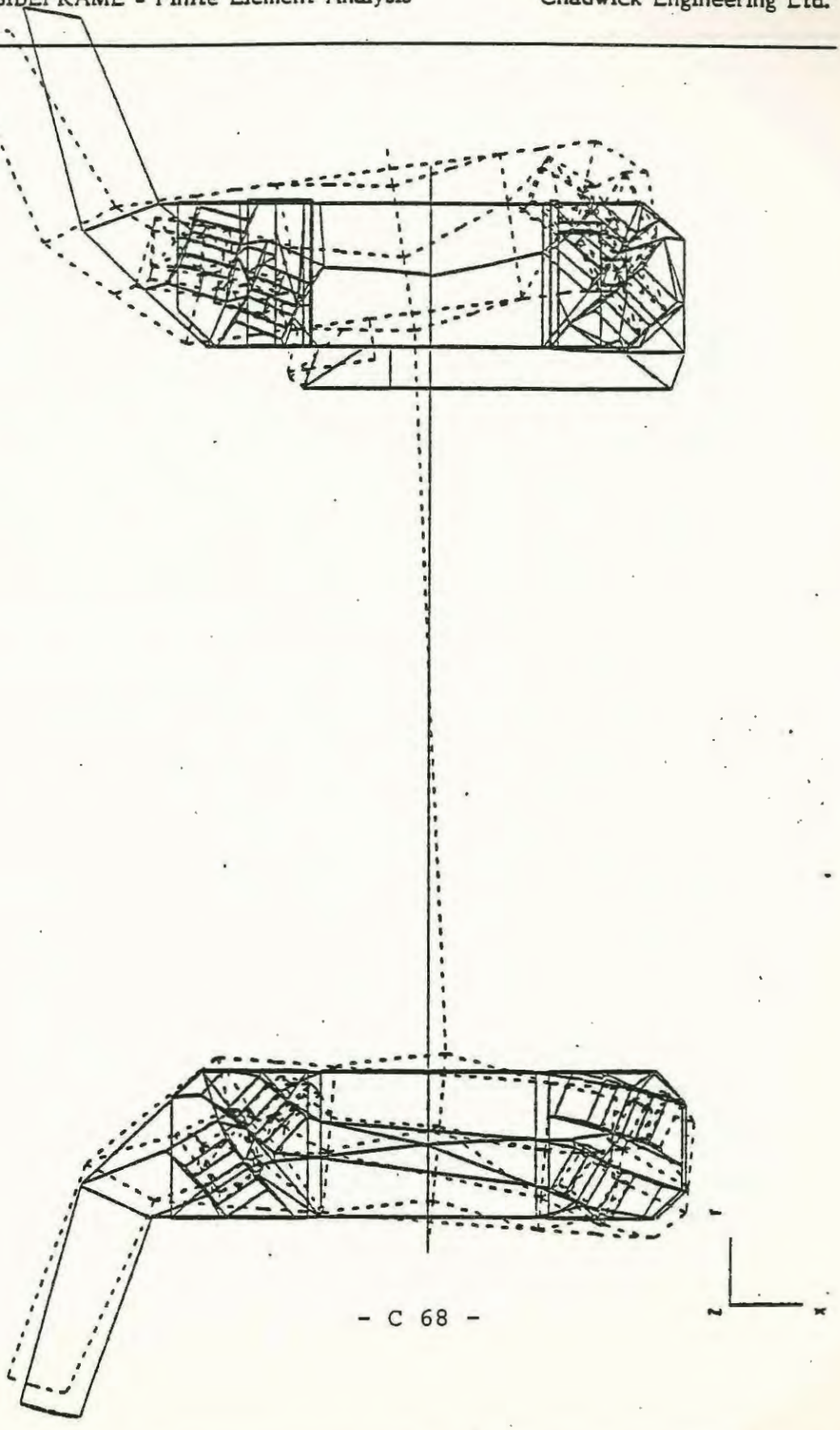

Figure 8 - ORIGINAL SIDEFRAME - DISPLACEMENTS DUE TO VERTICAL LOAD-CASE 4

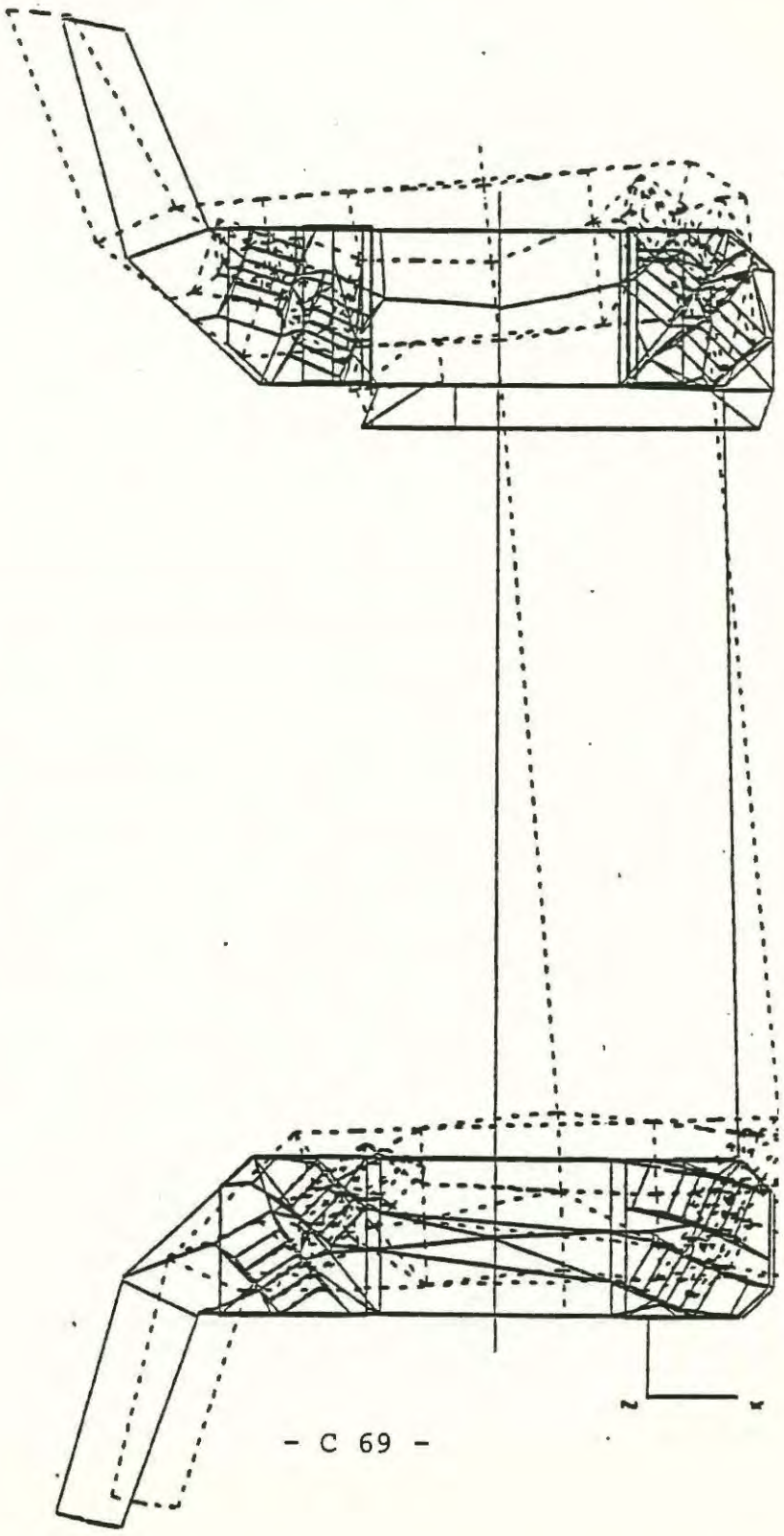

Figure 9 - MODIFIED SIDEFRAME - DISPLACEMENTS DUE TO COMBINED LOAD-CASE 1

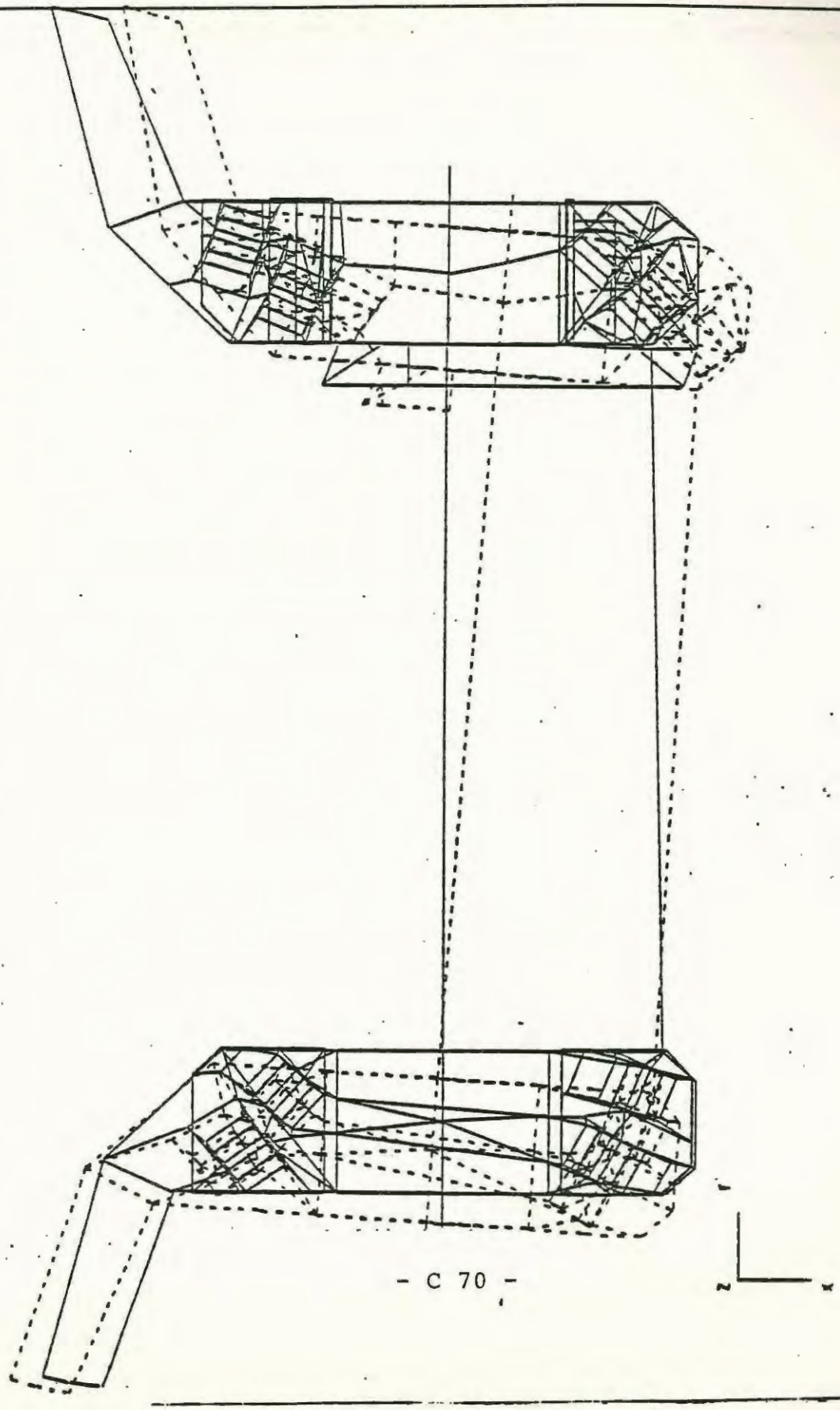

Figure 10 - MODIFIED SIDEFRAME - DISPLACEMENTS DUE TO LONGITUDINAL LOAD-CASE 2

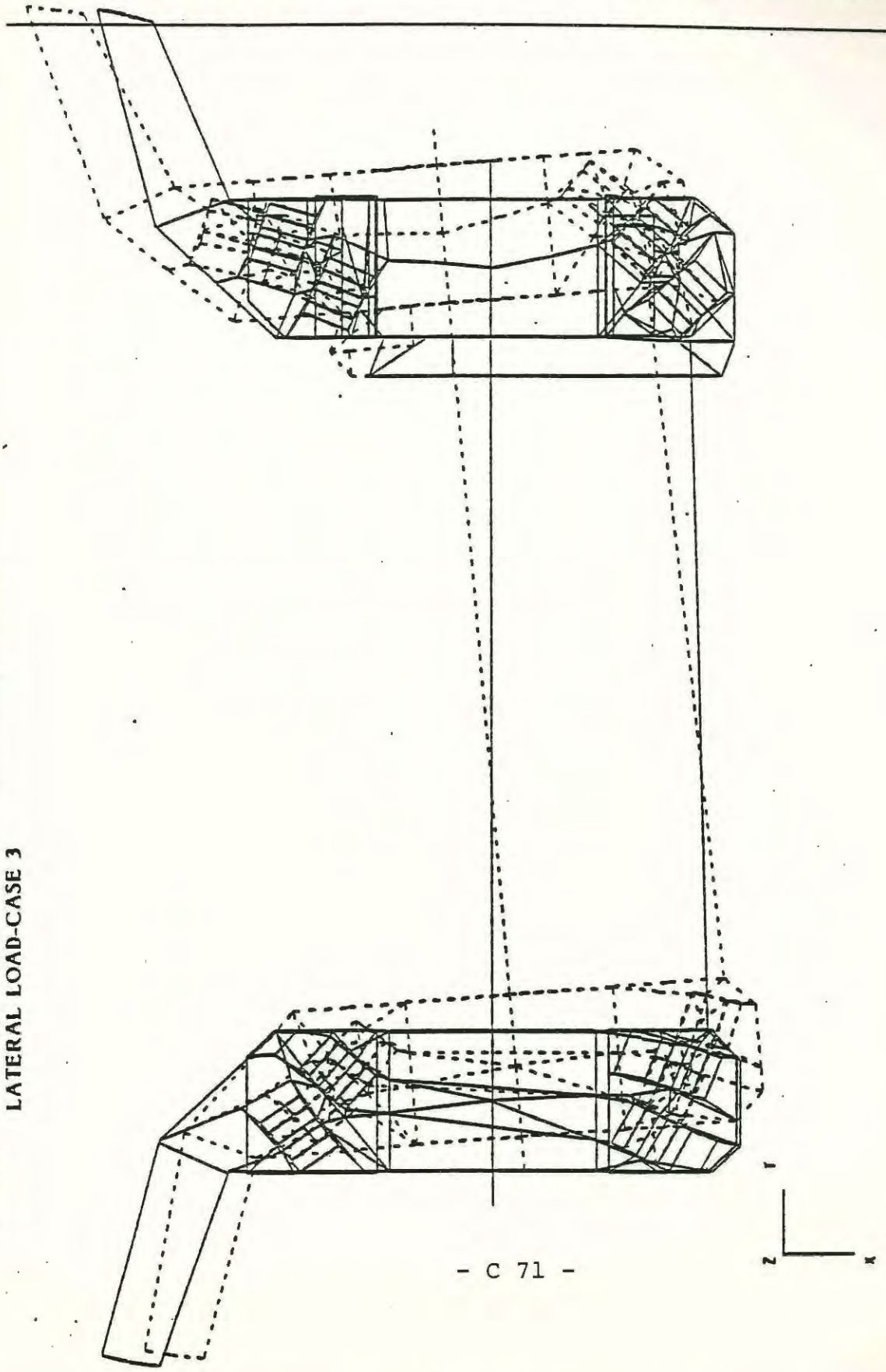

Figure 11 - MODIFIED SIDEFRAME - DISPLACEMENTS DUE TO LATERAL LOAD-CASE 3

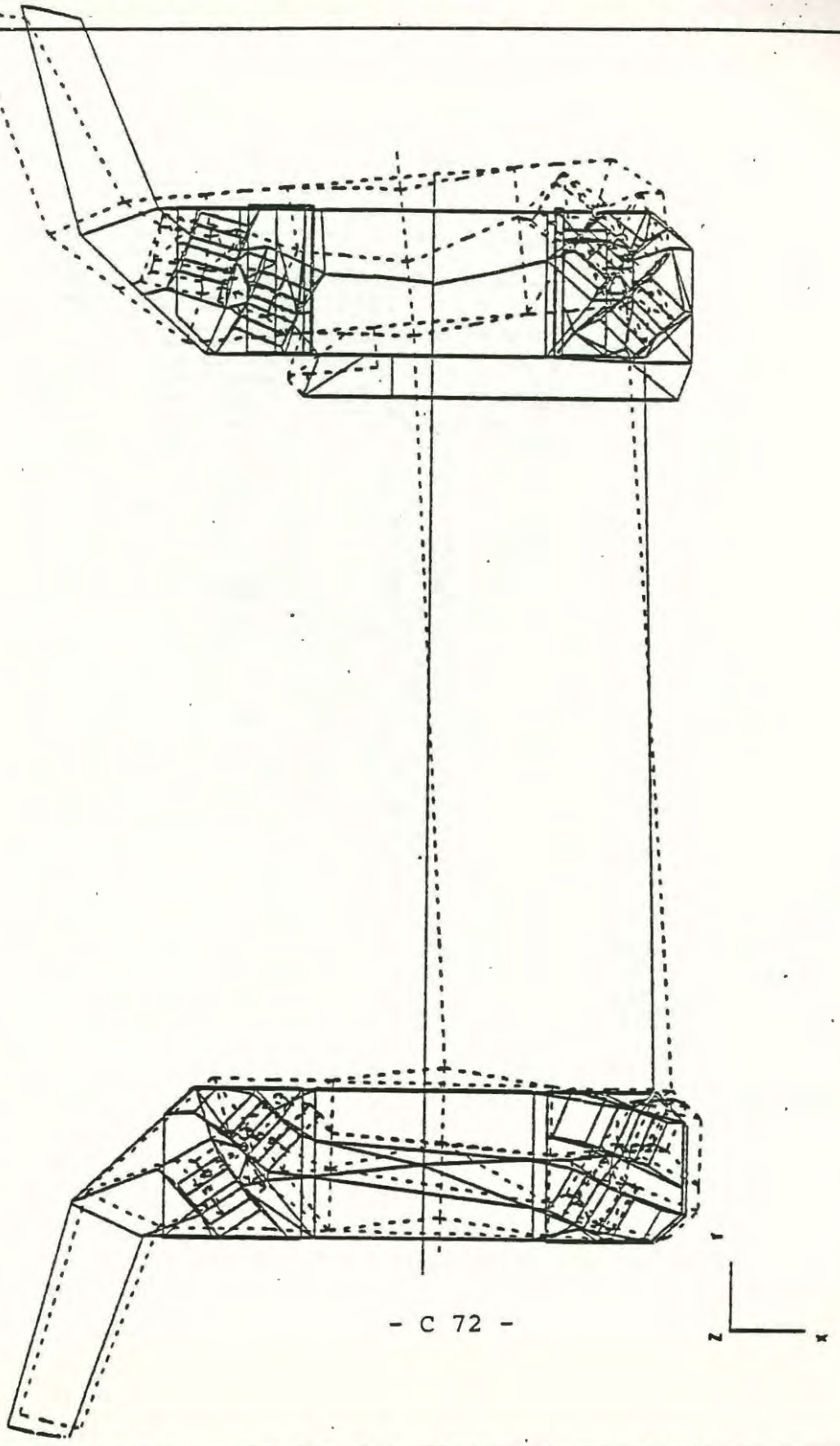

Figure 12 - MODIFIED SIDEFRAME - DISPLACEMENTS DUE TO VERTICAL LOAD-CASE 4

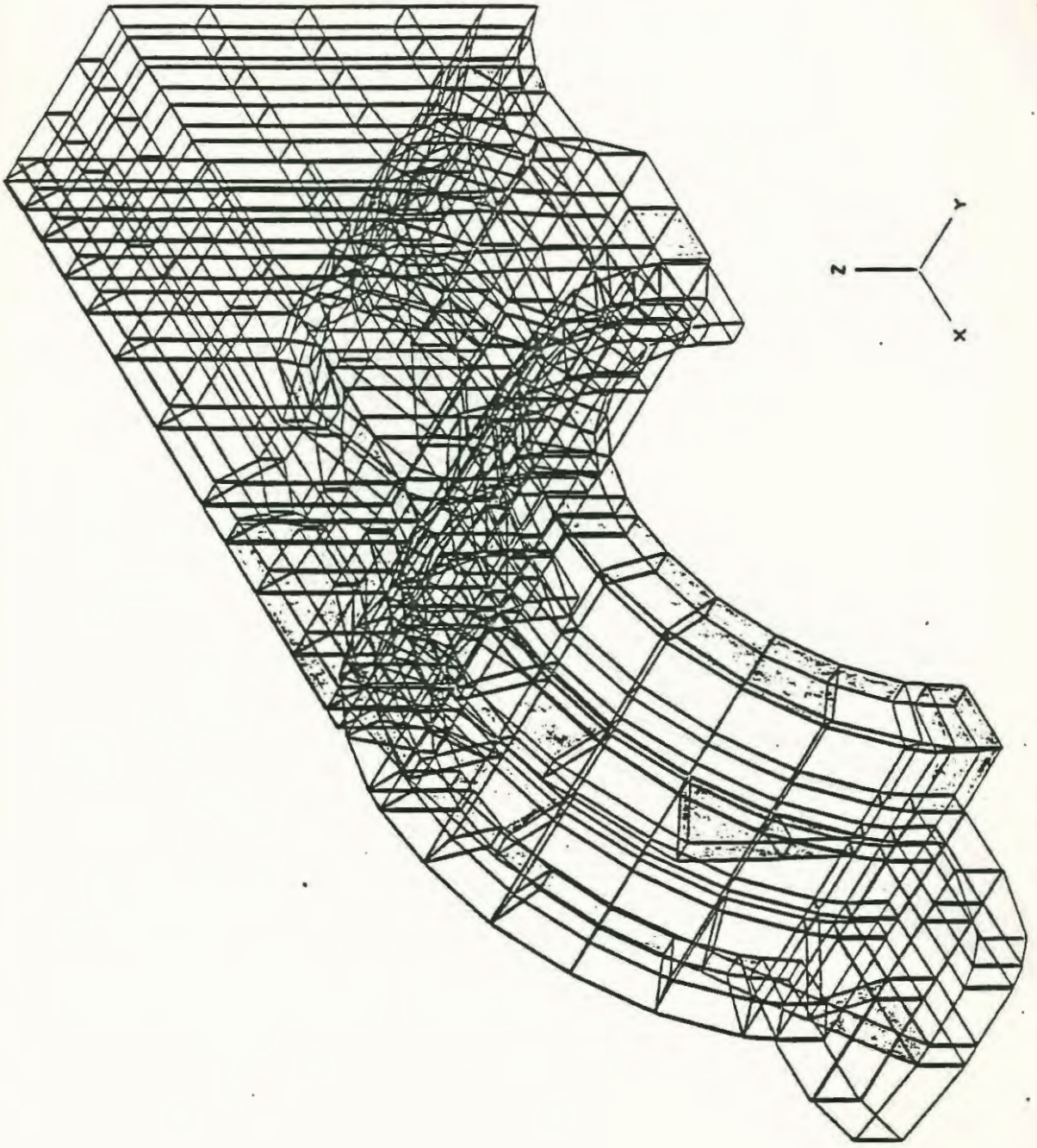

Figure 13 - ORIGINAL SIDEFRAME - STRESSES EXCEEDING 35 MPa

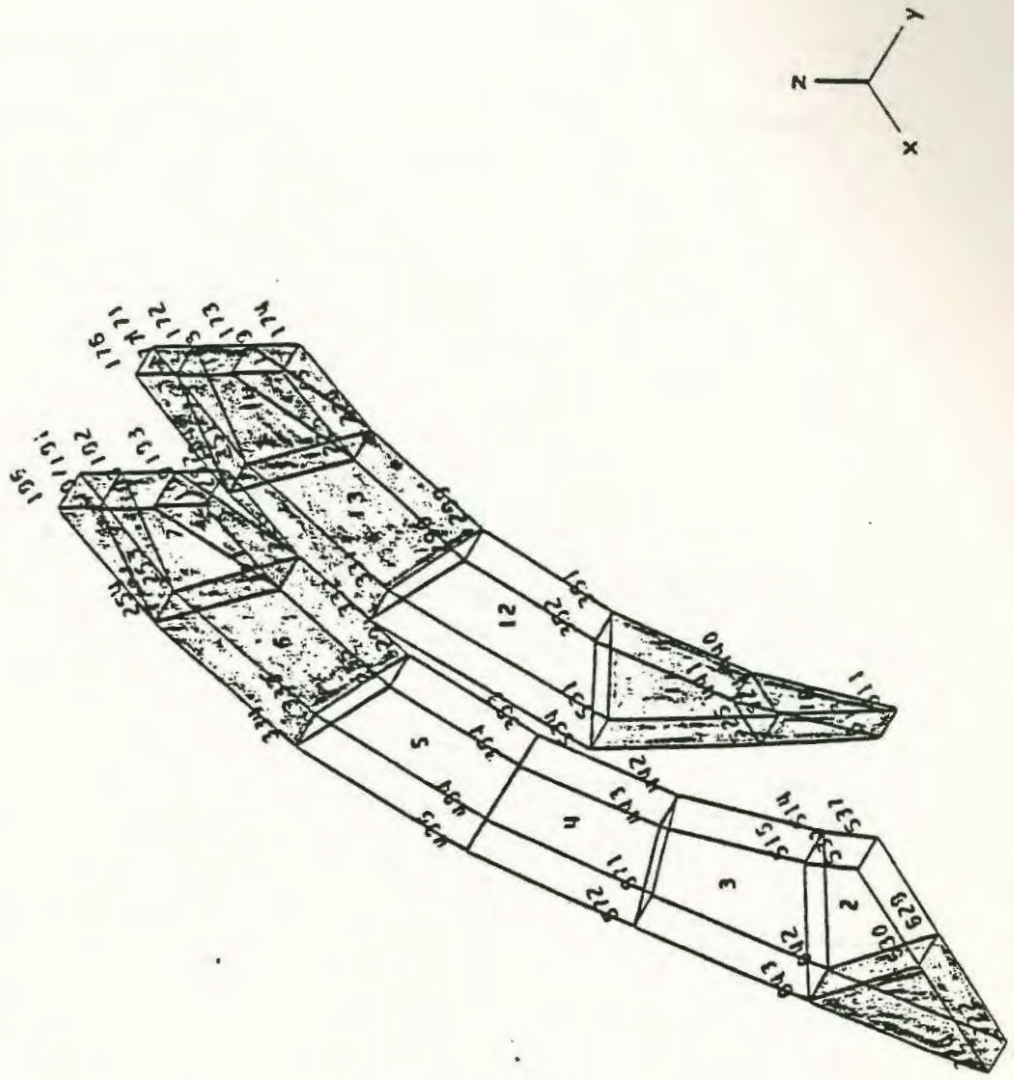

Figure 14 - ORIGINAL SIDEFRAME - STRESSES EXCEEDING 35 MPa.

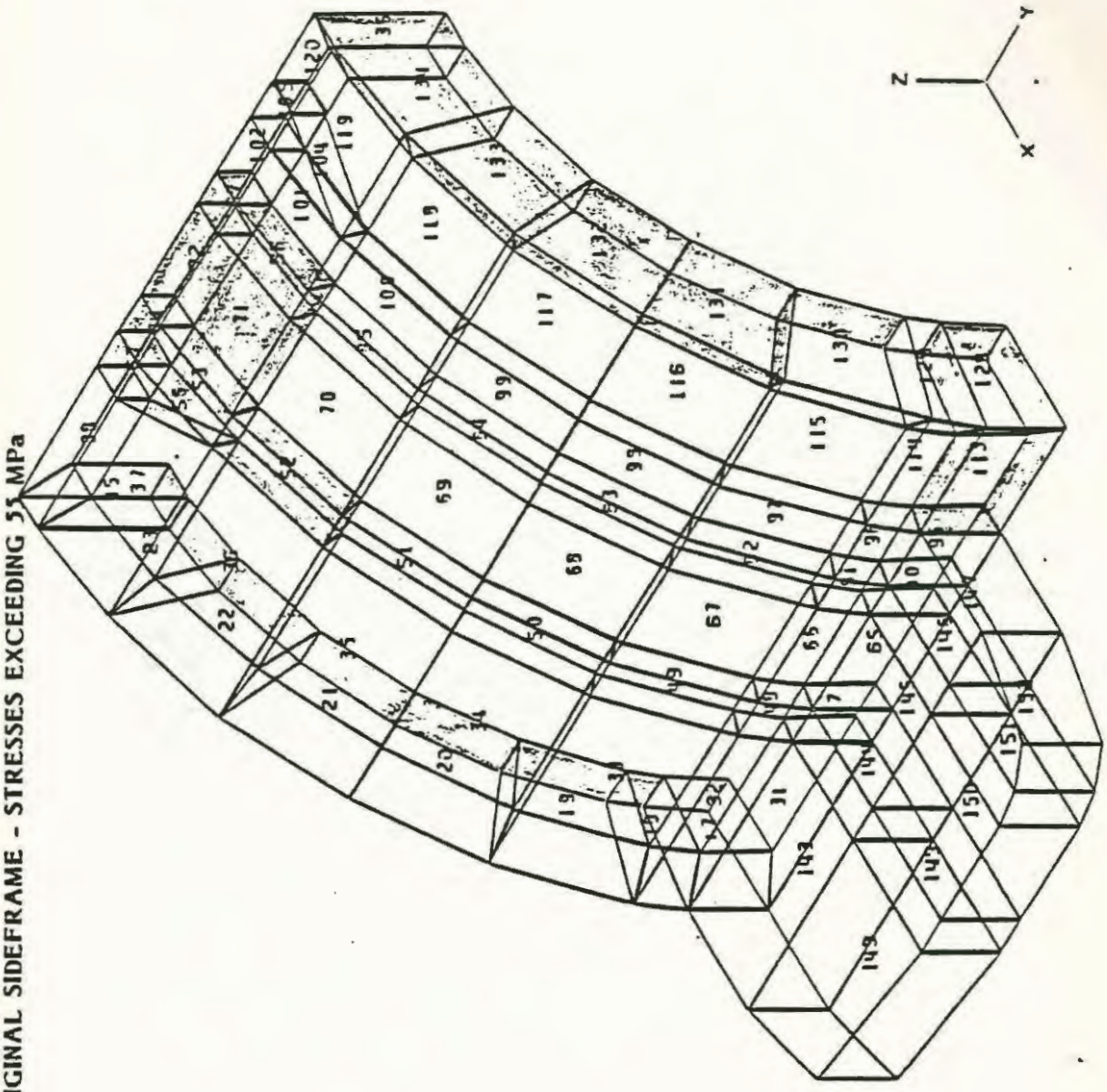

Figure 15 - ORIGINAL SIDEFRAME - STRESSES EXCEEDING 55 MPa

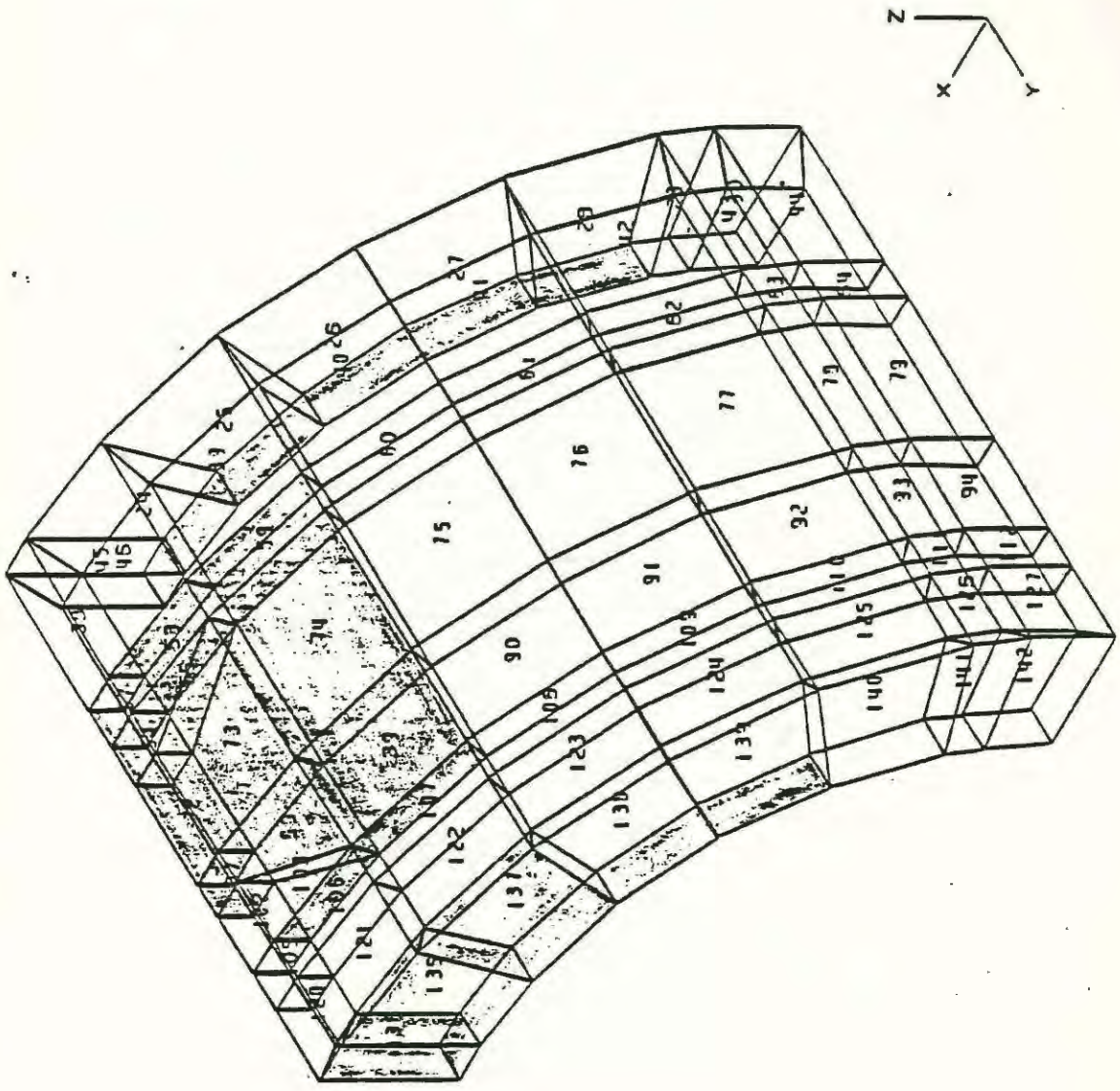

Figure 16 - ORIGINAL SIDEFRAME - STRESSES EXCEEDING 55 MPa

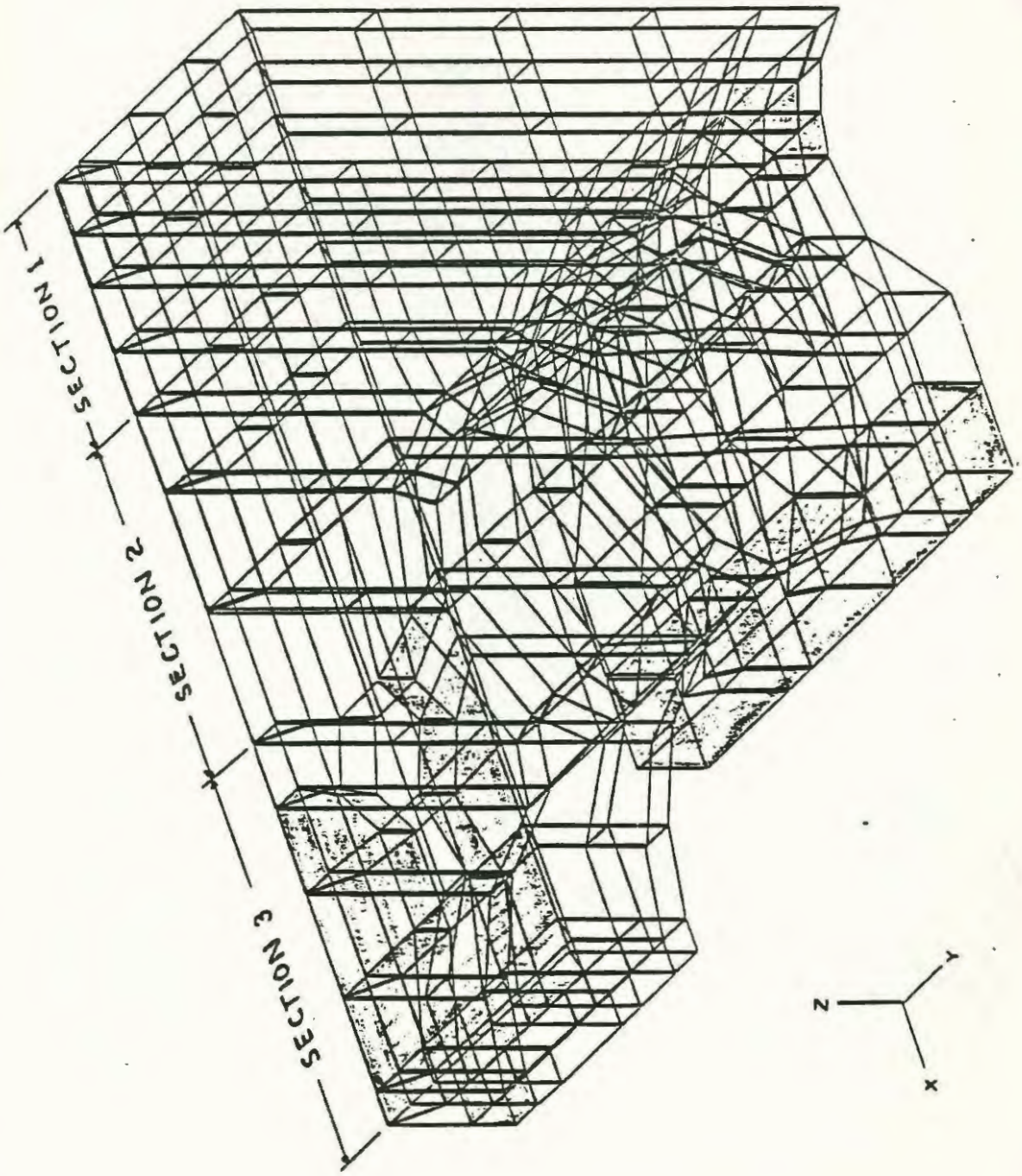

Figure 17 - ORIGINAL SIDEFRAME - STRESSES EXCEEDING 35 MPa

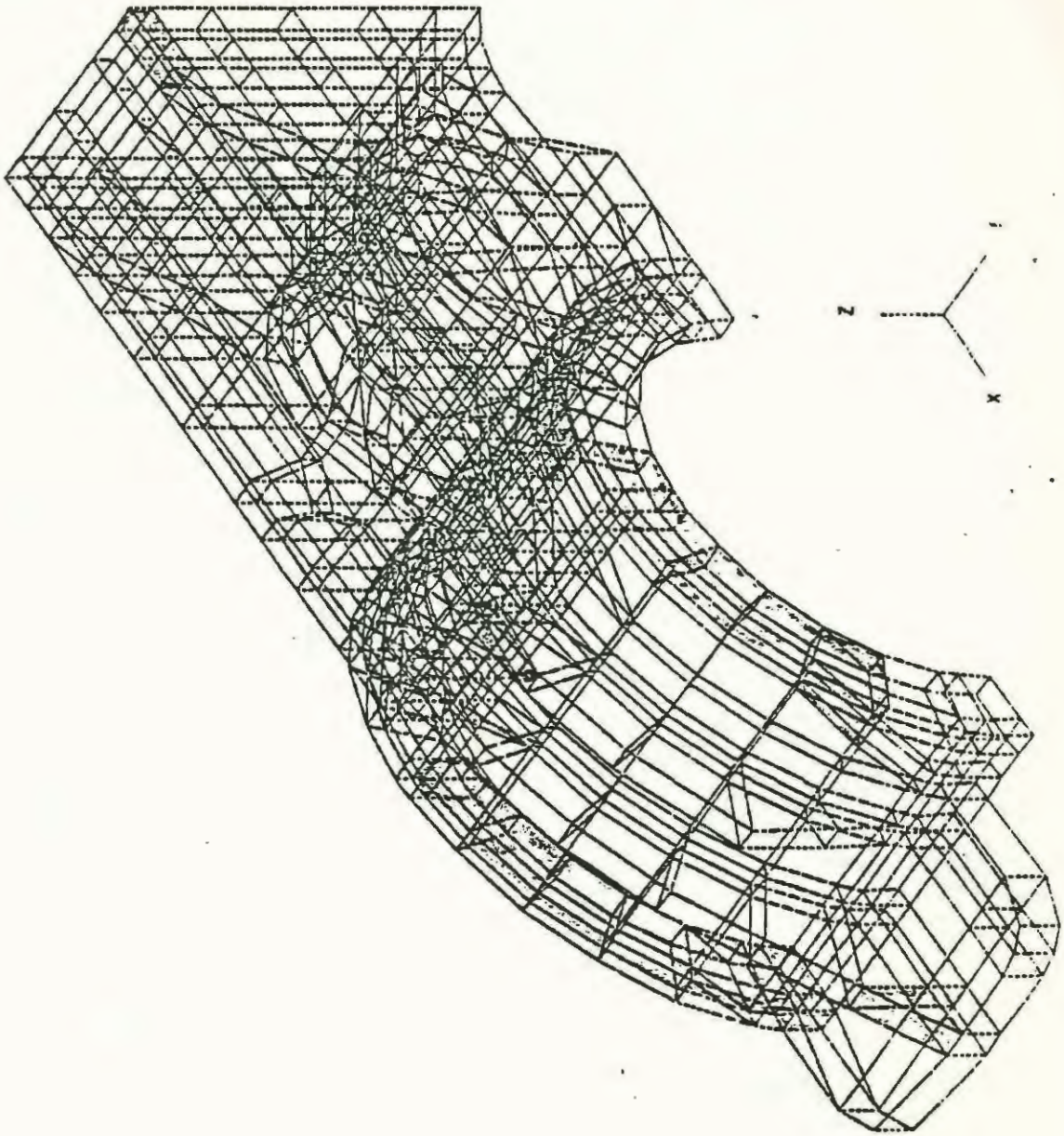

Figure 18 - MODIFIED SIDEFRAME - STRESSES EXCEEDING 55 MPa

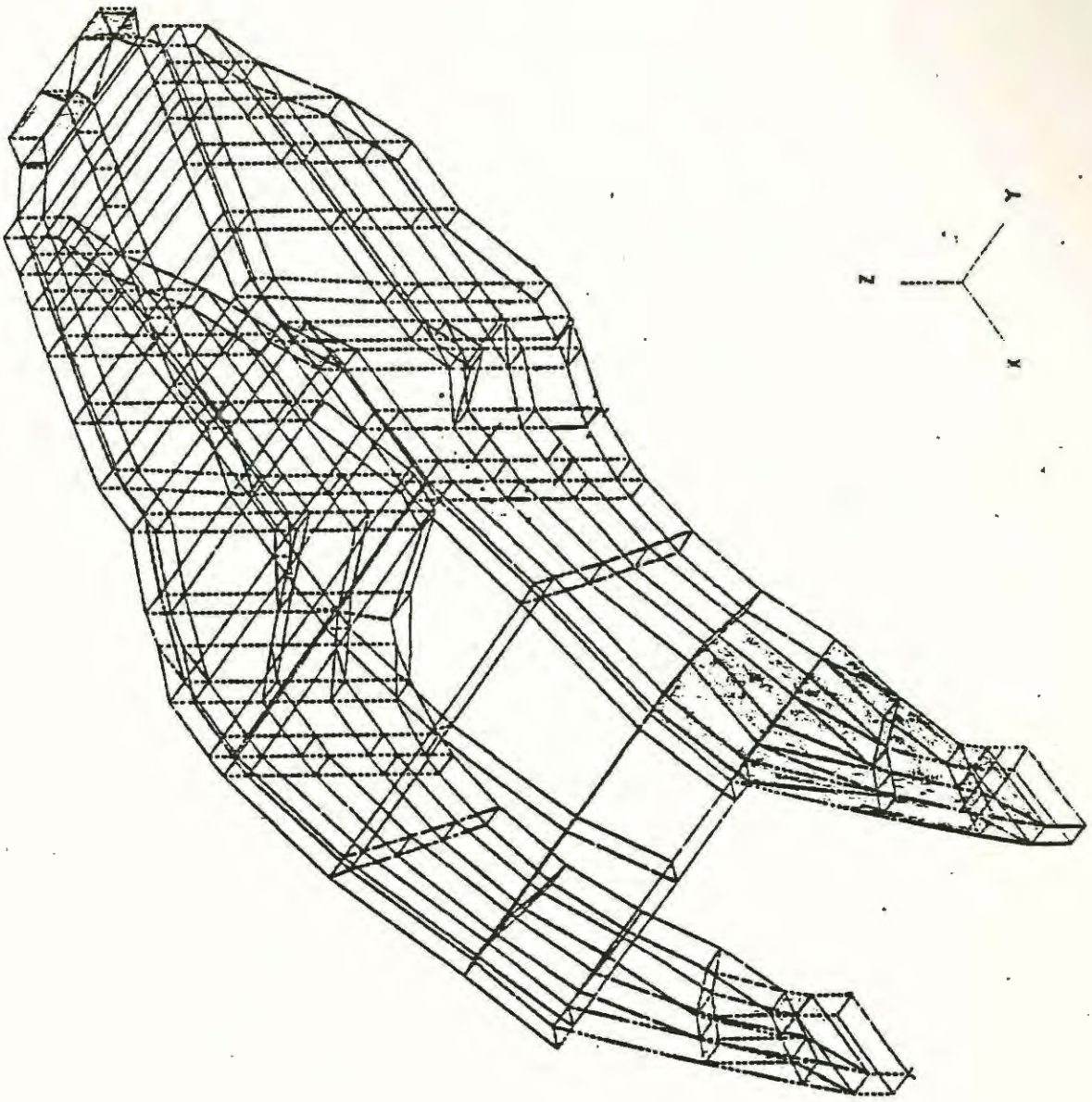

Figure 19 - MODIFIED SIDEFRAME - STRESSES EXCEEDING 55 MPa

Figure 20 - COMPARISON OF PRINCIPAL STRESSES - MODIFIED AND ORIGINAL (BRACKETED NUMBERS)

SIDEFRAMES

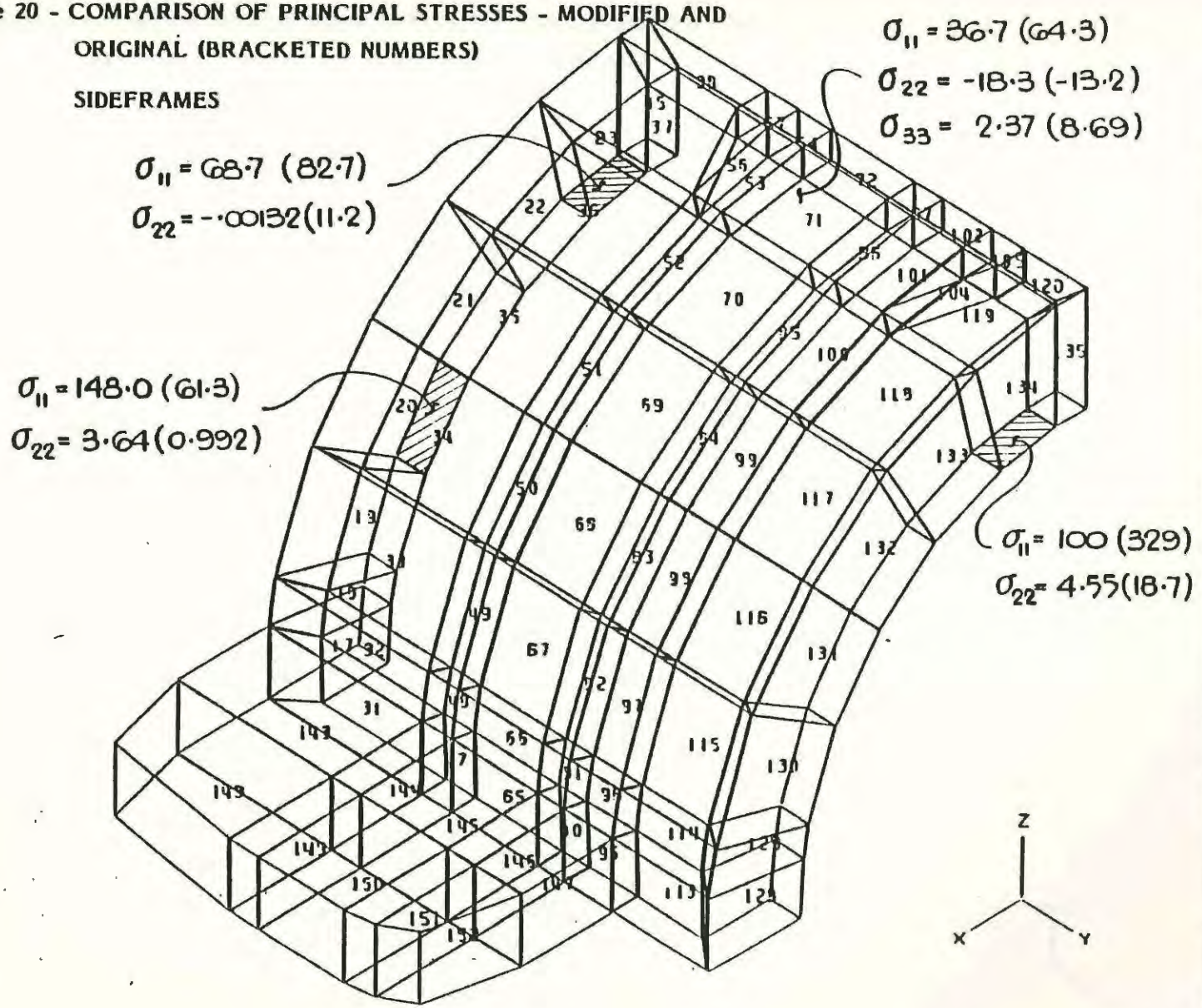

Figure 21 - COMPARISON OF PRINCIPAL STRESSES - MODIFIED AND ORIGINAL (BRACKETED NUMBERS) SIDEFRAMES

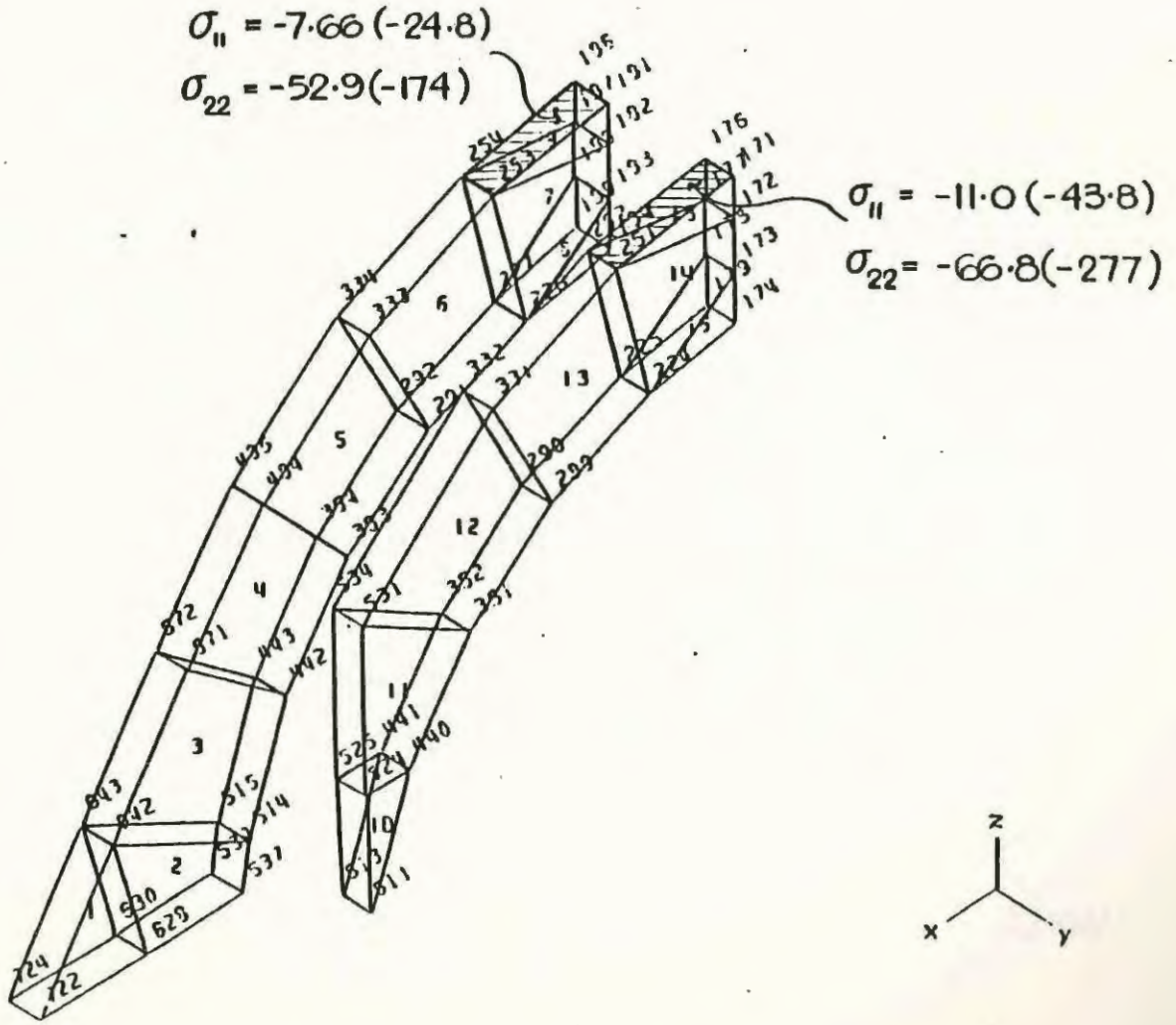

Figure 22 - PAD NORMAL FORCES ON JOURNAL HOUSING DUE TO A VERTICAL LOAD

Note: Normal Forces directed at an angle of 20° to horizontal.

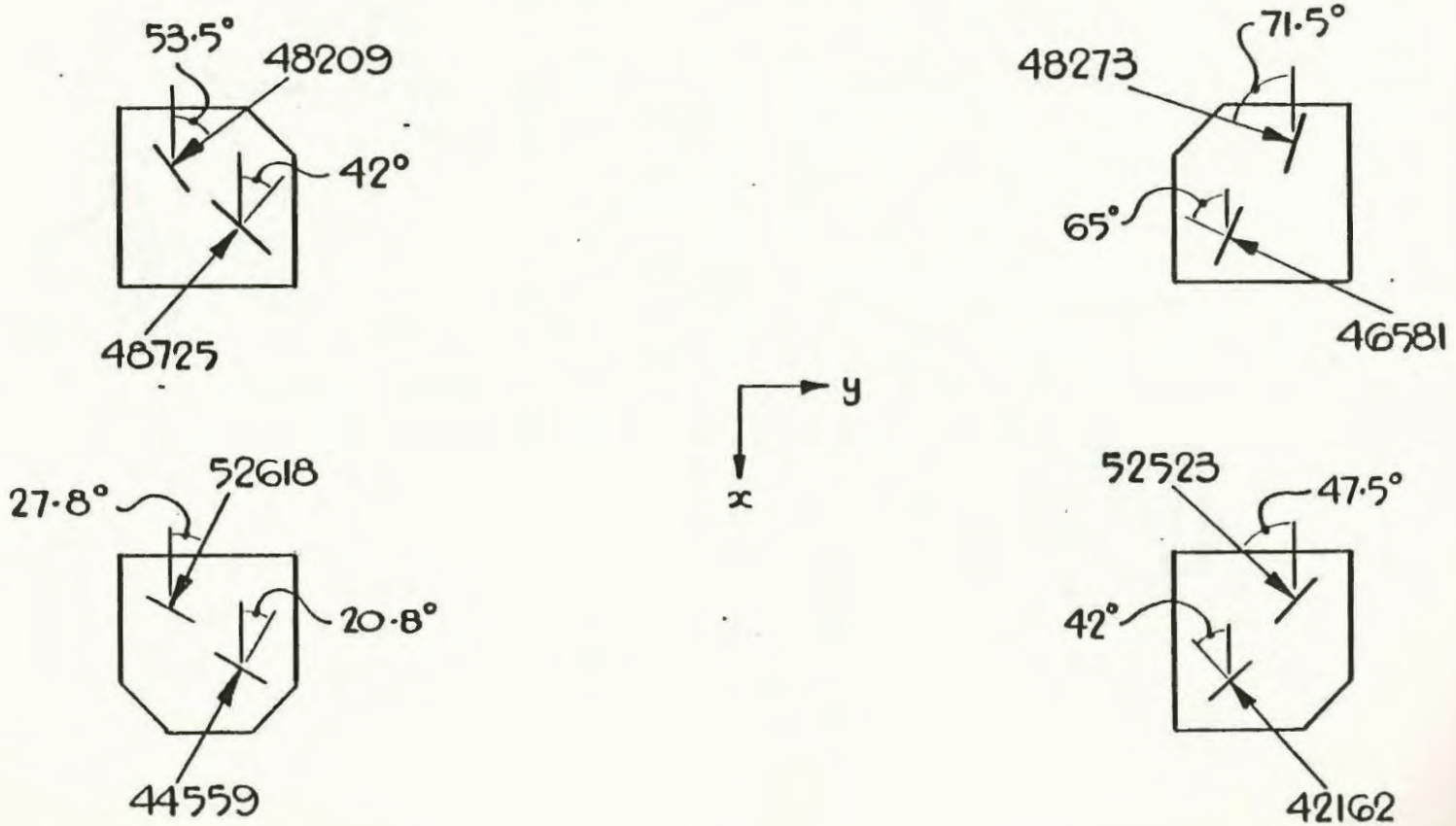

Figure 23 - PAD REACTION FORCES ON MODIFIED SIDEFRAMES DUE TO A VERTICAL LOAD

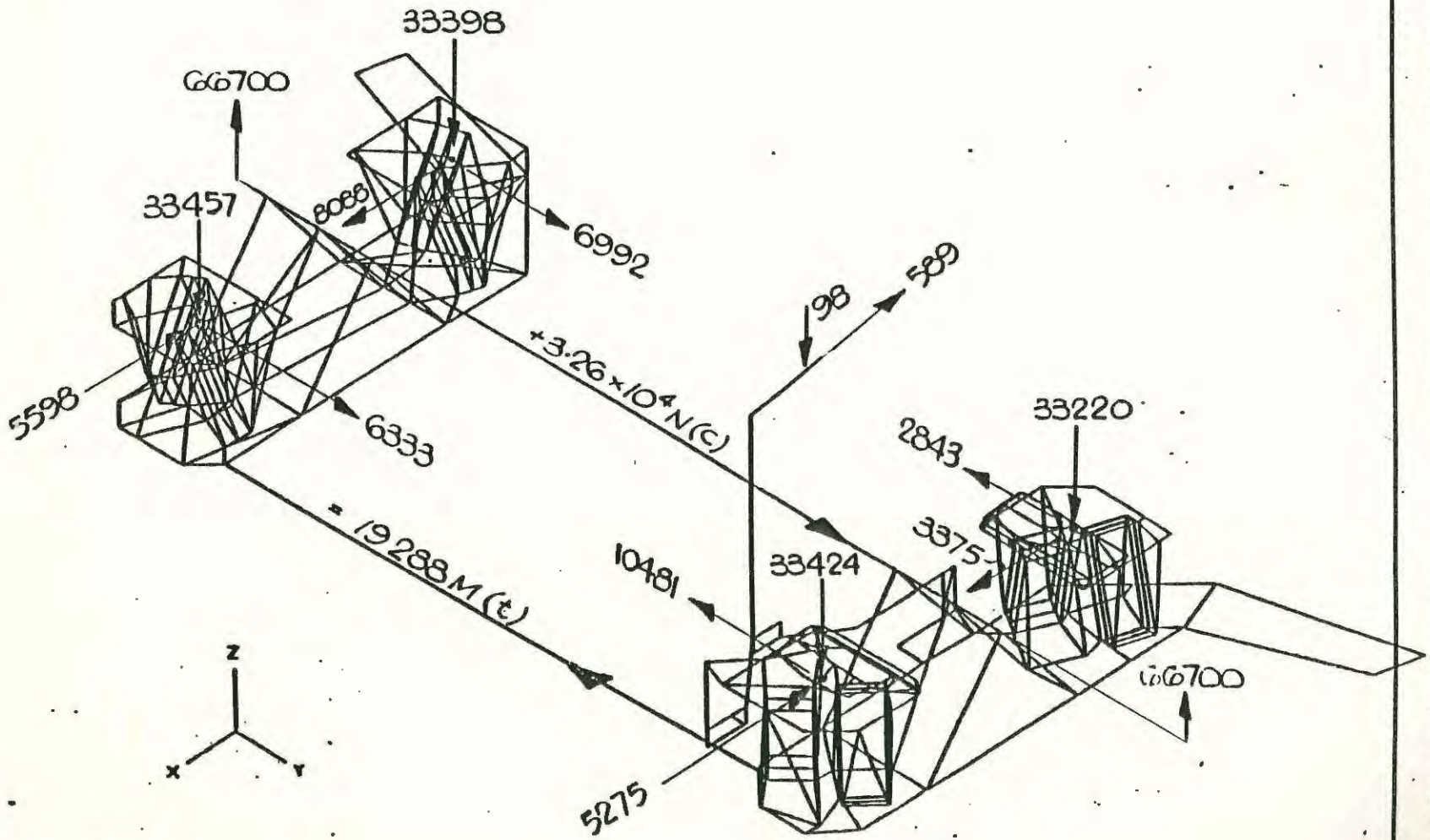

APPENDIX C

Part Two Sideframe and Reinforcement

Subpart B APPROXIMATE STRESS CALCULATIONS FOR MODIFIED SIDEFRAME

SIDEFRAME	Sx TOP	Sx BOTTOM	σ max (psi) TOP	BOTTOM
UNMODIFIED	2.28	2.78	-25200	47700
MODIFICATION				
1) Fig.A2 -1	22.7	22.4	- 2500	5900
2) Fig.A2 -2	28.1	28.7	- 2000	4600

A stress comparison was made by considering a ratio of Sx Top and Sx Bottom values between the unmodified and modified sideframes.

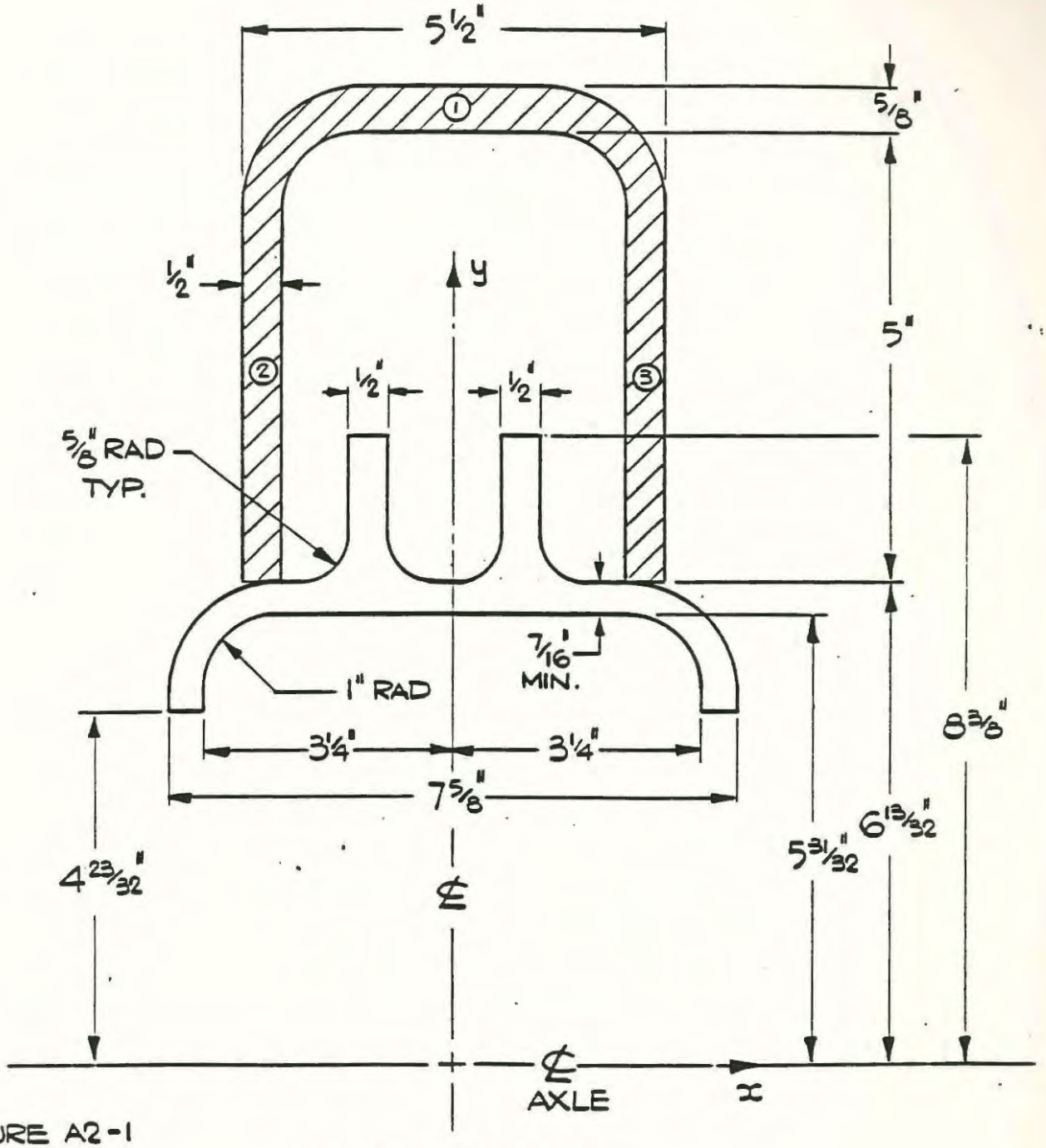

FIGURE A2-1

MODIFICATION 1

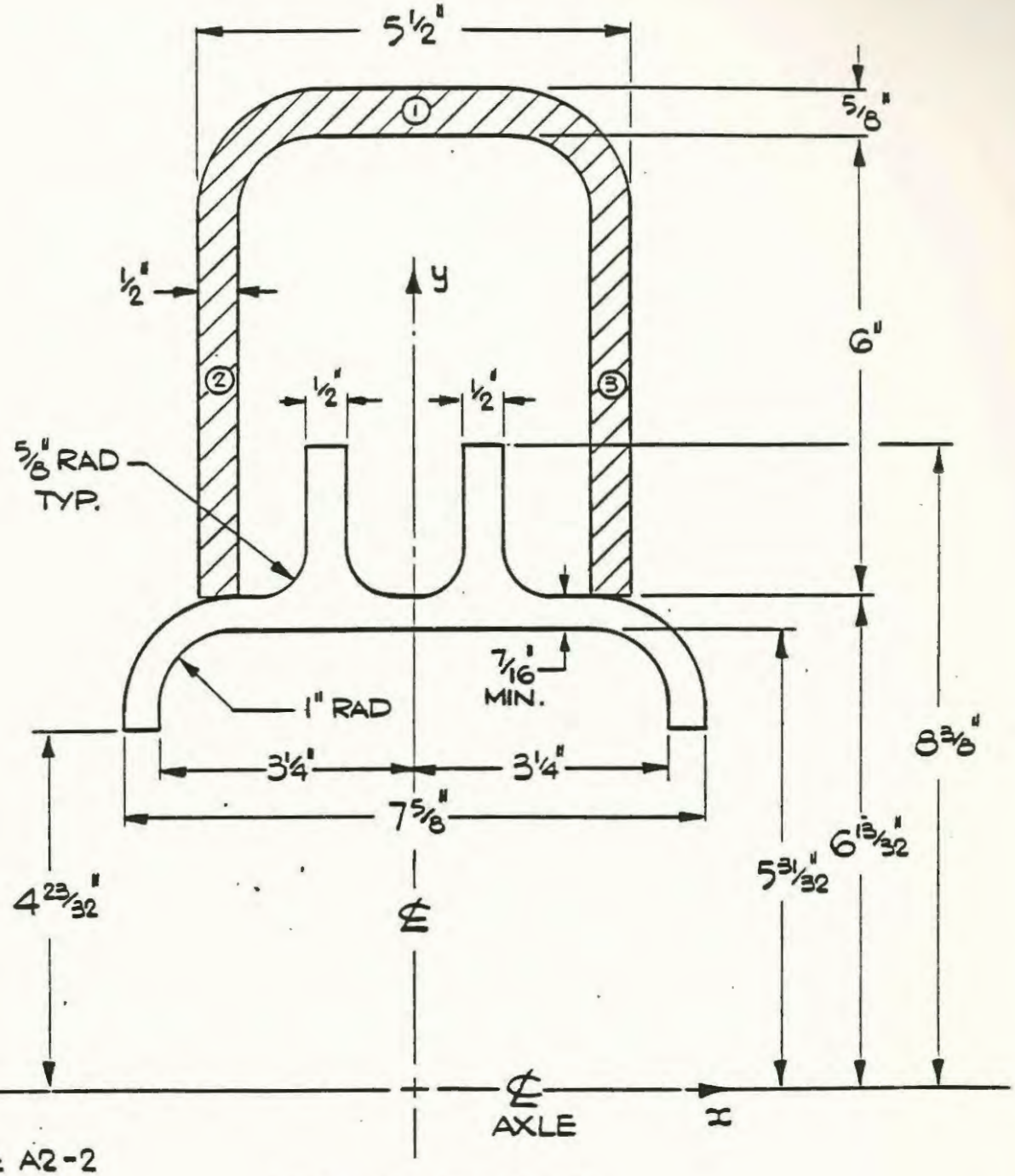

FIGURE A2-2

MODIFICATION 2

Chadwick
Engineering Ltd

:D Sherwood Avenue, Amherstview, Ontario K7N 1N2 (613) 384 2866

APPENDIX C

Part Three Revised Spring Pads

WMATA SIDEFRAME
FINITE ELEMENT ANALYSIS

Approved by: D. Chadwick

D. Chadwick, P.Eng.,
President,
Chadwick Engineering Ltd

Date: 14 Oct 83

TABLE OF CONTENTS

1. INTRODUCTION

Throughout the two previous WMATA sideframe analysis reports:

REPORT 1 : WMATA SIDEFRAME Finite Element Analysis - July 22 1983

REPORT 2 : WMATA SIDEFRAME Finite Element Analysis
Addendum 1 - Sideframe Reinforcement - Sept. 30 1983

every attempt was made to understand the response of this relatively complex system. Upon a close examination of the outboard normal pad forces and reactions it was discovered that the normal to each of these pads was in a direction which created a net moment on the sideframe. This was discussed with UTDC and it was decided to revise the orientation of these outboard pads and examine the effect of this change on the analysis.

2. SPRING PAD REVISION

Both pairs of outboard spring pads on the steering and non-steering sides were modified in such a way that their orientation in the horizontal plane remained the same while being rotated symmetrically about, for example, line AB shown in Figure 1. Thus the pad surface remains orientated at the same angle of approximately 20% relative to a vertical plane through AB. A comparison between the original housing and the revised journal housing can be examining the following figures.

	Original Housing	Revised Housing
Steering	Figure 1	Figure 3
Non-steering	Figure 2	Figure 4

A complete set of revised drawings are shown in Figures 5 to 11.

3. RESULTS OF ANALYSIS

The revised journal housing was subjected to the standard four load cases and the results were examined to determine it there were any dramatic change in the behaviour of the system.

3(i) Comparison of Deflections

In general there was a marginal increase in the movement of the journal housings shown in Figures 12 to 15. These Figures can be compared in a global sense to figures 9 to 12 in Report 2. Consequently the revised pad orientation made the system slightly more flexible.

3(ii) Comparison of Spring Pad Normal Forces - Vertical Load - Case 4

There was no significant change (maximum of 10%) in the magnitudes of the normal forces, as shown in Figures 16 and 17.

3(iii) Comparison of Reaction Forces - Combined Load - Case 1

It can be seen in Figures 18 and 19 that the reaction forces in the vertical and longitudinal directions (Z and X) were reduced by no more than 15%. These forces in the vertical plane are considered to be the major factors causing the excessive flexural stresses in the sideframe. It should be noted that there is a reduction of almost 50% in the lateral force which will reduce the torsional stresses significantly.

4. CONCLUSIONS

The revised journal housings did not result in significantly large changes in the primary reaction forces. As a result, the sideframe stresses would not be reduced to acceptable levels.

APPENDIX C

Part Three Revised Spring Pads

Subpart A Figures

Figure 1 - ORIGINAL JOURNAL HOUSING - STEERING LINK SIDE

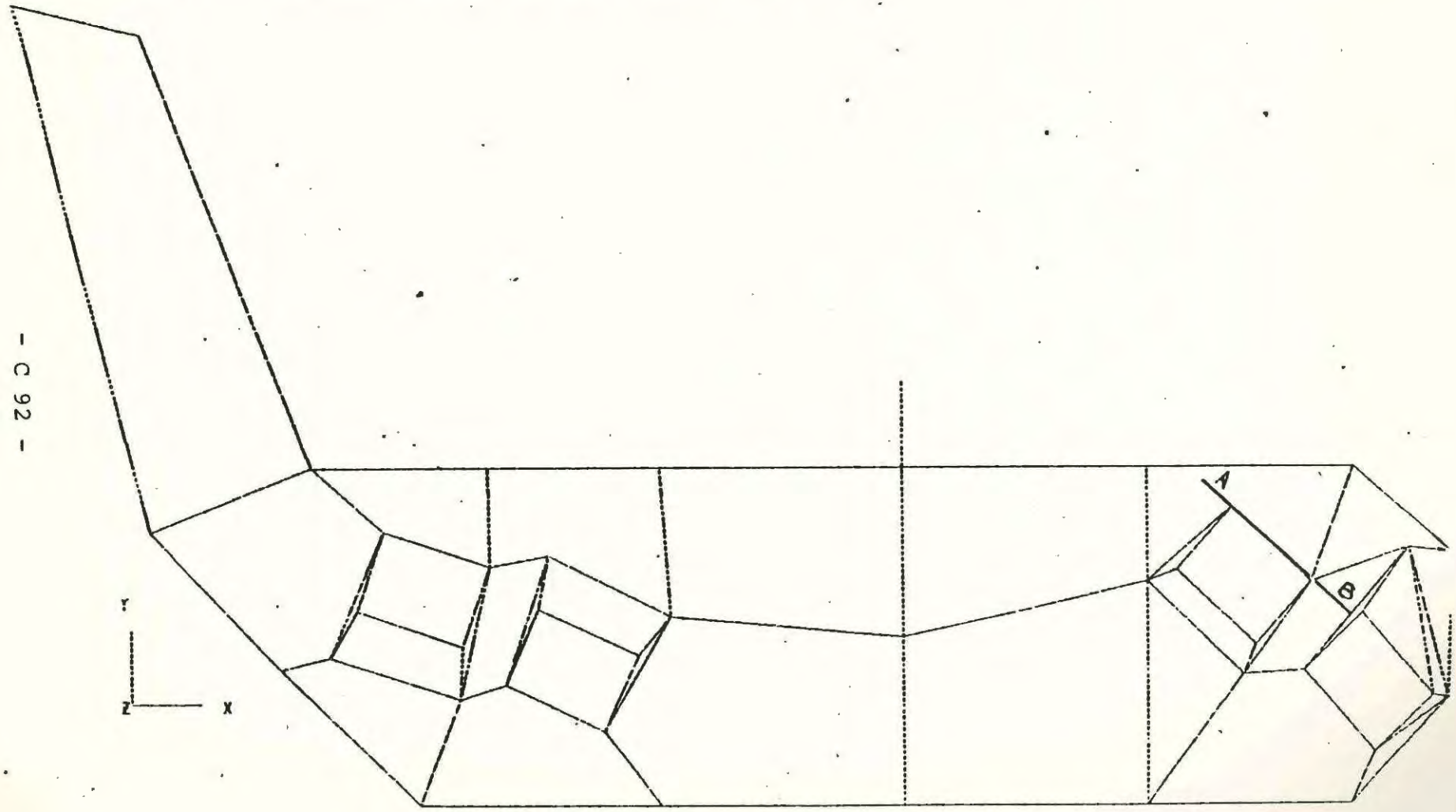

Figure 2 - ORIGINAL JOURNAL HOUSING - NON-STEERING LINK SIDE

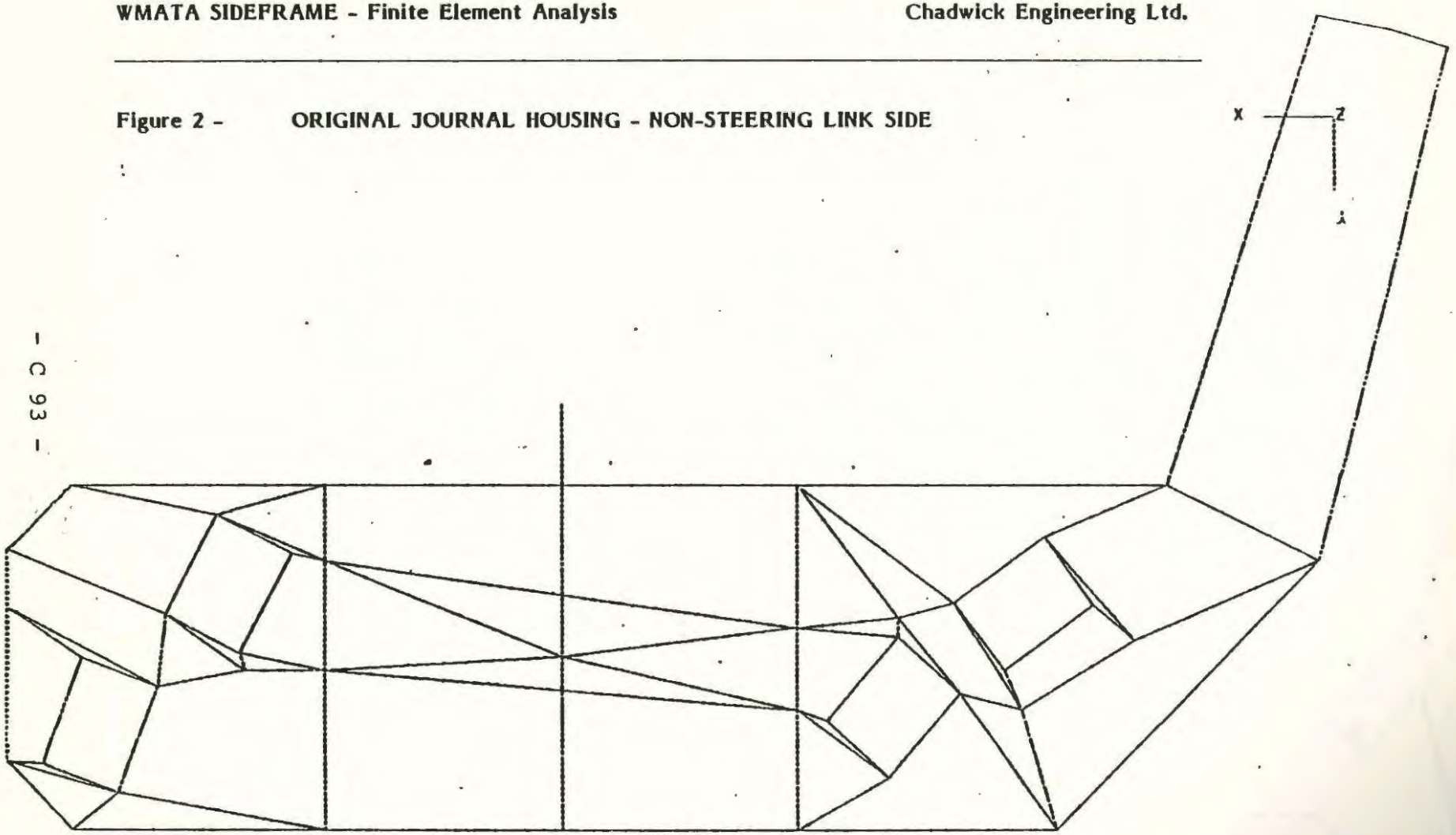

Figure 3 - REVISED JOURNAL HOUSING - STEERING LINK SIDE

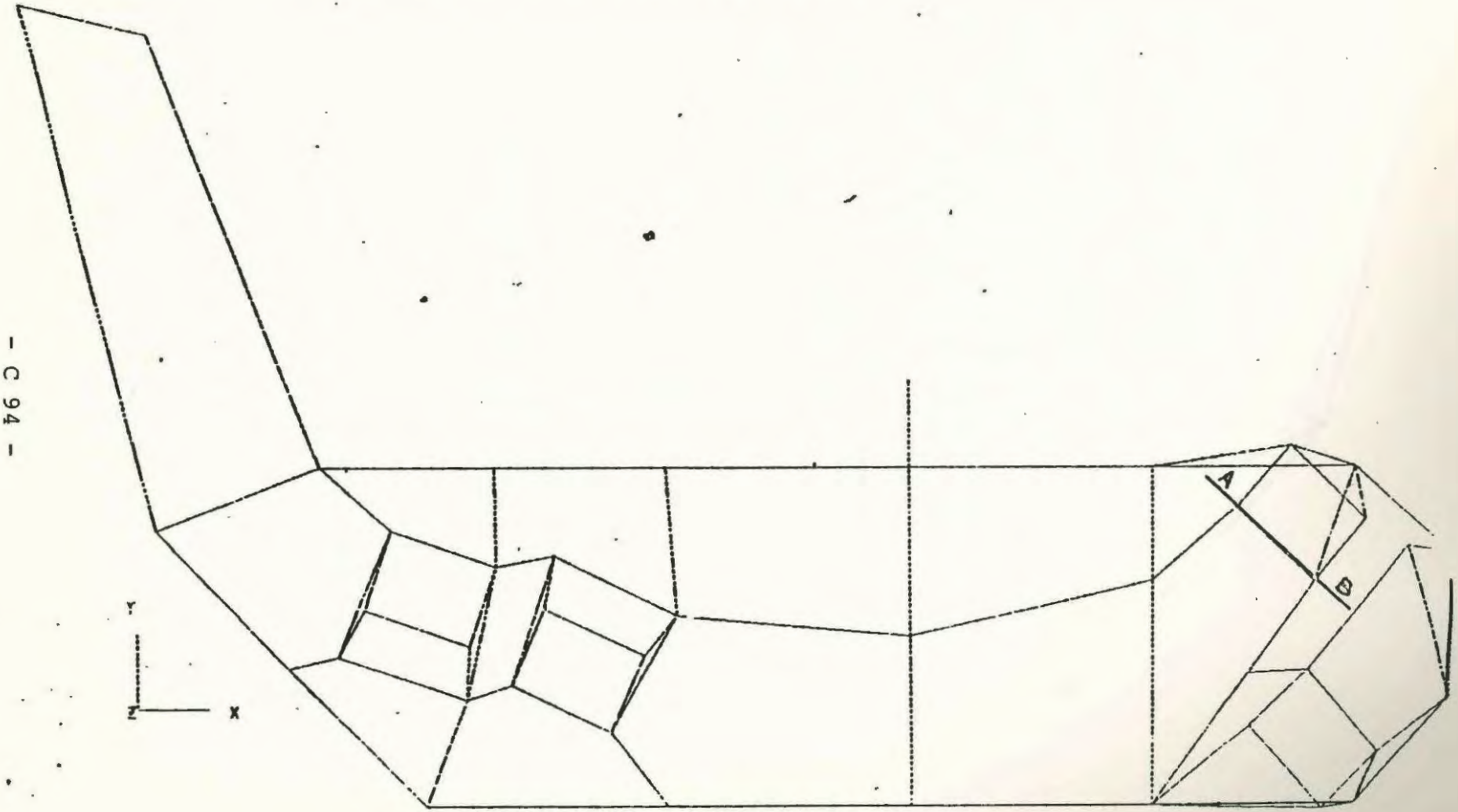

Figure 4 - REVISED JOURNAL HOUSING - NON-STEERING LINK SIDE

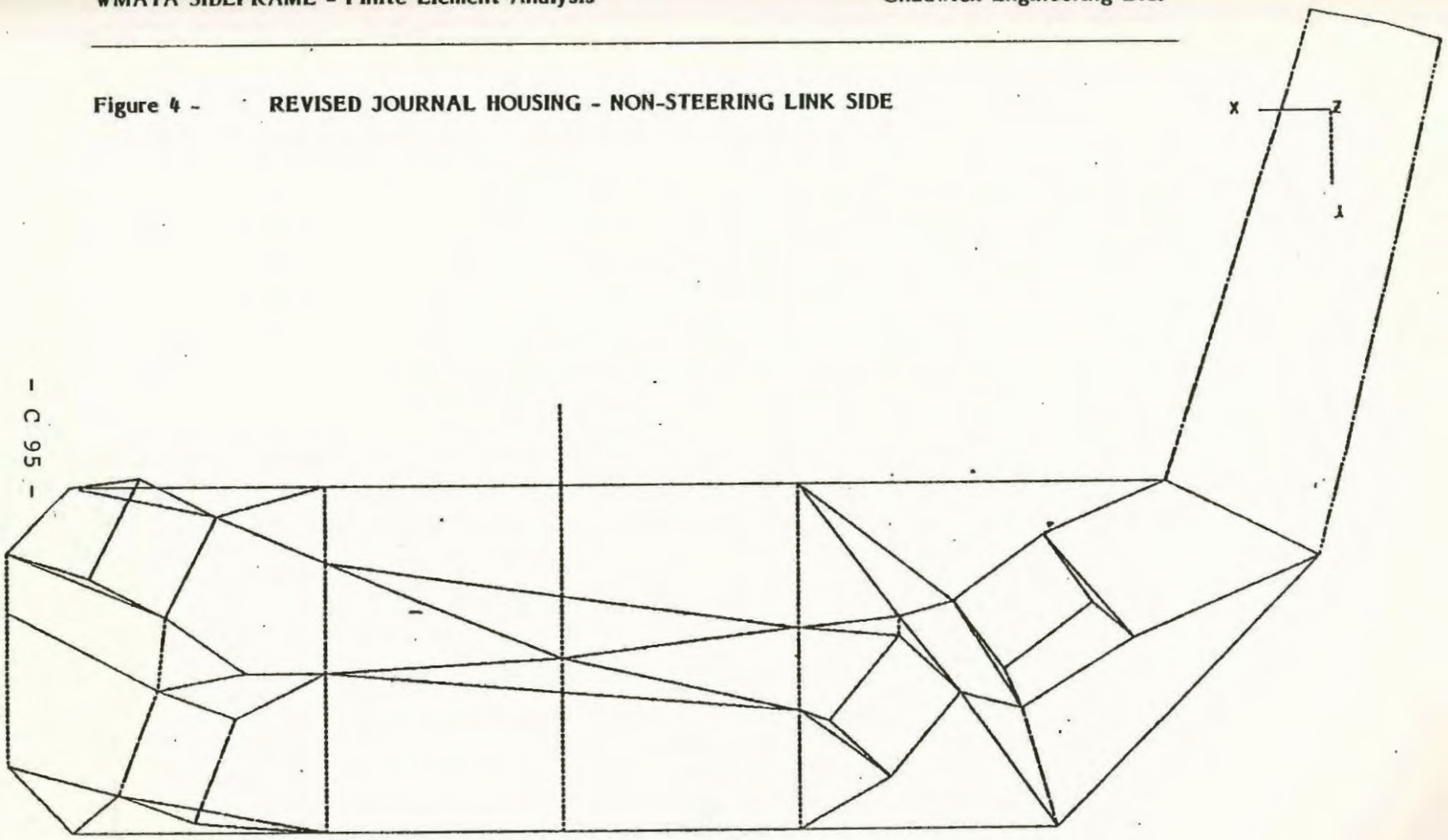

Figure 5 - REVISED JOURNAL HOUSING - GENERAL VIEW

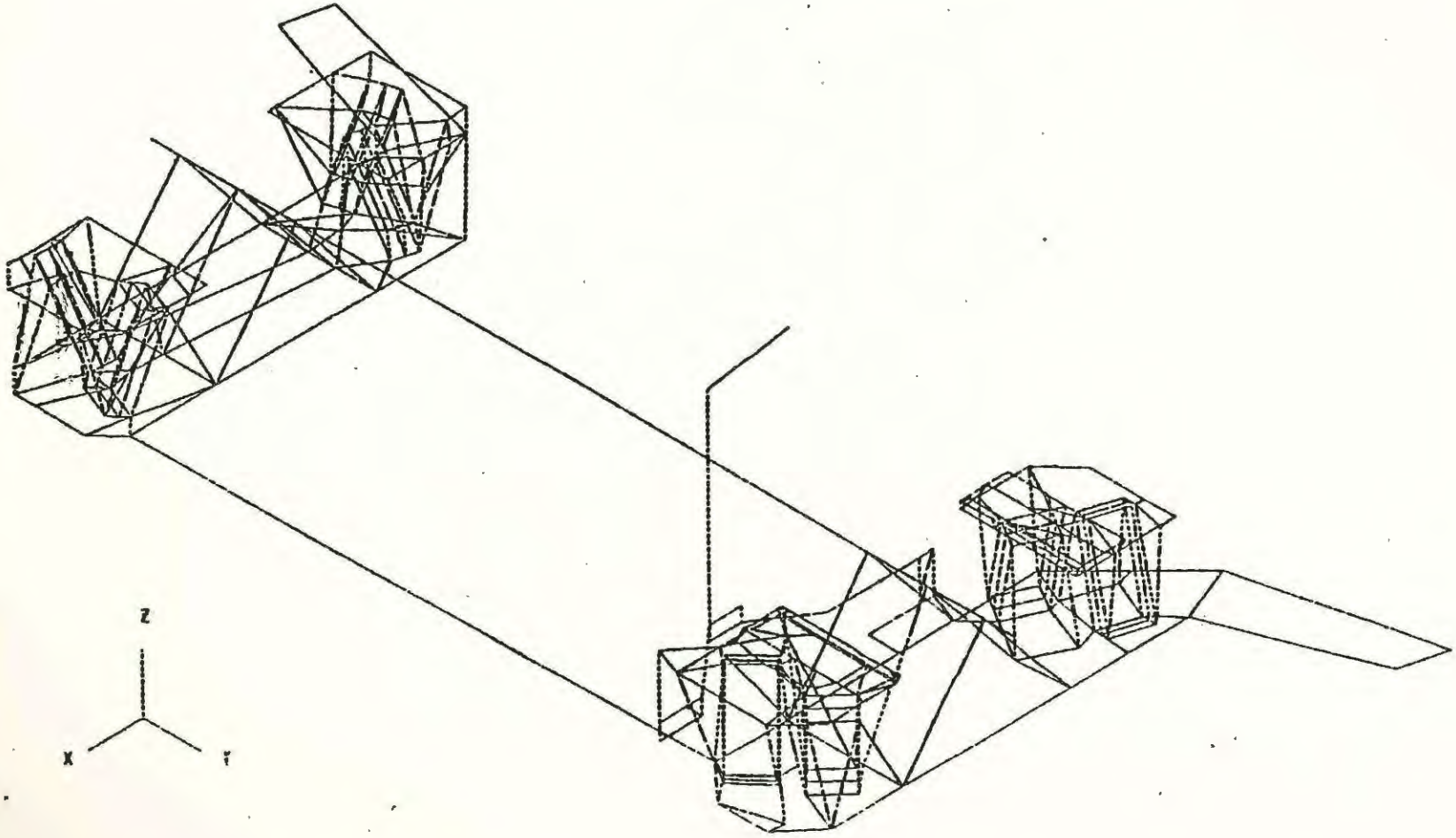

Figure 6 - REVISED JOURNAL HOUSING AND TOP BRACKETS - STEERING LINK SIDE

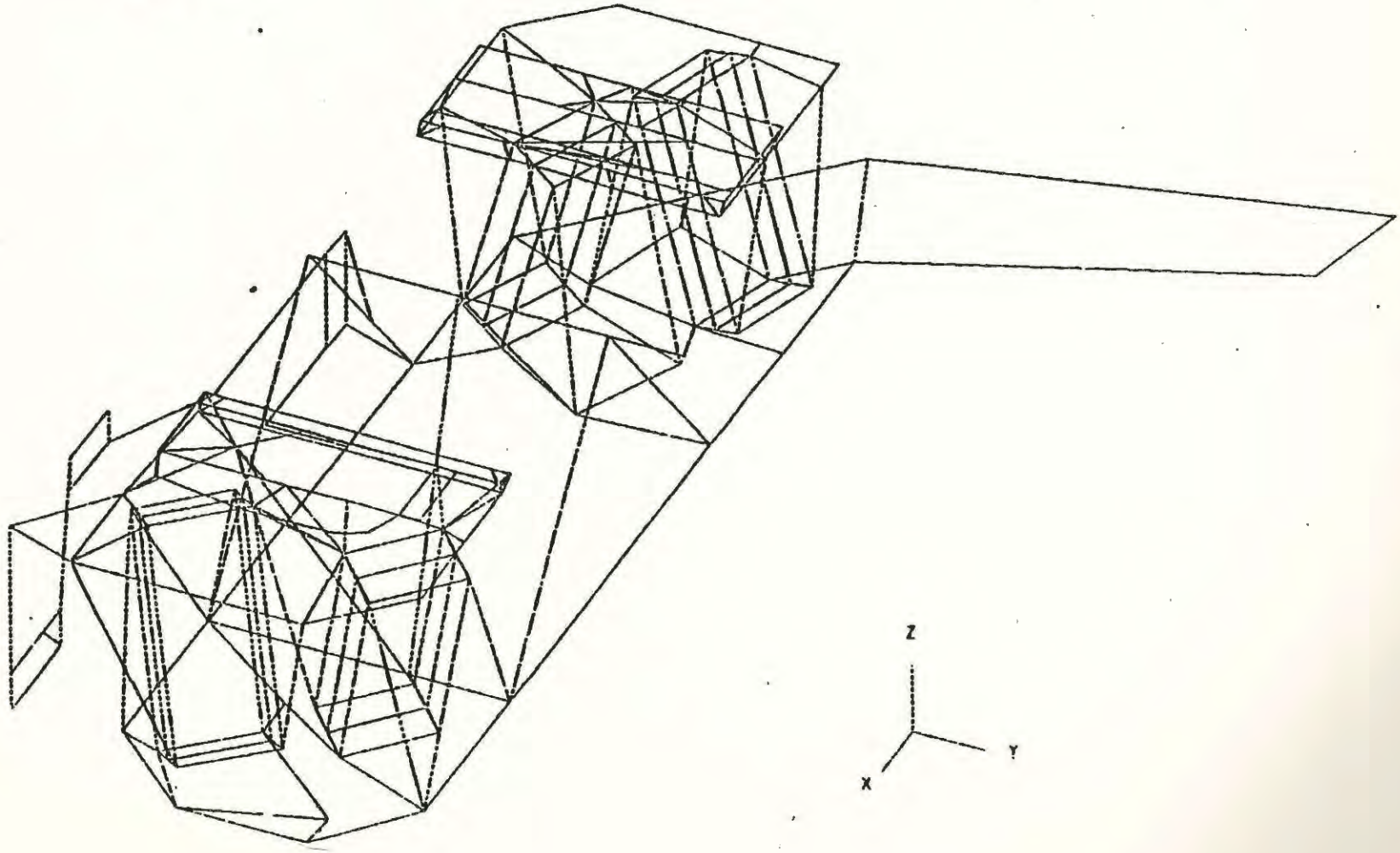

Figure 7 - REVISED JOURNAL HOUSING - STEERING LINK SIDE

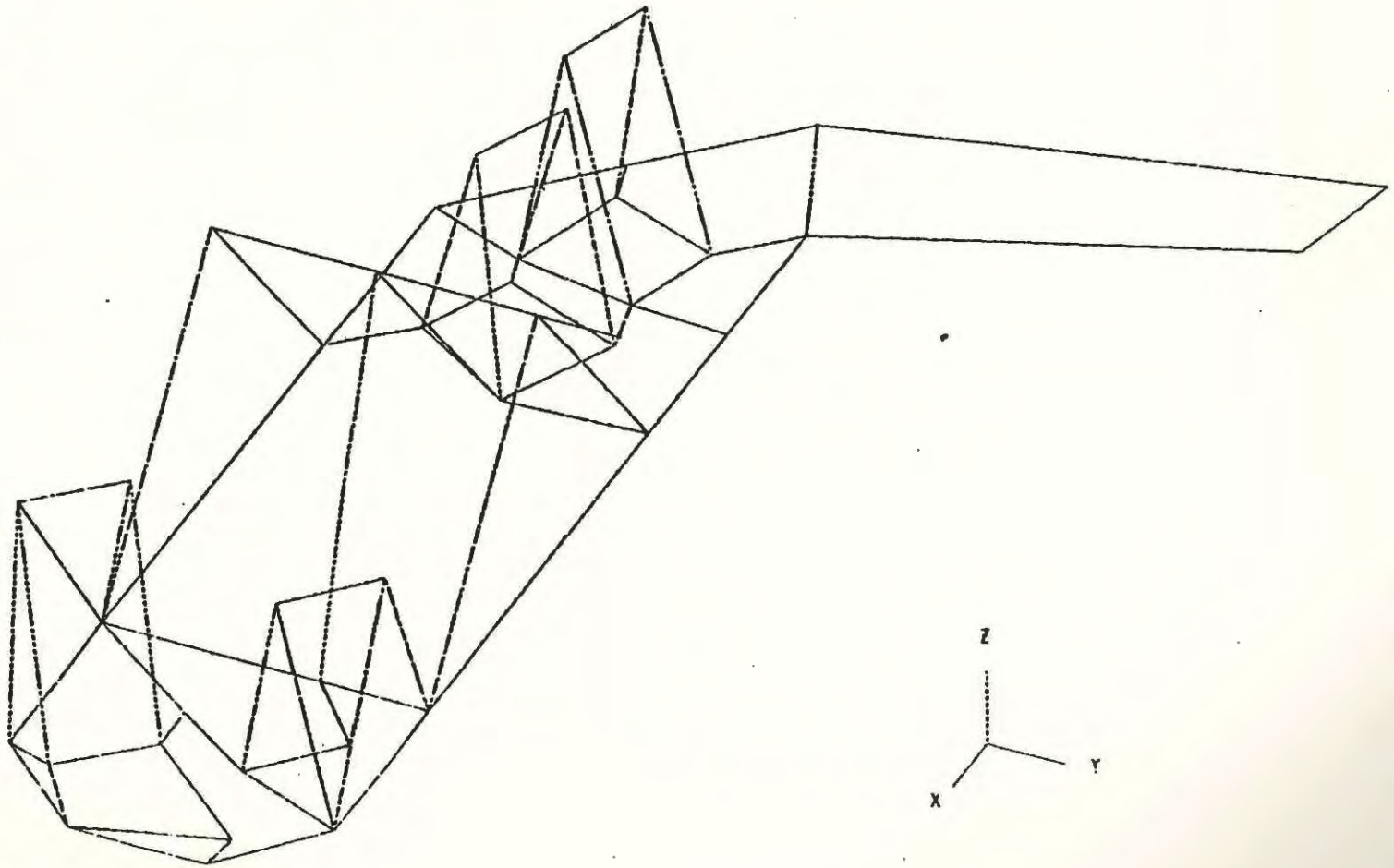

Figure 8 - SPRING PADS - STEERING LINK SIDE

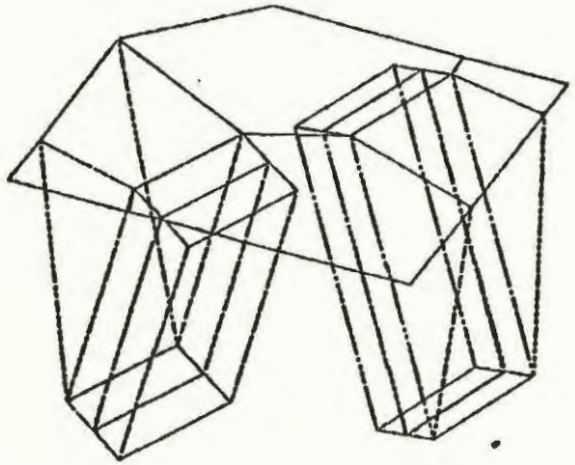

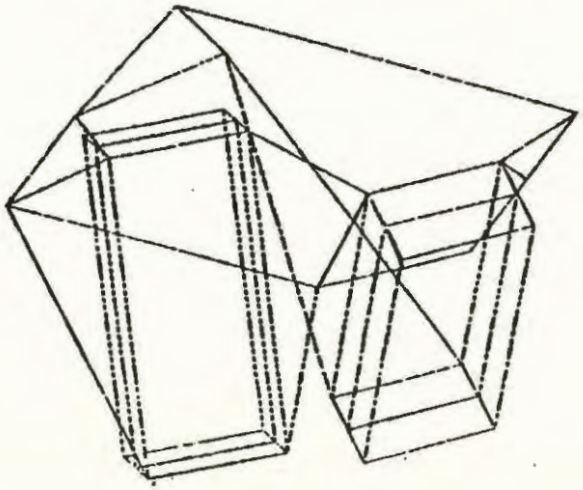

Figure 9 - REVISED JOURNAL HOUSING AND TOP BRACKETS - NON STEERING LINK SIDE

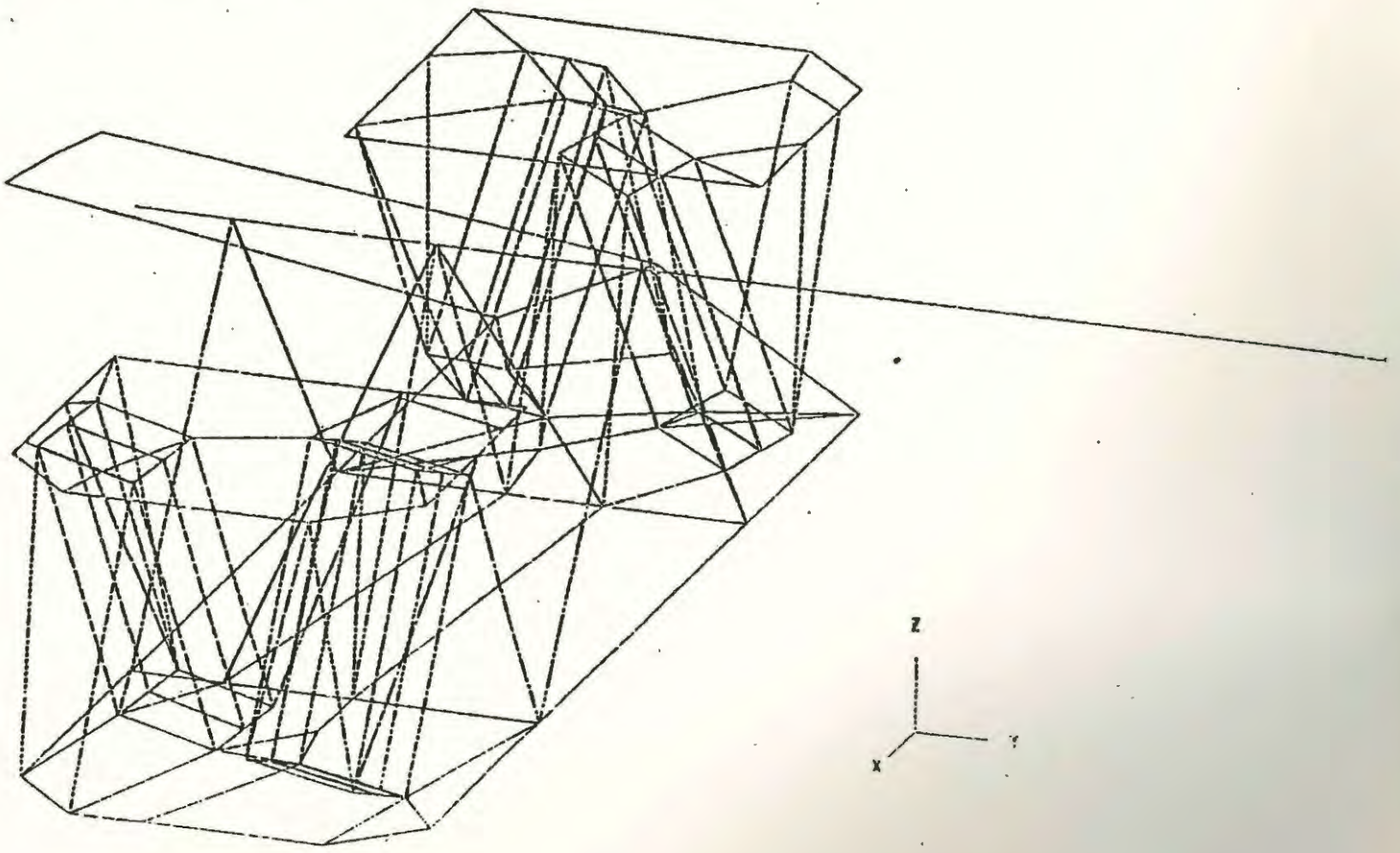

Figure 10 - REVISED JOURNAL HOUSING - NON-STEERING LINK SIDE

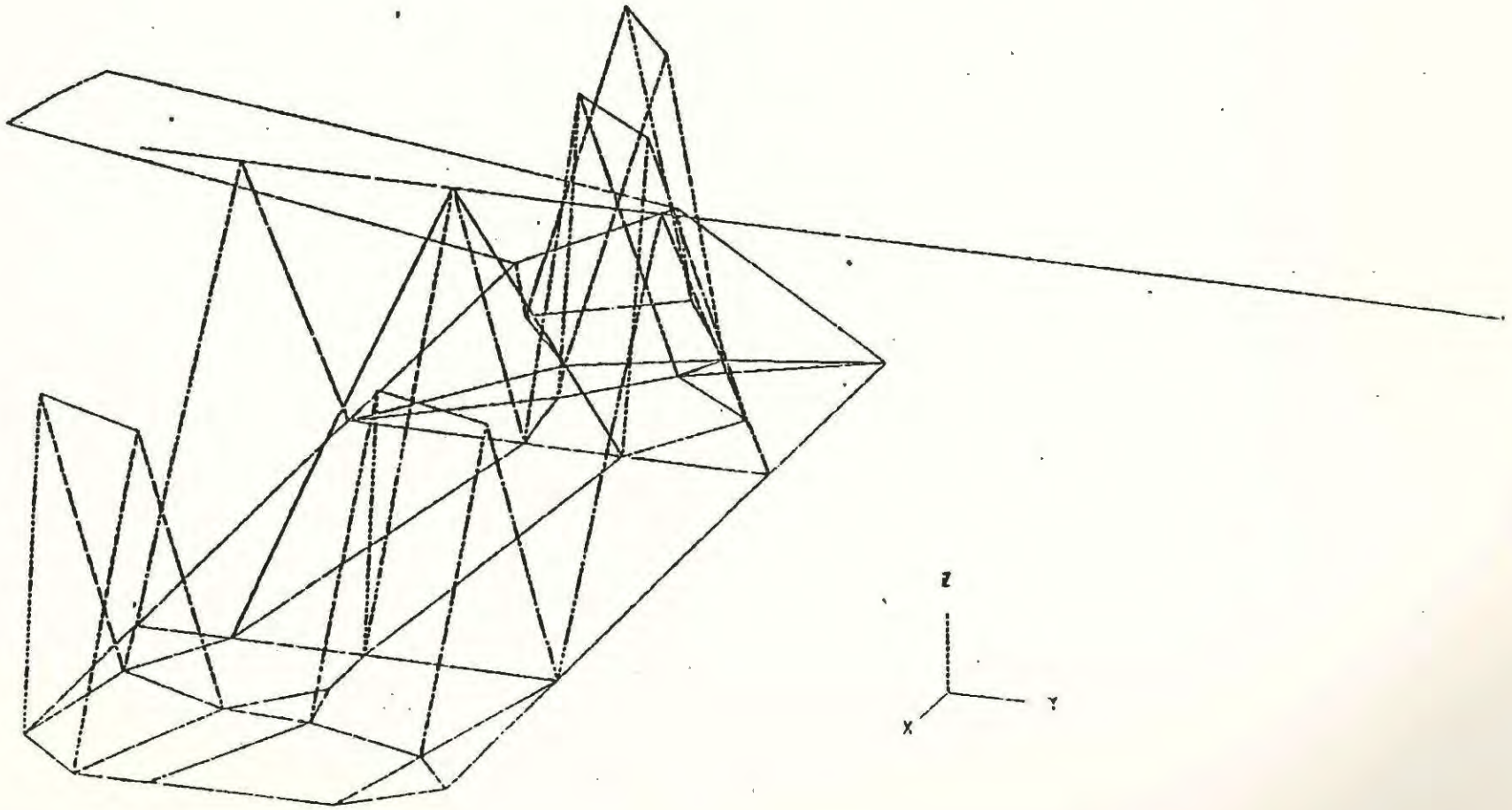

Figure 11 - SPRING PADS - NON-STEERING LINK SIDE

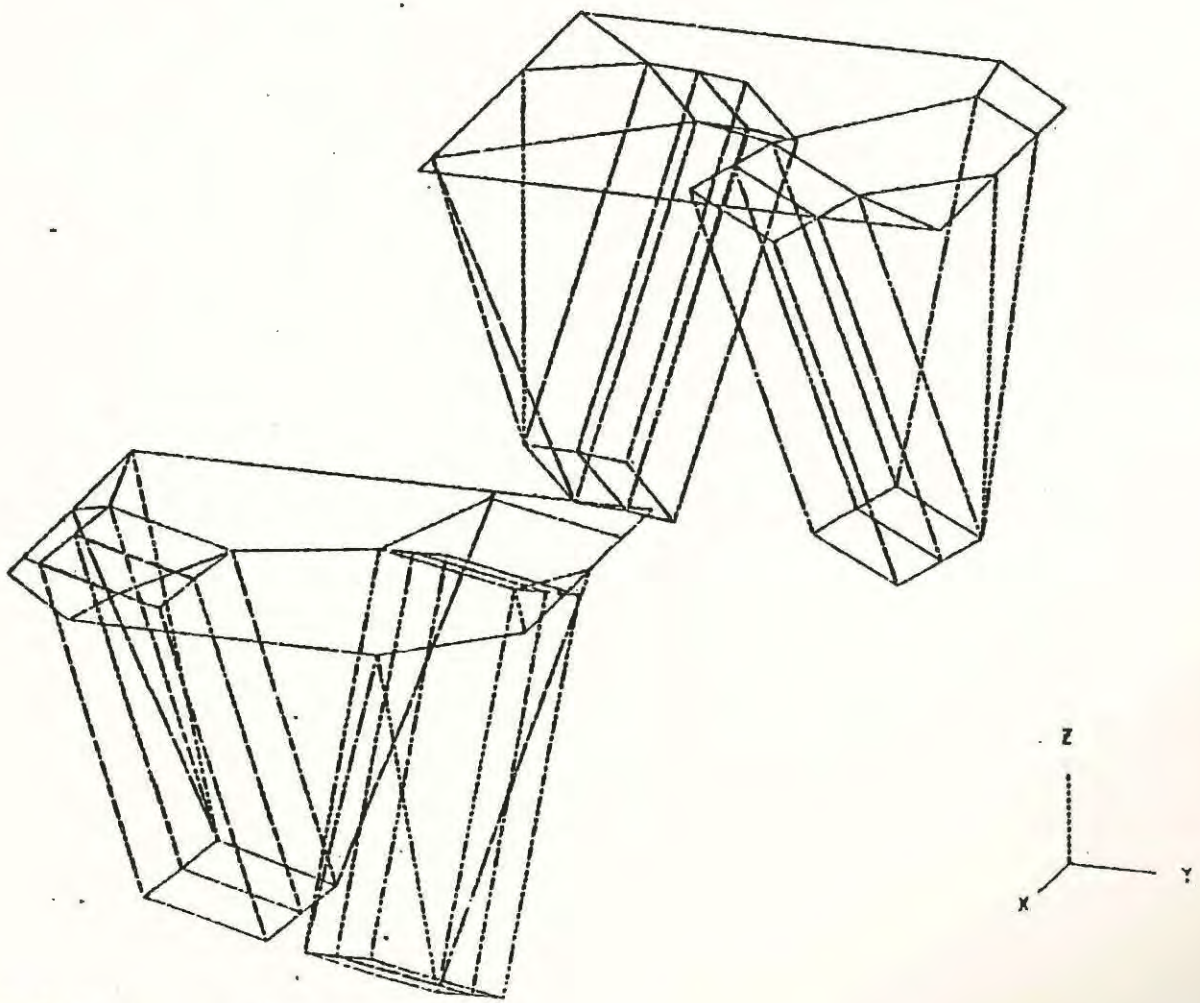

Figure 12 - REVISED JOURNAL HOUSING - COMBINED LOAD - CASE 1

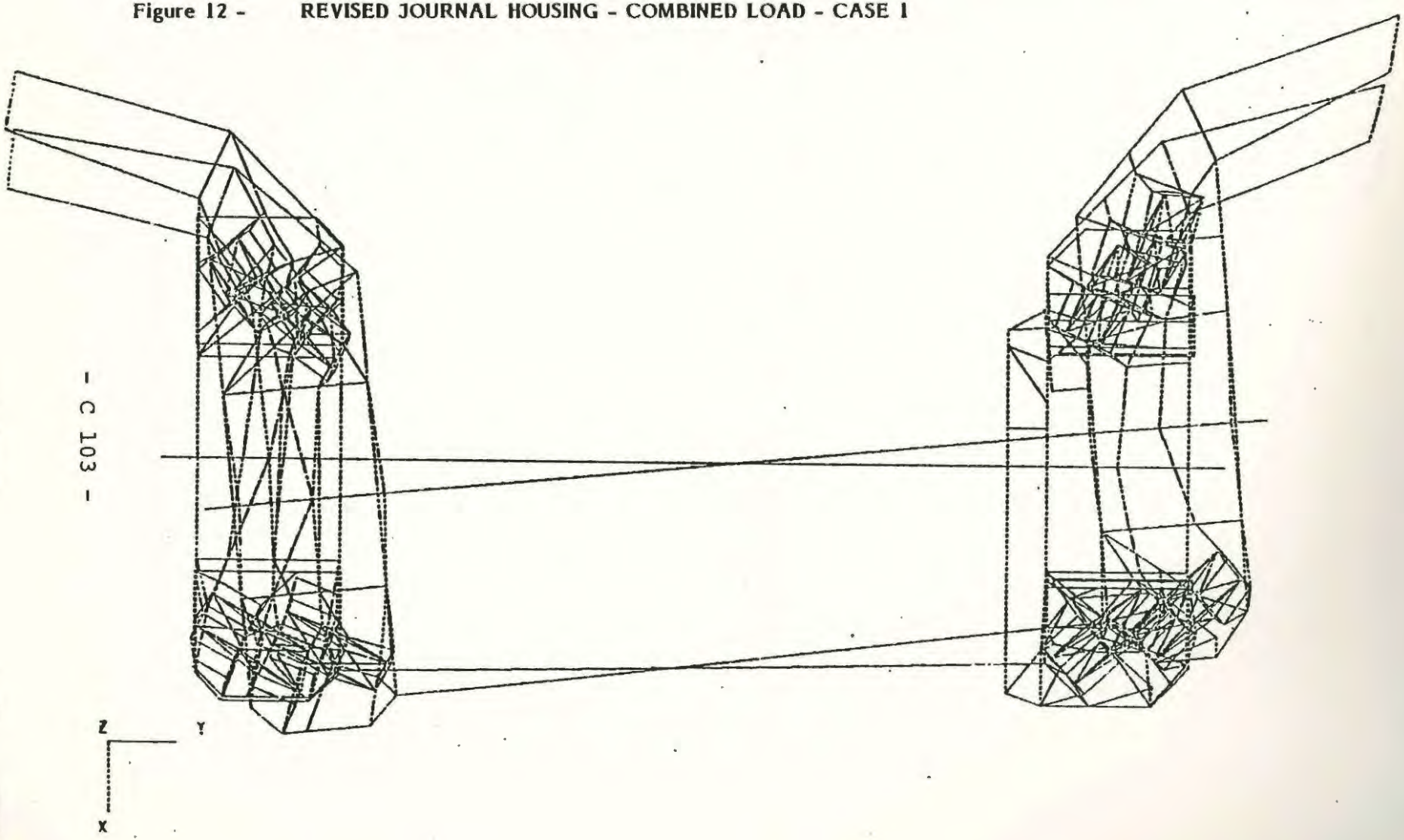

Figure 13 - REVISED JOURNAL HOUSING - LONGITUDINAL LOAD - CASE 2

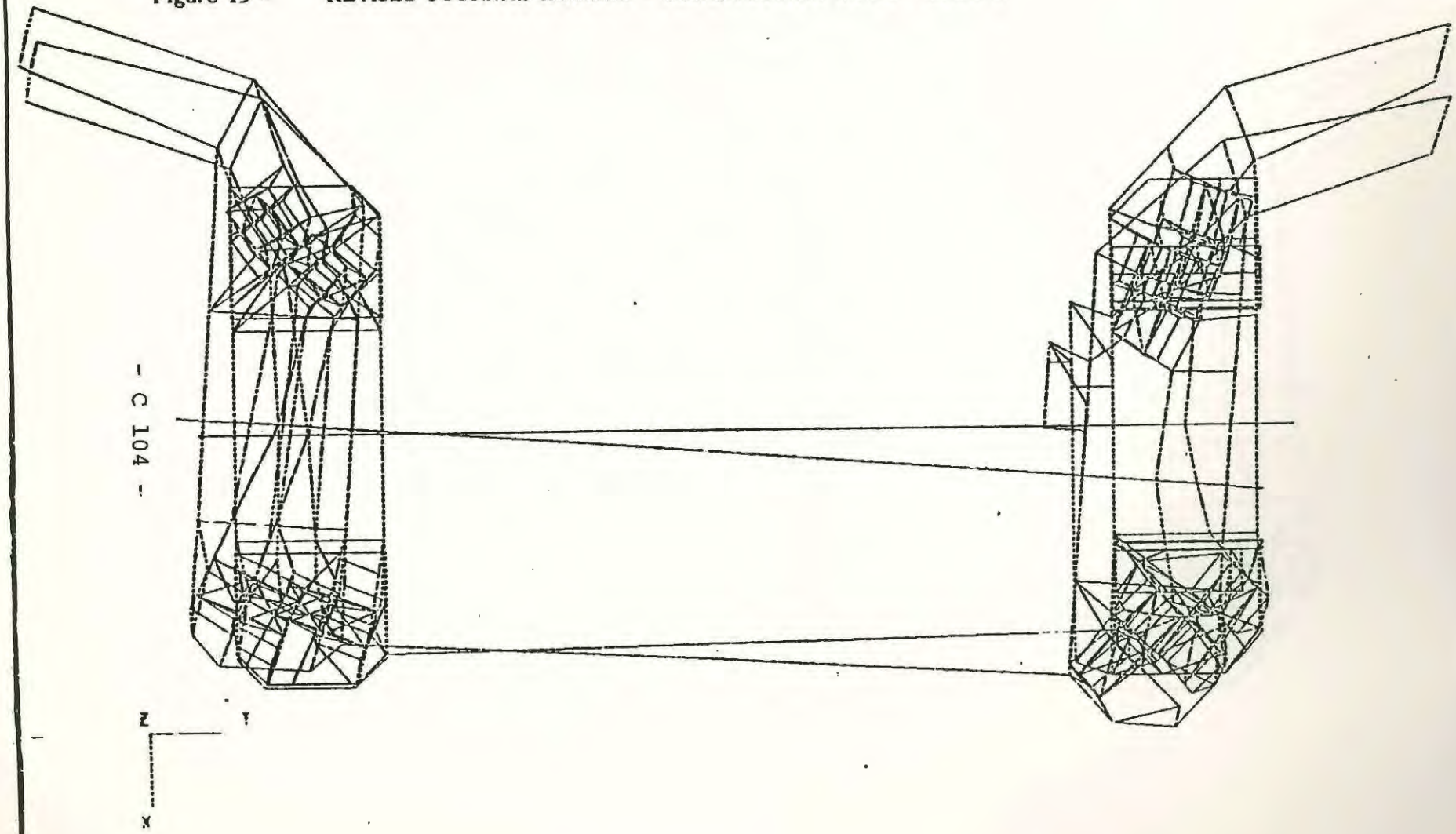

Figure 14 - REVISED JOURNAL HOUSING - LATERAL LOAD - CASE 3

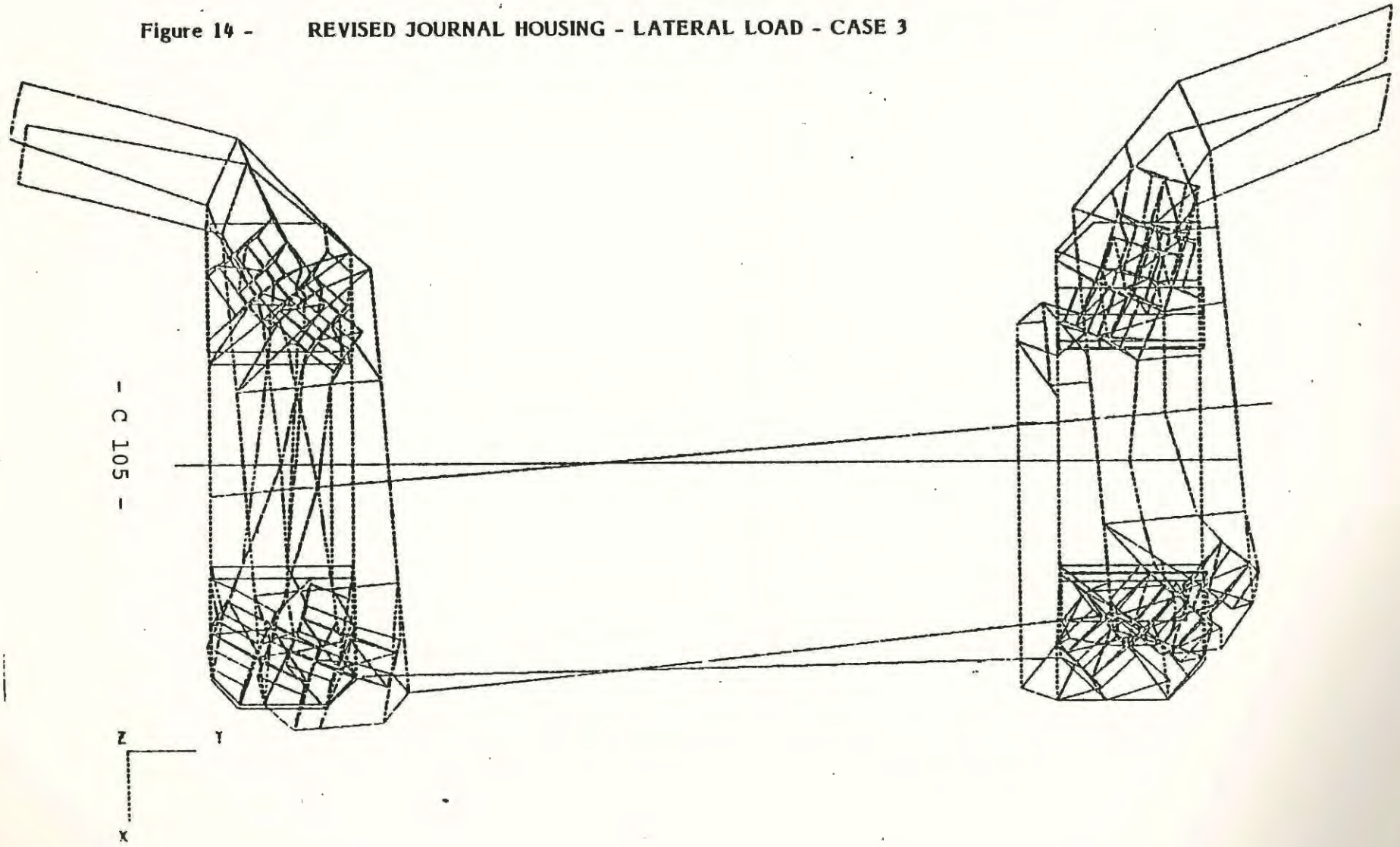

Figure 15 - REVISED JOURNAL HOUSING - VERTICAL LOAD - CASE 4

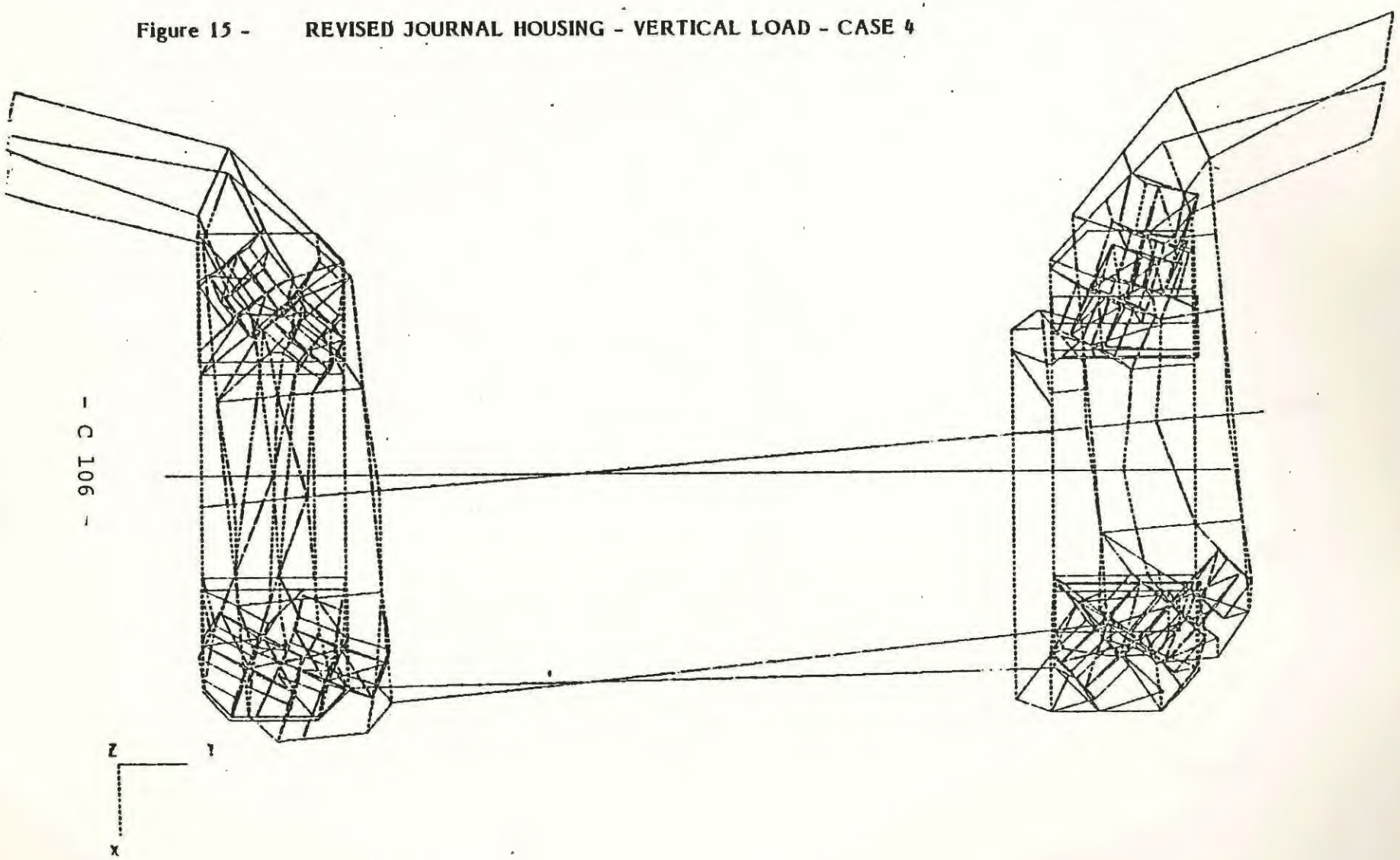

Figure 16 - ORIGINAL JOURNAL HOUSING - SPRING PAD NORMAL FORCES - VERTICAL LOAD - CASE 4

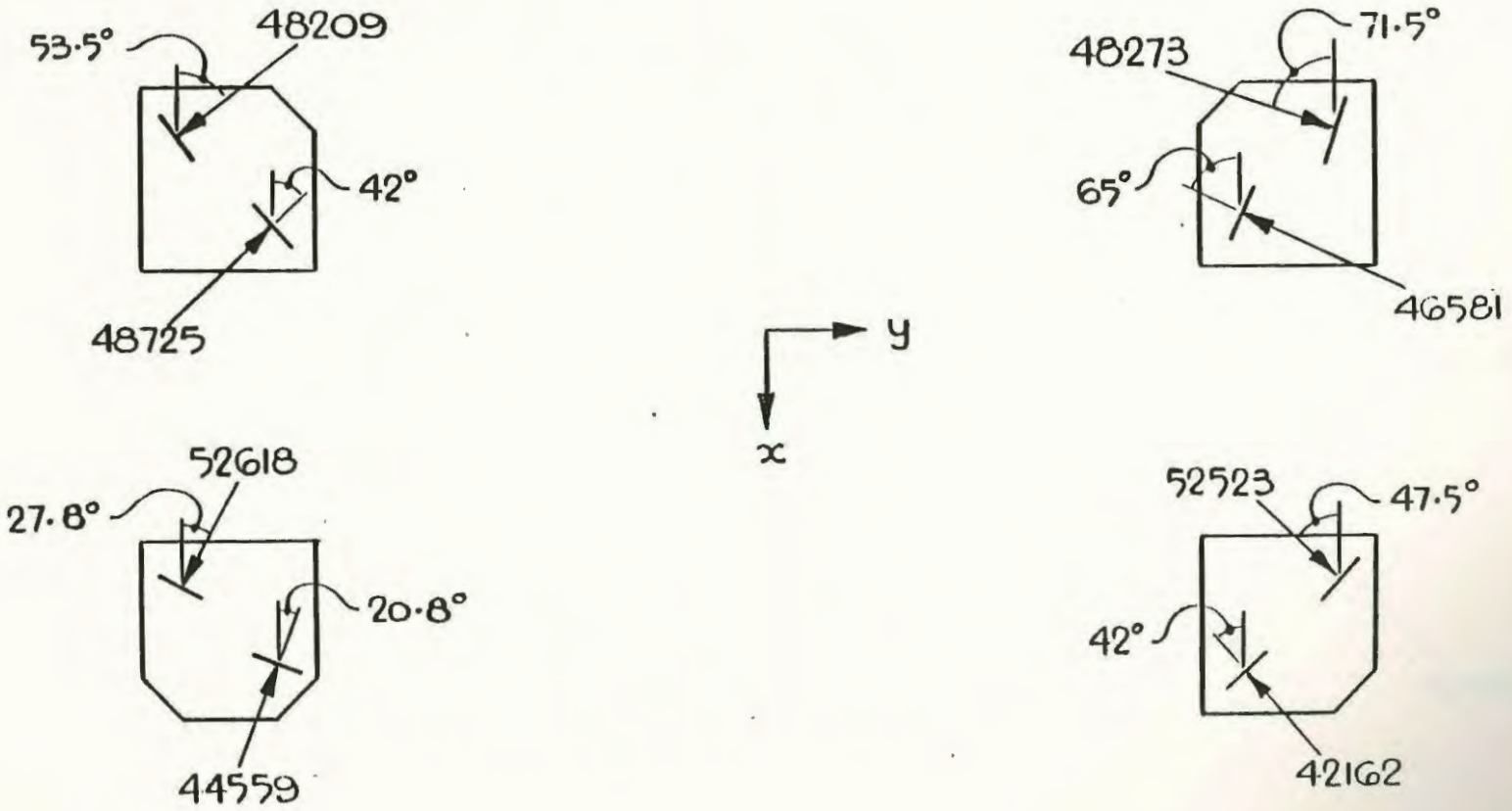

Figure 17 - REVISED JOURNAL HOUSING - SPRING PAD NORMAL FORCES - VERTICAL LOAD - CASE 4

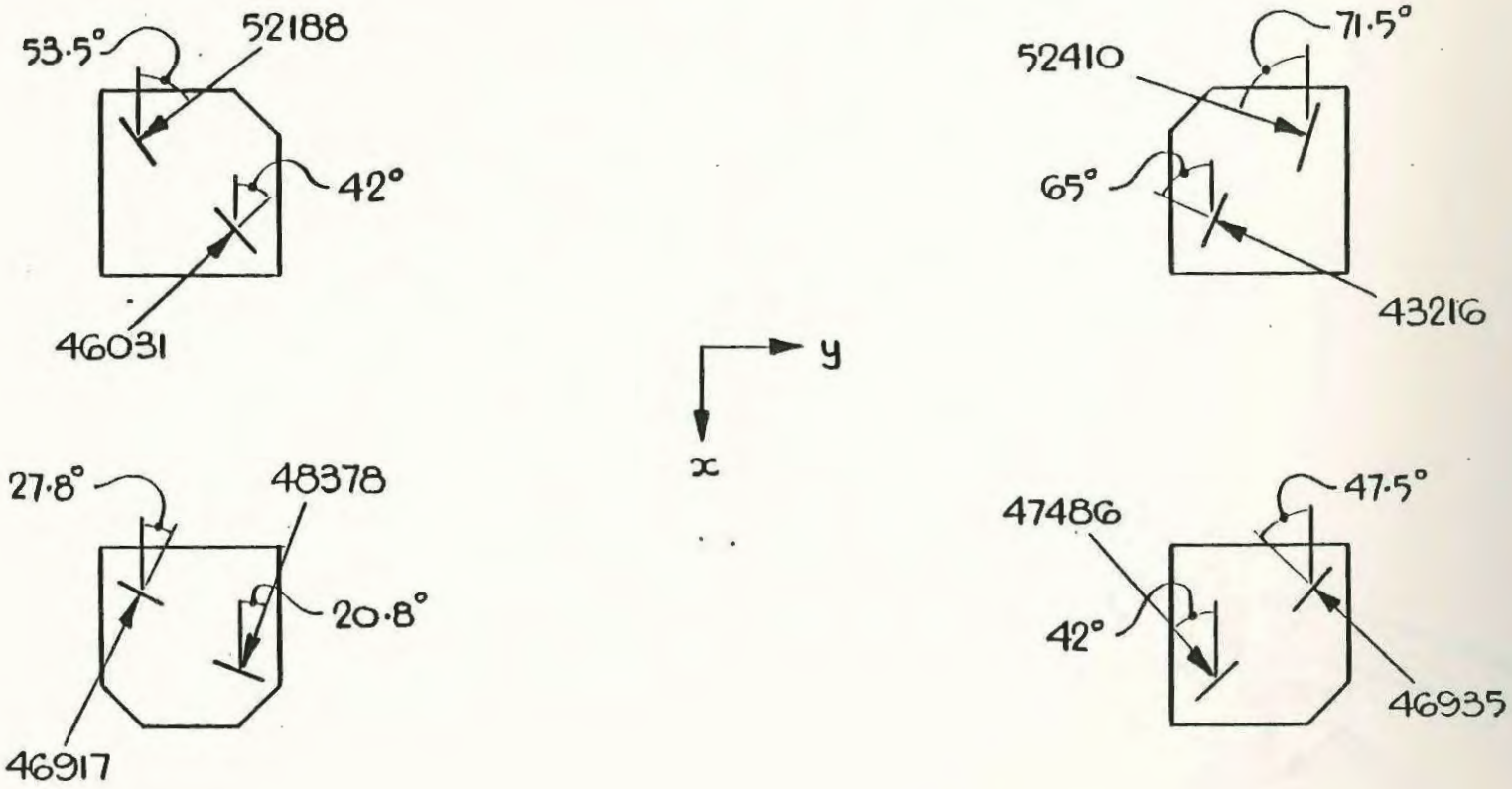

Figure 18 - ORIGINAL JOURNAL HOUSING - REACTION FORCES - COMBINED LOAD - CASE 1

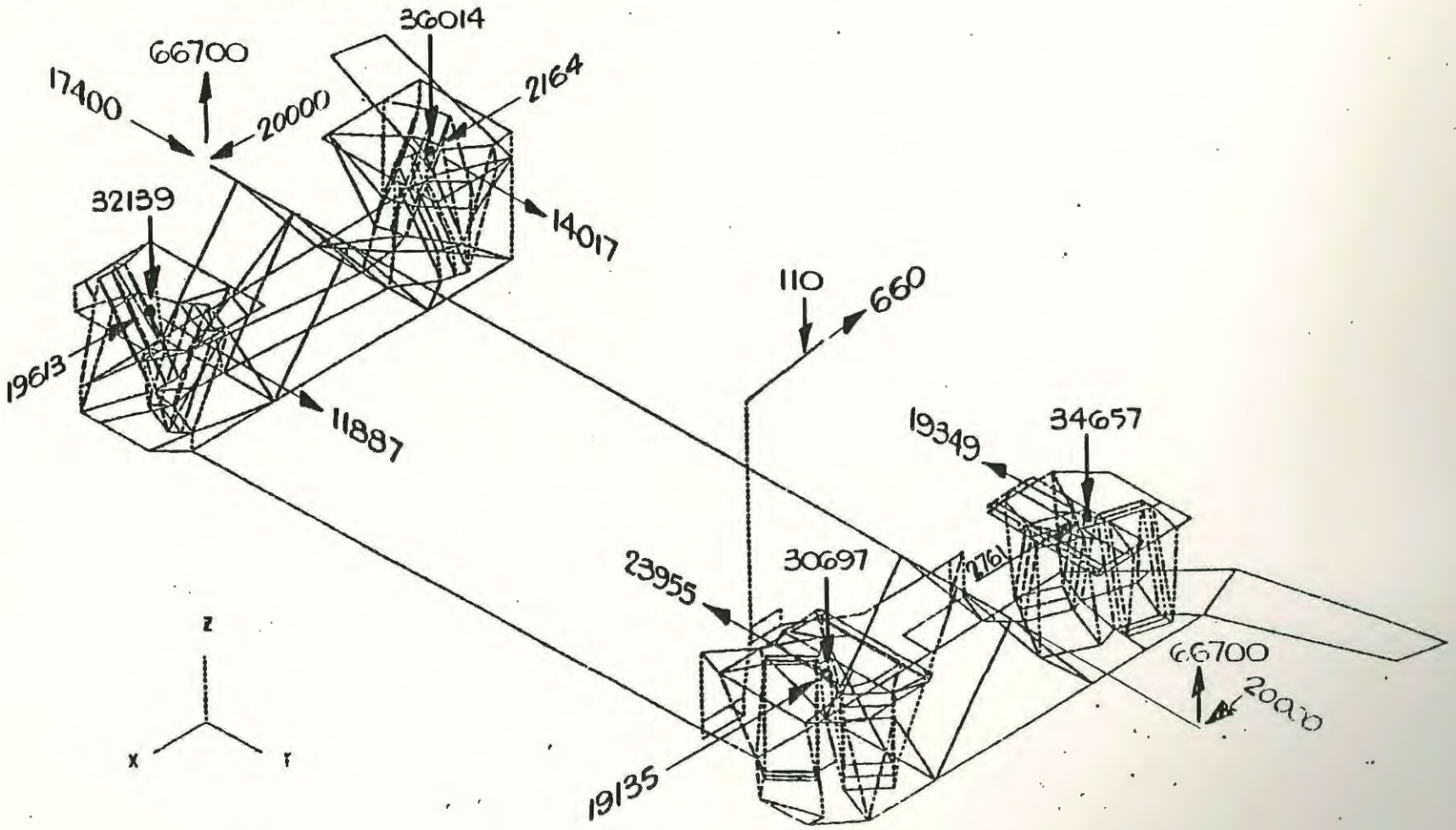

Figure 19 - REVISED JOURNAL HOUSING - REACTION FORCES - COMBINED LOAD - CASE 1